THE UNIVERSITY *of* EDINBURGH

FIRE RESISTANCE OF EARTHQUAKE DAMAGED REINFORCED CONCRETE FRAMES

Mariyana Aida Ab. Kadir

Doctor *of* Philosophy

The University *of* Edinburgh

2013

Declaration

This thesis and the research described within has been completed solely by Mariyana Aida Ab Kadir under the supervision of Prof. A.S Usmani and Dr. Martin Gillie.

Where other sources are quoted and references are given in details.

Mariyana Aida Ab. Kadir, 2013

Abstract

The topic of structural damage caused by fires following an earthquake (FFE) has been discussed extensively by many researchers for over a decade in order to bring the two fields closer together in the context of performance based structural engineering. Edinburgh University, Heriot-Watt University, Indian Institute of Technology Roorkee (IIT Roorkee) and Indian Institute of Science initiated a collaboration to study this problem under a UK-India Engineering Research Initiative (UKIERI) funded project. The first construction of a single-storey reinforced concrete frame at IIT Roorkee was completed in summer 2011; this is known as the Roorkee Frame Test 1 throughout this thesis.

This thesis presents the modelling of the Roorkee Frame Test 1 using the finite element method and assesses the capability of the numerical methodologies for analysing these two sequential events. Both two and three dimensional finite element models were developed. Beam and shell elements were chosen for the numerical modelling, which was carried out using the general purpose finite element package ABAQUS (version 6.8). The variation in material properties caused by these two types of loading, including strength and stiffness degradation, compressive hardening, tension stiffening, and thermal properties, is implemented in the numerical modelling. Constitutive material calculations are in accordance with EC4 Part 1.1, and all loading is according to IS 1893:2002 Part 1 (Indian Standard). The time-temperature curve used in the analysis is based on data from the test carried out.

The behaviour of the Roorkee Frame Test 1 when subjected to monotonic, cyclic lateral loading followed by fire is presented. The capacity of the frame when subjected to lateral loading is examined using a static nonlinear pushover method. Incremental lateral loading is applied in a displacement-controlled manner to induce simulated seismic damage in the frame. The capacity curve,

hysteresis loops and residual displacements are presented, discussed and compared with the test results. The heat transfer analysis using three dimensional solid elements was also compared against temperature distributions recorded during the Roorkee frame fire test. Based on the smoke layer theory, two emissivity values were defined.

In this study, the suitability of numerical modelling using ABAQUS to capture the behaviour of Roorkee frame test is examined. The results from this study show that the 3D ABAQUS model predicted more reliable hysteresis curves compared to the 2D ABAQUS model, but both models estimated the lateral load capacity well. However neither model was able to simulate the pinching effect clearly visible in the hysteresis curves from the test. This was due to non-inclusion of the bond slip effect between reinforcing bars and concrete.

The residual displacement obtained at the end of the cyclic lateral loading analysis from the 2D ABAQUS model is higher than that seen in the test. However, the result in the 3D ABAQUS model matched the trend obtained in the test. The both columns appear to stiffen under the heating and the residual displacement seems to recover slightly. Lateral displacements, obtained in the thermo-mechanical analysis of the numerical models, show that thermal expansion brings the frame back towards its initial position.

Finally, correlation studies between analytical and experimental results are conducted with the objective to establish the validity of the proposed model and identify the significance of various effects on the local and global response of fire resistance earthquake damaged of reinforced concrete frames. These studies show that the effect of tension stiffening and bond-slip are very important and should always be included in finite element models of the response of reinforced concrete frame with the smeared crack model when subjected to lateral and thermal loading. The behaviour of reinforced concrete

frames exposed to fire is usually described in terms of the concept of the fire resistance which defined in terms of displacement limit. This study shows the global displacement of the frame subjected to fire recover slightly due to the thermal expansion during the heating.

Publications

Conference Papers

Mariyana A. Ab-Kadir, J.Zhang, Asif S. Usmani; Experimental and Numerical Study on softening and Pinching Effects of Reinforced Concrete; 8th Asia Pacific Structural Eningeeirng and Construction Conference (APSEC) and 1st International Conference on Civil Engineering Research (ICCER), Surabaya, Indonesia, October 2012

Mariyana A. Ab-Kadir, Jian Zhang, Jian Jiang, Asif S. Usmani, Martin Gillie, Umesh K. Sharma, Pradeep Bhargava; Modelling of an Earthquake Damaged RC Frame Subjected to Fire;7th International Conference on Structures in Fire, Zurich, Switzerland, June 2012

Ab.Kadir M A, A.S Usmani, M. Gillie; Modelling of Reinforced Concrete Frames in Fire Following an Earthquake; Applications of Structural Fire Engineering, Prague, April 2011

Acknowledgements

A special thanks to my supervisor, Professor A.S Usmani for his expert advice support, patience, kindness and unending optimism. I'd also like to thank to my second supervisor, Dr. Martin Gillie for his valuable insight and support.

The financial support of the Universiti Teknologi Malaysia (UTM) and the Ministry of Higher Education Malaysia (MOHE) trust fund is gratefully acknowledged.

Thanks to all my colleagues in John Muir Building at the University of Edinburgh; you such my family while I'm away from them. You've made it cheerful and delight.

I'd variously like to thank to all Edinburgh University Fire Group; a real fire engineering group.

Thank you to all my friends, family members and particularly my mum for tireless support.

Importantly, thanks to my husband Marzukey. You've been constantly support and motivate me through this. Thanks to be a wonderful daddy and make the house running. To my daughter, Munaa Zahraa, who joined us throughout this research. Thanks for being a good girl and giving me unlimited happiness and pleasure.

Table of Contents

Declaration ..... **ii**

Abstract ..... **iii**

Publications ..... **vi**

Acknowledgements ..... **vii**

Table of Contents ..... **viii**

List of Figures ..... **xiii**

List of Tables ..... **xxi**

1 Introduction **1**

1.1 Background to the Project 1

1.2 Thesis Aims and Objectives 3

1.3 Outline of Thesis Chapters 4

2 Literature Review **7**

2.1 Introduction 7

2.2 Earthquake Effects on Building Structures 8

2.2.1 Consequences of an Earthquake 8

2.2.2 Factors Influencing the Extent of Earthquake Damage to Buildings 10

2.2.3 Non-Structural Damage 13

2.2.4 Active System Damage 14

2.2.5 Lifeline Systems Damage 14

2.2.6 Buildings Response 15

2.2.7 Strength and Ductility of Materials 16

2.2.8 Seismic Analysis 21

2.3 Behaviour of Reinforced Concrete Structures in Fire 25
2.3.1 Fire and its Consequences 25
2.3.2 Material 33
2.3.3 Structural Response to Fire 38
2.3.4 Fire Design Technique – Numerical Modelling 43
2.3.5 Failure Parameters of Structures Subject to Fire 43
2.4 Fire Following Earthquake (FFE) 45
2.4.1 Potential Effects on Building Fire Safety 48
2.4.2 Earthquake Loss Assessment 49
2.5 Conclusion 50
3 Preliminary Design and Test Set-Up 53
3.1 Introduction 53
3.2 Design Specification 55
3.3 Preliminary Design of the Roorkee Frame 56
3.3.1 Plastic Hinge 57
3.3.2 Static pushover analysis 58
3.4 Test Set-Up 62
3.4.1 Loading 62
3.4.2 Fire Loading 63
3.5 Conclusion 64
4 Development Numerical Models of the Roorkee Frame 69
4.1 Introduction 69
4.2 2D ABAQUS Model 70
4.2.1 Element Type and Meshing 72
4.2.2 Material Modelling of Concrete 73

4.2.3 Material Modelling of Reinforcing Steel 75
4.2.4 Interactive Modelling Between Concrete and Reinforcing Steel 76
4.2.5 Boundary Conditions and Imposed Loading 76
4.3 3D ABAQUS Model 78
4.3.1 Linear Drucker-Prager Model 79
4.3.2 Friction and Dilation Angle 82
4.4 2D OpenSees Model 83
4.4.1 Pinching4 Damage Model 83
4.5 Discussion and Conclusions 85
5 Simulation of The Response Due to Lateral Loading Using ABAQUS86
5.1 Introduction 86
5.2 Analysis 87
5.3 Analysis of results 89
5.3.1 Capacity curve of the frame 89
5.3.2 Cyclic lateral displacement loadings 95
5.4 Conclusion 100
6 Simulation of The Response Due to Fire Loading Using ABAQUS102
6.1 Introduction 102
6.2 Fire test 102
6.3 Numerical Heat Transfer Analysis 106
6.3.1 Heat Transfer Parameter Using in ABAQUS 112
6.4 Analysis of results 118
6.4.1 Temperature Distribution on the Bottom Beams (B1-B4) 120
6.4.2 Temperature Distribution in the Top Beams (B5 to B8) .. 123

6.4.3 Temperature Distribution in the Columns (C1 – C4)..... 125
6.4.4 Temperature Distribution through the Slab..... 127
6.5 Conclusions 129
7 Simulation of The Response Due to Thermo- Mechanical Loading131
7.1 Introduction 131
7.2 Thermal Loading 132
7.3 Analysis of Result..... 141
7.3.1 Horizontal Displacements after Thermo-Mechanical Loading 141
7.3.2 Reaction Forces of the Frame Due to Thermo-Mechanical Loading..... 151
7.3.3 Forces in the Frame Due to Thermo-Mechanical Analysis 153
7.3.4 Bending Moment at Plinth Beam after Thermo-Mechanical Analysis 157
7.3.5 Horizontal Displacements Due to Monotonic Loading Followed by Fire 161
7.4 Discussion and Conclusions 163
8 Summary, Conclusions and Recommendation for Further Work . 166
8.1 Introduction 166
8.2 Summary..... 167
8.2.1 Constitutive Models 167
8.2.2 Modelling and Analysis Methodology 168
8.2.3 Thermal Loading..... 170
8.2.4 Lateral displacement analysis 171
8.2.5 Thermo-mechanical analysis..... 172

8.3 Conclusions 173

8.4 Recommendation for Further Work 175

References 176

Appendix A 185

Appendix B 196

Appendix C 205

Appendix D 218

Appendix E 224

Appendix F 230

Appendix G 238

List of Figures

Figure 2-1 Earthquake effects on built environment [Reproduced from 20] 9

Figure 2-2 Roof drift and storey drift 15

Figure 2-3 Stress-Strain relationship of confined and unconfined concrete subjected to monotonic loading [Reproduced from 93] 17

Figure 2-4 Typical stress-strain relationship for concrete under cyclic compressive loading [Reproduced from 90] 18

Figure 2-5 Typical stress-strain relationship for reinforcing steel [Reproduced from 30] 19

Figure 2-6 Stress-strain schematic diagram with important characteristics of reinforcing steel bar subjected to cyclic loading [Reproduced from 30] 20

Figure 2-7 Cyclic straining of reinforcing steel for fy=380 MPa [Reproduced from 30] 20

Figure 2-8 Deformation and equivalent capacity curve of the structure sequence in pushover analysis procedure [Reproduced from 30] 24

Figure 2-9 Design fire with constant temperature 25

Figure 2-10 Parametric time-temperature curve [Reproduced from 32].....26

Figure 2-11 Swedish fire curve for different ventilation factors and fuel loads [Reproduced from 32].....29

Figure 2-12 Maximum temperature recorded in small-scale compartment during the steady burning period [Reproduced from 125] 31

Figure 2-13 Variation of thermal properties of concrete with different aggregates at elevated temperature [Reproduced from 81].....36

Figure 2-14 Variation of stress-strain in temperature [Reproduced from 83] 38

Figure 2-15 Uniform mean temperature and through depth thermal gradient over the cross-section of a beam [Reproduced from 76].....40

Figure 3-1 Description of the Roorkee frame study.....54

Figure 3-2 Design frame used in the modelling 55

Figure 3-3 Load Combination Mechanisms 57

Figure 3-4 Direct displacement base design [Reproduced from 104] 60

Figure 3-5 A simplified frame used in DDBD calculation.....60

Figure 3-6 The Roorkee frame assemblage tested in IIT Roorkee (a) Plan view (b) elevation view of the frame [Reproduced from 120].....65

Figure 3-7 Elevation view of the frame to show (a) the location of thermocouples (b) electrical strain gauges on the beams and the columns [Reproduced from 120].....66

Figure 3-8 A plan view of the frame to show the location of (a) L.V.D.T's (b) electrical resistance strain gauges in the slab [Reproduced from 120] 67

Figure 3-9 Pre-damage Roorkee frame with fireproof panel [Reproduced from 117] 68

Figure 4-1 Schematic front view of the 1x1 bay reinforced concrete frame 71

Figure 4-2 (a) Column and (b) beam cross-section with reinforcing steel details 71

Figure 4-3 Detailing of reinforced beam at slab level.....72

Figure 4-4 Node arrangement on the concrete section of the 2D beam element model 73

Figure 4-5 Node arrangement on the reinforcing steel of the 2D ABAQUS model 74

Figure 4-6 Response of uniaxial loading of concrete in tension and compression [Reproduced from 1].....75

Figure 4-7 Stress-strain relationship of reinforcing steel 76

Figure 4-8 2D beam model developed using ABAQUS 78

Figure 4-9 3D ABAQUS beam-shell element modelled using ABAQUS 6.8 80

Figure 4-10 The p-t stress plane [Reproduced from 1] 81

Figure 4-11 Illustrates the linear model in the deviatoric plane [Reproduced from 1] 82

Figure 4-12 Yield surface and flow direction in the p-t plane for the linear Drucker-Prager model [Reproduced from 1] 83

Figure 4-13The cross-section of the (a) column and (b) lower beam of the frame 84

Figure 4-14 Hysteresis curve of Pinching4 uniaxial material model in OpenSees [Reproduced from 94].....84

Figure 5-1 History of imposed lateral displacement on the frame used in numerical analysis.....88

Figure 5-2 History of imposed lateral displacement on the frame from the Test 1 [Reproduced from 120].....89

Figure 5-3 Capacity curve from 2D ABAQUS model and the test.....90

Figure 5-4 Capacity curve of 3D ABAQUS model and the test 91

Figure 5-5 Capacity curve of 2D ABAQUS model, OpenSees and the test 91

Figure 5-6 Illustration of the deformation of the frame under gravity loading 92

Figure 5-7 Illustration of the strain of the frame during at (a) monotonic loading=10mm (b) monotonic loading=50mm (push in positive x-direction).....93

Figure 5-8 Illustration of the strain of the frame during at (a) monotonic loading=75mm (b) monotonic loading= 100mm (push in positive x-direction).....94

Figure 5-9 Hysteresis curve of 2D ABAQUS model and the test 96

Figure 5-10 Hysteresis curve of 3D ABAQUS model and the test 97

Figure 5-11 Hysteresis curve of 2D model using ABAQUS and OpenSees.....98

Figure 5-12 Deformation shape of the frame from 2D ABAQUS model.....99

Figure 5-13 Deformation shape of the frame from 3D ABAQUS model.....99

Figure 6-1 Set-up of a brick masonry with a pool fire for test [Reproduced from 120] 104

Figure 6-2 Plan view of brick compartment.....104

Figure 6-3 Gas temperature curve of M1 thermocouple at A (TMRA) [Reproduced from 120].....105

Figure 6-4 Gas temperature curve of M1 thermocouple at B (TMRB) [Reproduced from 120].....105

Figure 6-5 Gas temperature curve of M1 thermocouple at C (TMRC) [Reproduced from 120].....106

Figure 6-6 3D Continuum frame modelled in ABAQUS version 6.8.....107

Figure 6-7 Total emittance of (a) water vapour (H_2O) and (b) carbon dioxide (CO_2) [Reproduced from 57].....109

Figure 6-8 The well-mixed case: An enclosure with uniform temperature, T_g, which is higher than the outside temperature, T_a [Reproduced from 73] 112

Figure 6-9 Compartment fire modelled in ABAQUS 6.8.....114

Figure 6-10 (a) Test setup for realistic compartment fire (b) Attainment of flashover in fire test [117] 115

Figure 6-11 Plan view of the lower frame.....116

Figure 6-12 Notation of beams, columns and slab in a compartment (Plan view) 117

Figure 6-13 Compartment fire modelled in ABAQUS 6.8.....117

Figure 6-14 Temperature distribution of the frame from the heat transfer analysis 118

Figure 6-15 Location of thermocouples in beams and columns in the test [117] 119

Figure 6-16 Temperature distributions in the plinth beam, B1 at the left side along the height (a) Test (b) Heat Transfer using ABAQUS.....121

Figure 6-17 Temperature distributions in the plinth beam,B1 at the middle side along the height (a) Test (b) Heat Transfer using ABAQUS.....122

Figure 6-18 Temperature distribution in the plinth beam, B1 at the right side along the height (a) Test (b) Heat Transfer using ABAQUS.....122

Figure 6-19 Temperature distributions in the top beam, B5 at the left side along the height (a) Test (b) Heat Transfer using ABAQUS.....124

Figure 6-20 Temperature distributions in the top beam, B5 at the middle side along the height (a) Test (b) Heat Transfer using ABAQUS.....124

Figure 6-21 Temperature distributions in the top beam, B5 at the right side along the height (a) Test (b) Heat Transfer using ABAQUS.....125

Figure 6-22 Temperature distributions in the column, C4 at the bottom side along the height (a) Test (b) Heat Transfer using ABAQUS.....126

Figure 6-23 Temperature distributions in the column, C4 at the middle along the height (a) Test (b) Heat Transfer using ABAQUS.....127

Figure 6-24 The five locations on the slab where the temperature distribution was recorded [117].....128

Figure 6-25 Temperature distributions in the slab at A (a) Test (b) Heat Transfer using ABAQUS.....129

Figure 7-1 Temperature distributions in the plinth beam, B1 from the Roorkee test 133

Figure 7-2 Temperature distributions in the top beam, B5 from the Roorkee test 133

Figure 7-3 Temperature distributions in the column, C4 from the Roorkee test 134

Figure 7-4 Temperature distributions in the slab, TSL-O from the Roorkee test 134

Figure 7-5 Nodes where the thermal loading applied at different heights of column.....135

Figure 7-6 Temperature variable input at specific points in beam section 136

Figure 7-7 The I-beam section modelled with wider web and temperatures points.....139

Figure 7-8 Representing beam B5 showing the location of the temperatures values at five points throughout the I-beam section 140

Figure 7-9 Representing column C4 showing the location of the temperatures values at five points throughout the I-beam section 140

Figure 7-10 Cross section of the slab showing the temperature points through its thickness.....141

Figure 7-11 Horizontal displacement of Nodes 3001 and 3019 during thermo-mechanical loading-2D ABAQUS Model 142

Figure 7-12 Horizontal displacement of Nodes 1 and 2 from 2D OpenSees model 142

Figure 7-13 Vertical displacement (U2) from 3D ABAQUS model (magnified to 5) 144

Figure 7-14 Horizontal displacement (U1) at slab level of node 3001 and 3019-3D ABAQUS Model 144

Figure 7-15 Horizontal displacement (U1) at slab level of node 3001 and 3019 from thermal analysis (undamaged frame)-3D ABAQUS Model...145

Figure 7-16 Horizontal displacement along the height of the right column.....145

Figure 7-17 Horizontal displacement along the height of the left column.....146

Figure 7-18 Vertical displacement (U2) at slab level of node 3001 and 3019 .147

Figure 7-19 Vertical displacement (U2) at slab level of node 3001 and 3019 (thermal loading on undamaged frame) 147

Figure 7-20 Vertical displacement (U2) at top beam of node 3010 (thermal loading analysis of undamaged frame).....148

Figure 7-21 Vertical displacement (U2) at the plinth beam of node 1210 149

Figure 7-22 Vertical displacement (U2) at the plinth beam of node 1210 (thermal loading analysis of undamaged frame).....150

Figure 7-23 Vertical displacement (U2) at mid slab level due to thermo-mechanical loading.....150

Figure 7-24 Vertical displacement (U2) at mid slab level (thermal loading analysis of undamaged frame) 151

Figure 7-25 Reaction force (RF1) in x-direction of the frame due to thermo-mechanical loading.....152

Figure 7-26 Reaction force (RF2) in y-direction of the frame due to thermo-mechanical loading.....153

Figure 7-27 Reaction force (RF3) in z-direction of the frame due to thermo-mechanical loading.....153

Figure 7-28 Shear force of both columns at 200mm below the slab 154

Figure 7-29 Shear force of both columns at 200mm above the plinth beam...154

Figure 7-30 Shear force profile of the plinth beam at 400mm from left hand column.....155

Figure 7-31 Shear force profile of the plinth beam at 400mm from right hand column.....155

Figure 7-32 Axial force profile at mid span of the plinth beam 156

Figure 7-33 Axial force of the plinth beam at 400mm from left hand column ..157

Figure 7-34 Axial force of the plinth beam at 400mm from right hand column 157

Figure 7-35 Bending moment profile at mid span of the plinth beam 158

Figure 7-36 Bending moment profile of the plinth beam at 400mm from left hand column.....158

Figure 7-37 Bending moment profile of the plinth beam at 400mm from right hand column.....159

Figure 7-38 Nodes on the frame 159

Figure 7-39 Bending moment profile of right hand column 160

Figure 7-40 Bending moment profile of the left hand column.....161

Figure 7-41 Horizontal displacement (U1) in x-direction of Nodes 3001 and 3019 subjected to monotonic lateral loading, 50mm followed by fire-3D Model.....162

Figure 7-42 Horizontal displacement (U1) in x-direction of Nodes 3001 and 3019 subjected to monotonic lateral loading, 70mm followed by fire-3D Model.....162

Figure 7-43 Horizontal displacement (U1) in x-direction of Nodes 3001 and 3019 subjected to monotonic lateral loading, 95mm followed by fire-3D Model.....163

List of Tables

Table 2-1 Previous recorded fire following earthquakes [Reproduced from 23] 46

Table 2-2 Summary of reported fire spread and extent of damage [Reproduced from 23] 47

Table 3-1 General details of the Roorkee frame 56

Table 3-2 Modification of column and beam detailing (where Φ is the bar diameter) 58

Table 3-3 Total mass of each storey 61

Table 3-4 Comparison of results from analytical solution and numerical analysis. 61

Table 3-5 Loading cases in each test planned [17] 63

Table 5-1 Displacement history used in cyclic analysis 87

Table 5-2 Area under the curve of ABAQUS models and the test 97

Table 5-3 Area under the hysteretic loop of 2D ABAQUS and OpenSees 2D model 98

Table 5-4 Area under the hysteresis curve 101

Table 6-1 Summarised burning mode according to diameter by Babrauskas. 107

Table 6-2 Kerosene parameter estimation for large pool burning rate [19,76] 111

Table 6-3 Parameter of emissivity for different areas used in heat transfer analysis using ABAQUS 116

Table 6-4 Details of location for recorded temperatures 120

Table 7-1 Thermal loading details 132

Table 7-2 Temperature values applied in the top beam 136

Table 7-3 Temperature values applied in the plinth beam 137

Table 7-4 Temperature values applied in the bottom level column 137

Table 7-5 Temperature values applied in the middle level column 138

Table 7-6 Temperature values applied in the top level column.....138

1

Introduction

1.1 Background to the Project

The possibility of fires following an earthquake has attracted considerable attention from many researchers for over a decade. Scawtorn et al. [113] in his studies of the 1906 San Francisco earthquake and the 1923 Tokyo earthquake, showed that in about 80% of cases, damage was due to the fires following the earthquake rather than the earthquake itself. This phenomenon leads to substantial loss of human life and damage to urban infrastructure and facilities.

There are various factors that can cause fires after an earthquake. Prior to the fire, the active and passive fire resistance system may be damaged by the earthquake. The probability of ignition is high because of toppled furniture, electrical malfunction, movement of hot equipment, and damage to fireproofing systems in buildings such as sprinklers and vertical pipes. This may pose a serious threat to the structural integrity of buildings, and be detrimental to the life safety of the occupants and rescue workers.

In the context of structural engineering, the seismic and fire design of a building are defined as two different fields, considered to occur separately. Essentially, seismic design codes are relevant for designing a structure for an expected level of earthquake and do not consider fire safety. To obtain a well-engineered structure under both earthquake and fire loading requires further understanding in these areas. It is prudent to consider such scenarios in the design of buildings constructed in seismic zones [96]. Consequently, understanding the performance and response of structures in fires following an earthquake is important.

Prompted by evidence from previous fires following earthquakes [113], the University of Edinburgh, in collaboration with Heriot-Watt University and the Indian Institute of Technology (IIT) Roorkee, carried out a research project to investigate the structural behaviour of a single storey reinforced concrete frame.

The frame was subjected to simulated seismic damage followed by fire. The first large-scale frame test was completed in March 2011 [120]. This frame setup is known as the Roorkee frame throughout this thesis. The test results were presented and discussed at various engineering conferences [120].

Modelling of the Roorkee frame using finite element methods (FEM) ABAQUS is presented in this thesis. The aims of this research are to assess the suitability of the numerical modelling method for analysing the frame. The commercial general purpose finite element package, ABAQUS [1] was used to develop numerical models of the Roorkee frame.

For numerical modelling comparison purposes, the Roorkee frame was modelled using Open System for Earthquake Engineering Simulation (OpenSees). OpenSees is an open-source object oriented software framework

generally used to simulate the seismic response of structural and geotechnical systems, and developed at the University of California, Berkeley. The analyses have been developed by other team members in the project [130].

[130].

1.2 Thesis Aims and Objectives

This PhD research has evolved as a direct result of the modelling of the Roorkee frame test. The primary aim of this research is to compare numerical modelling to experimental results. Different types of modelling techniques, concrete models, and element types were used. The key parameters investigated were the temperature distributions in the structural elements and the deflections of the beams, columns and slabs. Further research objectives are broadly summarised as follows:

- Investigate the structural behaviour of reinforced concrete subjected to monotonic lateral loading
- Understanding the behaviour of the frame under cyclic loading (which represents the simulation of earthquake damage)
- Understanding the variation of the compartment temperature in the thermal analysis
- Developing sequential analysis loading in order to consider the damage of a reinforced concrete frame subjected to earthquake loading followed by a fire
- Investigating the response of the earthquake damaged reinforced concrete frame subjected to elevated temperatures for one hour

1.3 Outline of Thesis Chapters

Chapter 2

Literature Review

An overview of the history of this field of research is outlined. Philosophies of earthquake and fire engineering are described in this chapter. The earthquake and fire design of a building are two different aspects of structural engineering; and how these areas affect each other are outlined in this section.

Chapter 3

Preliminary Design and Test Set-Up

Preliminary calculations for the Roorkee frame are presented. A simple analysis was carried out to understand the behaviour of the frame under lateral loading. The simple model was examined both analytically and numerically, and details of this are included in this chapter.

Chapter 4

Development of the Numerical Models of the Roorkee Frame

The behaviour of the Roorkee frame when subjected to thermal and mechanical loading was numerically investigated using ABAQUS. Both two and three dimensional finite element models were developed. The material behaviour and concrete models used are presented and discussed.

Chapter 5

Simulation of the Response Due to Lateral Loading

Monotonic and cyclic lateral loadings in displacement-control mode were used to simulate earthquake damage to the frame. The capacity curve obtained from

monotonic lateral loading was compared with both analytical solutions and OpenSees numerical modelling. The hysteresis curve from cyclic lateral loading was compared with the test results and the OpenSees numerical modelling results.

Chapter 6

Simulation of the Responses Due to Fire Loading Using ABAQUS

This chapter describes the thermal analysis of the Roorkee frame when numerically modelled using ABAQUS. The model used in this study was developed using three dimensional continuum elements. The temperature distributions within the structural elements are compared with the test results.

Chapter 7

Simulation of the Response Due to Thermo-Mechanical Loading of the Roorkee Frame

This chapter describes the thermo-mechanical analysis of the Roorkee frame using ABAQUS. The behaviour of the model subjected to one hour of heating following cyclic damage simulating an earthquake is discussed.

Chapter 8

Summary, Conclusion and Recommendation for Further Work

The final chapter reviews and summarises the main conclusions from the research conducted and makes recommendations for future work.

Appendix A – Preliminary design details

The preliminary design of the Roorkee frame is presented.

Appendix B – Material models used in numerical modelling

This appendix provides the detailed material model values used throughout the thesis.

Appendix C- Parametric study on beam elements using ABAQUS

A series of benchmark analyses using beam elements with varied reaction types, when loaded under uniformly distributed loading and varying temperature increases and gradients. The analytical solutions for the benchmark problems are presented. The numerical results are compared with analytical results.

Appendix D- Temperature distribution from the Roorkee frame test

Temperature distribution values at various depths within the columns, beams and slab throughout the Roorkee test are presented.

Appendix E - Temperature distribution from the heat transfer analysis

Temperature distribution values within the frame, taken from the heat transfer analysis carried out numerically using heat flux values from the Roorkee tests.

Appendix F- Temperature distribution details used for the I-beam section

This section presents the temperature distribution details used through the I-beam section, which is present in the 3D ABAQUS beam-shell element model in Chapter 5.

Appendix G – Publications

A selection of published papers from research completed for this thesis.

.

2

Literature Review

2.1 Introduction

This chapter presents an overview of earthquake resistant and fire safety design in three parts. First, the effect of earthquakes on reinforced concrete structures is considered. Secondly, the behaviour of structures at elevated temperatures is discussed. Finally, literature which considers the consequences when both of these events occur sequentially is presented.

Buildings constructed in seismic regions are exposed to earthquakes, and the level of structural damage caused can vary depending on the magnitude of the earthquake. However, fire in buildings is a reality and occurs for many different reasons. Factors which affect the behaviour of a building subjected to earthquake and fire are described. Changes in material behaviour and the response of the structure are addressed separately.

2.2 Earthquake Effects on Building Structures

The impact of earthquakes is widespread, and damage can vary widely. Only certain parameters will be discussed here, as the aim is to give readers sufficient information to quantify the damage caused to a structure in an earthquake, in order to predict the structure's response.

Structural damage due to an increase in initial lateral load during an earthquake has been investigated [15,88,137]. It is generally acknowledged that minor structural damage is permitted during an earthquake, but that collapse is never acceptable [106].

2.2.1 Consequences of an Earthquake

There are four possible phenomena caused by earthquakes – ground shaking, ground failure and tsunami. Each of these phenomena is briefly discussed. Fire is of particular interest in this study and is discussed in depth.

Figure 2-1 shows a diagram of the effects of an earthquake on the built environment. The phenomena effects due to earthquakes are shown within the box while the physical features from which they originate are in the ellipses.

2.2.1.1 Ground Shaking

Earthquakes are the result of a sudden release of energy induced by movements within the earth's crust. In 1963 and 1967, Evison, a seismologist, defined that earthquakes as a sudden movement of the earth's lithosphere (know as crust and upper mantle), accompanied by volume changes in relatively small volumes of the crust [38,39]. This mechanism may cause ground shaking.

As the earth vibrates, the infrastructure on the surface of the ground will respond to that vibration in varying degrees. Infrastructure that has been designed and constructed to be earthquake resistant can sustain earthquakes of a certain magnitude. Hence, the ground shaking of structures is a principal area of consideration in their design.

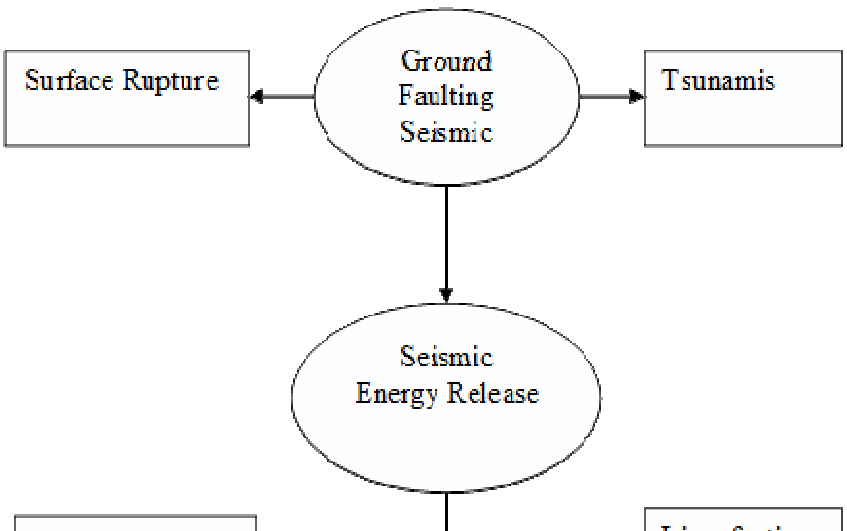

Figure 2-1 Earthquake effects on built environment [Reproduced from 20]

2.2.1.2 Ground Failure

While ground shaking is widely considered to be a principal cause of damage to structures and loss of life during earthquakes, ground failure is not believed to be a major cause of spectacular structural collapse. However it frequently causes major disruption particularly to fracture of lifelines such as gas mains. Detailed observation and investigation of the potential damage caused by ground failure induced in earthquakes has been made as far back as the two major earthquakes in 1964 in Alaska, USA and Niigata in Japan. Ground failure that occurs during the earthquake is caused by ground rupture along the fault zone, landslides, settlement and soil liquefaction. Boomer and Bird [18]

reviewed 50 of the past earthquakes and showed that ground failure contributed to damage in the built environment.

2.2.1.3 Tsunami

A tsunami is a series of sea waves due to an underwater earthquake or volcanic eruptions and other explosion beneath the sea floor. Obviously, tsunamis induce damage to the built environment in coastal areas. One of the worst that occurred was after the 1896 Meiji-Sanriku earthquake in Japan, which had a magnitude of 7.2. The waves measured between 75 and 100 ft in height, engulfing an entire village. Nearly 10,000 houses were destroyed and more than 17,000 people were reported dead [82].

2.2.2 Factors Influencing the Extent of Earthquake Damage to Buildings

The level of damage induced in buildings by earthquakes depends on many parameters, such as the frequency, amplitude (displacement, velocity and acceleration) of the ground motion, soil condition and the design of the building.

Fires which follow an earthquake occur due to failure of either the passive or active fire safety component. Structural and non-structural damage in buildings due to earthquakes may change the fire safety design in buildings. Failure of lifelines such as electricity supply, water supply, communication and transportation may cause delays to fire fighting and result in urban conflagrations. Therefore, earthquake damage increases the damaging effects of earthquake-induced fire [24]. This particular effect of an earthquake will be discussed in depth.

In general, buildings with a higher natural frequency and short natural period tend to suffer higher acceleration but smaller displacements. Buildings with lower frequency and a long natural period will experience lower acceleration but larger displacements. Resonance occurs when the frequency of ground motion is around the natural frequency of the building. This situation will cause amplification of the building response, seen in larger lateral displacements. Due to this effect, a building will suffer greater damage from ground motion at a frequency close to its own natural frequency.

The fundamental period of buildings can be numerically calculated. The typical formula in order to give the right vibration period of buildings as present in the building code and can be applied to a structure to determine the effectiveness of its earthquake resistant design [37,51,62,99,102,117,124]. Equation 2.1 is the empirical formulation of the natural period of a building according to Eurocode (EC8) [37].

$$T = C_t H \frac{3}{4} \tag{2.1}$$

Where:

T = natural period of a building;

C_t =0.75 for concrete frames;

H =is the height of the building (m).

Past earthquakes have shown that earthquake intensity is directly related to the type of soil layer supporting the building [9,21]. Structures built on solid rock or firm soil frequently perform far better than structures on soft soil. One of the reference cases is from the 1985 Mexico City Earthquake, where damage to structures on soft soil in Mexico City, 400km from the epicentre of the

earthquake, was significantly greater than at closer locations where soil was firmer [100].

The properties of the soil underlying buildings have a significant influence on the effects of an earthquake. For instance, stiff buildings constructed on strong subsoils and flexible buildings constructed on weak subsoils may both exhibit a greater response than that seen with an intermediate soil type. Ovando et al. [100], by using Terzaghi consolidation theory, have shown in their study on the soil in Mexico City that the subsoil properties have an effect on the seismic response.

Damage to structures in close proximity and those further from the epicentre of an earthquake is quite different. Wen et al. [134] showed, from the investigation of 21-storey buildings built in Hong Kong in the 1960s, that distance from the epicentre affects damage caused to the buildings.

The effect of earthquakes on structures depends on their design. The building codes permit limited deformation as long as the structures have the capability to sustain an earthquake load and prevent collapse.

The damage to buildings subjected to earthquakes is due to a combination of inadequate strength of the overall seismic resisting system, and poor distribution of strength over successive storeys leading to soft storey formation. Mahin et al. [88] and Johnston et al. [65] show failure due to discontinuity of the vertical elements of the lateral load resisting systems. This is due to excessive deformation resulting in formation of a soft storey, for example in the Olive View Hospital during the 1972 San Fernando earthquake. The inertia loads that develop due to acceleration of individual elements must be transferred from the individual reactive elements to the floor, to the vertical elements, to the

foundation and eventually to the ground. The lack of provision of an adequate load path through the individual elements in the system can result in partial or complete failure of the structure.

The building's configuration including its size and shape plays a role during earthquakes. The building configuration determines the way seismic forces are distributed within the structure. A regular building is shaped like a box, rectangular both in plan and elevation, and is inherently stronger than one that is irregular such as an L-shaped or U-shaped one. Irregularly shaped buildings will twist as they shake and increase the damage caused. Previous research shows that irregular buildings are more likely to fail during earthquakes [75,87].

2.2.3 Non-Structural Damage

Components or systems that are attached to the floors or walls of a building, and which are not part of the intended load-bearing structural system, are classified as non-structural elements. The non-structural elements include chimneys, ceilings, partition walls, doors, external glazing etc.

Moderate earthquakes with an intensity of MMS VII and above cause damage to non-structural elements due to the load applied as the building deflects [27]. Non-structural damage may allow the development of a larger fire due to the loss of exterior glazing, which may change the ventilation factors for a fire compartment. Fire separation suffers significant cracking due to earthquake motion and loses its fire integrity. For example in 1998, Rojahn [109] organised a seminar to consider the important issues in an earthquake and identified the principal issues induced by non-structural elements. The seminar encouraged more people to initiate further research and provided detailed reporting procedures for reconnaissance teams.

2.2.4 Active System Damage

Active fire safety systems in buildings, such as sprinkler systems, smoke detectors, fire alarms, and including mechanical systems, such as smoke control and pressurisation, will be vulnerable to failure in an earthquake. For instance, sprinkler systems are subjected to damage due to inertia load on the suspended pipe work and impact from suspended ceilings [48]. Fleeming [45] and Beattie [12,13] showed in their studies that the current seismic design codes are still inadequate to design buildings in earthquake zones. Dust dislodged resulting from structural or non-structural damage in buildings can prevent the smoke detectors from activating. There is little data on fire alarms efficiency after earthquakes [23].

2.2.5 Lifeline Systems Damage

Lifeline systems, including electric power, water supply, gas and liquid fuel, telecommunication and transportation, are vulnerable to damage by ground movement. Todd et al. [127] showed in their study that the 1994 Northridge earthquake damaged the water supply.

These factors influence the ability of the rescue, fire fighting and medical personnel to gain access and operate effectively in areas with major damage.

The longer the time it takes a fire fighter to arrive at the damaged area, the more difficult it is to control the fire in a building. This may lead to more severe damage of the building subjected to post earthquake fire.

2.2.6 Buildings Response

2.2.6.1 Drift

Ground acceleration induces deformation to buildings, which can be quantified by the roof drift (also known as lateral drift), Δ_{roof} or storey drift, Δ_i.

Figure 2-2 shows the configuration of drift on a building. Past earthquakes have shown damage to buildings due to both roof and storey drift. Excessive drift to both could cause damage to structural or non-structural elements and adjacent structures. Most building codes provide detailed provision for calculating acceptable seismic drift for buildings in seismic regions. For example, the storey drift ratio limitation from UBC [62] is between 2% to 2.5%.

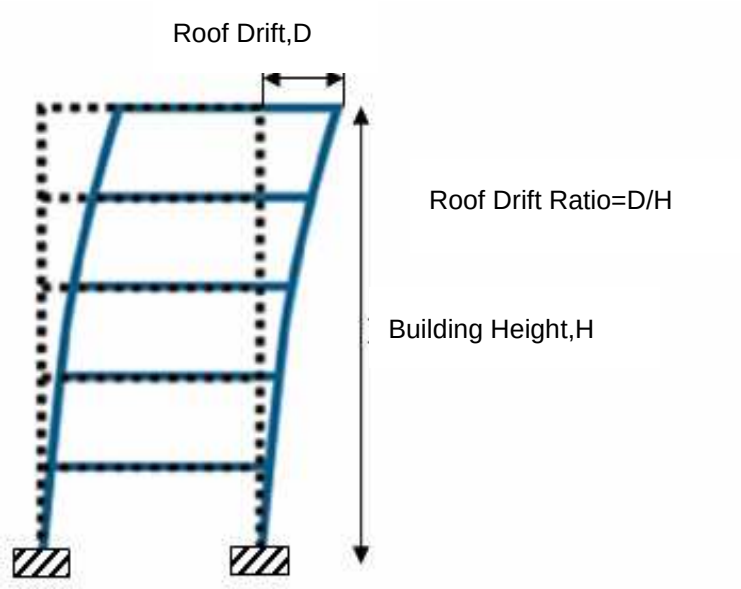

Figure 2-2 Roof drift and storey drift

2.2.6.2 P-Delta Effects

Gravity loading needs to be taken into account due to the incremental lever arms which result from lateral deflection of the building. This creates a second order moment which contributes to the overturning and torsional moments, and is commonly known as the P-Delta effect. This effect is associated with the magnitude of the applied axial load (P) and a displacement (Delta). The P-Delta

effect and the influence it has on structural response has been the subject of significant research in recent decades.

Current international design codes, such as EC8 [37], impose limits on the P-Delta ratio. The P-Delta ratio affects the value of the maximum inelastic response displacement. This refers to the ratio of the secondary moment to the primary moment. According to EC8 [37], P-Delta effects are not to be taken into account if the ratio is ≤0.01 in all storeys.

In low-rise buildings the P-Delta effect is not significant, since the total lateral displacements are kept relatively small by the storey drift limit. However, in high-rise buildings, where the lateral displacement may be much larger, satisfying the maximum drift requirement does not ensure that the P-Delta effects will be negligible [122].

2.2.7 Strength and Ductility of Materials

2.2.7.1 Concrete

The behaviour of concrete is largely dependent upon its load history. In cyclic loading, the change in stiffness in the stress-strain relationship, unloading strains on the envelope curve, unloading plastic residual strains, and reloading strains at the end of reloading curves are the major parameters that control the general behaviour of concrete under cyclic loading.

Another factor that affects the behaviour of concrete is its confinement. Concrete which is confined by a suitable arrangement of transverse reinforcement results in a significant increase in both the strength and the ductility of the compressed concrete [90].

Figure 2-3 shows the stress-strain relationship of confined and unconfined concrete for monotonic loading. Martinez-Rueda and Elnashai [93] have produced a new concrete model based on the limitations of the stress-strain

relationship of confined concrete in cyclic loading in Mander et al. [90]. Bahn and Thomas [8] investigated the behaviour of concrete under various types of loading and proposed a numerical expression and diagram to be used for cyclic loading. Figure 2-4 shows the degradation of compressive strengths due to cyclic loading.

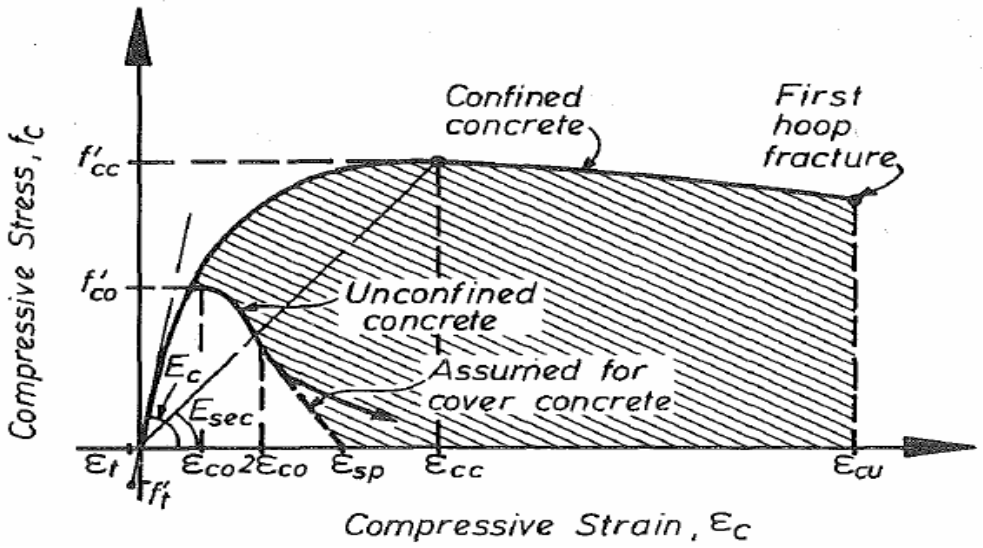

Figure 2-3 Stress-Strain relationship of confined and unconfined concrete subjected to monotonic loading [Reproduced from 93]

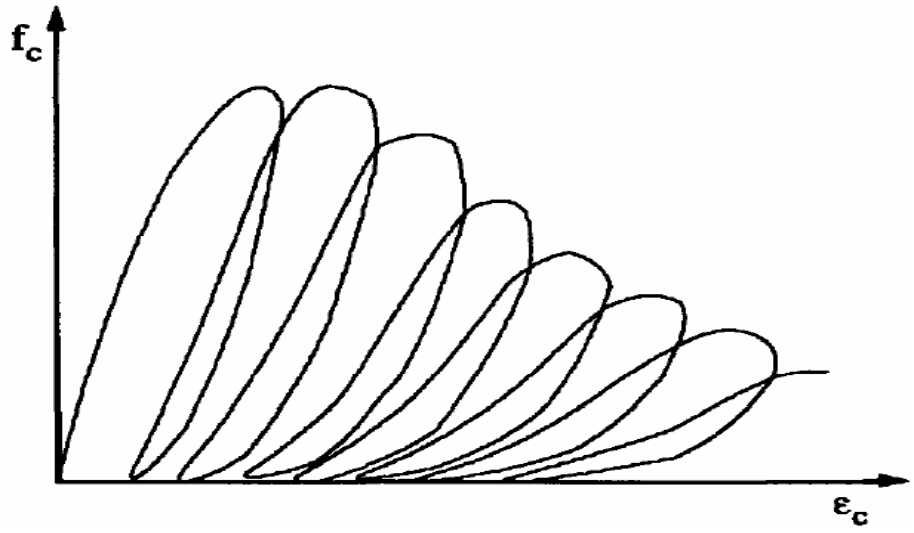

Figure 2-4 Typical stress-strain relationship for concrete under cyclic compressive loading [Reproduced from 90]

The concrete model for cyclic loading is characterised by the way the degradation of strength and stiffness are modelled. It can be achieved by using the capacity curve to specify the unloading, reloading branches, inelastic strain and strength degradation.

2.2.7.2 Reinforcing Steel

Cyclic loading may cause repeated compression and tension in concrete elements. When concrete cover spalls or cracks due to cyclic loading, the reinforcing steel left will determine the durability of the element. Therefore, the behaviour of the reinforcing steel may control the response of reinforced concrete structural elements subjected to cyclic loading.

Figure 2-5 shows the stress-strain relationship of reinforcing steel commonly used in concrete construction under monotonic loading. The initial linear elastic stress-strain relationship up to yield stress, f_y is followed by a yield plateau or subsequent region of strain hardening. After maximum stress is reached, typically at $f_{su} = 1.5 f_y$, strain softening occurs. However, in cyclic loading, the yield plateau is suppressed and the stress-strain curve behaves differently.

The stress-strain relationship of reinforcing steel bars under cyclic loading must estimate the following characteristics: elastic, yielding and hardening branches in the first excursion; Bauschinger effects and reduction of the yield stress after load reversal, which increases with the enlargement of the plastic strain component of the last excursion; and isotropic strain hardening, which consists of an increase in the capacity curve, proportional to the plastic strain component of the last excursion, as shown in Figure 2-6.

Figure 2-7 shows the behaviour of reinforcing steel in compression and tension under cyclic loading.

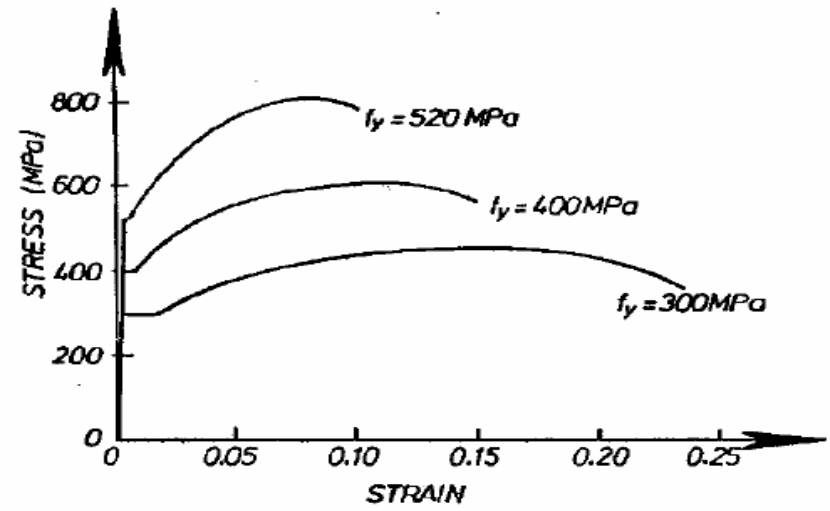

Figure 2-5 Typical stress-strain relationship for reinforcing steel [Reproduced from 30]

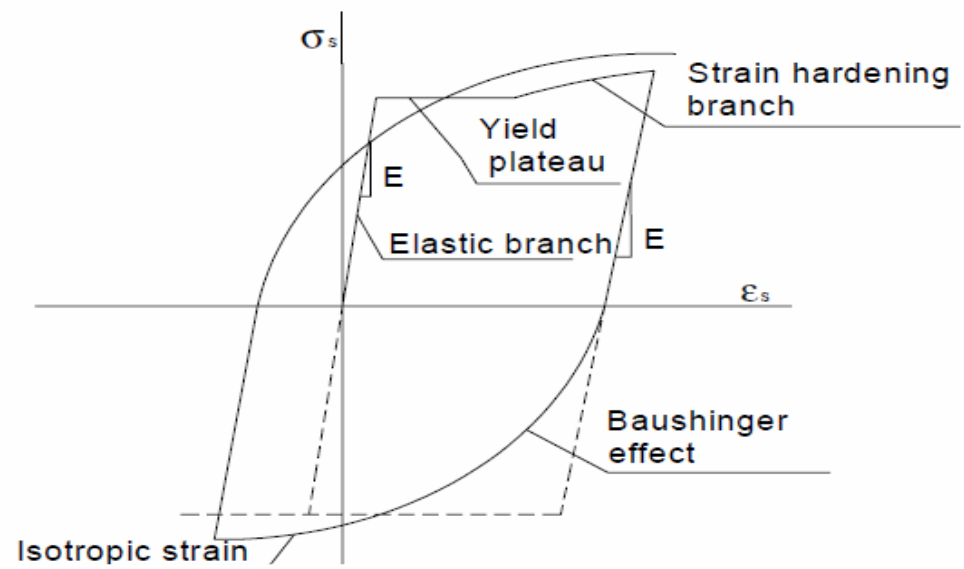

Figure 2-6 Stress-strain schematic diagram with important characteristics of reinforcing steel bar subjected to cyclic loading [Reproduced from 30]

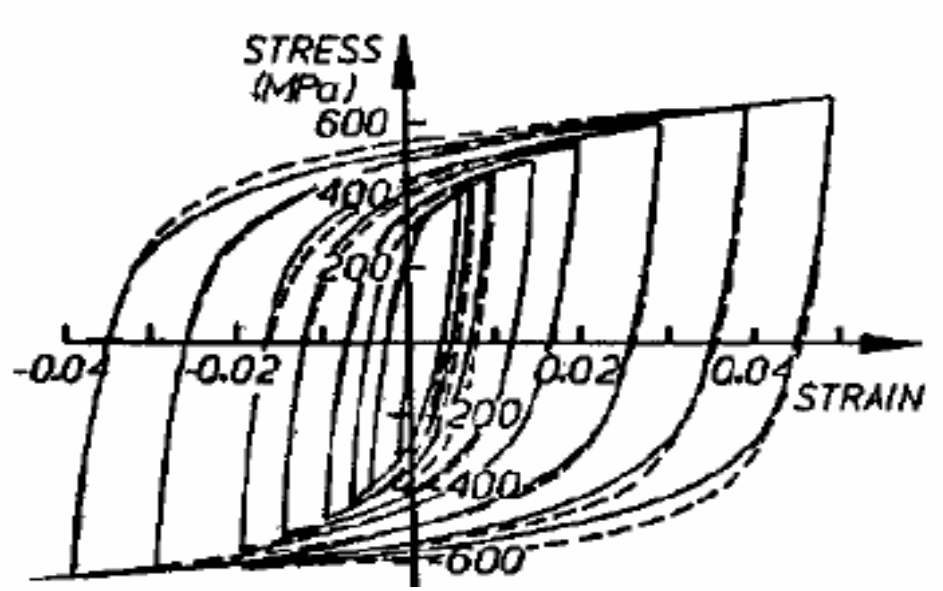

Figure 2-7 Cyclic straining of reinforcing steel for fy=380 MPa [Reproduced from 30]

2.2.8 Seismic Analysis

The seismic analysis approach is to calculate the response of a building when subjected to earthquake motion. It can be analysed using five approaches as listed below.

1. Equivalent Static Analysis
2. Response Spectrum Analysis
3. Linear Dynamic Analysis
4. Nonlinear Static Analysis
5. Nonlinear Dynamic Analysis

The equivalent static analysis approach defines a series of forces acting on a building to represent the effect of earthquake ground motion. It assumes that the building responds in its fundamental mode. This approach is appropriate for a low-rise building which twists less when the ground moves. The response of a

building when subjected to earthquake ground motion is defined as a combination of many mode shapes. At each mode, the response of the building is read from the design spectrum, based on the model frequency and the modal mass. This combination provides the magnitude of forces in all directions (for example in the x,y and z-axes) and then shows the effects on the building.

The dynamic approach is required for tall buildings, buildings with torsional irregularities and other more complex building characteristics [31]. Seismic input is modelled using either a model spectral analysis or a time history analysis. This seismic approach is considered as a time domain analysis.

Nowadays a number of computational tools have been developed for dynamic analysis, however there are still some gaps concerning its complexity and suitability for research and practical design applications. This is possibly because of the limited training given to civil engineers in structural dynamics, and the difficulties encountered by design offices in utilising advanced software for dynamic analysis.

Nonlinear static approach is applicable when the building is expected to remain nearly elastic at the particulate level of ground motion. The nonlinear static pushover analysis tries to address the difficulties faced by structural engineers in seismic design. Mwafy and Elnashai [97] made a comparison between static pushover and dynamic analysis of 12-storey reinforced concrete buildings with different characteristics, subjected to natural and artificial earthquake records. The have found that the static pushover analysis for seismic design is more appropriate for low rise and short period frame structures. However well-designed buildings but with structural irregularities, the results show good correlation with the dynamic analysis approach.

2.2.8.1 Nonlinear Static Pushover Analysis

This analysis is a simple technique for estimating the strength capacity of the structure in the post-elastic range. This type of analysis is used in this study to determine the capacity of the frame.

In the past twenty years, a number of researchers have presented the procedure of the static pushover [25,40,112]. This analysis technique is recommended as a tool for design and assessment purposes by FEMA 273 in the National Earthquake Hazard Reduction Program 'NEHRP' [41].

Furthermore, this method was accepted by the Structural Engineers Association of California, SEAOC (Version 5) [116].

2.2.8.2 Pushover analysis formulation

Pushover analysis is the nonlinear incremental-iterative solution for equilibrium, as shown in Equation 2.2.

$$KU = P \tag{2.2}$$

Where:

K is the nonlinear stiffness;

U is the displacement vector;

P is the load vector applied laterally over the height of the structure.

For multi-storey building lateral load a force control mode that has a necessarily constant ratio throughout the analysis is applied. Reaction vector, P^e, as in

Equations 2.3 and 2.4, is obtained at the end of each iteration, and is calculated from the assemblage of all finite element contributions.

$$\Delta U = [K_T]^{-1}.(\lambda.P_0 - P^e) \tag{2.3}$$

Where:

ΔU is the calculated displacement increment within an iteration;

K_T is the current nonlinear stiffness matrix;

λ is the load factor within the corresponding loading increment;

P_0 is the initial load;

P^e is the equilibrated load (reaction) of the previous iteration.

$$P^e = \sum \int_V B^T.\sigma_{NL}.dV \tag{2.4}$$

Where:

B is the strain-displacement matrix of each element;

σ_{NL} is the element nonlinear stress vector as determined by its material constitutive law.

The out-of-balance forces are iteratively re-applied until convergence to a specified tolerance is reached [10]. This procedure continues until a predefined limit state is reached or until structural collapse is detected. The target limit state for a new structure corresponds to the deformation caused by the specified design earthquake taken from the building code; and for an existing building is the drift which corresponds to structural collapse for assessment purposes. The procedure for pushover analysis enables prediction of the deformation at member and structure level, and progress on the overall capacity curve of the structure, as shown in Figure 2-8. However, the accuracy of pushover analyses depends on several factors, such as the distribution pattern

of lateral load along the height (triangular, uniform, etc.), the magnitude of the lateral load, the number of load steps, the convergence criteria and the iterative strategy.

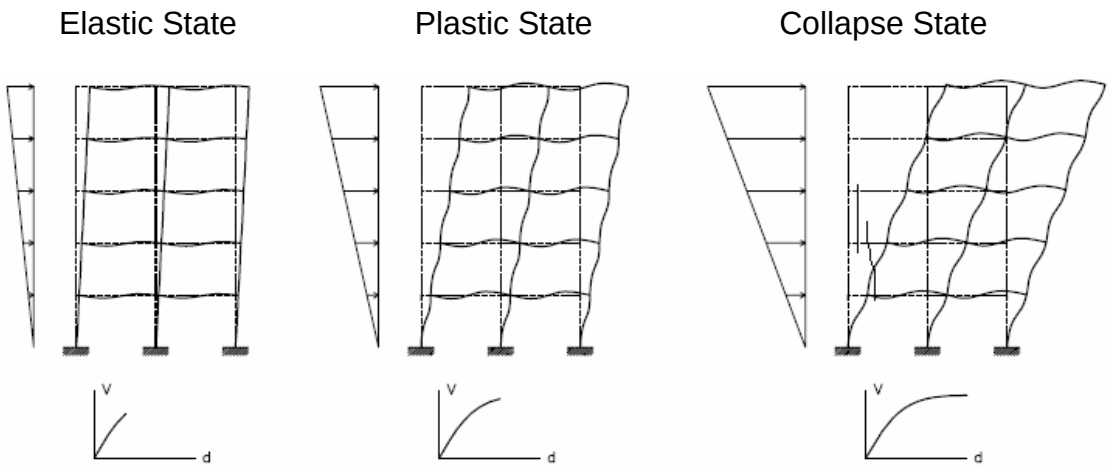

Figure 2-8 Deformation and equivalent capacity curve of the structure sequence in pushover analysis procedure [Reproduced from 30]

2.3 Behaviour of Reinforced Concrete Structures in Fire

In this section the factors of structure's response due fire are discussed.

2.3.1 Fire and its Consequences

Conventionally, for a given situation, design fire scenarios are calculated either through hand calculations, parametric fires (time-temperature curves) as specified in the codes and standards, or through real fire data taken from tests.

2.3.1.1 Hand Calculation

Although the design fire information obtained by hand calculation is a simple and rough approximation, it is sufficiently accurate for a simple design. The temperatures are assumed to be constant throughout the burning period, as

shown in Figure **2-9.** The maximum temperature and the duration of the burning period of the curve are defined either by assumption or using the equation by Kawagoe [67].

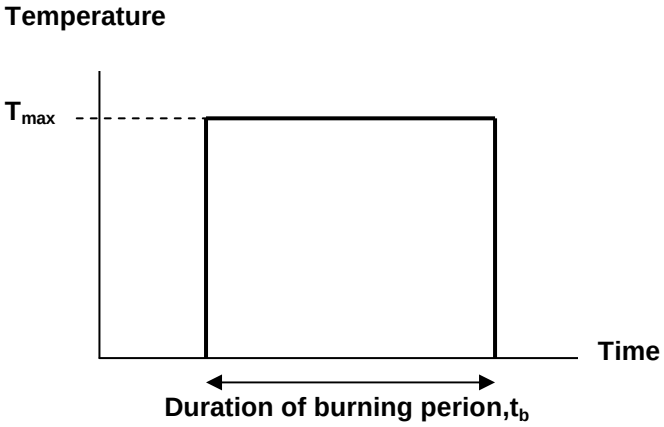

Figure 2-9 Design fire with constant temperature

2.3.1.2 Parametric Fire

Most research done to evaluate the fire performance of building materials and structural elements around the world relies on full-size fire-resistance tests. The design fire used in the fire resistance test is known as the `parametric fire' or `standard fire'. The parametric fire is obtained from the design codes or standards of the country. There are several examples of parametric fires like British Standard BS 476 Part 20-23 [28], Eurocode 1 [34], Australian Standard AS 1530 Part 4 [111], ASTM E119 [4] and ISO 834 [62]. The most widely used in fire testing is ASTM E119 and ISO 834.

Figure 2-10 shows the comparison of parametric time-temperature curves from ASTM E119, ISO 894 and Eurocode 1. At the beginning of the burning time, the temperature curce from ASTM E119 and ISO 894 look similar to each other. After 30 minutes, the temperature calculated from ASTM E119 is slightly higher than that usimg ISO 894. There are several equations to define the temperature

in ASTM E119. One of the simplest ways is derived by Lin [83].as in Equation 2.5.

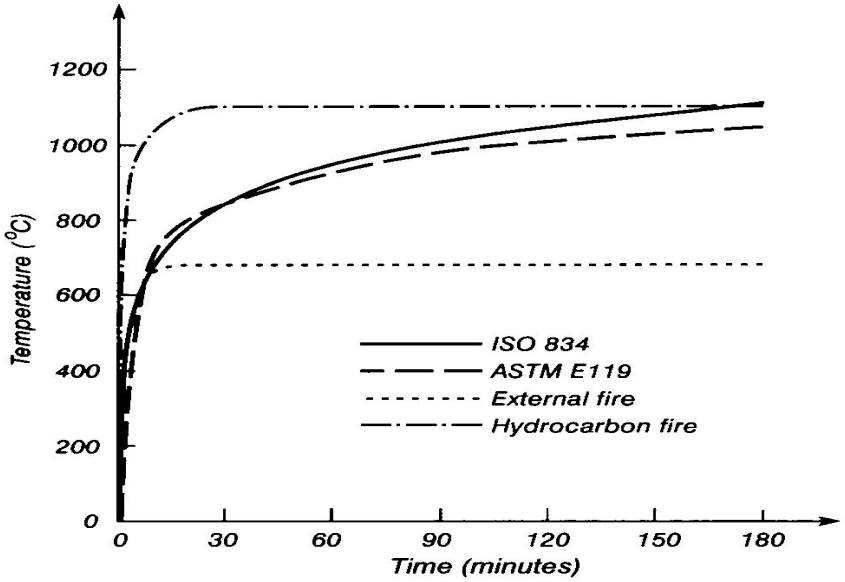

Figure 2-10 Parametric time-temperature curve [Reproduced from 32]

$$T(^0C) = 750\left[1 - e^{-3.79553\sqrt{t_h}}\right] + 170.41\sqrt{t_h} + T_0 \quad (2.5)$$

Where:

t_h=time (hours);

T_0=ambient temperature (^{0}C).

The temperature curve derived from ISO 834, is shown in Equation 2.6, where t is the time in minutes.

$$T(^oC) = 345\log_{10}(8t + 1) + T_0 \quad (2.6)$$

Another two parametric fires are shown in Figure 2-11, they are calculated from Eurocode 1 [34]. The hydrocarbon time-temperature curve is used when the structural member is assumed to be engulfed in flames from a large pool fire. The hydrocarbon time-temperature curve is obtained from Equation 2.7.

$$T = 1080(1 - 0.325e^{-0.167t} - 0.675e^{-2.5t}) + T_0 \quad (2.7)$$

For structural members designed to be located outside a burning compartment, the external time-temperature curve is used and can be derived from Equation 2.8.

$$T = 660(1 - 0.687e^{-0.32t} - 0.313e^{-3.8t}) + T_0 \quad (2.8)$$

2.3.1.3 Time-Temperature Curve for Real Fire

The time-temperature curve can be based on data from real fires. This data varies with parameters such as the size of ventilation, fuel load, and surface lining characteristics of the compartment material. In 1970, Magnusson and Thelandersson [86], studied these effects that influence the time-temperature curves. They derived the curves from the heat balance calculation, using Kawagoe's equation to calculate the burning rate of ventilation controlled fires.

Their research has been referenced by other researchers around the world for real fire exposure. These curves are often known as the 'Swedish' fire curves, as shown in Figure 2-12. Each of the graphs in the figure shows a different ventilation factor with increasing fuel load marked. The hand calculated design fire shows a constant temperature throughout the duration of the burning time, while in these real time-temperature curves a decreasing temperature is seen after flashover occurs.

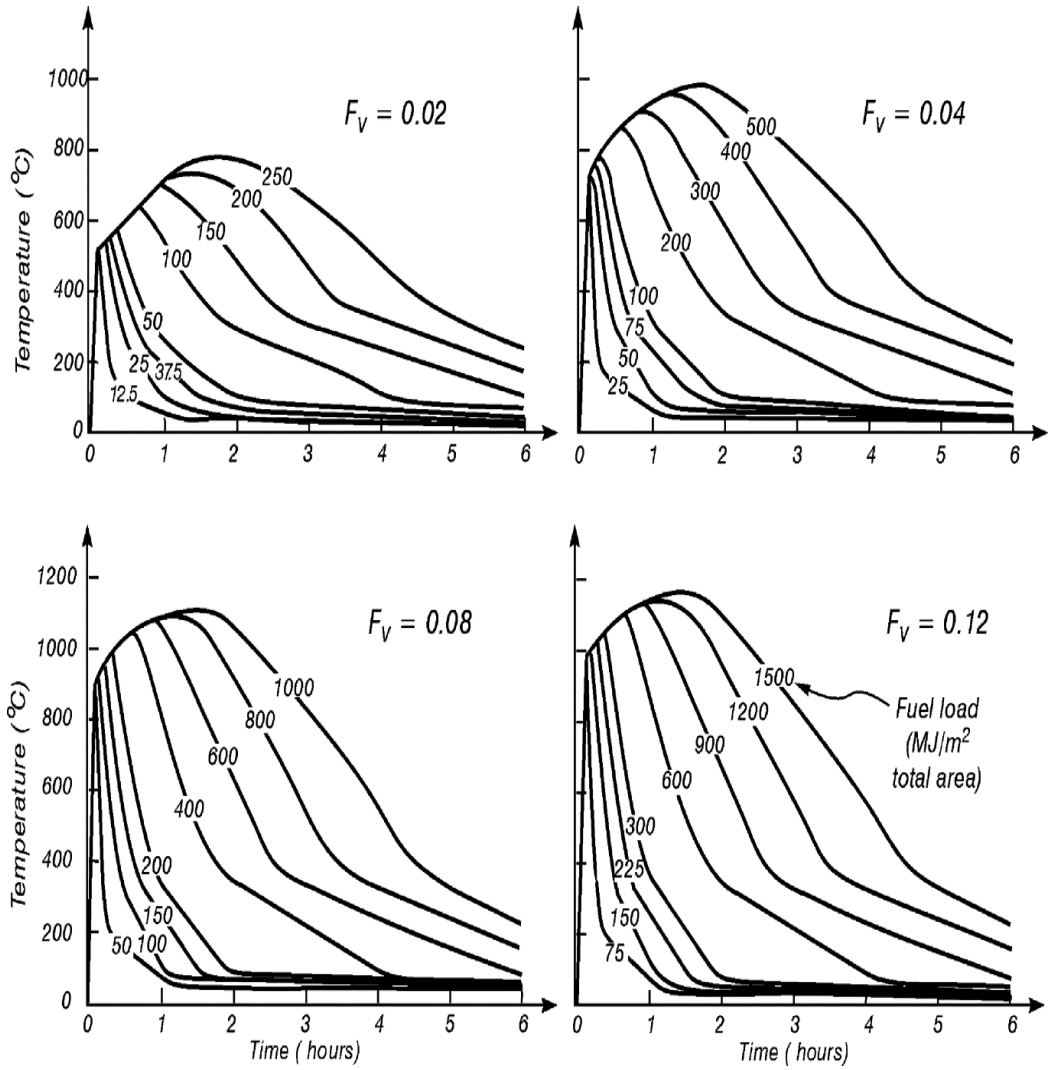

Figure 2-11 Swedish fire curve for different ventilation factors and fuel loads [Reproduced from 32]

2.3.1.4 Rate of Burning

The duration of the burning period for a single room can be estimated by using Equation 2.9 derived by Kawagoe [67]. Kawagoe conducted many experiments and has shown in his reports that the rate of burning depends on the rate of burning of wood fuel, the ventilation area, the ventilation controlled heat release

rate and the energy content of fuel available for combustion. The equation is only appropriate for fuel from wood cribs [32].

$$t_b(\text{sec}) = \frac{E}{Q_{vent}} \tag{2.9}$$

$$m = 0.092 A_v \sqrt{H_v} \tag{2.10}$$

$$Q_{vent} = \dot{m} \Delta H_c \tag{2.11}$$

Where:

m = the rate of burning of wood fuel (kg/s);

H_v = the height of the window opening (m);

A_v = area of the window opening (m^2);

E = energy contents of fuel available for combustion (MJ);

Q_{vent} = ventilation controlled heat release rate;

ΔH_c = heat of combustion of the fuel (MJ/kg).

2.3.1.5 Maximum Temperature

Defining the maximum temperature is an essential part of the design fire. Law [80] developed an empirical equation for this value as shown in Figure 2-12. The figure used was reported by Thomas and Heselden [125] based on the recorded maximum temperature during the steady burning period for a large number of wood cribs in small-compartments.

The equation was then recapitulated by Walton and Thomas [132], as shown in Equation 2.12.

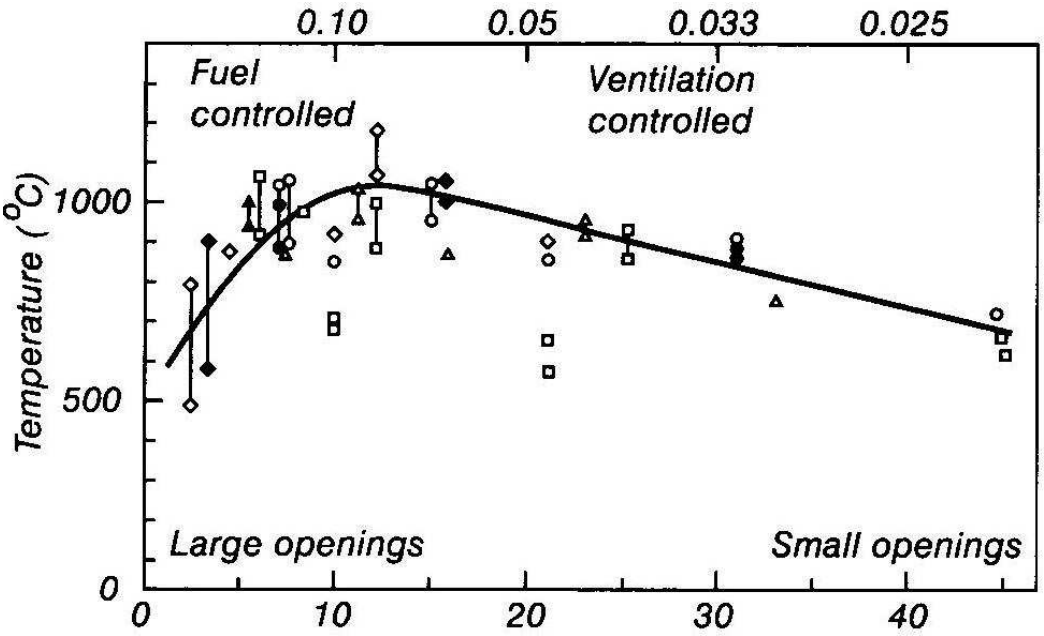

Figure 2-12 Maximum temperature recorded in small-scale compartment during the steady burning period [Reproduced from 125]

When the fuel load in the compartment is high, Equation 2.12 is applied. However, for low fuel loads, Equation 2.13 is used.

$$T_{\max}(^0C) = \frac{6000(1-e^{-0.1\Omega})}{\sqrt{\Omega}}\,\mathrm{T} \tag{2.12}$$

$$\Omega(MW) = \frac{A_t - A_v}{A_v\sqrt{H_v}} \tag{2.13}$$

$$T = T_{\max}(1-e^{-0.05\psi}) \tag{2.14}$$

$$\Psi = \frac{L}{\sqrt{A_v(A_t - A_v)}} \tag{2.15}$$

Where:

A_t = total internal area of the bounding surfaces including opening (m^2);

A_v = area of the window opening (m^2);

L = fire load (kg).

2.3.1.6 Rate of Temperature Decrease

The decreasing temperature in the time-temperature curves post-flashover is affected by the shape and material of the fuel load, the size of the ventilation openings and the thermal properties of the lining materials.

2.3.1.7 Fuel Load

There are two types of fuel load, liquid or solid materials. The consuming time of liquid or molten material is short leading to a short burning period. Solid material burns more slowly and consistently, for instance, wood will generally burn at a predictable rate.

2.3.1.8 Ventilation Opening Size

Another factor that influences the rate of temperature decrease is the size of ventilation opening. If the ventilation opening is large, it will allow rapid heat loss from the compartment by convection and radiation, while small ventilation openings trap the heat for a longer period.

2.3.2 Material

The behaviour of heated structures is affected by the change in the mechanical and thermal properties of the construction materials. Changes in the properties of concrete and steel at ambient and elevated temperatures have been discussed by a number of researchers [70, 71,114] and described in books [11, 29,105]. The aim of this section is to provide the reader with a brief summary of the main characteristics and trends that govern a material's behaviour at both ambient and elevated temperatures. This study's primary focus is concrete, which will be discussed in detail; steel will be considered more briefly.

2.3.2.1 Concrete

Concrete is commonly considered to have good fire resistance. However, when it is exposed to heat, chemical and physical reactions occur at elevated temperatures, such as loss of moisture, dehydration of cement paste and decomposition of aggregate. These changes result in a breakdown of the structure of the concrete, affecting its mechanical properties. Although it is possible to describe the qualitative processes that concrete undergoes as it is heated, to predict exactly the quantitative behaviour for anything other than a precisely known mix of materials is very challenging.

2.3.2.1.1 Physical Behaviour of Concrete at Elevated Temperature

Concrete is a composite material that consists essentially of a binding medium within which are embedded particles of aggregate, water, and cement paste. Its mechanical properties, such as strength, modulus of elasticity and volume deformation, decrease remarkably on increasing temperature, which results in deterioration of the structural quality of the concrete [114]. A number of researchers have focused on the chemical and physical changes within concrete, such as the decomposition of calcium hydroxide ($Ca(OH)_2$), the

incompatibility of the aggregate-cement paste boundary and the crystal transformation of quartz (SiO_2) [77].

In the last decade, there has been extensive research on the fire performance of concrete and most studies have concentrated on aspects such as types of aggregate, addition of fibres, heating rate, maximum temperature level, methods of testing and many more [103].

Different mix proportions in concrete production have a huge influence on how the behaviour of concrete changes when it is exposed to fire. Due to varying compositions of different concretes, the strength loss at 120^{o}C can range from 30% to 100% [71]. The cement type and different water-cement ratio have been shown to have little effect on the compressive strength. It has been found that one of the main factors affecting concrete compressive strength with temperature is the type of aggregate [11].

The well-known types of aggregate used in concrete are calcareous and siliceous. Although the behaviour of these two types of concrete is different, the processes that they undergo on heating are similar in nature.

2.3.2.1.2 Properties of Concrete at Elevated Temperatures

Concrete exposed to fire undergoes severe micro-structural changes. These changes alter the mechanical properties of Portland cement concrete. The physical and chemical changes in concrete under fire exposure depend on the matrix composition as well as the type of aggregate (mineralogical characteristics, dilation, etc.).Other factors that have an effect are the water-cement ratio, the porosity, humidity and age of the concrete.

When the cement paste is exposed to increasing temperatures the following effects occur. At 100^{o}C, the expulsion of water due to evaporation begins. Then, with increasing temperature up to 180^{o}C, dehydration of the hydrate calcium silicate occurs. At 500^{o}C, the composition of calcium hydroxide alters and at around 700^{o}C calcium silicate begins to hydrate. The changes in concrete induced by increasing temperature are more evident when the temperature surpasses 500^{o}C. At this temperature level, most changes experienced by concrete can be considered as being irreversible. Visual observations, such as colour change, cracking and spalling, are the first step in investigating the effect of fire exposure on reinforced concrete structures.

Concrete is not only affected by the temperature level; the degree of concrete damage also depends on the exposure time and the type of cooling experienced. Previous studies have shown that most alterations are produced in the first two hours of exposure to high temperatures. They also affirm that, in general, the strength of concrete shown in tests performed at high temperatures is higher than that obtained for the same specimens once they have cooled. The strength reduces more when the specimens are rapidly cooled. This phenomenon can be attributed to the micro- cracking produced in the material by tension strain.

Among the most significant changes to concrete exposed to high temperatures are dehydration of cement paste, increased porosity, modification of moisture content, thermal expansion, retraction, alteration of pore steam pressure, strength loss, thermal cracking due to thermal incompatibility, thermal bowing, thermal creep and thermal spalling due to the excessive pore steam pressure. The spalling effect is often seen in concrete element at the structural level. This phenomenon is often seen when high strength concrete is exposed to fire [2]. It is not clear if damage makes it more or less likely. “Spalling” is thought to occur due to the high pressure of steam being generated by the free water in the

pores of the concrete, and by restrained thermal expansion [123]. In damaged structures, the steam may be released by the damage and there may be a reduction in restraint, therefore, “spalling” may be reduced.

2.3.2.1.3 Thermal Properties of Heated Concrete

The thermal properties of concrete exposed to high temperature will also change, such as the reduction of specific heat capacity and conductivity, and a minor reduction in the material’s density. The changes in thermal properties are due to the evaporation of water. Susan et al. and Wickstrom et al. have shown that when the temperature rises between 100°C to 120°C, the specific heat capacity of the concrete will suddenly increase and then return to the original value [78,135]. The value of the specific heat capacity depends on the moisture content of the concrete being modelled. The reduction in conductivity on heating is caused by cracking and degradation.

Figure 2-13 shows the variation in thermal specific heat capacity and conductivity of concrete with different aggregates as a function of temperature.

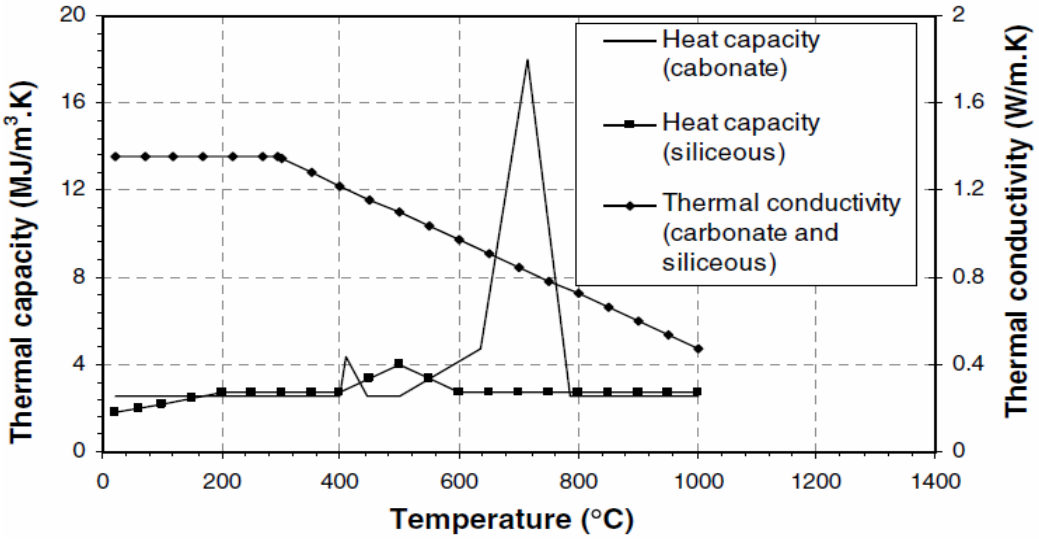

Figure 2-13 Variation of thermal properties of concrete with different aggregates at elevated temperature [Reproduced from 81]

2.3.2.1.4 Mechanical Properties of Heated Concrete

There is a degradation of stiffness, strength and thermal expansion of the material at elevated temperature.

When the concrete is exposed to elevated temperatures, there is a little loss in strength as the chemicals in the concrete change as described above. Above 500^{o}C, the reduction in compressive strength is rapid [54]. However, Khoury [69] has shown that the choice of certain aggregates can increase the temperature at which significant reduction occurs to 600^{o}C. In contrast to steel, concrete does not return to its original strength when it returns to ambient temperature; the degree of recovery is uncertain, ranging from a further reduction to some recovery [55,114,138].

Scheinder has shown that the degradation of stiffness is a linear pattern between 200^{o}C and 700^{o}C [115].

Figure 2-14 shows the relationship of stress-strain for normal strength concrete at various temperatures. From the figure, it can be seen that the properties of concrete vary significantly with temperature, with a large decrease in strength (stress) once the temperature exceeds 500^{o}C [83]. Changes in thermal expansion primarily depend on the type of aggregate used – siliceous aggregates tend to expand the most on heating, followed by calcareous, while light-weight aggregates show almost no expansion [73].

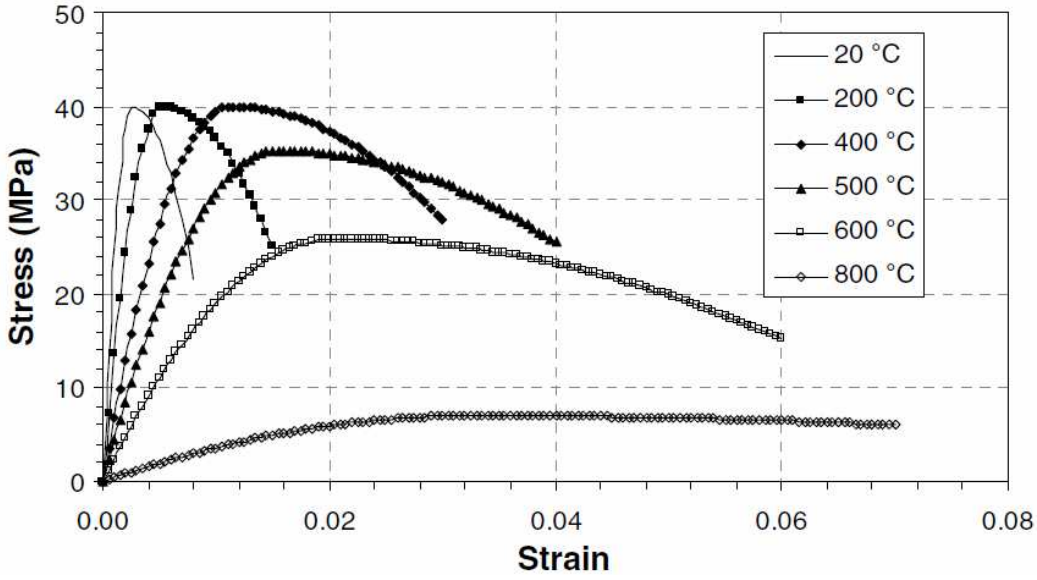

Figure 2-14 Variation of stress-strain in temperature [Reproduced from 83]

2.3.2.2 Reinforcing Steel at Elevated Temperature

The behaviour of steel is much more sensitive to high temperature and less complex than concrete. It is generally acknowledged that when steel is exposed to high temperature it will suffer a loss of strength and stiffness. At above 700^{o}C, the load bearing capacity of the steel will be reduced to about 20% of its design value. The behaviour of steel and concrete as used in this study is referenced in the well known books by Bazant [11], Buchanan [29] and Purkiss [105].

2.3.3 Structural Response to Fire

High temperatures lead to changes in the mechanical properties of structural materials, as discussed in the previous section. The response of structural elements at elevated temperatures is different depending on the type of restraint [131]. In principle, the behaviour of structures subjected to high temperature is a combination of the thermal strain and mechanical strain, as

shown in Equation 2.16. The physical response of structural elements subjected to high temperature, otherwise known as total strain, is described as its deformation shape. Mechanical strain, $\varepsilon_{mechanical}$ depends on the stress state in the structure.

$$\varepsilon_{total} = \varepsilon_{thermal} + \varepsilon_{mechanical} = \delta, \text{ where } \varepsilon_{mechanical} \to \sigma \quad (2.16)$$

When the thermal strain, ε_{strain}, is allowed to develop in an unrestricted manner, the heated structure behaves in a different manner due to the thermal strain (see Equation 2.17). In this situation, there is no external load, axial expansion or thermal bowing. Thermal stress and plastification occur when the thermal strain is fully restrained without external loads being present, as shown in Equation 2.18.

$$\varepsilon_{total} = \varepsilon_{thermal} \text{ and } \varepsilon_{total} \to \delta \quad (2.17)$$

$$0 = \varepsilon_{thermal} + \varepsilon_{mechanical}, \text{ where } \varepsilon_{mechanical} \to \sigma \quad (2.18)$$

2.3.3.1 Temperature Distribution

The temperature distribution through the depth of the beam can be described by several methods: 1. Temperature values at specific points though the depth of the beam;2. Uniform mean temperature, ΔT; and 3. A gradient, $T,_y$. Figure 2-15 illustrates the temperature regime in a beam heated from underneath $(T_2 > T_1)$. In the study, the temperature values at specific points throughout the section are used to define the temperature.

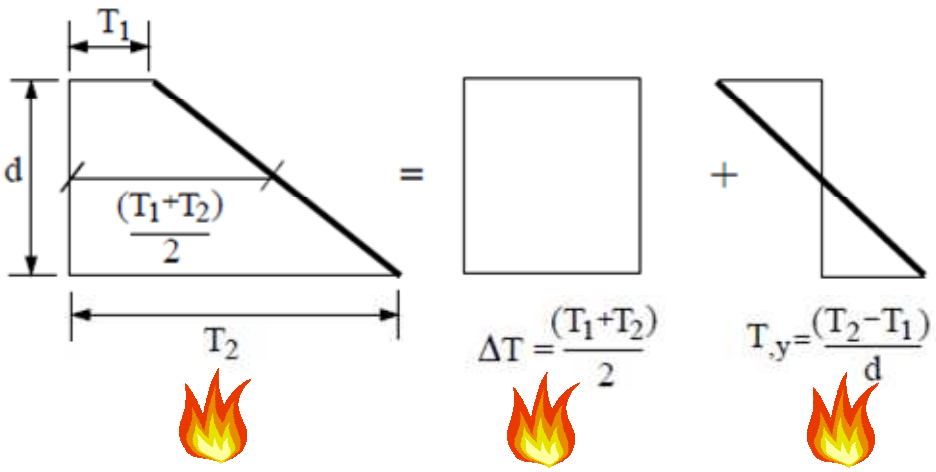

Figure 2-15 Uniform mean temperature and through depth thermal gradient over the cross-section of a beam [Reproduced from 76]

Uniform mean temperature increases to a structural element induce strain due to thermal expansion, as shown in Equation 2.19. The expansion coefficient depends on the material properties.

$$\varepsilon_T = \alpha \Delta T \tag{2.19}$$

Where:

α is an expansion coefficient;

ΔT is a uniform mean temperature rise.

When a structural element is heated on one surface, the temperature difference induces a uniform curvature, ϕ along the length due to the thermal gradient $T,_y$. Thermal curvature strain, ε_ϕ is calculated as a result of the shortening of the structural length due to curvature along the length of the beam; the shortening

is interpreted as the contraction strain. The thermal curvature strain is shown in Equation 2.20.

$$\varepsilon_{\phi} = 1 - \frac{\sin(l\phi/2)}{l\phi/2} \tag{2.20}$$

Where:

ϕ is a uniform curvature along the length, $\phi = \alpha T_{,y}$;

l is a length of the element.

2.3.3.2 Restrained Type

Structural behaviour of structural elements subjected to high temperature is affected by the type of end restraint. Insufficient end translational restraint to thermal expansion leads to expansion displacement. The effect of curvature strain induced by thermal gradients in structural elements, whose ends are rotationally restrained, produces a large hogging bending moment throughout the length of the member without deflection. In the case of curvature, strain effects in structural elements where ends are only translationally restrained are to produce tension. Usmani AU *et al*. [131] described in detail the end restraints which affect the structural response at high temperatures.

2.3.3.3 Cracking

Cracking is driven by similar factors to those that lead to spalling. The thermal expansion and dehydration of heated concrete leads the formation of fissures on the surface. The fissures contribute to the direct heating of the reinforcing steel, which leads to more thermal stresses and results in further cracking.

Geogali and Tsakiridis [49], in their study, have shown that the temperature of the fire contributes to the penetration depth of cracks.

2.3.3.4 Structural Stability

High temperatures change the chemical properties of concrete. Therefore, after a fire the changes in the structural properties of concrete do not fully reverse themselves. This behaviour is opposite to that of a steel structure, where the cooling effects (following fire) lead to restoration of the material properties.

Due to the change of the concrete material properties in fire, in some circumstances, a concrete structure can be considerably weakened after a fire even though there is no visible damage.

2.3.3.5 Fire Resistance

Fire resistance is defined as the period of time of fire exposure after which failure occurs. Even though concrete is known as an incombustible material, it still needs protection when subjected to high temperatures (due to material degradation in fire). High temperatures reduce the fire resistance of structural elements. In certain circumstances, fire resistance is provided to structural elements either to control the spread of fire or to prevent structural buildings from collapse. For concrete structures, fire resistance can be achieved by providing the appropriate depth of structural element and thickness of concrete cover depending on their function. The 2006 International Building Code (IBC), ACI 216.1 and AC1 318 provide tables with various assemblies of building materials and finishes providing specific fire endurance.

2.3.4 Fire Design Technique – Numerical Modelling

The numerical modelling method used is intended to replicate the standard test. The aims are to calculate the critical temperatures and to represent all aspects of structural behaviour that would occur in a real fire.

In the mid 1990s, the ability of computers to model structures subject to fire was used extensively by researchers. However, finite element models were fairly limited in their range of capability [33]. They performed reasonably well for a specific task but were limited to single elements in isolation. Subsequently, as computer tools became more powerful and the need for the full behaviour of structural elements subject to fire became significant, the finite element tools used became more advanced.

The computer software available can be divided into two categories. The software aimed purposely at structural fire engineering problems, such as Vulcan [110] and SAFIR [46]. This software was developed and validated [48,60] by researchers at the Universities of Sheffield and Liege. Second is the finite element method (FEM) such as ABAQUS [1] and ANSYS [3] were developed for the general purpose of structural modelling. They have a huge range of functionality with some parts being applicable to the field of structural fire engineering. The ability of the software to model structures subject to fire has been validated by a number of researchers [50,59,78].

2.3.5 Failure Parameters of Structures Subject to Fire

Parameters for the failure of structures due to fire can be interpreted by a number of definitions of failure. Each of these definitions comes from a particular way of measuring the structures behaviour in fire. This definition can be used as a structural limitation either for assessment of the existing structures or in the design state to resist fire. Modelling of structures using the finite

element method is one way to identify the failure parameters. There are two main failure parameters that are used in this study, as discussed below.

2.3.5.1 Deflection

The maximum deflection of a structural element is defined as the ratio of deflection to element length. The limit on the ratio varies depending on the provision in the design codes to minimise the effect of movement. For example, a limit for deflection is given in the British Standards, as in Equation 2.21, which is applied when the deflection has already exceeded L/30 [28].

$$\frac{L^2}{9000d} \tag{2.21}$$

Where:

d is the distance from the top of the section to the bottom of the design tension zone;

L is the span.

2.3.5.2 Stress and Strain of Reinforcing Steel

The behaviour of the stress and strain of reinforcing steel is used as an indicator to failure when reinforced concrete is subjected to a fire. A simple indication of failure in reinforced concrete structures is the critical temperature of reinforcing steel, usually taken as 593^{o}C. At this temperature the yield stress of the reinforcing steel reaches half of its ambient capacity [74]. The rupture strain of reinforcing steel can also be used as a failure parameter in reinforced concrete structures. According to Eurocode 3 [36], the ultimate strain for steel at any temperature is taken as 0.2. This failure parameter can be easily measured

by numerical analysis of structures in comparison with experimental testing due to the difficulties of placing a strain gauge inside the reinforced concrete element.

2.4 Fire Following Earthquake (FFE)

Post earthquake, there are several factors that influence the level of damaged caused to the fire safety system. Several are discussed below.

The probability of fire following an earthquake (FFE) was first recorded in the early twentieth-century. In 1998, Botting Russ [24] reported that in 15 out of 40 of his studies on major earthquakes a significant conflagration occurred following the earthquake. The fires following the earthquakes occurred due to the failure of buildings' fire safety and damage of lifelines such as electricity, water supply and transportation. Even though the number of conflagrations is quite small, the effects of such disasters are enormous. Table 2-1 shows summaries of 15 major earthquakes with fire ensuing afterwards.

Botting and Buchanan [23] in their study show the ignition source, fire spread, damage to buildings, lifelines and suggestions for mitigation of particular issues. Even though history has shown that many countries have experienced fire following an earthquake in the past, only Japan has shown any immediate response by initiating research to address the problem [113].

This clearly shows that fires following an earthquake have to be considered from the early design stage. The seismic and fire design of a building structure are two different fields in structural engineering. To obtain a well-engineered structure with respect to both seismic and fire design requires expertise in both fields.

Table 2-2 shows the fire spread mechanism and the level of fire damage for each earthquake.

Table 2-1 Previous recorded fire following earthquakes [Reproduced from 23]

Earthquake	Year	Fire following earthquake
San Francisco	1906	50 (all grew quickly to conflagration)
Tokyo	1923	134 (all grew quickly to conflagration)
Napier	1931	3 (started in Chemists' shops; later caused conflagration)
Long Beach	1933	15 (confined to buildings of fire origin)
Niigata	1964	9 (one caused conflagration in a residential area)
San Fernando	1971	116 (3 in broken gas lines in streets)
Managua	1972	4 – 5 (developed to a conflagration)
Morgan Hill	1984	3 – 4 (confined to buildings of fire origin)
Mexico city	1985	200 fires reported within 24 hours (confined to buildings of origin).
Edgecumbe	1987	No fires reported.
Whittier	1987	58 structure fires (confined to bldg of origin) and 75 gas fires in first 5 hours.
Loma Prietta	1989	27 in first 2 hours (confined to buildings of fire origin)
Hokkaido Nansei-oki	1993	Initial fire outbreak immediately developed to a conflagration.
Northridge	1994	50 structure fires in first 2 hours, and 110 over 6 hours (most confined to bldg)
Kobe	1995	89 fires in first 14 minutes (about 50% grew to conflagration) 205 fires reported on the first day, with 240 fires reported four days later.

Table 2-2 Summary of reported fire spread and extent of damage [Reproduced from 23]

Earthquake	Year	Fire following earthquake induced damage
San Francisco	1906	Fire spread by direct flame impingement and thermal radiation. Spot ignitions by burning brands. Buildings were 90% wood up to 5 storeys. Problem with wind. 28,000 buildings destroyed over an area of 10 sq km
Tokyo	1923	Severe conflagration. Rapid fire spread through closely spaced dwellings. Problem with wind. 450,000 houses destroyed over an area of 38 sq km.
Napier	1931	Fire spread by wind-driven flames, flame impingement and burning brands. Major conflagration destroyed 4 hectares of city buildings.
Niigata	1964	Conflagration in high-density residential areas. Burning oil slick on tsunami-driven water.
Managua	1972	Conflagration in downtown burned for one week. Fire spread from storey to storey. Modern tall concrete buildings were burned out.
Morgan Hill	1984	Fire spread between structures due to flying brands (wind speed 7 m/s).
Mexico city	1985	No major conflagrations. No wind. No buried gas pipelines. Gas tank fire spread to two adjacent buildings.
Whittier	1987	No reported fire spread beyond the structures of the fire origin.
Loma Prietta	1989	Fire spread by radiant heat from apartment building fires. No wind.
Hokkaido Nansei-oki	1993	Conflagration in residential and industrial area. Fire spread by radiant ignition, exterior fuel tanks and flying brands. Metal roofs limited the fire spread. Fire progressed relatively slowly (35 m/hour).
Northridge	1994	Most fires confined to building of origin due to light winds, good building construction and building separation, and fire fighting. Fire spread between mobile homes by thermal radiation. 110 fires under control within 6 hours.

Kobe	1995	Severe conflagration. Fire spread by direct flame contact on collapsed wooden buildings. Solvents and plastics assisted fire spread. Cars helped to spread fire across narrow streets. Fire spread via windows. Non-combustible buildings stopped fire spread. Little wind. 69,000 buildings destroyed in 65 hectares.

2.4.1 Potential Effects on Building Fire Safety

Based on the study by Scawthorn [113] a number of potential effects of earthquakes on buildings that have to be considered when studying the impact of earthquakes on fire safety were identified. Four identical potential effects of building fire safety will be discussed in this chapter.

Earthquakes may damage or fracture gas and electrical pipelines in the seismic area. If the automatic detector fails during the earthquake event, this may lead to accidental ignition [24]. Appliances in the building, including candles, also contribute to the potential sources of ignition in the days following the earthquake [137].

Fire and smoke spread within a short duration due to damaged passive fire protection and building services. The passive fire protection in the buildings acts to contain fires or retard the spread of the fire. Examples of passive fire protection in buildings are fire-resistant walls, floors and doors.

Another factor is the delay in the evacuation of occupants from the damaged building. This may be caused by structural damage to stairs, obstruction of the escape routes and loss of lighting. Alarm systems in the buildings are important as they provide an early warning to occupants allowing them sufficient time to escape. Frequently, there is a faster response to fire alarms activated at home

compared to in a larger building [26]. Inoperative alarm systems caused by an earthquake event may delay the response of the occupants in buildings.

Due to damage to communication and transportation systems during an earthquake, fire services may have to take a detour to reach the area, which will increase the time taken to respond to a fire. This may result in a lack of fire service intervention to control the fire spread and facilitate escape.

2.4.2 Earthquake Loss Assessment

The loss assessment of damage induced by earthquakes has been progressively developed. Studies have been done in the macro-scale, particularly for use by local authorities for planning the mitigation of damage to lifelines and utilities after an earthquake [44]. The assessment is based on information from past earthquakes and there is considerable uncertainty in the loss estimation process [52].

In the 1994 Northridge and the 1995 Kobe earthquake loss assessments of damage induced by the earthquakes, the effect of potential conflagration due to fire following the earthquake was recognised [127]. Fires following an earthquake affect the local economy, cause casualties and cause damage to buildings that may sometimes exceed that caused by the earthquake itself [96].

Following both earthquakes, macro-scale assessment has changed the assessment of individual elements and provides information for individual buildings based on the vulnerability of the particular elements and systems to develop damage assessment. In 2000 Sekizawa et al. [119] developed an assessment of fire spreading in a building following an earthquake based on observed damage, ignition and fire spread during a recent earthquake in Japan.

They also proposed a simplified model of structural response to predict the earthquake actions on individual building elements.

2.5 Conclusion

A detailed background study on earthquake engineering and fire engineering and how these two fields relate to each other was presented. Building responses to both earthquake and fire were discussed. To provide a detailed understanding, the changes to material properties by earthquake damage and heating due to fire were presented.

According to seismic building codes, the buildings in seismic regions are designed to sustain certain earthquake intensity without consideration of design for fire, while fire design always focuses on the undamaged structural condition. Fire behaviour is the main contributor to the performance of structural response.

Based on the history of earthquakes, the possibility of fire following an earthquake is a serious consideration. The failure of short circuits from structural damage, damage to the sprinkler system, fracturing of gas or electricity connections during the earthquake all can lead to the spread of fire. The effect of sequential phenomena was discussed.

3

Preliminary Design and Test Set-Up

3.1 Introduction

This chapter reports the test of a full-scale one-storey reinforced concrete frame subjected to cyclic loading and a subsequent fire. The test was the result of a collaboration between the Indian Institute of Technology Roorkee (IIT Roorkee) and the University of Edinburgh, funded by the UKIERI. The project plan of this research is shown in

Figure 3-1. The coloured boxes show the stage that which were involved and presented through out the thesis. At the design stage of the Roorkee frame, all the members of the project were involved. The test of the Roorkee frame was carried out at IIT Roorkee and most of the numerical analyses were carried out at the University of Edinburgh [17].

The objective of the project was to investigate the behaviour of the reinforced concrete frames first subjected to simulated earthquake loading followed by a

fire. It was planned that the test frame would be subjected to cyclic lateral loading at the slab level to simulate the motion of an earthquake. The damaged frame was then exposed to a pool fire for one-hour and its behaviour was monitored and recorded. The first large-scale sequential loading test of the Roorkee frame was completed in summer 2011. The results of the test have been presented at various engineering conferences and in journals [17,120].

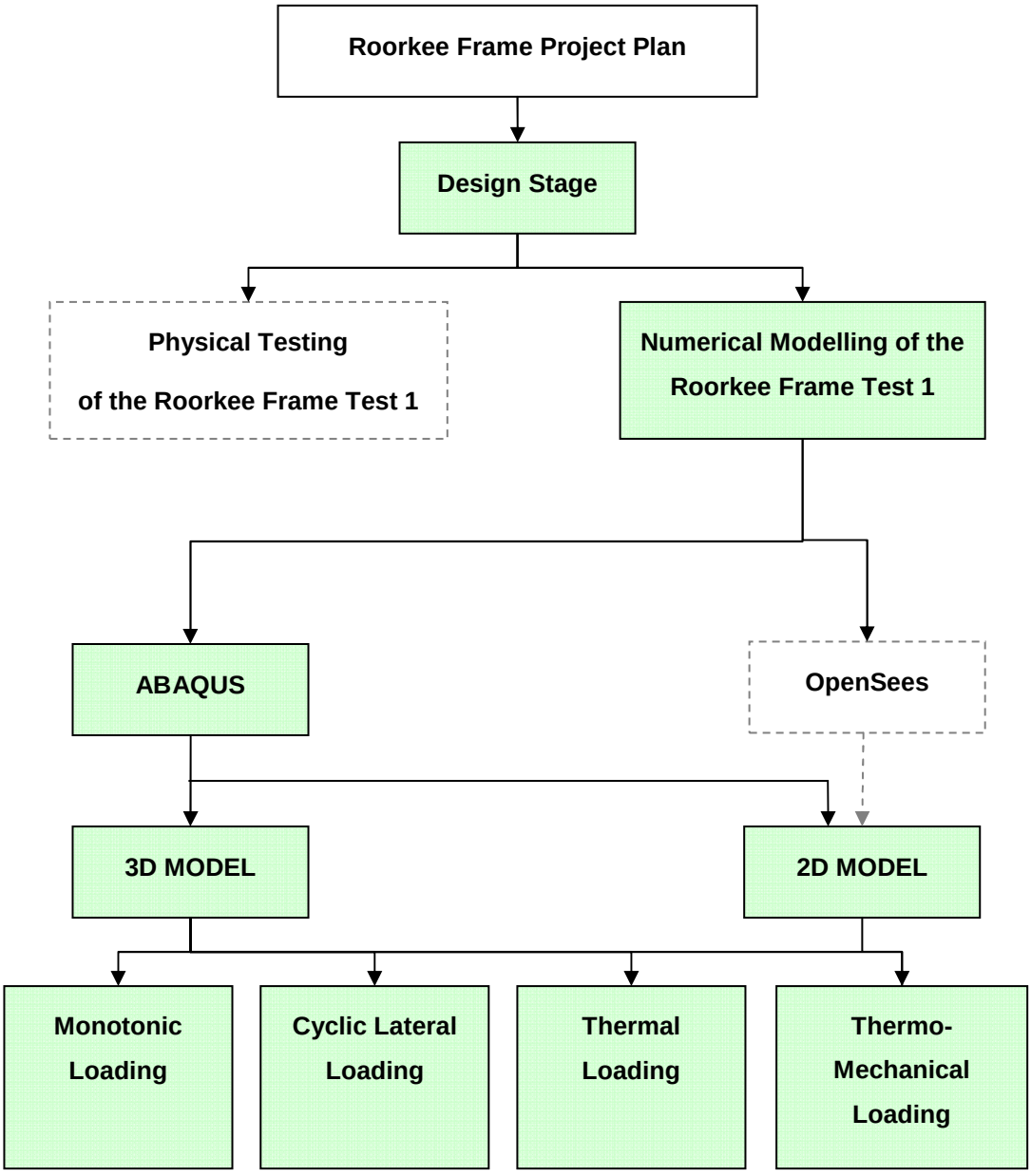

Figure 3-1 Description of the Roorkee frame study

This chapter presents the methodology of the first Roorkee Frame Test 1, and describes preliminary simple analytical modelling carried out to understand the behaviour of the frame right up to peak load.

3.2 Design Specification

The design of the frame was carried out in early 2009, in accordance with the seismic design code, Indian Standard (IS) 1893: Part 1(2002) [63]. A single storey reinforced concrete frame section of 5.8m height was designed, as part of a four storey office building located in seismic zone IV.

Figure 3-2 is showing the elevation of the frame used in the numerical analysis. According to the IS, zone IV corresponds to a severe intensity zone that is prone to major property damage; a zone factor of 0.24g was considered. The 0.24g is defined as the peak ground acceleration (PGA) that could give potential moderate damage after an earthquake motion.

Figure 3-2 Design frame used in the modelling

The building elements and loading details are shown in Table 3-1. It should be noted that the simulated gravity loads (dead load and 25% of imposed loads) on the structure is considered in the seismic loading combination calculation.

The combination loading on the frame was calculated and the frame element details are shown in Appendix A.1.

Table 3-1 General details of the Roorkee frame

Building elements details (mm)	Material	Loadings details
Column: 300 x 300 Beam: 230 x 230 Thickness of slab: 120	Grade of concrete: M30 Grade of steel: Fe415 Density of concrete: 25 kN/m^2	Floor finishing: 1 kN/m^2 Live load: 2 kN/m^2

3.3 Preliminary Design of the Roorkee Frame

The general concept of earthquake resistant design involves ‘failure’ or yielding of the beam prior to failure of the continuous columns taking place in the frame. This design method is known as ‘strong column weak beam’. Failure of the column can affect the stability of the whole building, while failure of a beam causes localized effects; therefore, it is better to have yielding in the beams than in the columns. In this approach, a plastic hinge is formed at the end of the beam and energy dissipation occurs there. While beams are permitted to yield, the columns remain elastic. Generally, reinforced concrete beams exhibit more ductile behaviour than reinforced concrete columns. In order to ensure that plastic hinges form in the beam, prior to the columns of a frame, the elements may need to be redesigned.

The plastic hinge phenomenon has been investigated analytically using the stiffness method and numerically using SAP2000, ABAQUS [1] and SeismoStruct [118]. SeismoStruct is a freely available finite element package used to predict large displacement behaviour of space frame under both static and dynamic loading, including geometry nonlinearity and material inelasticity.

SAP 2000 is a commercial finite element programme which was also used to predict the capacity of the frame.

3.3.1 Plastic Hinge

A plastic hinge is used to describe the deformation of a section of a beam or column where plastic bending occurs. The loading calculations in Appendix A.1 suggested column sizes of 300x300mm with 8 reinforcing bars of 12mm diameter within; and beams of 230x230mm with 3 reinforcing bars of 16mm diameter at top and bottom, and 2 reinforcing bars of 12mm diameter in the middle.

Figure 3-3 shows the load combinations used in the analysis, with the lowest load factor at collapse, λ=6.71. The detailed results obtained from the analytical and numerical solutions show that plastic hinges occur first in the column rather than in the beam, as shown in Appendix A.2. Therefore, the detailing of the elements was revised to ensure that the desired ‘strong column weak beam’ behaviour was achieved in the design.

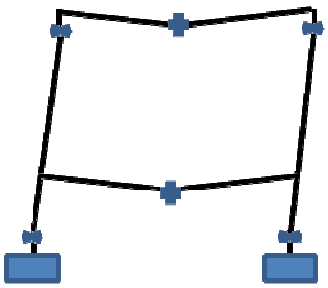

λ=6.71

Figure 3-3 Load Combination Mechanisms

Table 3-2 shows the modified detailing of the column and beam. The final element details, shown in Case II, were used in the test and in numerical modelling.

Table 3-2 Modification of column and beam detailing (where Φ is the bar diameter)

Case	Column		Beam		
	Size (mm)	Reinforcing steel (mm)	Size (mm)	Reinforcing steel (mm)	
				Top	Bottom
I	300x300	8-12Φ	230x230	3-16Φ and 2-12Φ	3-16Φ and 2-12Φ
II	300x300	8-20Φ	230x230	3-16Φ	3-16Φ

3.3.2 Static pushover analysis

The capacity of the frame was predicted by subjecting it to lateral loading using the static pushover analysis approach. The theory of static pushover analysis was discussed in detail in Chapter 2. It was carried out by applying increasing lateral displacement at the slab level. The reaction force at the base of the frame was plotted against displacement and this is known as the capacity curve.

Based on the capacity curve the target displacement of the frame was obtained and used in cyclic analysis. The prediction of the capacity of the frame was calculated numerically using SAP2000, ABAQUS, and SeismoStruct.

The direct displacement base design procedure (DDBD) [104] was used in the analytical solution. The DDBD characterizes the structure by the effective stiffness of the frame, K_e at maximum displacement, Δ_d. The calculation of the effective stiffness and maximum deflection of the frame is shown below. The

values were compared with the numerical analyses listed above to determine whether the numerical modelling packages performed as expected.

Figure 3-4 illustrates the fundamentals of the direct displacement base design proposed by Priestley et al. [104]. The DDBD simplifies the building as a single-degree-of-freedom (SDOF) structure, representing its performance at the peak displacement response (Figure 3-4 (a)). Figure 3-4 (b) presents the bilinear envelope of the lateral force-displacement response of the SDOF structure. The damping of the structure is defined according to its displacement ductility and the type of structure involved (Figure 3-4 (c)). Based on the design displacement obtained, the effective period, T_e, can be read from the displacement spectra for different levels of damping (Figure 3-4 (d)). Table 3-3 is show calculation of total mass of the frame.

Figure 3-5 shows the simplified test frame arrangement for use in the DDBD. Table 3-4 shows the effective stiffness and design displacement of the frame obtained from the analytical solution and numerical analysis. The effective stiffness obtained from ABAQUS is 13% higher than the analytical solution. This may be due to the continuum elements used in ABAQUS, which model the frame as over-stiff. SeismoStruct and SAP2000 give a frame stiffness of about 4% and 10.5% lower than the analytical solution. The base shear-displacement curve from the numerical analyses is presented in Appendix A.3.

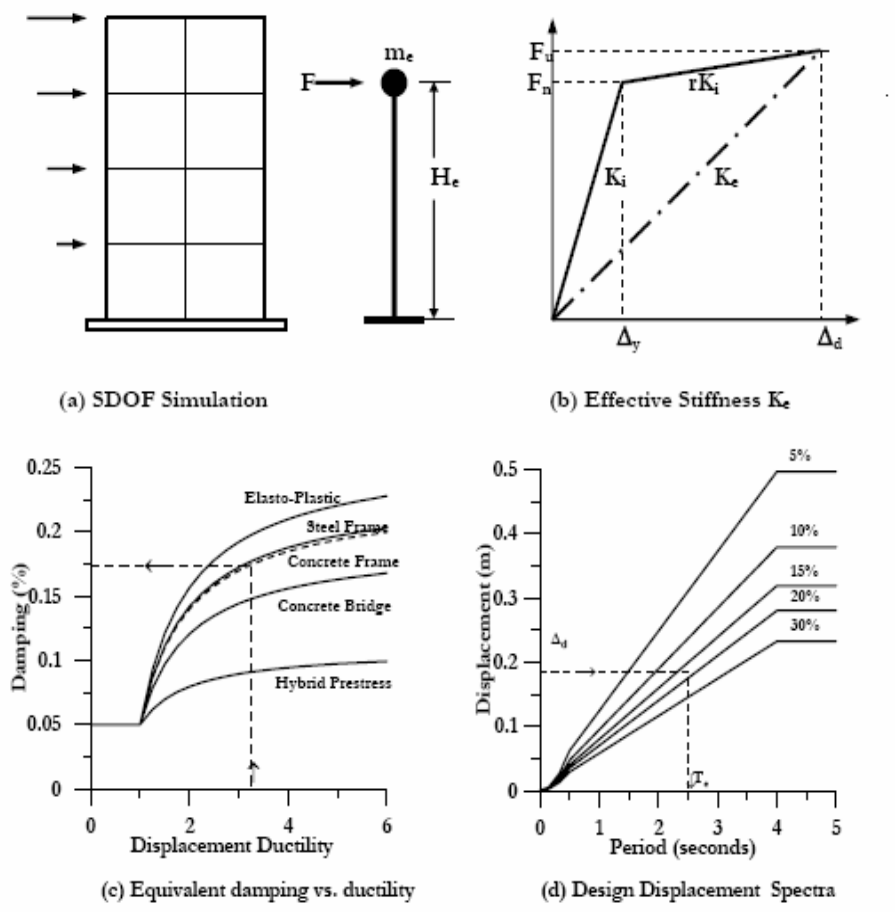

Figure 3-4 Direct displacement base design **[Reproduced from 104]**

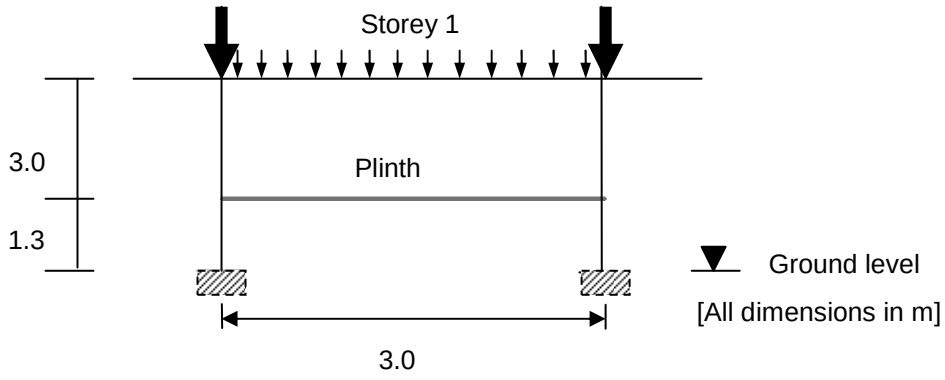

Figure 3-5 A simplified frame used in DDBD calculation

Table 3-3 Total mass of each storey

Storey i	Height H_i, (m)	Mass m_i,(kg)	Storey displacement Δ_i, (m)	$m_i\Delta_i$, (kg.m)	$m_i\Delta_i^2$, (kg.m^2)
1	4.3	227800	0.108	24488.5	105300.55
Plinth beam	1.3	26230	0.033	853.45	1109.485
Total				25341.95	

$$\text{Equivalent design displacement, } \Delta_d = \frac{\sum_{i-=1}^{n} m_i\Delta_i^2}{\sum_{i=1}^{n} m_i\Delta_i} = 0.105m \quad (3.1)$$

$$\text{Equivalent mass of the frame, } m_e = \frac{\sum_{i=1}^{n} m_i\Delta_i}{\Delta_d} = 24141kg \quad (3.2)$$

$$\text{Effective stiffness of substitute frame, } K_e = \frac{4\pi^2 m_e}{T_e^2} = 2.5x10^6\ N/m \quad (3.3)$$

Table 3-4 Comparison of results from analytical solution and numerical analysis.

Analysis method	Effective stiffness, K_e (x10^{6}N/m)	Design Displacement, Δ_d (m)
Analytical solution (DDBD) [104]	2.5	0.105
SeismoStruct [118]	2.4	0.12
ABAQUS [17]	2.85	0.1
SAP2000 [17]	2.25	0.12

3.4 Test Set-Up

After the agreement of the preliminary design of the Roorkee frame, the first large-scale construction began in 2010. The test frame was built on a strong-floor with a reaction wall at IIT Roorkee. The construction of the frame was done by casting the foundation of the columns first, followed by the columns up to the soffit of the plinth beams. Then the plinth beams together with 3.0m height of columns were assembled, followed by the rest of the columns. The top beam and the slab were erected last. Sand-filled hessian bags were used to simulate the gravity loading on the Roorkee frame. Figure 3-6 shows the elevation of the Roorkee frame on site.

During the construction of the frame, it was instrumented with a number of thermocouples and thermal flux meters, Linear Variables Displacement Transducers (LVDT) and strain gauges. The instruments were installed to capture the displacement, strain values and temperature distribution during the test. Figure 3-7 and Figure 3-8 show the full details of their location within the elements.

3.4.1 Loading

Three major tests were planned for the Roorkee frame to investigate the behaviour of the (simulated) earthquake damaged reinforced concrete frame followed by fire as shows in Table 3-5. The Roorke frame Test 1 and the fire loading was completed. The others test (which in progress) will take into account the weakness obtained from the Test 1 and some modifications are made in order to get better results.

The earthquake was simulated by applying severe incremental lateral loading and unloading. The cyclic lateral loads were applied in quasi-static mode using a pair of hydraulic double rams against a reaction wall at the slab level. The

hydraulic rams were mounted with pressure sensors to measure the lateral loads, while the horizontal displacements at the slab level were measured using LVDTs.

Table 3-5 Loading cases in each test planned [17]

Test	Simulated seismic load	Fire load (for 1 hour)	Test completed
1	Displacement beyond peak lateral load	900^{o}C -1000^{o}C	Summer 2011
2	None	900^{o}C -1000^{o}C	Yes
3	Moderate displacement (30% of the displacement corresponding to peak lateral force)	900^{o}C -1000^{o}C	In progress
4	Severe displacement (70% of the displacement corresponding to peak lateral force)	900^{o}C -1000^{o}C	Not started yet

3.4.2 Fire Loading

A 1.0m x1.0m x 0.05m oil pool steel tray was located in the centre of the compartment in the pre-damaged frame. Kerosene was continuously supplied to the oil pool using a galvanized iron pipe of 0.254m diameter. The oil flow during the test was controlled using a fixed head to maintain a designed peak flow rate. The exterior of the frame was covered by fireproof panels made of iron and mild steel using stainless steel rods. Figure 3-9 shows the assembled pre-damaged Roorkee Frame Test 1 with fireproof.

3.5 Conclusion

This chapter presented the details of the Roorkee frame. The aim of the preliminary design was to obtain an optimum design for the reinforced concrete frame subjected to earthquake considering quantity and diameter of reinforcement bars required. The design stage was undertaken about 8 to 10 months before the tests began.

The frame has been analysed analytically and numerically without any reference to previous studies to investigate the peak load, target displacement and location of the plastic hinge when subjected to monotonic lateral loading. The analytical solution and numerical analysis of the frame proved to be in good agreement.

The overview of the frame test set-up is presented at the end of this chapter to provide an understanding of the Roorkee frame test. It is planned to have several tests and some of the tests are still in progress (see Table 3-5). It should be noted that only the first test was completed during this research, and it is known as Roorkee Frame Test 1. Consequently, the validation of the numerical model throughout this thesis is limited to the first Roorkee Frame Test 1.

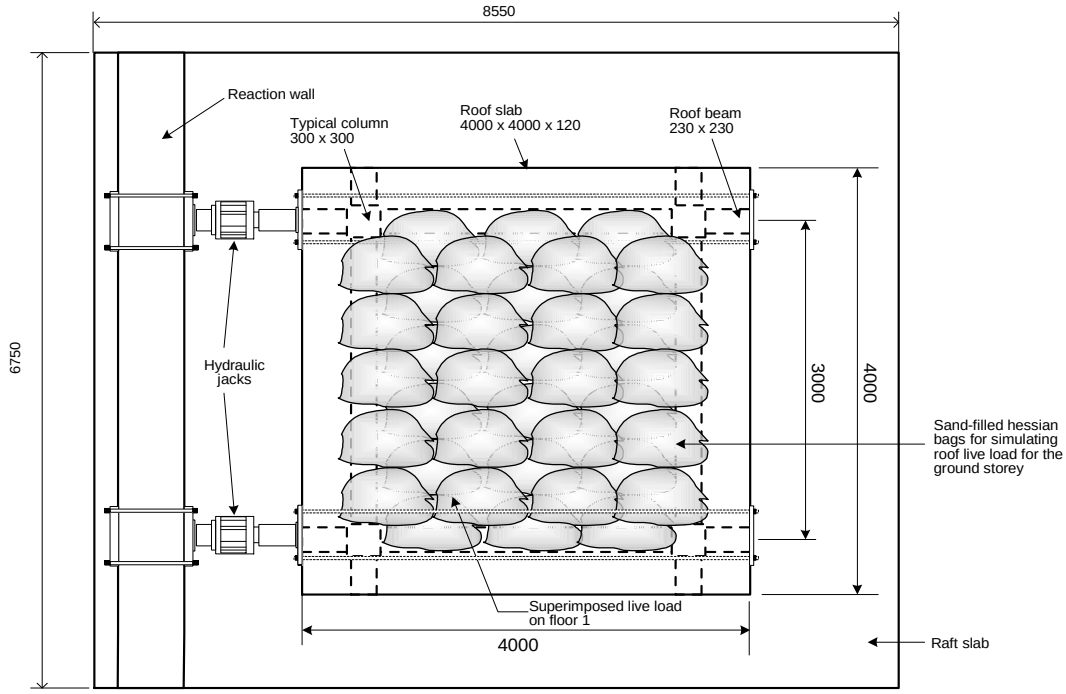

(a) Plan of the test setup (at X-X)

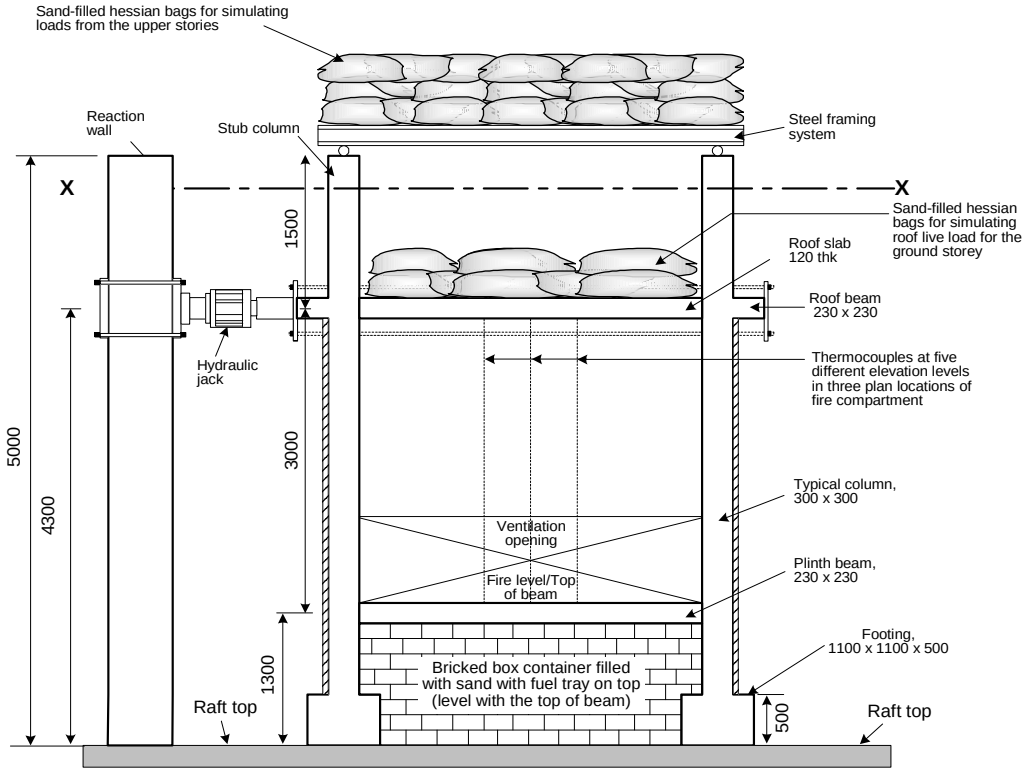

(b) Elevation of the test setup

Figure 3-6 The Roorkee frame assemblage tested in IIT Roorkee (a) Plan view (b) elevation view of the frame **[Reproduced from 120].**

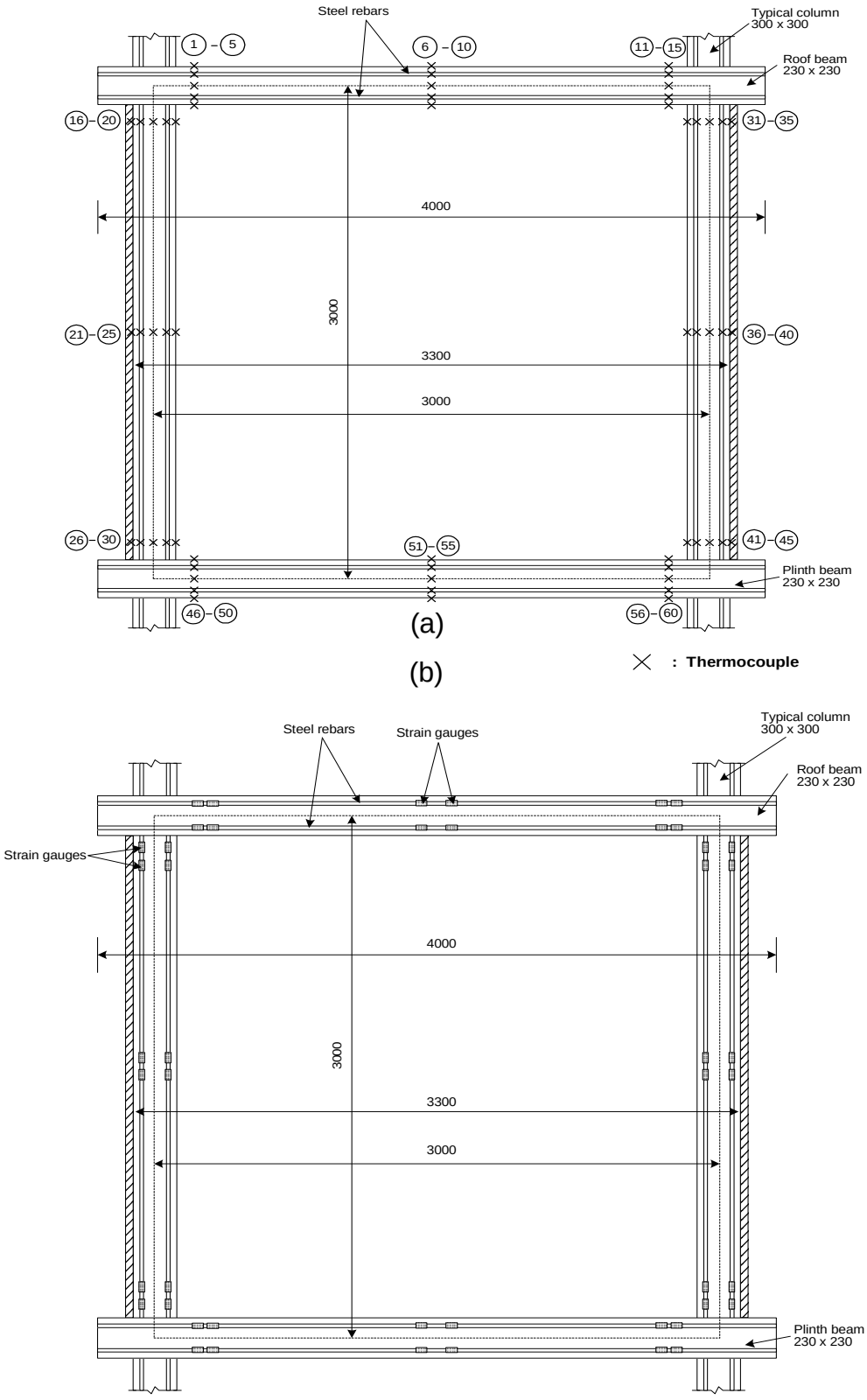

Figure 3-7 Elevation view of the frame to show (a) the location of thermocouples (b) electrical strain gauges on the beams and the columns [Reproduced from 120]

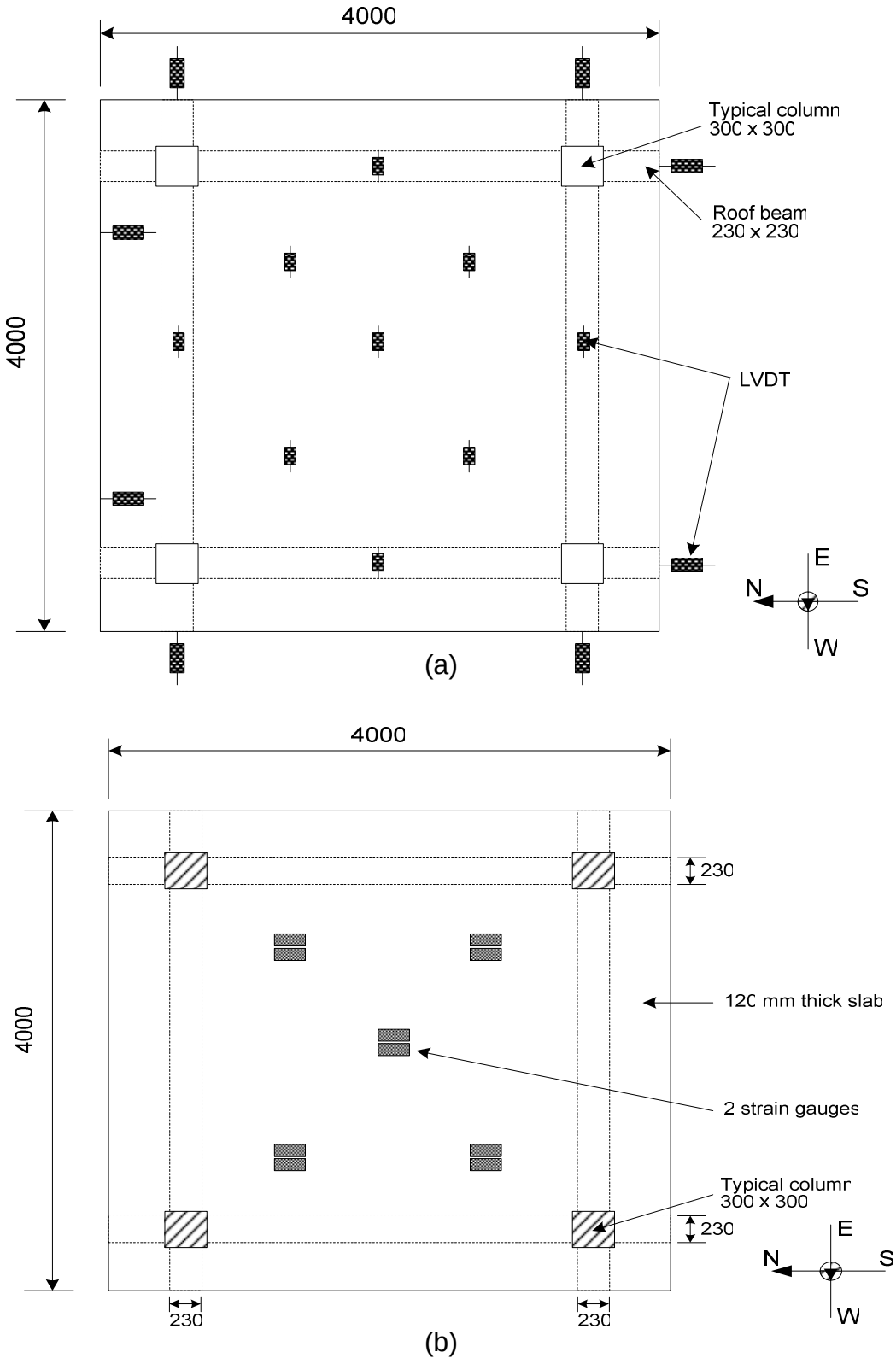

Figure 3-8 A plan view of the frame to show the location of (a) L.V.D.T's (b) electrical resistance strain gauges in the slab **[Reproduced from 120]**

Figure 3-9 Pre-damage Roorkee frame with fireproof panel **[Reproduced from 117]**

4

Development Numerical Models of the Roorkee Frame

4.1 Introduction

This chapter presents the details of numerical modelling of the (simulated) earthquake damaged reinforced concrete frame subjected to fire. ABAQUS [1] and OpenSees [94] models are developed to illustrate the behaviour of the Roorkee frame test. The numerical modelling of the reinforced concrete frame is studied in three parts.

First, the static pushover analysis is performed. The reinforced concrete frame was subjected to lateral loading in displacement control mode up to 100mm (in positive x-direction) at the slab level. The loading value used was the random number to calculate the response of the frame subject to lateral loading. The capacity curve of the frame obtained from the analysis was plotted. From the curve a target displacement was chosen and used in the cyclic loading and thermo-mechanical analysis.

Secondly, the frame is loaded with cyclic lateral loading in displacement control mode at the slab level.

Finally, the frame was released from the lateral displacement and exposed to a fire for 1 hour. The temperature-time history used was based on the compartment temperature test results.

4.2 2D ABAQUS Model

The 2D ABAQUS model was developed using beam elements. A schematic front view of the 1x1 bay of the generic frame designed for the purpose of this research is shown in

Figure 4-1. The structure is one storey high (5.8m), similar to the construction of the tested frame in Roorkee. It comprises of two 300x300 columns, eight 230x230mm beams with 3.0m length, and a 120mm thick slab. Eight reinforcing steel bars of 20mm diameter were used as the main reinforcement in both columns, and six reinforcing steel bars of 16 mm diameter were used in the beams.

The slab was reinforced with 8mm reinforcing steel bars in both directions at the top and bottom. Figure 4-2 and Figure 4-3 show the section details for the reinforced columns, beams and slab.

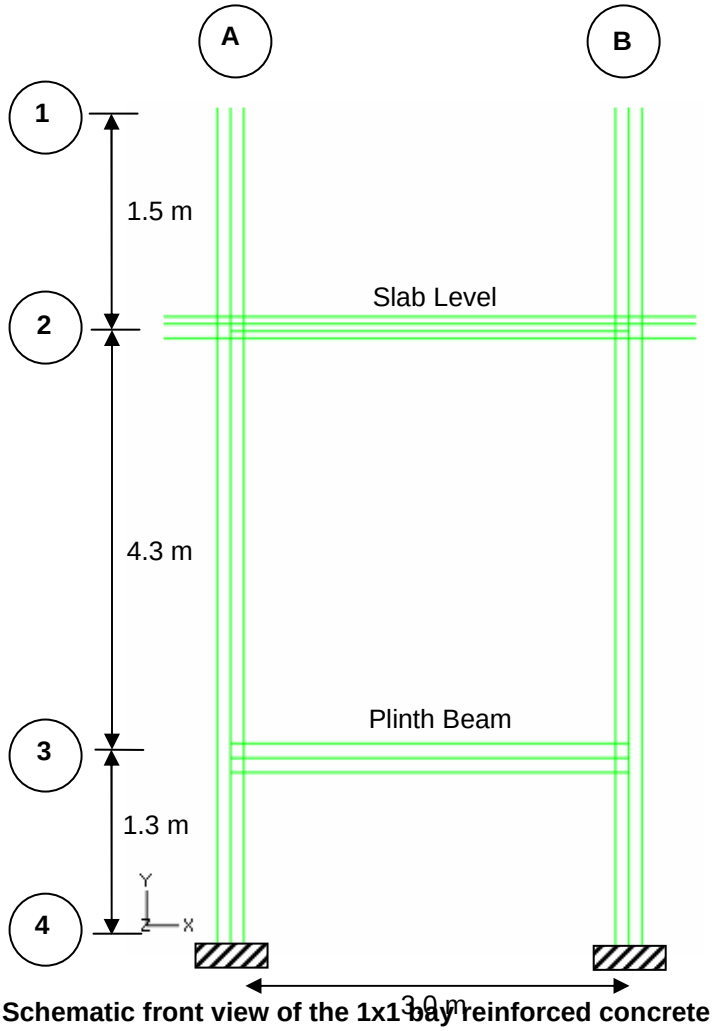

Figure 4-1 Schematic front view of the 1x1 bay reinforced concrete frame

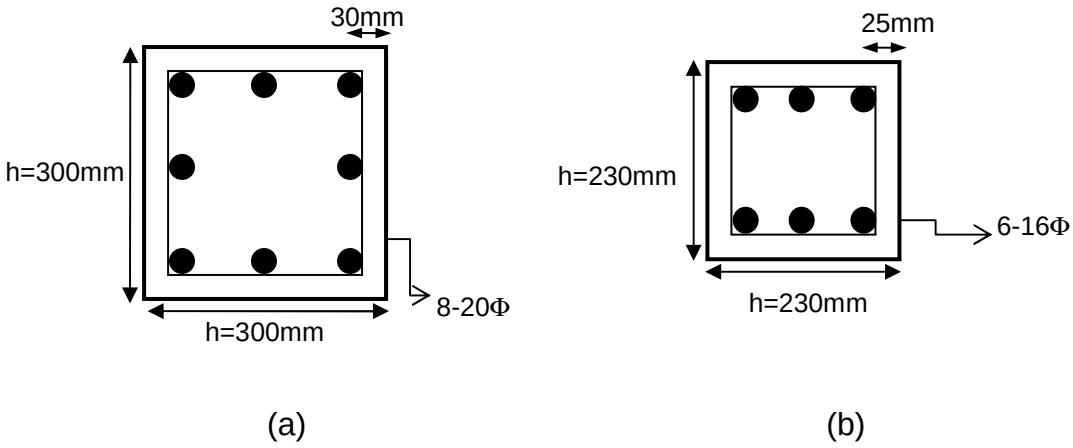

Figure 4-2 (a) Column and (b) beam cross-section with reinforcing steel details

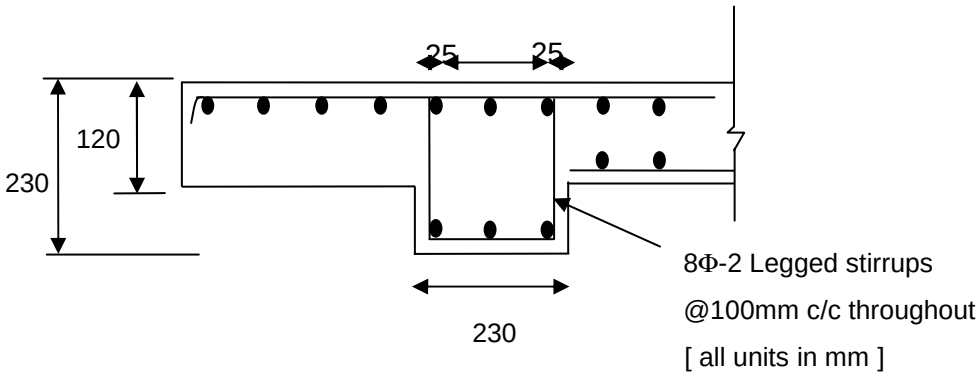

Figure 4-3 Detailing of reinforced beam at slab level

4.2.1 Element Type and Meshing

The concrete sections were modelled using the linear Timoshenko beam element (B21) which allow modelling of transverse shear strain. Two node linear truss elements (T2D2), which only permit axial forces, were used to model the reinforcing steel of the frame. The 2D ABAQUS beam element model contains 104 elements of concrete and 227 elements of reinforcing steel. The elements are shorter at the joints, with longer ones used in the middle section. This is to take into account plastic hinge formation in the beams and columns. The arrangement of the nodes in the model is shown in

Figure 4-4 and

Figure 4-5.

The top beam and slab at slab level are modelled monolithically, or, in other words, are modelled as a T-beam section. A grid system is used for naming the structural members of the frame. For instance the beam named Slab Level AB2 lies between gridlines A and B and along gridline 2 (see

Figure 4-1).

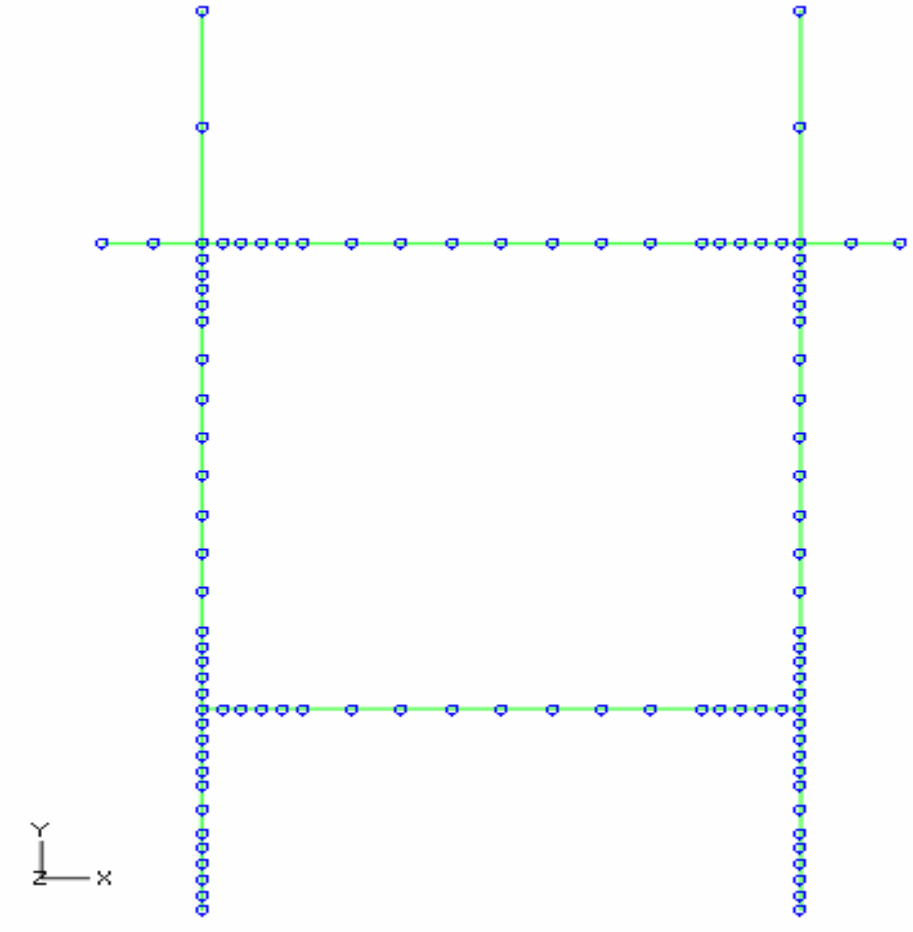

Figure 4-4 Node arrangement on the concrete section of the 2D beam element model

4.2.2 Material Modelling of Concrete

In the conventional concrete model in ABAQUS, the behaviour of concrete under compressive stress is usually represented by a plasticity based model, while the behaviour under tensile stress is expressed using the smeared cracking model. Although the smeared cracking model works well for monotonic loading, for cyclic loading it often encounters numerical difficulty in the analysis. To account for this situation, the concrete damaged plasticity model was used with ABAQUS version 6.8.

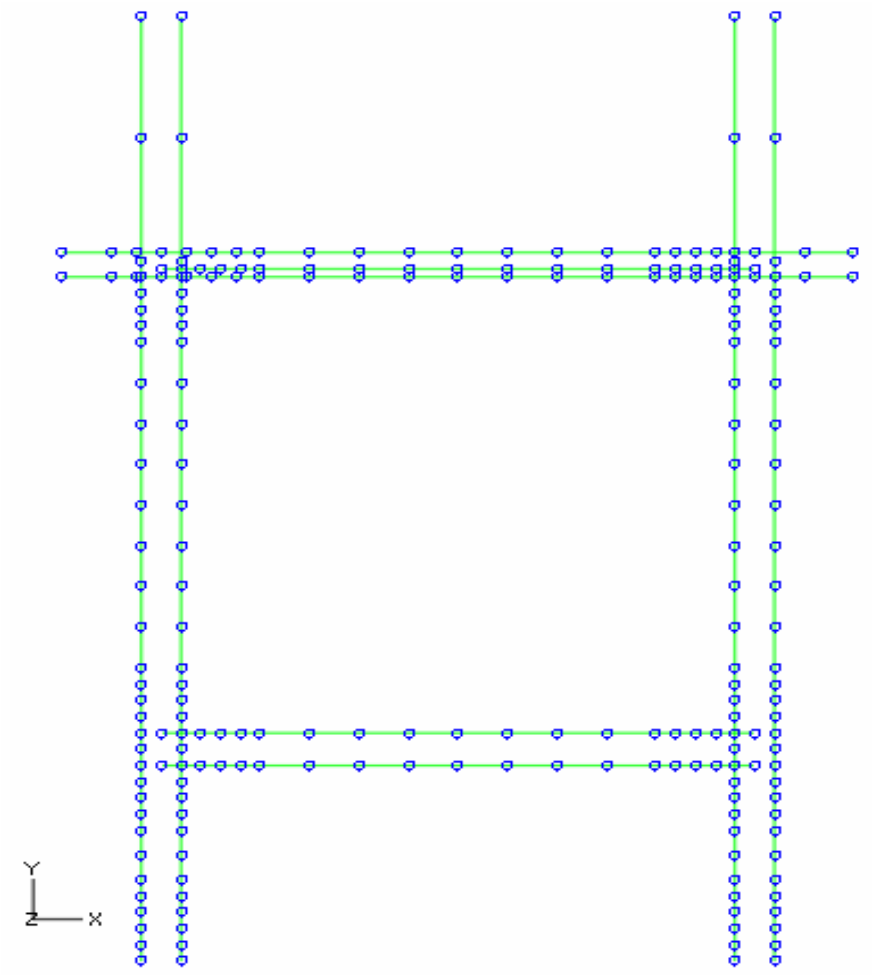

Figure 4-5 Node arrangement on the reinforcing steel of the 2D ABAQUS model

Under uniaxial cyclic loading conditions most quasi-brittle materials, including concrete, show complex degradation mechanisms. During changes of load, reduction of the elastic modulus occurs. As the load changes from tension to compression the compression stiffness recovers with the closure of the crack. This behaviour is often known as the 'unilateral effect', and is described in the concrete damaged plasticity model by scalar degradation in tension, d_t and compression, d_c.

When the load changes from tension to compression; after crushed micro-cracks have occurred, the stiffness in tension will not be restored. This behaviour is illustrated by ABAQUS [1] in default values $w_t = 0$ and $w_c = 0$, where w_t and w_c are, respectively, the weight factor for the tensile and compressive stiffness restoration under cyclic loading.

Figure 4-6 illustrates the response of uniaxial loading of concrete in tension and compression.

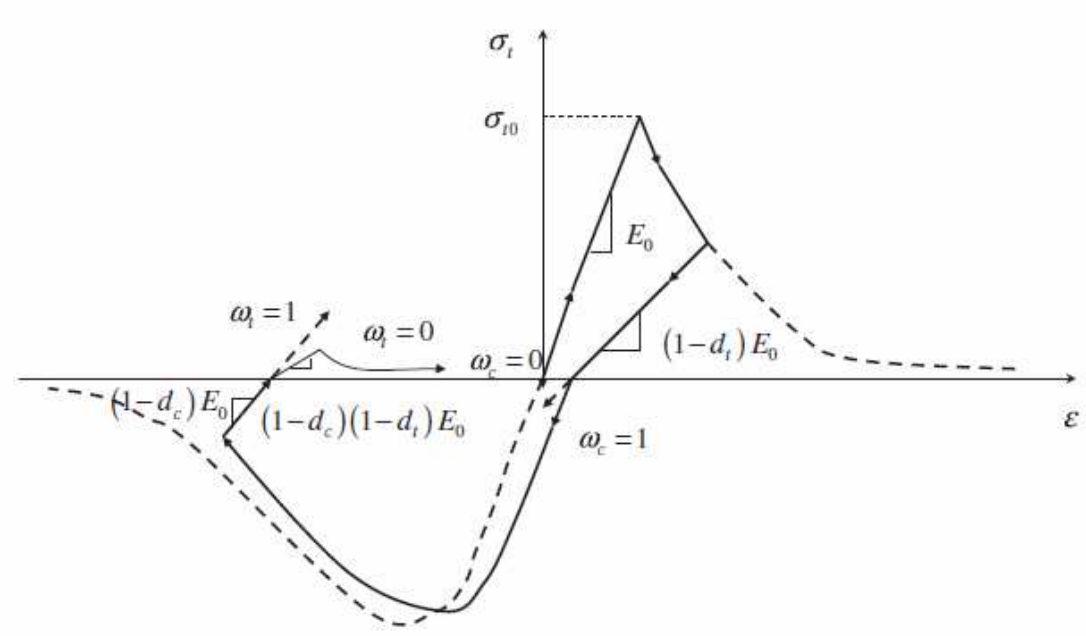

Figure 4-6 Response of uniaxial loading of concrete in tension and compression [Reproduced from 1]

4.2.3 Material Modelling of Reinforcing Steel

In this study the behaviour of the reinforcing steel bars is defined as bilinear, as shown in

Figure 4-7. The reasons for this approximation are due to computational convergence issues in the analysis, in which the behaviour of the reinforced concrete members are greatly affected by the yielding of the reinforcing steel.

Therefore, it is advisable to take advantage of the 2% strain-hardening behaviour of steel to improve the numerical stability of the solution.

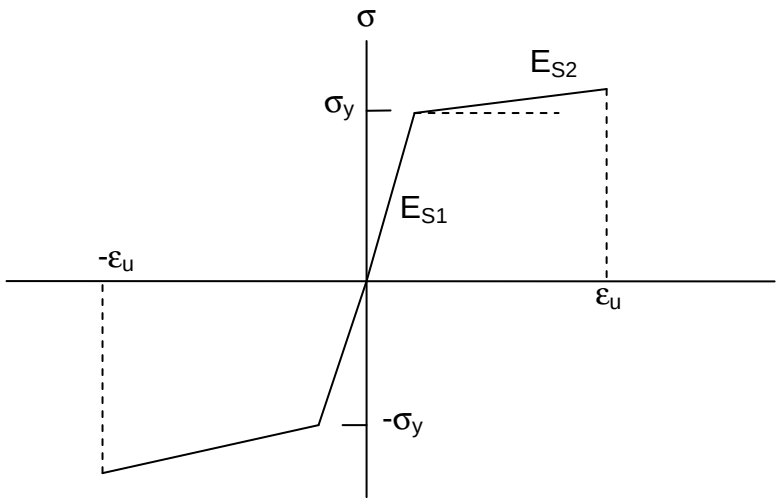

Figure 4-7 Stress-strain relationship of reinforcing steel

4.2.4 Interactive Modelling Between Concrete and Reinforcing Steel

The concrete columns and beams are constrained by the 'Interaction' module 'Tie' command. The Tie command in ABAQUS is used to bind two types of element, therefore, the relative slip between them is considered to be close to zero. The reinforcing steel bars and concrete are tied together and move together throughout the analysis. The connection between the columns and the beams is considered to have a little slip in the joint region.

4.2.5 Boundary Conditions and Imposed Loading

The base of both columns is fixed at A4 and B4 (see

Figure 4-1). Each column is axially loaded with an 80kN load at A1 and B1 (see

Figure 4-1) and the slab, AB2 (see

Figure 4-1) is loaded with a uniformly distributed load of 2.3kN/m^2, which comprises the dead and live load.

Generally, the loading of the frame is divided into two categories for mechanical analysis: first, the imposed load throughout the frame, and, secondly, the lateral load at A2 of the frame (see

Figure 4-1). Two load steps are used for static pushover analysis, and 14 load steps for static nonlinear cyclic loading analysis. For thermo-mechanical analysis, another step is introduced to apply the compartment fire to the frame.

Monotonic lateral loads are applied using displacement control to calculate the capacity curve of the frame. Cyclic loads are used similarly to simulate earthquake motion on the frame. This lateral loading is imposed at A2 (see

Figure 4-1). The specific method is as follows: the axial load is applied at the top of the two columns (A1 and B1,see

Figure 4-1) acting vertically downwards, while the distributed load is applied on top of the slab (AB3) and plinth beam level (AB3) – these loadings are set as a loading step.

After the axial and distributed loads are applied fully, cyclic loading in lateral displacement control mode is applied in order to obtain the load-displacement curves for the frame. This load is used at A2 for the ‘push step’ and at AB2 for the ‘pull step’. The frame is then released from the lateral loading before the frame is exposed to the compartment fire. Figure 4-8 shows the boundary and loading model diagram of the reinforced concrete frame.

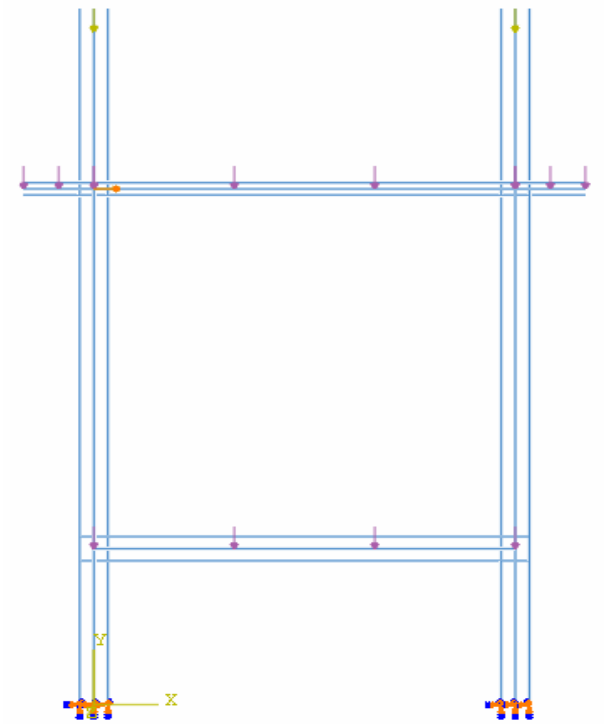

Figure 4-8 2D beam model developed using ABAQUS

4.3 3D ABAQUS Model

In the 3D ABAQUS model, the linear Drucker-Prager model is used for concrete instead of Concrete Damage Plasticity (CDP), as the CDP model is not available for 3D beam elements. The 3D ABAQUS model is developed using beam and shell elements. Figure 4-9 shows the frame modelled using ABAQUS version 6.8. The columns and the beams of the frame were modelled using 3D beam elements (B31), one of the Timoshenko beam types which allows for transverse shear deformation. This beam in space uses linear interpolation between two end nodes. The slab of the frame is modelled using shell elements (S4R). The S4R shell type, which is the conventional stress and displacement shell with four nodes with reduced integration, was used in the analysis.

The reinforcing steel bars are modelled using three dimensional, two node truss elements (T3D2). The T3D3 truss type contains two node straight truss

elements, uses linear interpolation for position and displacement, and has a constant stress.

Tie constraints were used to tie the reinforcing steel to the concrete. All the imposed loadings and boundary conditions are the same as applied to the 2D ABAQUS model.

4.3.1 Linear Drucker-Prager Model

In the 3D ABAQUS model, the linear Drucker-Prager model is used for concrete instate of Concrete Damage Plasticity because it is not available for 3D beam element. The Drucker-Prager model is considered to be one of the most simple plasticity models available for pressure dependent materials, with clear limitations in its application to reinforced concrete structures. This model incorporates isotopic hardening.

The nonlinear behaviour of concrete can be modelled using the concepts of classical plasticity, provided that an adequate yield function is introduced in order to reflect the different responses of concrete under tension and compression [89].

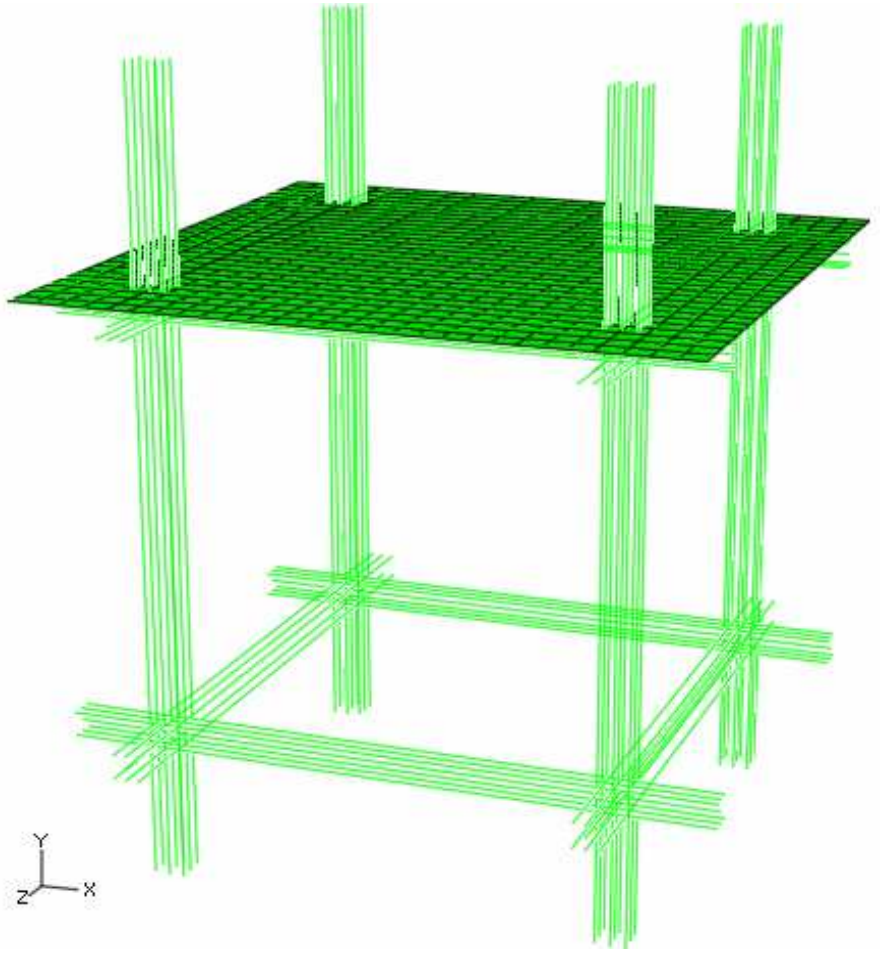

Figure 4-9 3D ABAQUS beam-shell element modelled using ABAQUS 6.8

The linear Druker-Prager criterion is based on the shape of the yield surface in the meridional plane, as shown in

Figure 4-10. It involves all three stress invariants. This material model provides for a possibly noncircular yield surface in the deviatoric plane. This matches the different yield values in triaxial tension and compression associated with inelastic flow in the deviatoric plane, and separate dilation and friction angles. Figure 4-11 illustrates the typical yield or flow surfaces of the linear mode in the deviatoric plane. To ensure the yield surface remains convex, the K value is derived as being between 0.778 and 1.0. The linear Drucker-Prager criterion is written as in Equation 4.1.

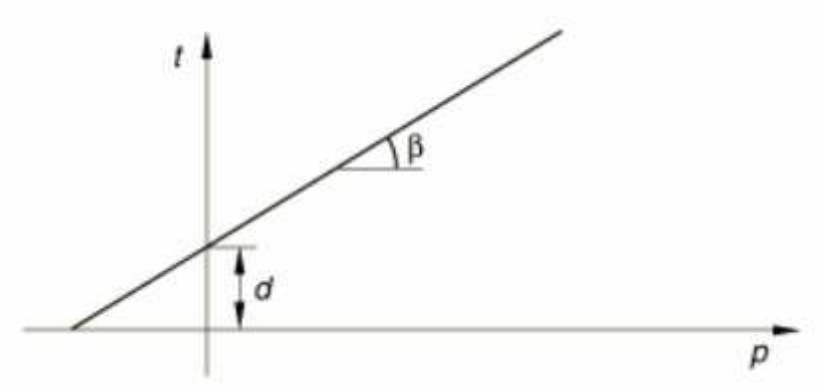

Figure 4-10 The p-t stress plane [Reproduced from 1]

$$F = t - p\tan\beta - d = 0 \tag{4.1}$$

$$G = t - p\tan\psi \tag{4.2}$$

Where:

F is linear Druker-Prager

$\beta(\theta, f_i)$ is the slope of the linear yield surface in the p-t stress plane; commonly known as the friction angle of the material;

d is the cohesion of the material;

G is flow potential;

$K(\theta, f_i)$ is the ratio of the yield stress in triaxial tension to the yield stress in triaxial compression;

$t = \frac{1}{2}\left[1 + \frac{1}{K} - \left(1 - \frac{1}{K}\right)\left(\frac{r}{q}\right)^3\right]$;

p = the equivalent pressure stress, $-\frac{1}{3}trace(\sigma)$;

$\psi(\theta, f_i)$ = the dilation angle in p-t plane

Plastic flow in the linear Drucker-Prager model is derived as in Equation 4.2. Where $\psi(\theta, f_i)$ is the dilation angle in the p-t plane.If the material model is in uniaxial compression, the linear yield criterion precludes friction angle, $\beta > 71.5^0$ and dilation angle, $\psi > 71.5^0$.

In the case of granular materials, the linear Drucker-Prager model is normally used with non-associated flow in the p-t plane. The flow is assumed to be normal to the yield surface in the deviatoric principal stress plane. The dilation angle, ψ, parallel to the t-axis in the p-t plane, is usually smaller than the friction angle, β, as shown in Figure 4-12.

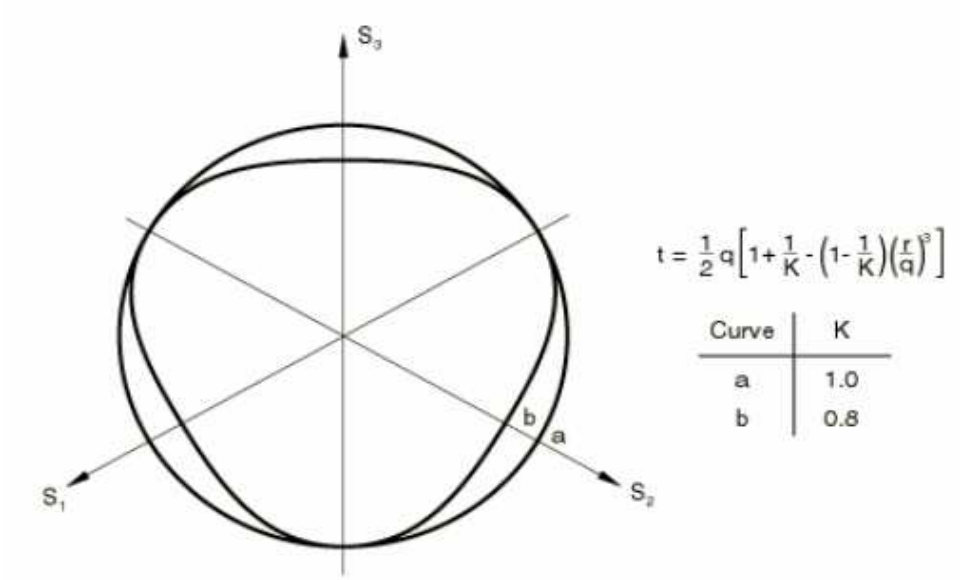

Figure 4-11 Illustrates the linear model in the deviatoric plane [Reproduced from 1]

4.3.2 Friction and Dilation Angle

The friction angle, β, can be derived using the Mohr Columb theory. In this study, the friction angle, β, is calculated by the ratio of the compressive strength to the tensile strength of the concrete (f_c / f_t). The dilation angles are more complicated and a value of half the friction angle has been widely used. In

this study, the ratio used for f_c / f_t is 10, therefore the friction angle, β, used is 55^o and the dilation angle, ψ, is 27.5^o.

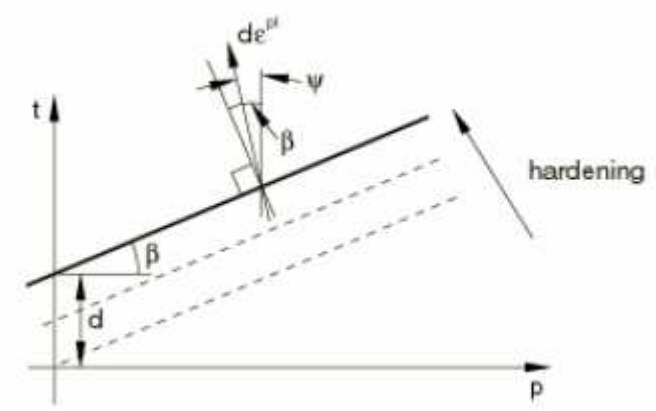

Figure 4-12 Yield surface and flow direction in the p-t plane for the linear Drucker-Prager model [Reproduced from 1]

4.4 2D OpenSees Model

The 2D ABAQUS model is compared with 2D OpenSees model which was developed by others team member of this project. The 2D OpenSees model is developed using nonlinear beam–column elements. The cross-section of the beam and the columns is modelled as double the size of the existing section to represent the full frame. The cross-section of the beam and column is shown in Figure 4-13. Pinching and stiffness degradation are considered in this model by using the uniaxial material model, Pinching4. This material model is used at both ends of the beams.

4.4.1 Pinching4 Damage Model

Figure 4-14 llustrates the hysteresis curve of the Pinching4 uniaxial material model. Degradation of the stiffness and strength are assumed due to the imposed load history. Two types of damage are defined: energy and cycle damage. In the case of damage due to displacement as well as energy effects,

the energy damage type is used. The cyclic damage type represents damage due to displacement as well as damage due to accumulated load cycles. This type is specified in this model.

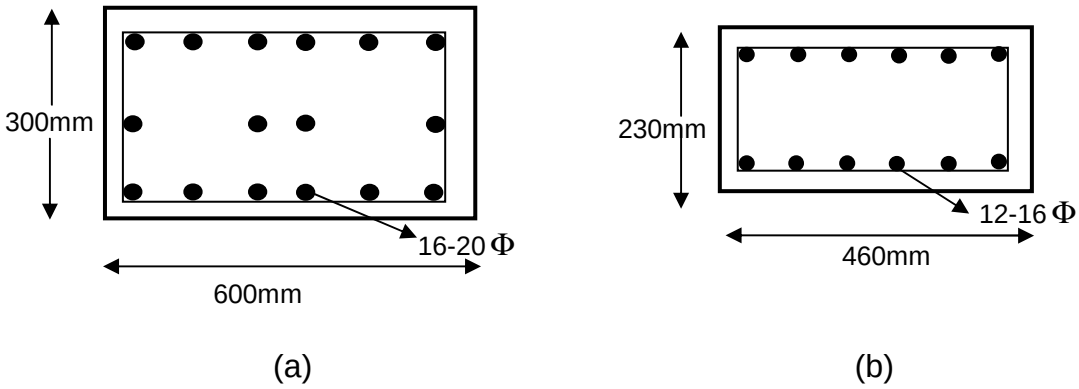

Figure 4-13The cross-section of the (a) column and (b) lower beam of the frame

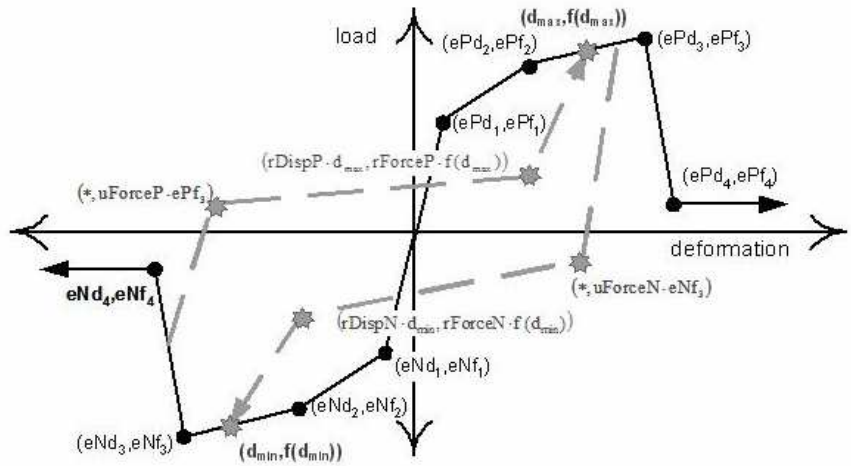

Figure 4-14 Hysteresis curve of Pinching4 uniaxial material model in OpenSees [Reproduced from 94]

4.5 Discussion and Conclusions

This chapter presents the numerical modelling of the Roorkee frame using ABAQUS and OpenSees. The 2D ABAQUS models were developed using ABAQUS and OpenSees, while the 3Dmodel was developed using ABAQUS only. It should be noted that the OpenSees model was developed by others team members of the project and only the results of obtained from the analysis is used for comparison purposes.

The concrete damage plasticity concrete model was used in the 2D ABAQUS model. Damage parameters were considered in order to take the effects of damage due to cyclic loading into account. This concrete model could not be used with 3D beam elements, therefore the Druker-Prager concrete model was used in the 3D ABAQUS model. It should be noted that a pinching effect in the reinforcing steel is not considered in these models.

In the 2D OpenSees model, the cyclic damage hysteresis was considered as the only factor that affected pinching development. The Pinching4 uniaxial material model was defined at the joints of the frame to represent this behaviour.

5

Simulation of The Response Due to Lateral Loading Using ABAQUS

5.1 Introduction

The behaviour of the frame subjected to lateral loading is numerically investigated. Cyclic analysis in the test was done by applying a lateral load to the frame using hydraulic jacks at the slab level as described in the previous Chapter. In the numerical modelling, the frame was subjected to lateral loading in displacement control mode to generate hysteretic behaviour of the frame.

This chapter presents the numerical analysis of the Roorkee Frame Test 1 using ABAQUS. The results have been compared with the test and with OpenSees [91,92,120]. The OpenSees analyses have been developed by another team working on this project [91, 120].

5.2 Analysis

The capacity of the frame is investigated using the static pushover analysis method. The frame was subjected to a monotonically increasing pattern of lateral displacements and the base shear was calculated.

Based on the target displacement obtained from this analysis, increasing displacement loading over seven cycles was used to simulate earthquake damage. Cyclic loading in the test was achieved by applying a lateral load to the frame using a hydraulic jack at the slab level in load control mode. However, in the numerical simulation, the frame was subjected to equivalent cyclic lateral displacements in displacement control mode.

The displacement history used in the numerical analyses was obtained by idealising the displacement history from Test 1 as shown in Figure 5-1 and Figure 5-2, respectively. A step-by-step procedure was used to increase the displacement applied to reach the target displacement in the positive x-direction (95mm) and in the negative x-direction (80mm). Table 5-1 shows the displacement applied at any particular time step. After the target displacement was applied the frame was released from any lateral restraint resulting in zero base shear.

Table 5-1 Displacement history used in cyclic analysis

Time	Displacement Applied (mm)
0	-19
10	19
20	-30
30	35
40	-39

50	49.8
60	-61
70	68.8
80	-79.6
90	95
100	Released boundary at slab level

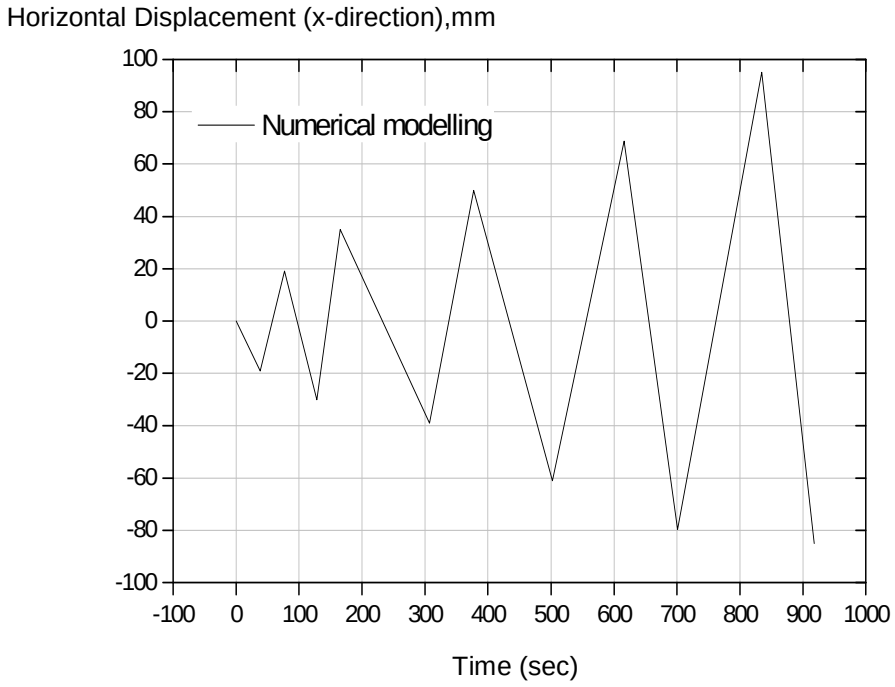

Figure 5-1 History of imposed lateral displacement on the frame used in numerical analysis

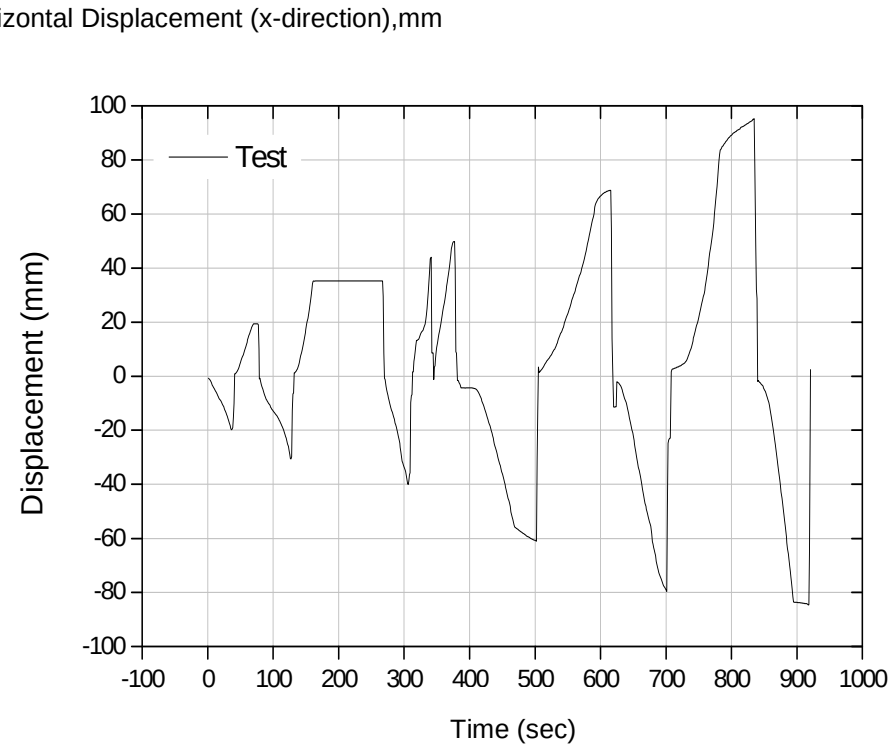

Figure 5-2 History of imposed lateral displacement on the frame from the Test 1 [Reproduced from 120]

5.3 Analysis of results

5.3.1 Capacity curve of the frame

The capacity curves obtained from numerical modelling and from the test were compared. Figure 5-3 shows the pushover analysis of the 2D ABAQUS model compared with the Roorkee frame test. The base shear of the 2D ABAQUS model is higher than the test result at a lower displacement. When the loading is increased from 20mm to 75mm the strength of the frame obtained from the 2D ABAQUS model is between 10% and 15%. At the target displacement of 76mm and above, the curve remained flat.The capacity curve obtained from the 3D ABAQUS model is shown in Figure 5-4. Both the 3D ABAQUS model and the test data shows similar base shear at displacements of less than 15mm. At larger displacements the base shear obtained from the 3D ABAQUS model is higher than the test data. The maximum base shear of the frame subjected to

cyclic loading from the 3D ABAQUS model is 317kN, while the test value is 315kN.

The capacity curve illustrated the nonlinear response of the frame under lateral displacement. From Figure 5-3 and Figure 5-4, it is seen that the frame behaved elastically until the displacement was 20mm. The numerical model response is almost identical to the test result except it is a bit higher than the test frame at the larger displacements.

Figure 5-5 shows the capacity curve for the 2D ABAQUS and OpenSees models, compared with the test data. The 2D ABAQUS model shows a higher capacity compared with results obtained from the OpenSees model. For the OpenSees model, the base shear for the frame is close to the test result up to 60mm displacement and is 5%-15% lower at higher displacements.

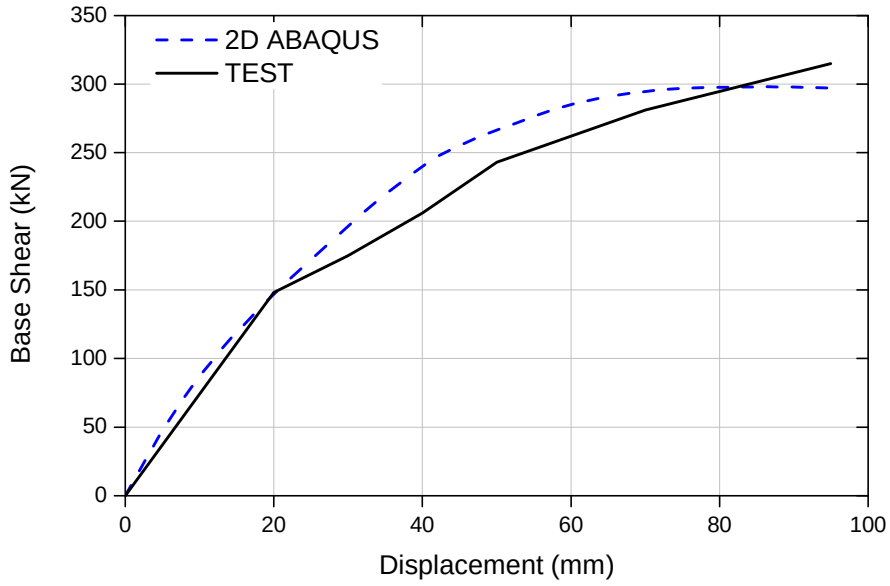

Figure 5-3 Capacity curve from 2D ABAQUS model and the test

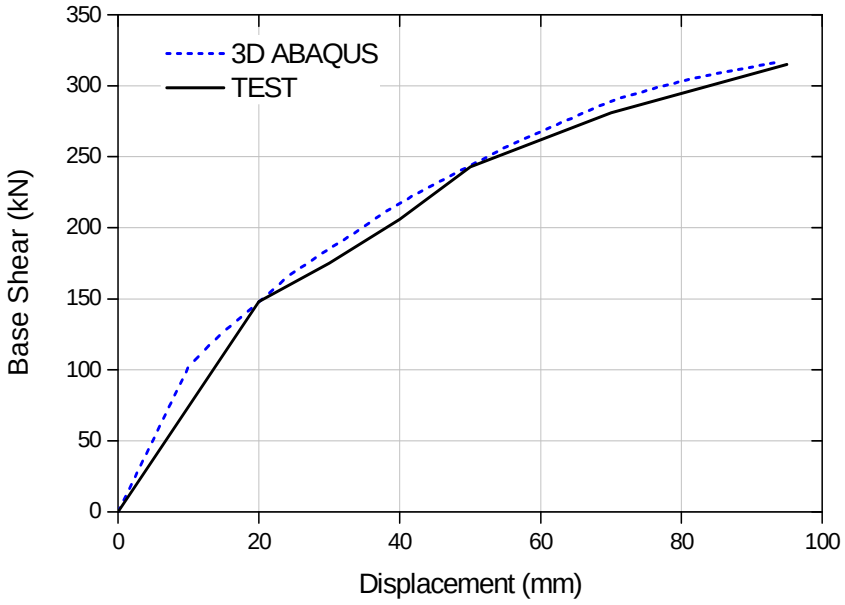

Figure 5-4 Capacity curve of 3D ABAQUS model and the test

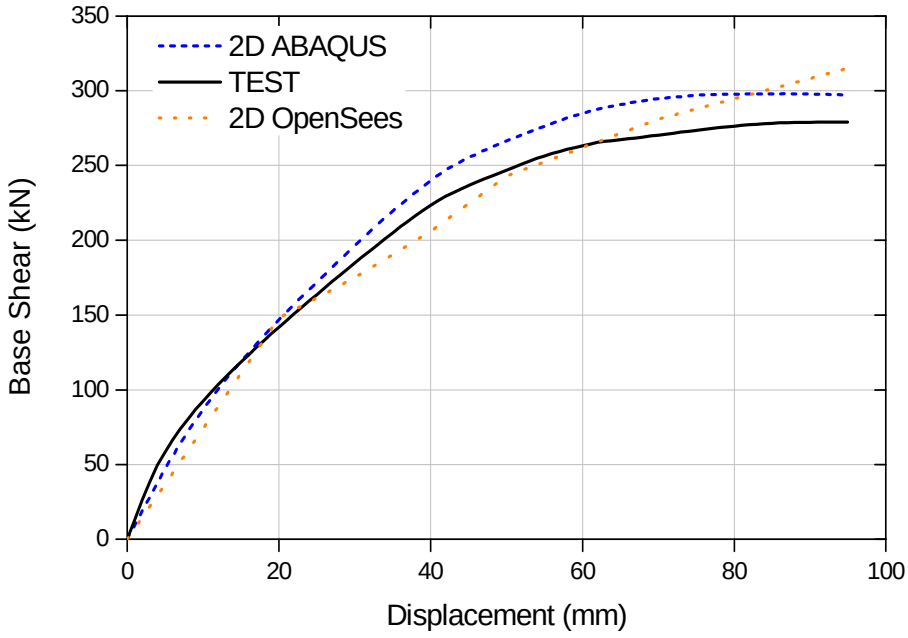

Figure 5-5 Capacity curve of 2D ABAQUS model, OpenSees and the test

Deformation shape of the frame under gravity loading is shown in Figure 5-6. The magnitude deformation of the frame is dominant in the first floor where the loading calculated from slab and from the upper stories.

Figure 5-8 and Figure 5-8 and show the progress of deformation damage of the frame on gravity loading, and during the monotonic loading. The figures clearly show that the maximum plastic strain (PE) in the frame occurs in the beam prior in the column. Hence, the frame has strong column and weak beam behaviour when subjected to lateral loading.

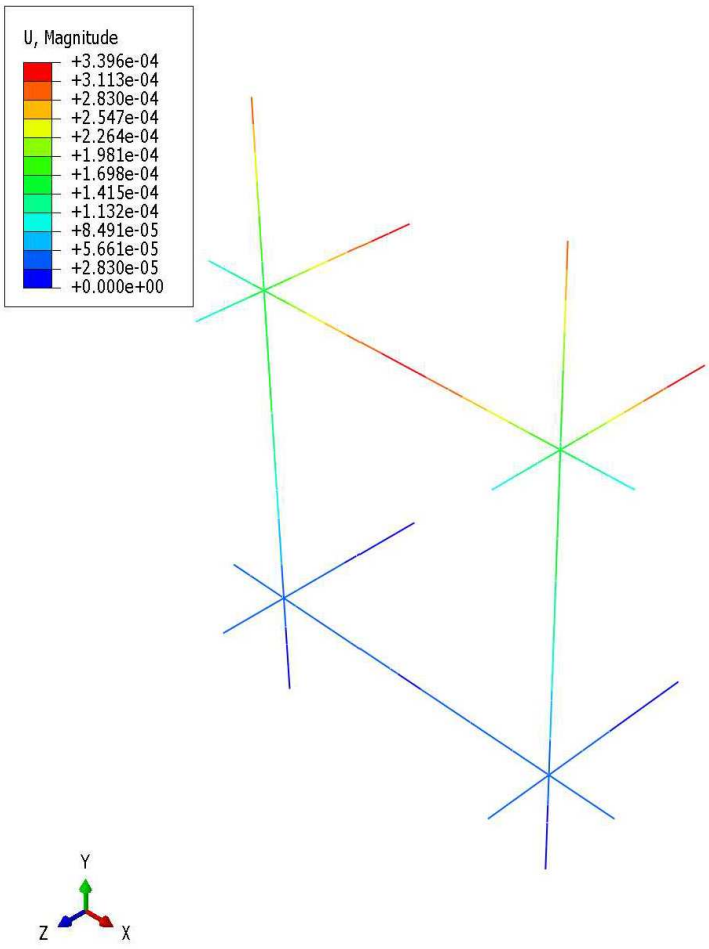

Figure 5-6 Illustration of the deformation of the frame under gravity loading

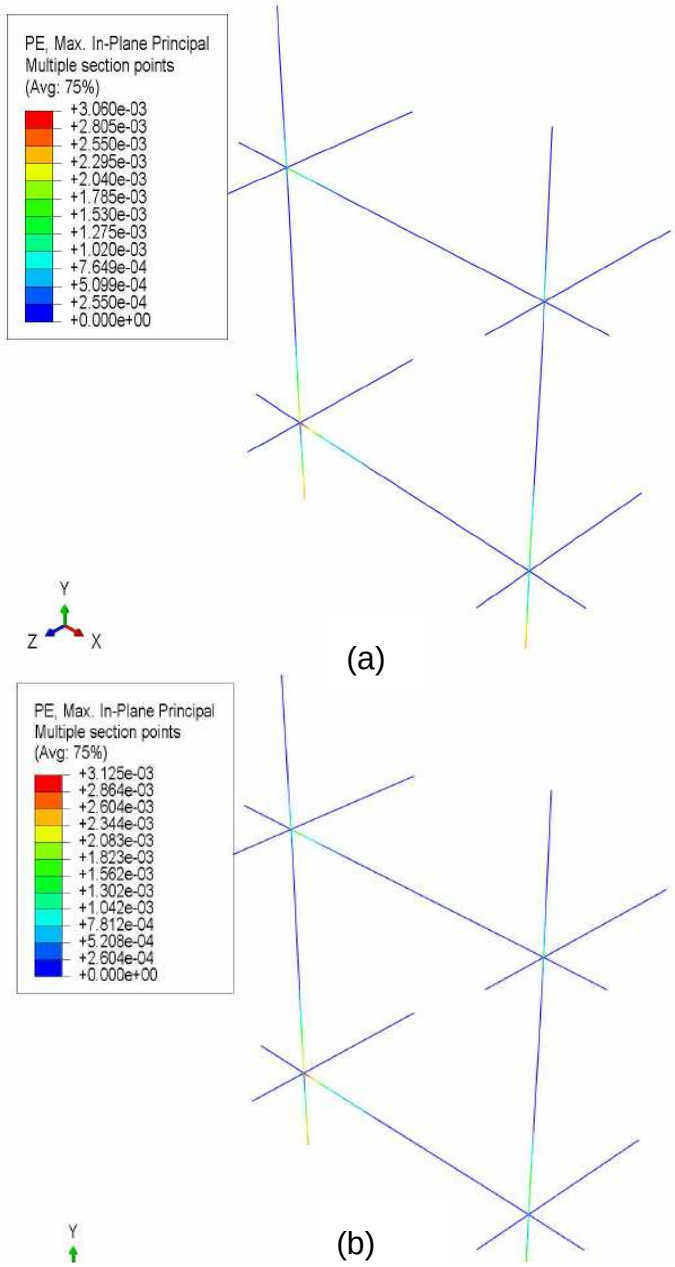

Figure 5-7 Illustration of the strain of the frame during at (a) monotonic loading=10mm (b) monotonic loading=50mm (push in positive x-direction)

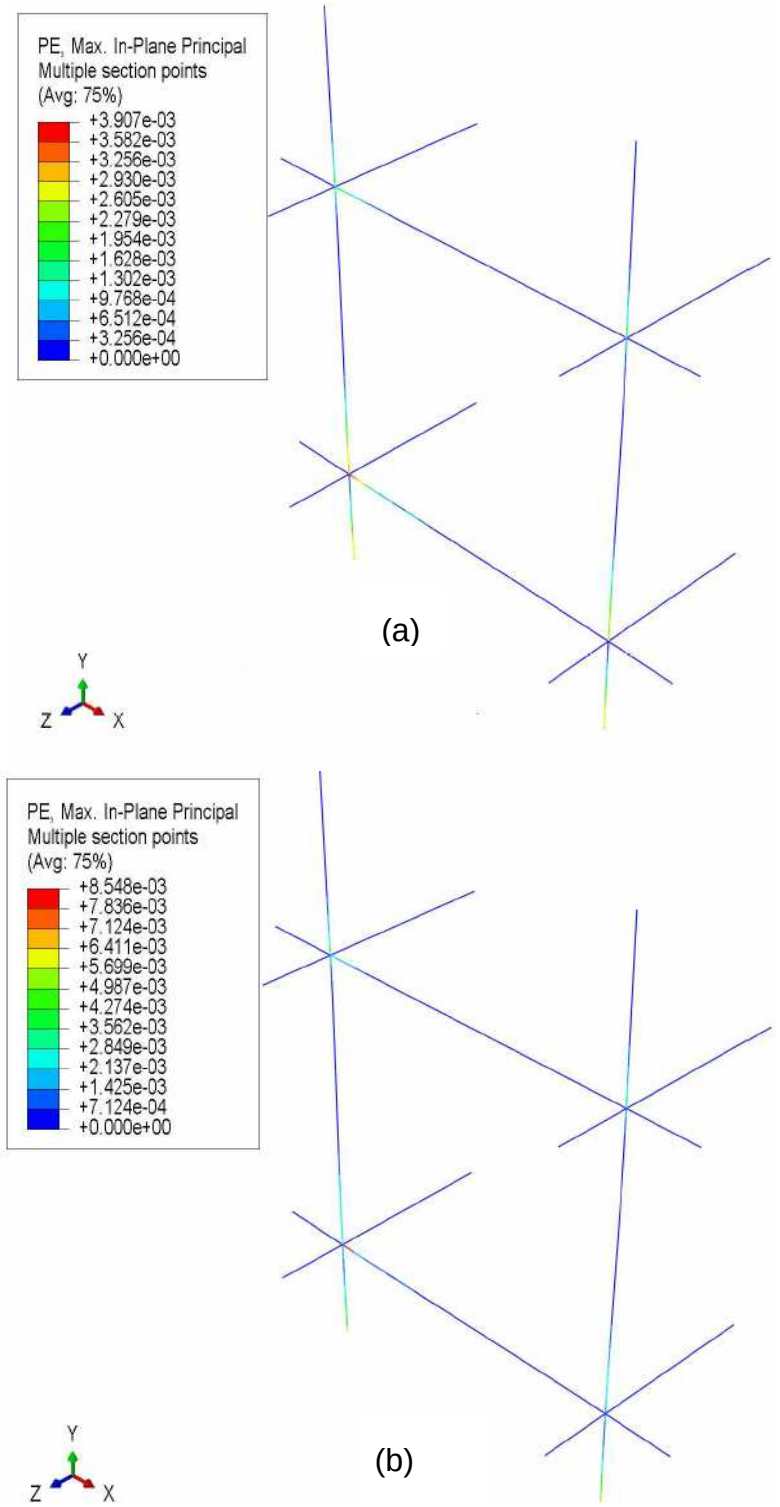

Figure 5-8 Illustration of the strain of the frame during at (a) monotonic loading=75mm (b) monotonic loading= 100mm (push in positive x-direction)

5.3.2 Cyclic lateral displacement loadings

The hysteresis curve of the ABAQUS models as compared to the test results are shown in Figure 5-9 and Figure 5-10. From the figures, the ABAQUS models show the strength envelope, or capacity curve, precisely. However, when the deformation increases, the area under the loop varies dramatically. As expected, the pinching type effect is absent in the ABAQUS models, as this is not taken into consideration (as discussed in the previous chapter). This is clearly described that bond slip is not considered in the modelling.

The Drucker-Prager model used in the 3D ABAQUS model gives a more reliable hysteresis curve compared to the concrete damage plasticity one used in the 2D ABAQUS model. The 3D ABAQUS model behaves similarly to the Roorkee frame test at low displacement loading as shown in Figure 5-10. Base shear from the loading path of the 3D ABAQUS model is 8% to 10% higher than the test result value. However, for the unloading path the ABAQUS models give significantly different values compared to the test result (15% to 25%). The relative displacement obtained from the 3D ABAQUS model is more reliable compared to the 2D ABAQUS model.

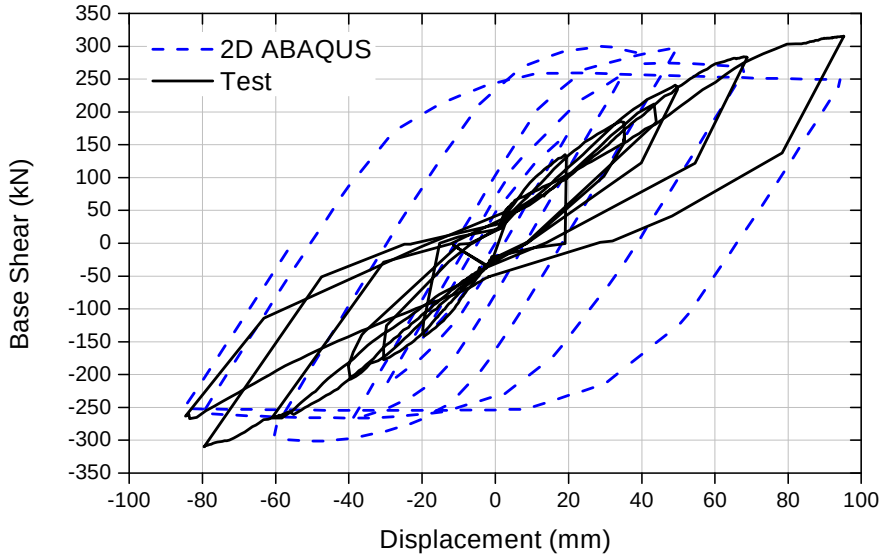

Figure 5-9 Hysteresis curve of 2D ABAQUS model and the test

The area under the curve represents the hysteretic dissipated energy obtained from the numerical simulation and test results. The hysteretic dissipated energy is similar for both the numerical simulation and the test when the deformation is small. Table 5-2 shows the area under the curve for the ABAQUS models and the test.

The 2D ABAQUS model gives about two times of the area under hysteresis curve and the 3D ABAQUS model gives about 20% higher than the test result.

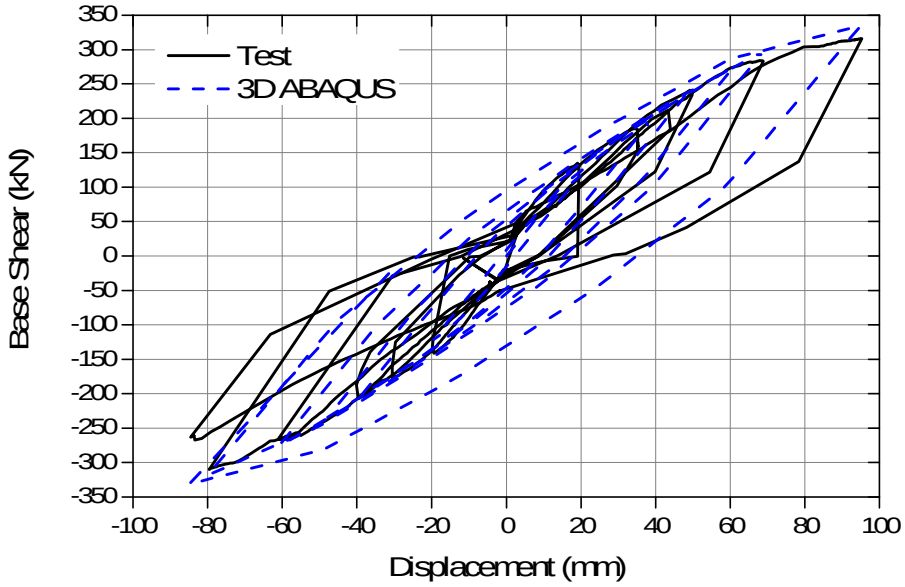

Figure 5-10 Hysteresis curve of 3D ABAQUS model and the test

Table 5-2 Area under the curve of ABAQUS models and the test

Analysis Types	Test	ABAQUS Models	
		2D	3D
Area under the curve, x10^4 Joule (J)	5.4	13	6.5

Figure 5-11 shows the hysteresis curve obtained from ABAQUS and OpenSees for the 2D model. The pinching effect is obvious in the data from the OpenSees model due to the material pinching behavior used in the analysis. The material model used in the analysis is capable of simulating the hysteresis behaviour of the reinforced concrete frame due to cyclic loading and unloading. Nevertheless, at higher displacements, the base shear obtained from the OpenSees model is 17% higher than the base shear obtained in the test.

Table 5.3 shows the area under the hysteresis curve from the ABAQUS and OpenSees models. The energy dissipation obtained from the OpenSees model is lower than the test result. However the dissipated energy from the ABAQUS model is twice the test result. The OpenSees model has underestimated the dissipated energy of the reinforced concrete frame under cyclic load, while the ABAQUS models give the opposite result.

Deformed shape of the frame taken from the numerical models are shown in

Figure 5-12 and Figure 5-13. These figures show the deformation of the frame at the final displacement step plotted using a magnification factor of 5.

Table 5-3 Area under the hysteretic loop of 2D ABAQUS and OpenSees 2D model

Computational Software	Area under the curve, ($x10^4$)Joule (J)
ABAQUS 6.8	13
OpenSees	3

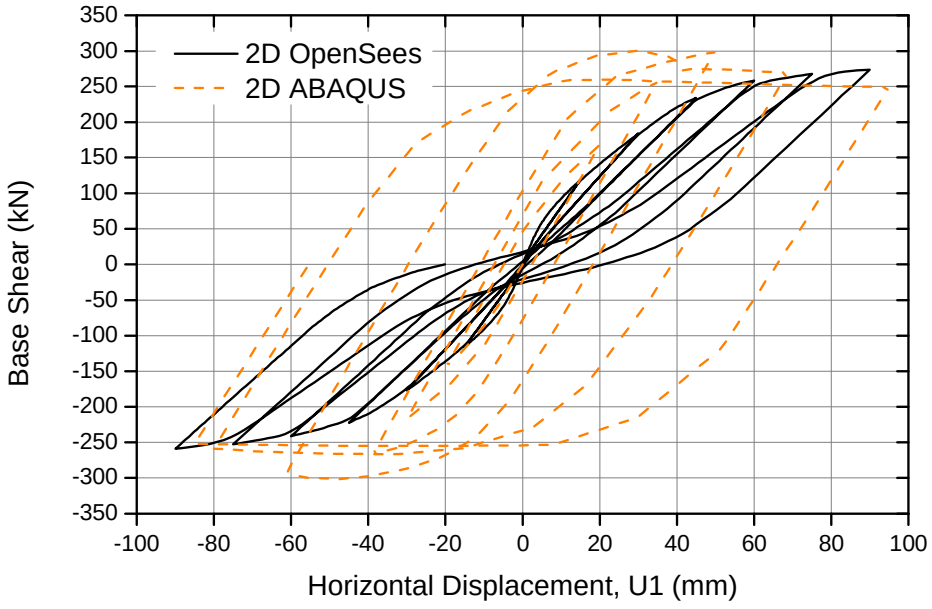

Figure 5-11 Hysteresis curve of 2D model using ABAQUS and OpenSees

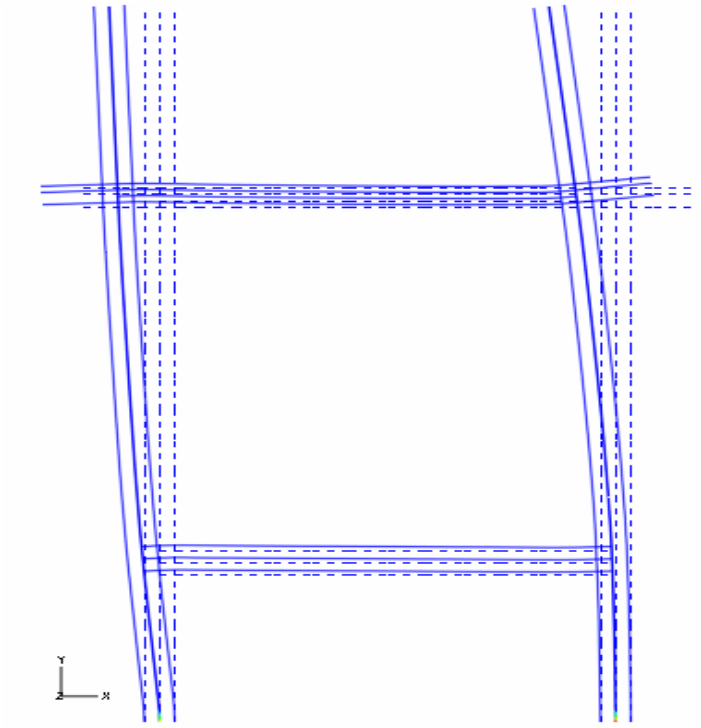

Figure 5-12 Deformation shape of the frame from 2D ABAQUS model

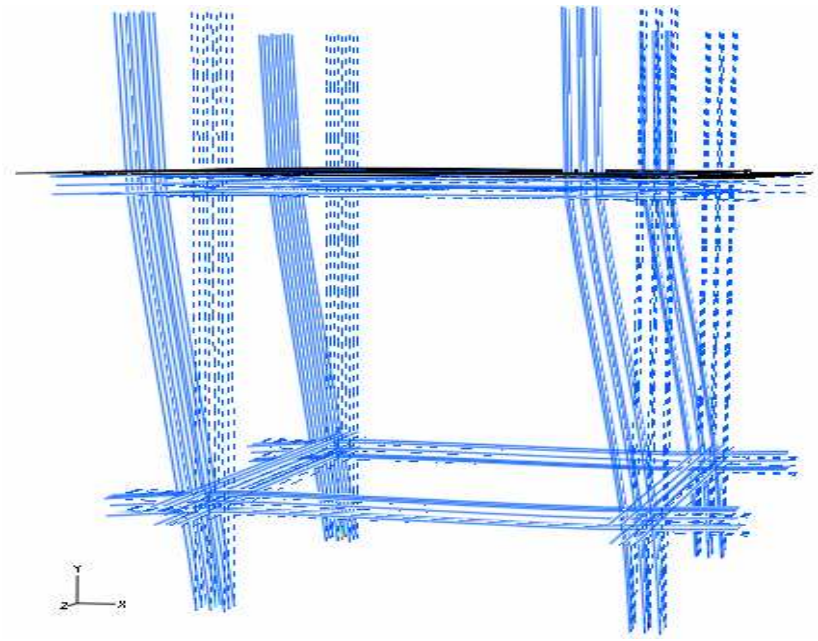

Figure 5-13 Deformation shape of the frame from 3D ABAQUS model

5.4 Conclusion

A full 2D ABAQUS model using beam elements, and 3D ABAQUS model using beam and shell elements, has been analysed and compared with available test data and OpenSees simulation. Concrete damage plasticity has been used for modelling the concrete of the frame in 2D and the Drucker-Prager concrete model is implemented in 3D. Both of these models do not consider the pinching effect in the reinforcing steel.

Pushover analysis has been performed to represent the displacement of the frame when subjected to lateral loading. Initially the base shear from the test is higher than that predicted in the numerical analysis. The maximum displacement obtained from both analyses is 95mm and it is used as the target displacement in the cyclic analysis.

In general, there was a correlation between the numerical and test data for the target displacement from monotonic loading analysis.

Based on the target displacement obtained from the pushover analysis, seven cyclic lateral displacements were considered to simulate damage from an earthquake. The ABAQUS models were capable of presenting the strength and stiffness degradation of the frame during the cyclic loading. The residual displacement observed at the slab level from the 2D and 3D ABAQUS models, the OpenSees model and the test result was 55mm, 27mm, 19mm and 19mm respectively. ABAQUS models gave higher residual displacements compared to the test and OpenSees results. This shows that the models developed in ABAQUS were less elastic compared to the real frame. The pinching effect is obviously shown in the capacity curve plotted from the test and the OpenSees model. Neither of the ABAQUS models with the concrete damage plasticity nor

the Drucker-Prager material models showed pinching due to progressive degradation upon repeated lateral loading.

Table 5-4 shows the area under the hysteresis curve calculated from the ABAQUS models and the test. The hysteresis dissipated energy shows that the 2D ABAQUS models under small deformation (30mm) gave about 20% lower values than the test result. The 3D ABAQUS model gives values higher than the test results. At higher displacements the dissipated energy obtained from ABAQUS is higher than the test value. The 3D ABAQUS model gives much better results compared to the 2D ABAQUS model.

Table 5-4 Area under the hysteresis curve

Analysis Type	Small deformation (<30mm)	Large deformation (80mm)
Roorkee Frame Test 1	6.7×10^3 Joule	5.4×10^4 Joule
2D ABAQUS	5.5×10^3 Joule	13.1×10^4 Joule
3D ABAQUS	2.9×10^3 Joule	6.5×10^4 Joule

6

Simulation of The Response Due to Fire Loading Using ABAQUS

6.1 Introduction

The purpose of performing heat transfer analyses is to numerically estimate how much heat is transferred between a fire, the fire gases, the fuel bed and the surfaces in an enclosure. This is essential to gain knowledge of the temperature distribution in the elements during a fire.

In this study the numerical heat transfer analysis was performed based on the gas temperatures obtained from fire tests done in the Indian Institute of Technology (IIT) Roorkee in 2009 [120].The temperature distribution data obtained using ABAQUS 6.8 was compared and discussed with the test data.

6.2 Fire test

The fire duration used in this study was one hour, with flashover occurring in less than 5 minutes, and the post flashover temperature reaching 900^{o}C to

1000^{o}C. Preliminary design of the fire was done by Prof. Jose Torero from University of Edinburgh. Pre-testing of the compartment fire was done in IIT Roorkee to determine the desired fire design parameters.

In the fire test, a brick masonry compartment of size 3.0 x 3.0 x 3.0 m was constructed. To obtain fast flashover (less than 5 minutes), it is important to make sure that the smoke accumulates rapidly and heats up the compartment quickly. Therefore, the compartment was designed with a 1m high ventilation opening along the full length of one side of the compartment. The fire compartment was continuously fed by a 1.0m x 1.0m tray of kerosene. To maintain the design fire post flashover with the chosen ventilation opening, a peak burning rate of 0.117kg/m^{2}s and peak fuel flow rate of 1.43x10-4m^3/s is required.

Three rod mineral insulated (MI) steel thermocouples of 6.0mm diameter were positioned vertically in the compartment to capture the gas temperatures. Figure 6-1 shows the constructed brick compartment on site. The locations of thermocouples are detailed in

Figure 6-2.

The gas temperatures within the compartment were measured using thermocouples at four different heights from the floor level of the compartment. Each plan location consisted of five MI thermocouples at elevations of 0.90 m, 1.60 m, 2.30 m and 2.90 m from the floor level of the compartment, which equate to the notation of TMRA1, TMRA2, TMRA3 and TMRA4 respectively, in the temperature-time curve, as shown in Figure 6-3, Figure 6-4 and Figure 6-5. No heat flux gauges were installed during the fire test, therefore only the

compartment temperatures obtained from the thermocouples at various heights detailed above were recorded.

Figure 6-1 Set-up of a brick masonry with a pool fire for test [Reproduced from 120]

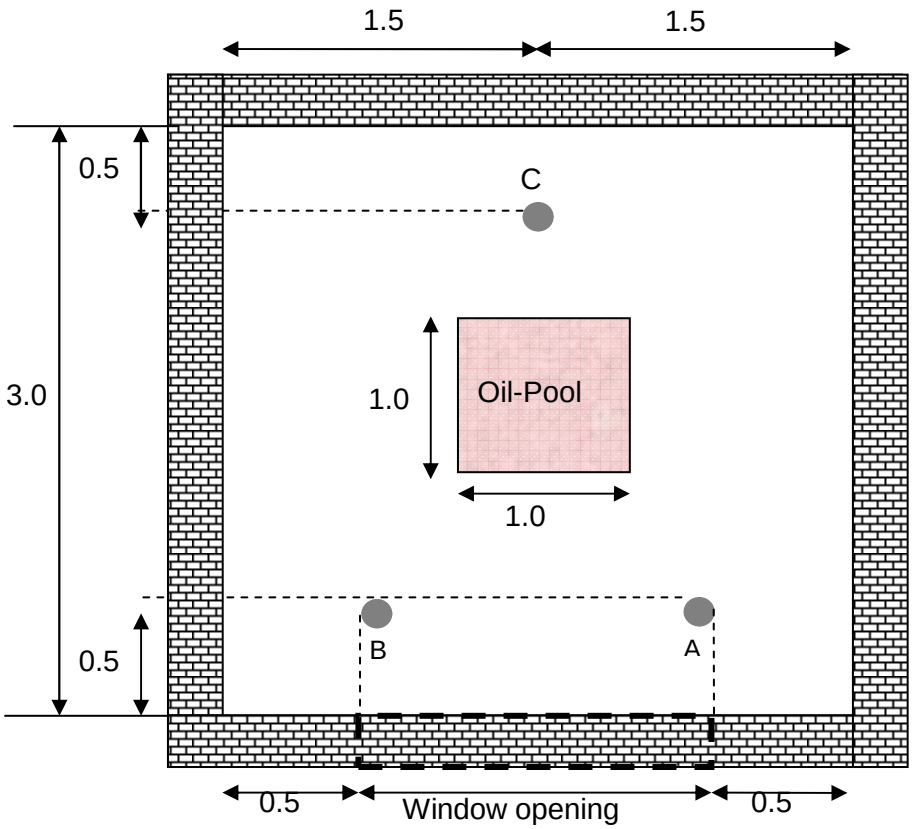

Figure 6-2 Plan view of brick compartment

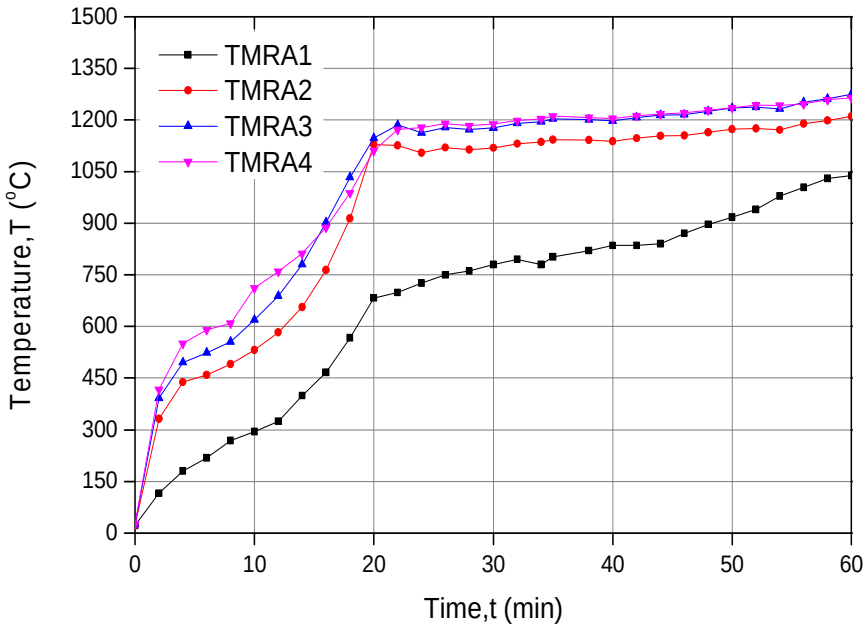

Figure 6-3 Gas temperature curve of M1 thermocouple at A (TMRA) [Reproduced from 120]

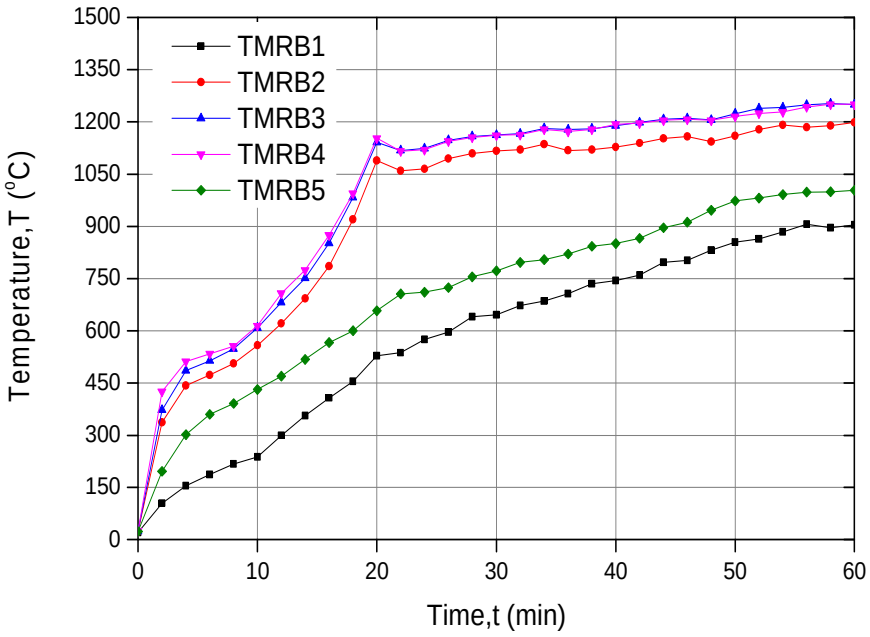

Figure 6-4 Gas temperature curve of M1 thermocouple at B (TMRB) [Reproduced from 120]

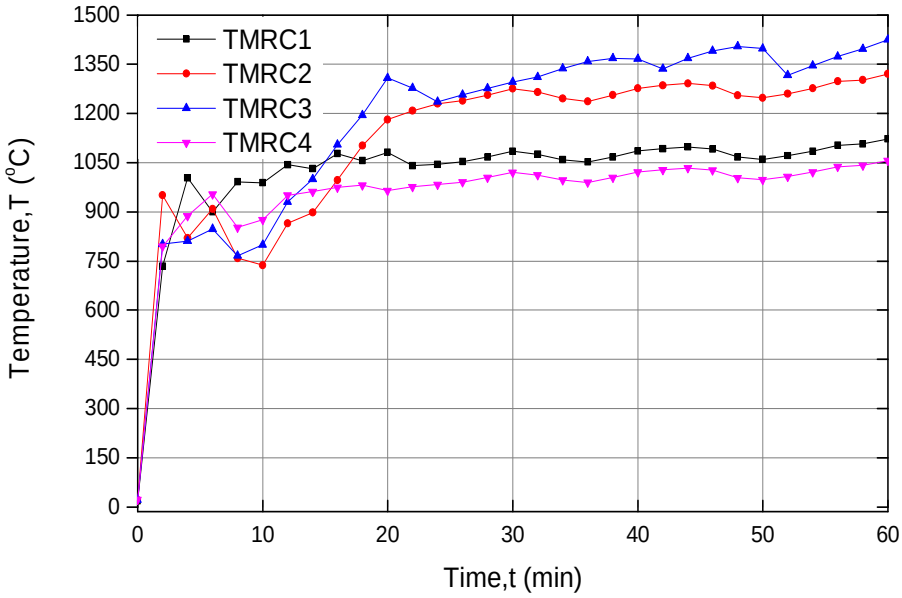

Figure 6-5 Gas temperature curve of M1 thermocouple at C (TMRC) [Reproduced from 120]

6.3 Numerical Heat Transfer Analysis

The heat transfer analysis was performed using ABAQUS version 6.8 [1] to get the temperature distribution through the elements of the frame. 3D continuum elements (DC3D8) were used to model the frame. Figure 6-6 shows the configuration of the continuum frame modelled for heat transfer analysis in ABAQUS.

Fire growth occurs in the compartment due to heat transfer to other combustible material, which is modelled in ABAQUS by means of convection and radiation. Babraukas [7] showed in his study that heat transfer with radiation mode effect is dominant when the pool diameter is 1.0 m or bigger. Table 6-1 shows the relationship between the fire pool size and burning mode. The maximum heat release rate (HRR) based on the experimental data by Babrauskas [6] is shown in Equation 6.1.

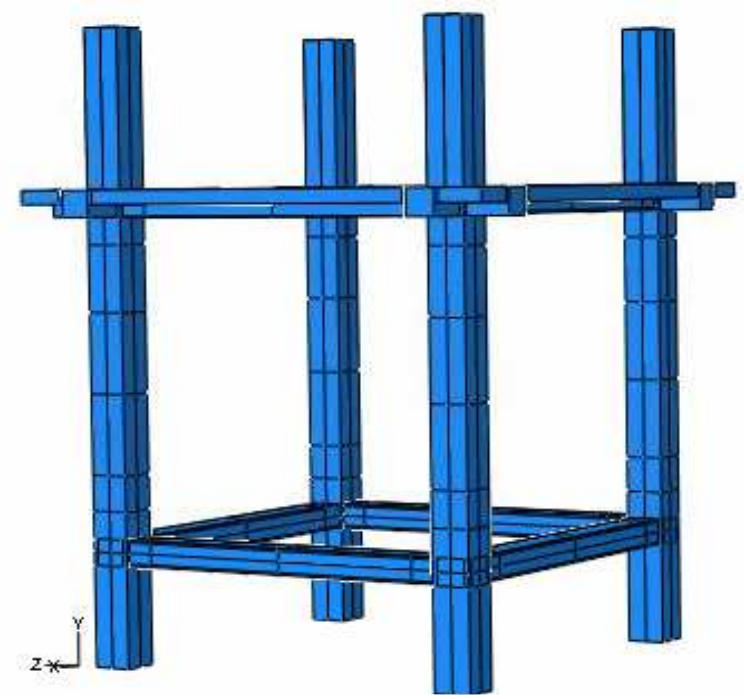

Figure 6-6 3D Continuum frame modelled in ABAQUS version 6.8

One type of radiation is known as thermal radiation. This is electromagnetic energy occurring at wavelengths from 2μm to 16μm. This is the net result of radiation emitted by radiating substances, such as water (H_2O), carbon dioxide (CO_2) and soot in the flame. Thermal radiation is the most significant mode of heat transfer in situations in which a target is located laterally to the fire source exposure. The radiated heat is transferred directly to nearby objects.

Table 6-1 Summarised burning mode according to diameter by Babrauskas [Reproduce from 7]

Pool Fire diameter (m)	Burning Mode
<0.05	Convective, laminar
<0.2	Convective, turbulent
0.2 to 1.0	Radiative, optically thin
>1.0	Radiative, optically thick

$$\dot{Q} = \dot{m}'' \Delta H_{c,eff} A_f (1 - e^{-k\beta D}) \quad (6.1)$$

Where:

Q =heat release rate (HRR) of the fire (kW);

m'' =burning or mass loss rate per unit area per unit time (kg/m^2-sec);

$\Delta H_{c,eff}$ =effective heat of combustion (kJ/kg);

A_f =horizontal burning area of the fuel (m^2);

$\kappa\beta$ =empirical constant (m^{-1});

D= diameter of burning area (m), $\sqrt{\frac{4A_f}{\pi}}$ for non-circular pools.

Flame height (H_f) typically depends on the flame being either laminar (short) or turbulent (tall). Equations 6.2 and 6.3 defined by Heskestad [55] and Thomas and Heselden [122] are widely used to determine the flame height of pool fires.

$$H_f = 0.235\dot{Q}^{\frac{2}{5}} - 1.02D \quad (6.2)$$

$$H_f = 42D\left(\frac{\dot{m}''}{\rho_a\sqrt{gD}}\right) \quad (6.3)$$

Where:

H_f =flame height (m);

Q =heat release rate (HRR) of the fire (kW);

D = diameter of burning area (m);

m'' =burning or mass loss rate per unit area per unit time (kg/m^2-sec);

ρ_a =ambient air density (kg/m^3);

g =gravitational acceleration (m/sec^2).

When heat transfer in radiation mode is analysed using ABAQUS the emissivity, ε, must be defined. In reality combustion gases are complex in terms of their radiative properties, due to the presence of gases, H_20 and $C0_2$, which radiate discretely over wavelength bands that can overlap, while soot radiates continuously over a wide range of wavelengths. Hottle [57] developed an emittance chart, as shown in

Figure 6-7, which was derived as an approach to compute the total emissivity of H_20 and $C0_2$. The chart is based on temperatures over the path length and concentration of gases, and is expressed in partial pressure.

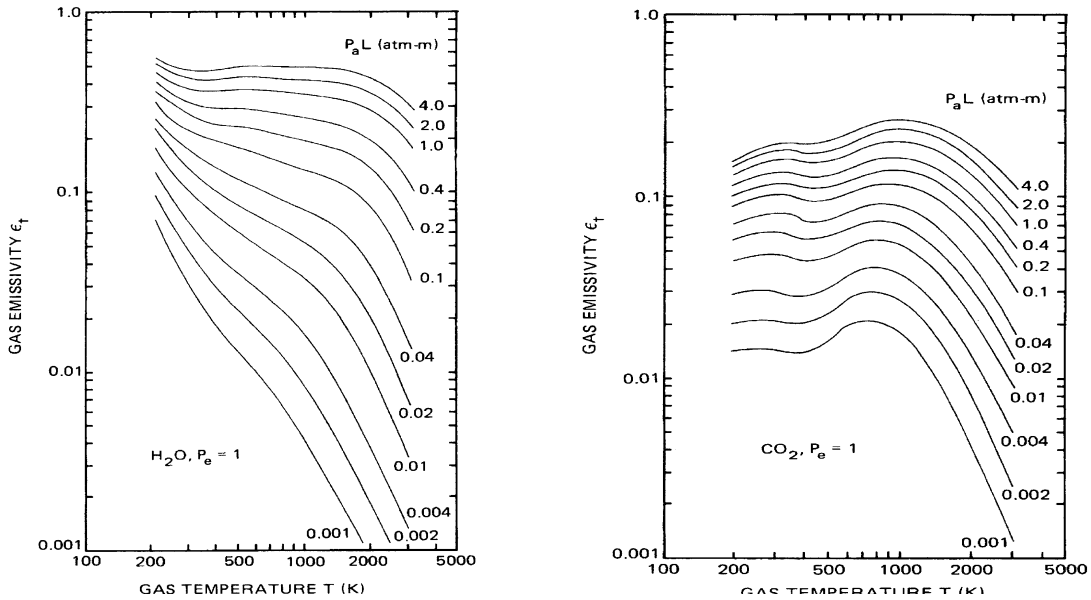

Figure 6-7 Total emittance of (a) water vapour (H_2O) and (b) carbon dioxide (CO_2) [Reproduced from 57]

Tien et al. [126] present the approximation of emissivity due to H_20 and $C0_2$, as shown in Equation 6.4.

$$\varepsilon = \varepsilon_{H_2O} + \varepsilon_{CO_2+[correctionfactorduetooverlapwavelenght]} \quad (6.4)$$

Equation 6.5 represents the total emissivity between two species (1 and 2) where the absorption coefficients are known.

$$\varepsilon_{1+2} = \frac{1}{\sigma T^4}\left\{\int_0^\infty E_{b,\lambda}\left[(1-e^{-\kappa_{\lambda,1}L}) + (1-e^{-\kappa_{\lambda,2}L}) - (1-e^{-\kappa_{\lambda,1}L})+(1-e^{-\kappa_{\lambda,2}L})\right]d\lambda\right\} \quad (6.5)$$

If grey gas approximations are used for each species, the emissivity equation can be calculated by using Equation 6.6, as shown below.

$$\varepsilon \equiv \frac{\int_0^\infty (1-e^{-\kappa_{\lambda,1}L})E_{b,\lambda}d\lambda}{\sigma T^4} \approx 1-e^{-\kappa_1 L} \quad (6.6)$$

When the grey gas approximation of $k_{\lambda,1}$ is altered, then the total emissivity between two species is as in Equation 6.7.

$$\varepsilon_{1+2} = \varepsilon_1 + \varepsilon_2 + \varepsilon_1\varepsilon_2 \quad (6.7)$$

Equation 6.7 is the based on Equation 6.4. This equation serves to combine the soot, ε_s and gas, ε_g contribution to the flame and smoke radiation, for instance, as in Equation 6.8.

$$\varepsilon \approx \varepsilon_g + \varepsilon_s + \varepsilon_g\varepsilon_s \quad (6.8)$$

In a compartment smoke layer, the products of H_20 and $C0_2$ can contribute about ε_g ~0.3 and ε_s ranging from nil to 0.7, taking the total ε up to a maximum of 1.0. The total ε depends on the path length, if long enough, it can make ε the maximum value of 1.0.

According to Babraukas, the emissivity is derived as in Equation 6.9.

$$\varepsilon = (1 - e^{-\kappa\beta D}) \tag{6.9}$$

The equation consists of an extinction coefficient, κ, a 'mean beam length corrector', β and D, the diameter of the pool fire. This value is defined depending on the fuel type used in the pool fire.

According to the parameters of kerosene, as shown in Table 6.2, the emissivity in the whole compartment calculated using Equation 6.9 is 0.9829.

Table 6-2 Kerosene parameter estimation for large pool burning rate [19,76]

Oil type	Density (kg/m3)	Mass loss rate, $m\&''$	Δh_g (kJ/kg)	Heat of Combustion Δh_C ,(MJ/kg)	Empirical Constant $\kappa\beta$,(m^{-1})	κ (m^{-1})	T_f (K)
Kerosene	820	0.039 (± 0.003)	670	43.2	3.5 (± 0.8)	2.6	1480

6.3.1 Heat Transfer Parameter Using in ABAQUS

Heat fluxes onto the frame surfaces are assumed to be dominated by convection and radiation. The convective mechanism in this study used a convection heat transfer coefficient, h_f of 25kW/m^2. This is a typical value used in structural fire analysis. The radiation mode is affected by the soot height in the compartment fire. In this study, the soot height is considered to vary, in order to estimate the emissivity value of the frame exposed to the fire.

The compartment was designed based on the assumption of the smoke layer that might occur during the fire. Figure 6-8 The well-mixed case: An enclosure with uniform temperature, T_g, which is higher than the outside temperature, T_a [Reproduced from 73]shows the behaviour of the smoke in a well-mixed case. From the figure, the height of smoke and air flow can be estimated using Equation 6.10 by Klote and Milke [73].

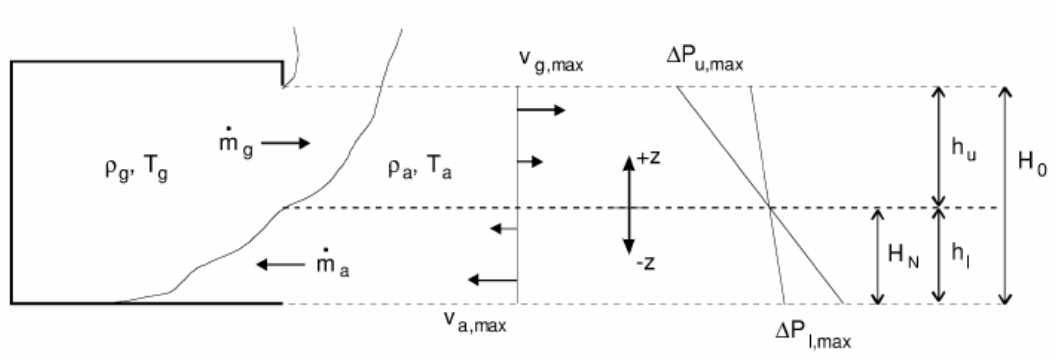

Figure 6-8 The well-mixed case: An enclosure with uniform temperature, T_g, which is higher than the outside temperature, T_a [Reproduced from 73]

Where:

ρ_g is density of gas in enclosure;

ρ_a is density of gas at ambient ;

T_g is temperature in enclosure;

T_a is ambient temperature;

$\dot{m}_a$ is mass of the gas at ambient temperature;

$\dot{m}_g$ is mass of the gas in enclosure;

H_0 is opening of enclosure;

H_N is reference height of the gas;

h_u is height of outgoing gas;

h_1 is height of incoming gas .

Equation 6.10 shows how to calculate the value of h_1 in the well-mixed case. If the reference point is the bottom of the opening, then $H_N = h_1$ [73].

$$h_1 = \frac{H_0}{1+\left(\frac{\rho_a}{\rho_g}\right)^{1/3}} \tag{6.10}$$

Welty et al. [133] derived Equation 6.11 to relate temperature to density.

$$T = \frac{353}{\rho} \tag{6.11}$$

Where:

T=temperature in Kelvin [K];.

ρ =density in [kg/m^3].

Based on the frame configuration used in this study, values of $T_g = 1400^0 C$ and $T_a = 20^0 C$ are derived. Therefore, $H_N = h_i = 0.357m$, according to Equation 6.10. The compartment of the frame in this study is divided into three areas, as shown in Figure 6-9.

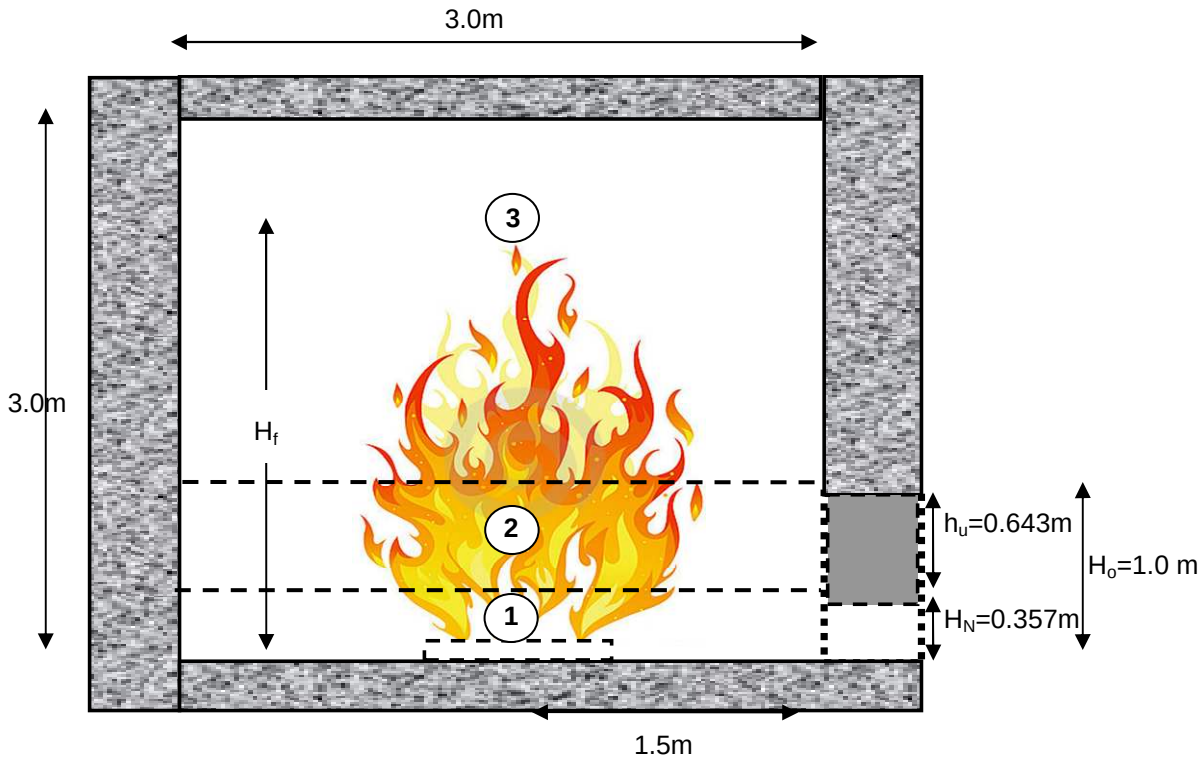

Figure 6-9 Compartment fire modelled in ABAQUS 6.8

From Figure 6-9 area number 3 is assumed to be filled with smoke. Area number 2 has smoke only in its upper region. Area number 1 is assumed to contain little smoke.

The limited information from the fire test means some assumptions must be made for the numerical analysis. The assumptions are made based on the information gained from the test data. One is made by interpretation of Figure

6-10, which was observed during the fire test. Figure 6-10(b), shows that wind flow occurs to the right compared to the left side of the compartment. The dimensions of the pool fire in the fire test changed due to spill effects. This phenomenon led to the temperature data on the plinth beam-right (B1-right) being much lower compared to the plinth beam-left (B1-left) (see Figure 6-16 and Figure 6-18).

(a) (b)

Figure 6-10 (a) Test setup for realistic compartment fire (b) Attainment of flashover in fire test [117]

Based on the smoke height and the temperature curves obtained from the fire test, the compartment fire was analysed using ABAQUS, with temperatures applied at different heights and locations in the compartment.

Figure 6-11 Plan view of the lower frame

and

Figure 6-12 show the area where each time-temperature curve relates to, with the notation of the beam and column given for further reference. The time-temperature curve A (TTA) is applied to column C1, half-length of beams B1, B4, B5, B8 and slab area SLA. TTB is applied to column C2, half-length of beams B1, B2, B6, B7 and slab area SLB. TTC is applied to columns C3, C4,

half-length of beams B2, B4, B6, B8, whole length of beams B3 and B7, and slab area SLC. The emissivity value varies with different smoke layers as discussed previously. Table 6-3 shows the emissivity value used in each case.

Table 6-3 Parameter of emissivity for different areas used in heat transfer analysis using ABAQUS

Cases	Area / emissivity, $\varepsilon = \varepsilon_g + \varepsilon_s$		
	AHT1	AHT2	AHT3
CHT1	0.3 ($\varepsilon_s = 0$)	0.6415	0.9829
CHT2	0.3 ($\varepsilon_s = 0$)	0.9829	

Two fire phenomena CHT1 and CHT2 (see Table 6-3) are considered in this study. The areas at different heights in the compartment are referred to as AHT1,AHT2 and AHT3 as shown in

Figure 6-13 where AHT1 is the area located near to the opening, AHT3 is the area located at the top of the compartment and AHT2 is the area considered between AHT1 and AHT3.

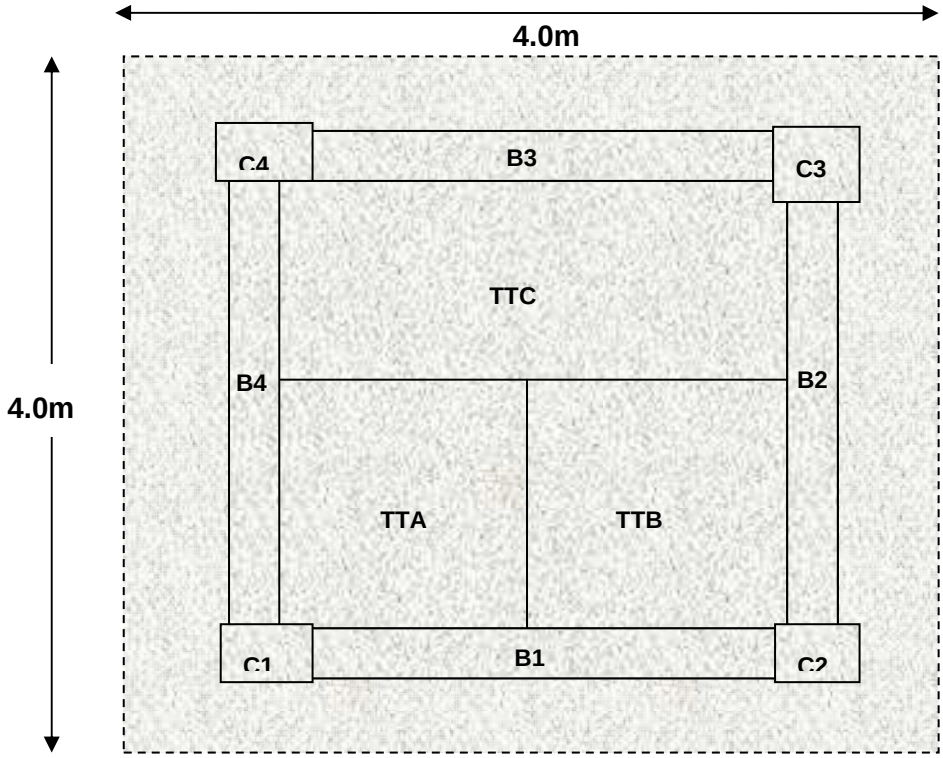

Figure 6-11 Plan view of the lower frame

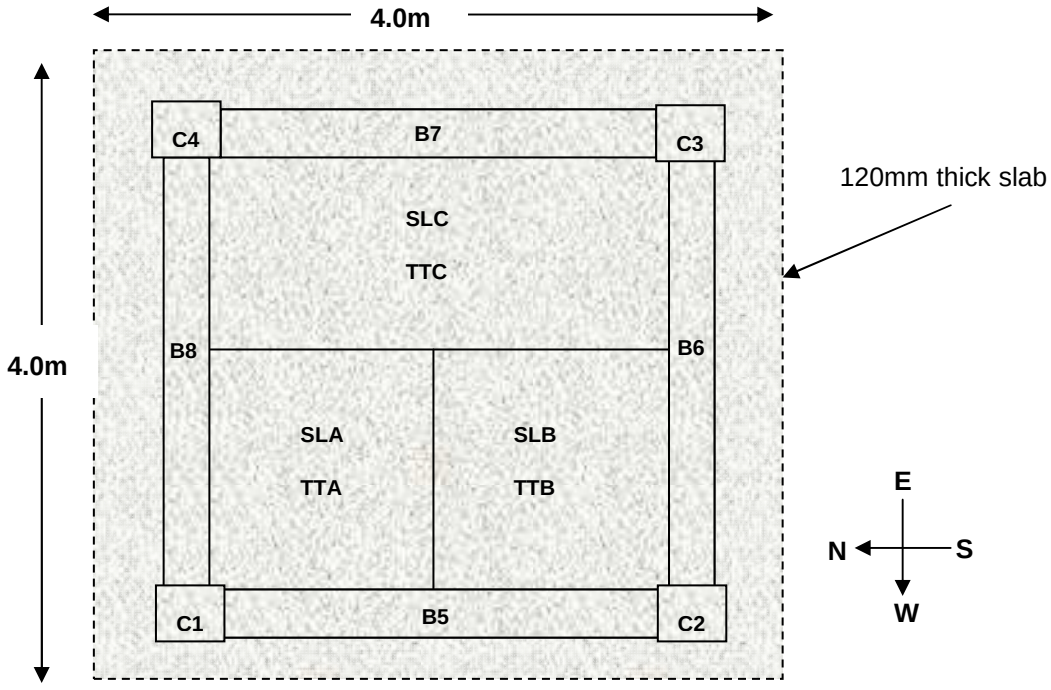

Figure 6-12 Notation of beams, columns and slab in a compartment (Plan view)

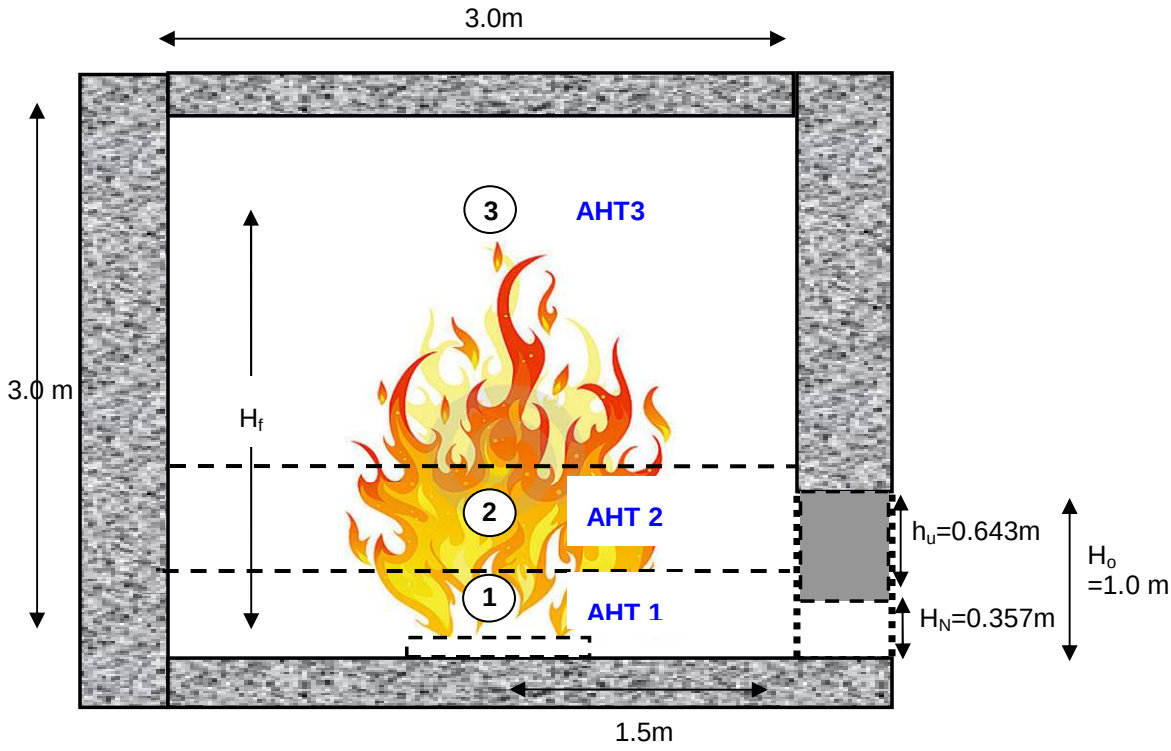

Figure 6-13 Compartment fire modelled in ABAQUS 6.8

6.4 Analysis of results

The temperature distribution in area AHT1 is the same in both cases CHT1 and CHT2, albeit the emissivity value in CHT1 is lower than CHT2. The temperature distribution through the elements of the frame at AHT2 in both cases is similar. Figure 6-14 shows the temperature distribution of the frame after 1 hour of fire.

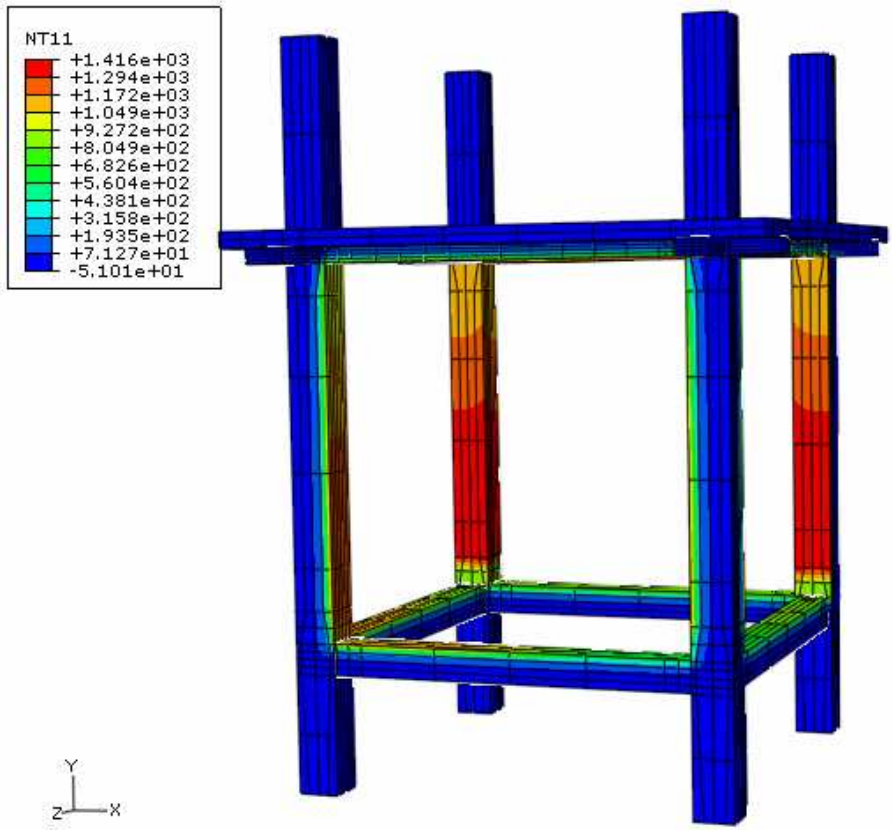

Figure 6-14 Temperature distribution of the frame from the heat transfer analysis

The temperature distribution within the frame from numerical analysis and test data is compared. Due to the failure of the thermocouples at elevated temperature, most of the temperature distribution data within elements is not present. The temperature results from case CHT2 are compared with the test data. All the temperature distributions from the test and numerical analysis are given in Appendix D and Appendix E respectively. In the test, thermocouples were embedded in each element, the location where the temperature distribution was recorded is shown in

Figure 6-15.

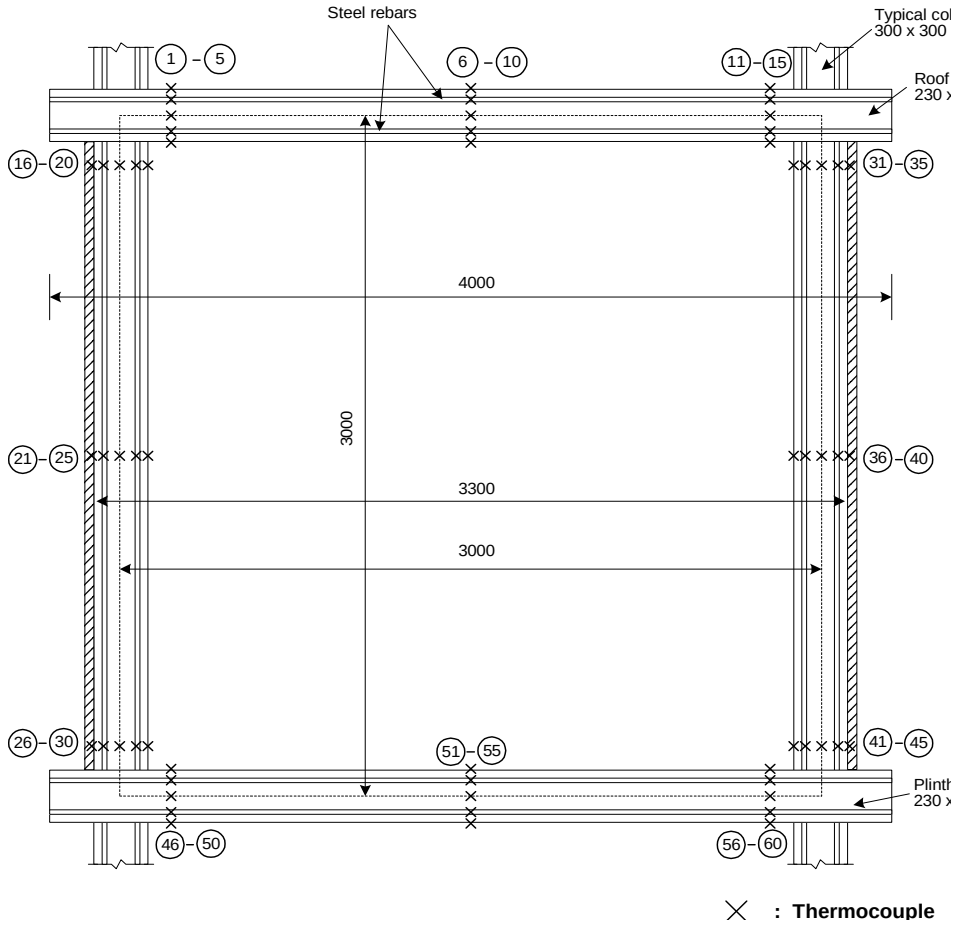

Figure 6-15 Location of thermocouples in beams and columns in the test [117]

Table 6-4 shows the location of temperature distributions calculated within the frame in the numerical analysis. For the beam, the location of the temperature recorded is measured from the nearest column. For the columns, it is measured from the base.

Table 6-4 Details of location for recorded temperatures

Elements	Left / Bottom (m)	Mid (m)	Right / Top (m)
Bottom and Top beam	0.2	1.35	0.2
Column	1.115	1.355	2.365

6.4.1 Temperature Distribution on the Bottom Beams (B1-B4)

The temperature distribution is recorded by thermocouples embedded at 5 depths within the elements. The 5 points are measured as 5mm, 25mm, 115mm, 205mm and 225mm from the base of the beam, as shown in Appendix D.1. B4, at mid span of the beam, experienced the highest temperature during the test. The numerical analysis agrees with this, B4 shows the highest temperature on the surface (Appendix E.1).

The temperature distributions though beam B1 provide the most detailed results obtained from the test, therefore a comparison is made between the results of the test and the numerical analysis in this beam. Figure 6-16 shows a comparison of the temperature distribution in B1 at the left side. The temperature distribution through B1 at mid span is shown in Figure 6-17. Figure 6-18 shows the comparision of the temperature distribution of B1 at the right side.

The temperature distributions at depth 25mm and above obtained from the test and numerical analysis agree with each other. Both show the same pattern of the temperature increment throughout the heating. However at depth 5mm, temperature obtained from the numerical analysis is higher than that from the test. The significant different of these temperature is might be due to two reasons. First, in the test the compartment temperature was measured using three thermocouples. In the test only one of the results was decided to use. Therefore, the compartment temperature in the numerical analysis is lower than in the test. Secondly, the effects of emissivity value used in the heat transfer in the compartment might cause this happened.

From the results, the temperature distribution through beam B1 at mid span is similar in both the numerical analyses and the test up until 50 minutes. For the right and left side of B1 the temperature distribution from the numerical analysis

is higher than the test results. In the test, the left side temperature of the frame is higher than the right side. This might be due to wind effects. This can be clearly seen from Figure 6-10 (b). This is not replicated in the numerical analysis.

For beam B2, only one temperature is available from the test result, for the top surface on the right side. The numerical result and the test result for B2 at 50 minutes are about 850^{o}C and 780^{o}C, respectively.

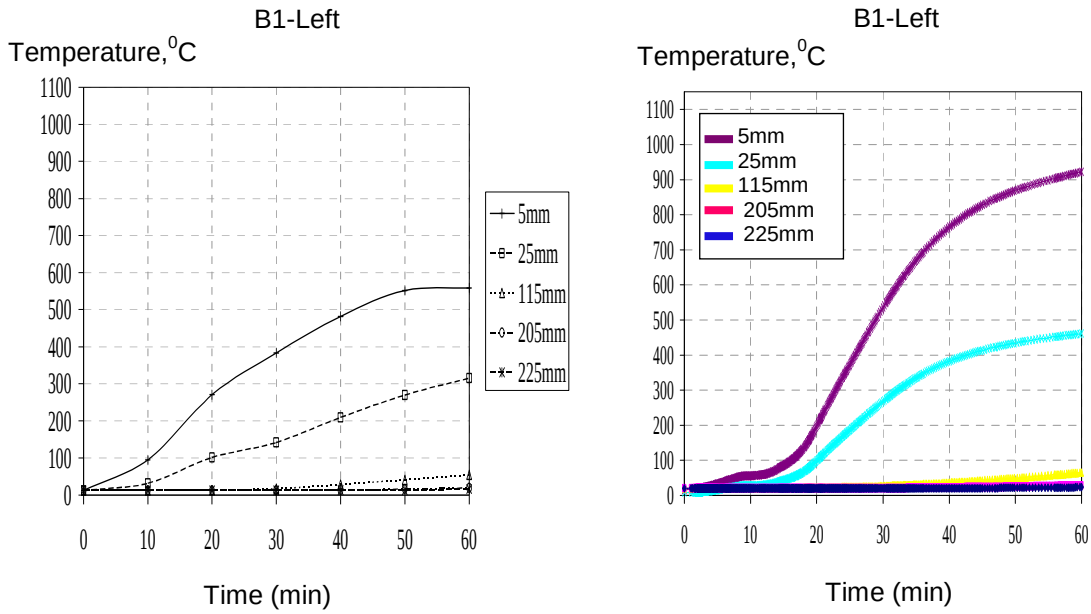

(a) (b)

Figure 6-16 Temperature distributions in the plinth beam, B1 at the left side along the height (a) Test (b) Heat Transfer using ABAQUS

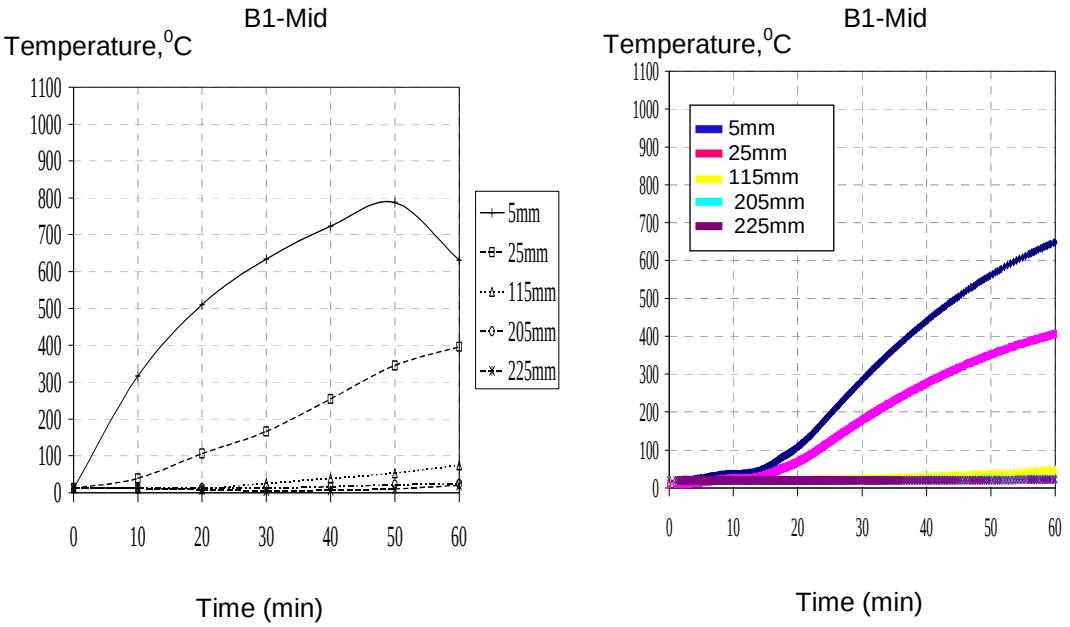

(a) (b)

Figure 6-17 Temperature distributions in the plinth beam,B1 at the middle side along the height (a) Test (b) Heat Transfer using ABAQUS

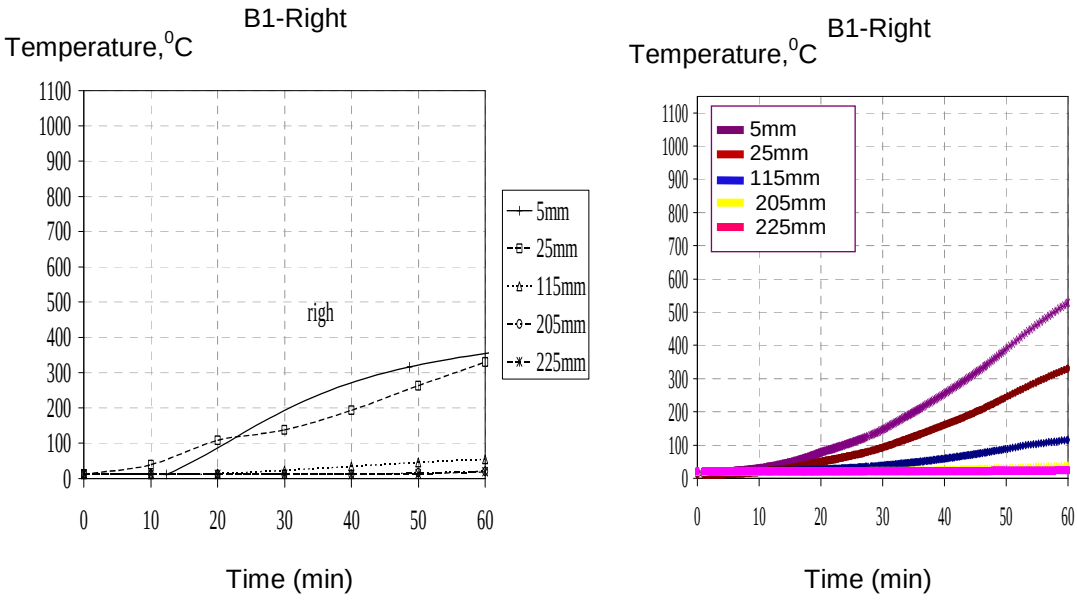

(a) (b)

Figure 6-18 Temperature distribution in the plinth beam, B1 at the right side along the height (a) Test (b) Heat Transfer using ABAQUS

The numerical analysis shows a temperature distribution through the beam depth for B3. At 60 minutes, the results for the numerical analysis and the test data, except for the right side, is comparable.

6.4.2 Temperature Distribution in the Top Beams (B5 to B8)

Appendices D.2 and E.2 show the temperature distribution of the top beam from the test and numerical heat transfer analysis. Temperature distribution data is available for beams B5 and B7, from the test. Data is not available for beams B6 and B8. The temperature gradient within the top beams increased as the time increased. However, in the last 10 minutes the temperature gradients in the top beams decreased.

In the numerical analysis, the temperature gradient through the top beams increased during the fire. The temperatures on the surface of all the top beams is higher thatn the temperature obtained from the test. Figure 6-19,Figure 6-20 and Figure 6-21 show the temperature distribution of beam B5 captured through it depth.

The temperature distribution seen in the test and the heat transfer analysis agrees well for the first 20 minutes. The temperature distribution in the test slowly increased while in the heat transfer analysis the temperature increased about 50% faster than that obtained in the test.

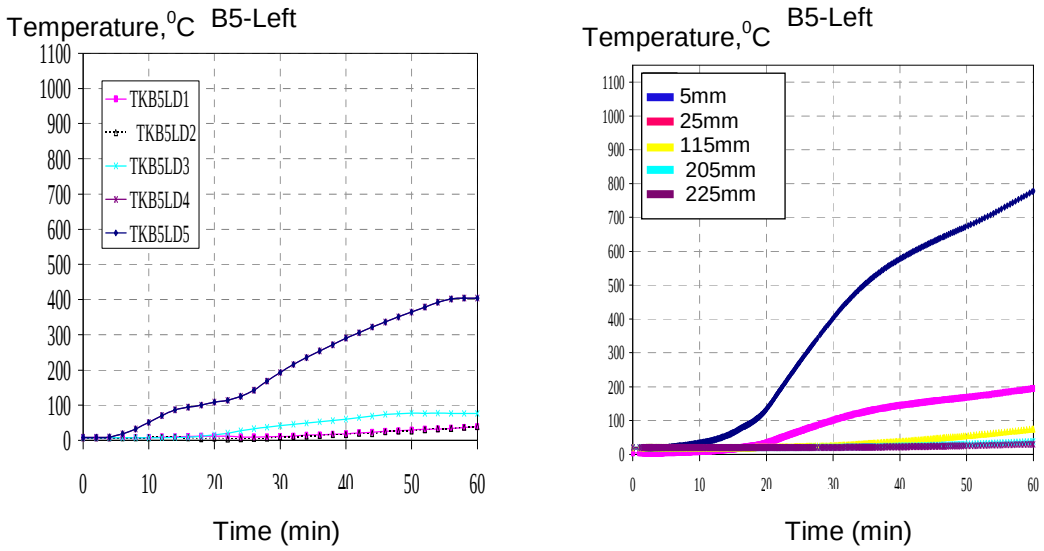

(a) (b)

Figure 6-19 Temperature distributions in the top beam, B5 at the left side along the height (a) Test (b) Heat Transfer using ABAQUS

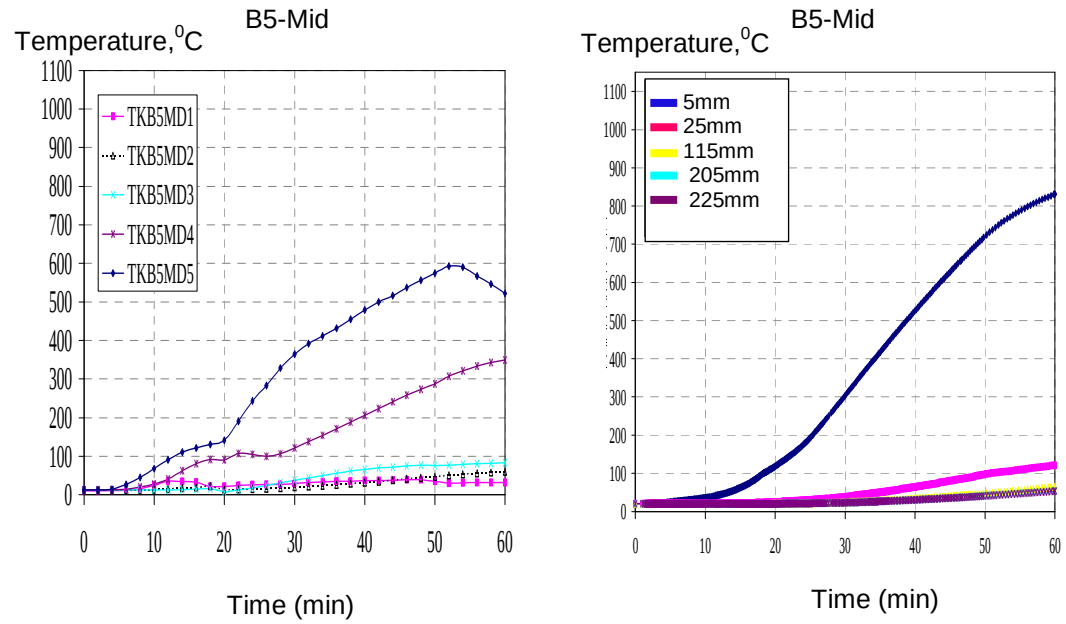

(a) (b)

Figure 6-20 Temperature distributions in the top beam, B5 at the middle side along the height (a) Test (b) Heat Transfer using ABAQUS

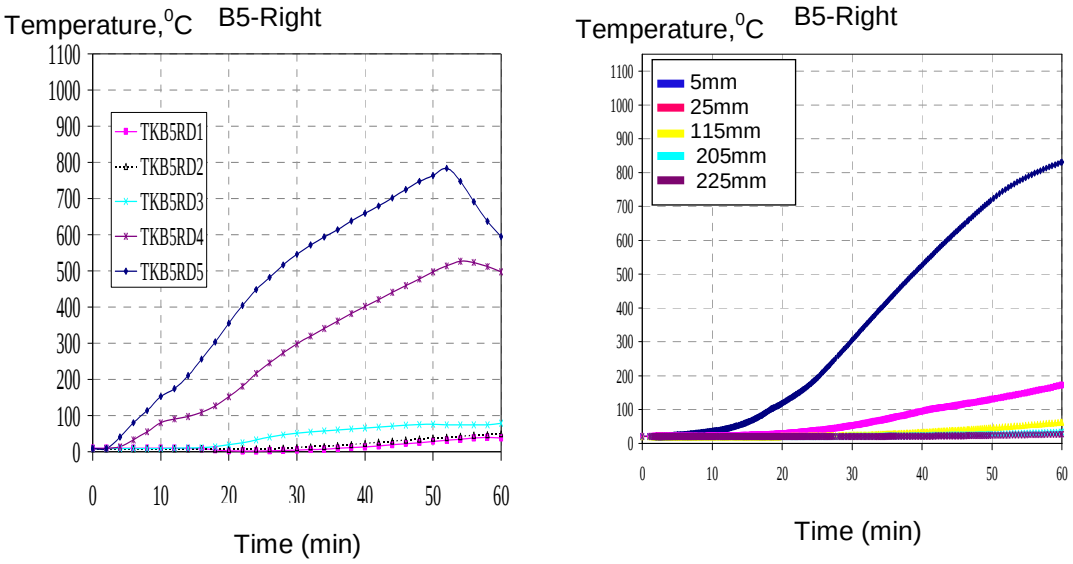

(a) (b)

Figure 6-21 Temperature distributions in the top beam, B5 at the right side along the height (a) Test (b) Heat Transfer using ABAQUS

6.4.3 Temperature Distribution in the Columns (C1 – C4)

The temperature distribution in the columns C1, C2 and C4 is available from the test data. Temperature distribution within the columns was captured in both the loading direction and perpendicular to the loading direction. The temperature distribution for all the columns obtained from the test and the heat transfer analysis is shown in Appendices D.3-D.4 and E.3-E.4.

The temperature distribution in the columns is captured at 5 points along the cross-section. The 5 points are measured as 5mm, 40mm, 150mm, 260mm and 295mm from the column surface. The average temperature recorded for the columns in the test is between 500^{o}C and 1030^{o}C, while the average of the temperature distribution obtained from the heat transfer analysis is between 700^{o}C and 1080^{o}C.

The temperature gradient in the columns obtained from the test shows a gradual increase as the time of exposure increases. In the last 10 minutes, most of the points show a decrease in temperature gradient. This might be due to the fuel running out at the end of the test. The temperature gradient in the column from the heat transfer analysis rises quickly from the beginning of the analysis until a time of 30 minutes, then increases slowly until the end of 1 hour.

Figure 6-22 and Figure 6-23show the temperature distribution within column C4 from both the test and heat transfer analysis.

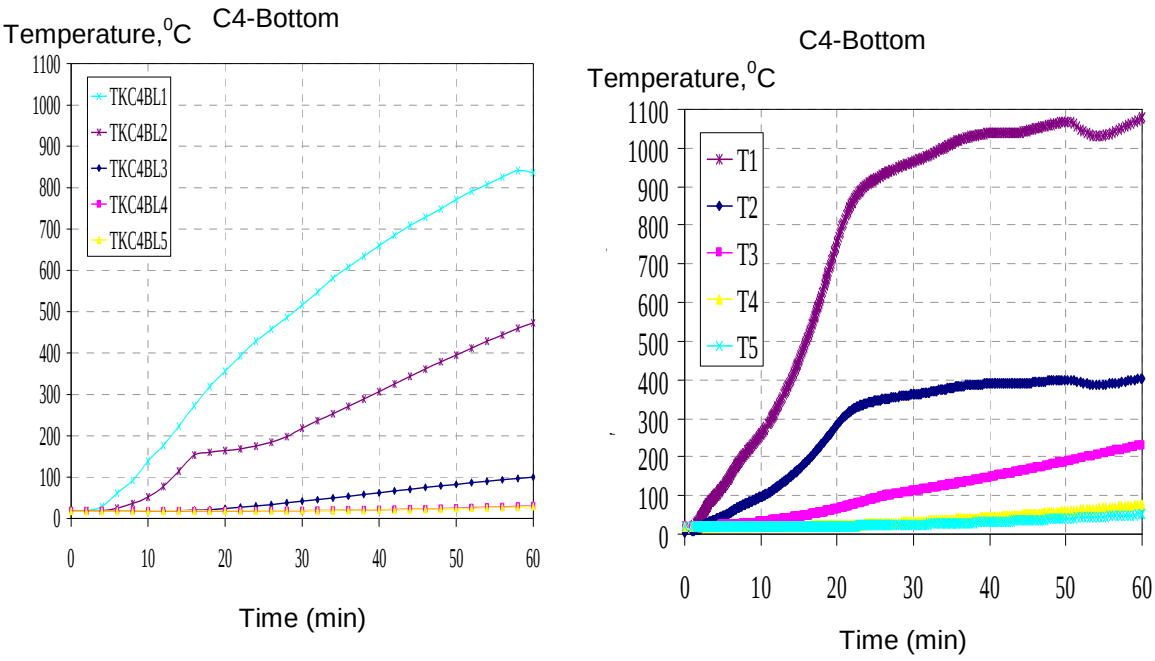

Figure 6-22 Temperature distributions in the column, C4 at the bottom side along the height (a) Test (b) Heat Transfer using ABAQUS

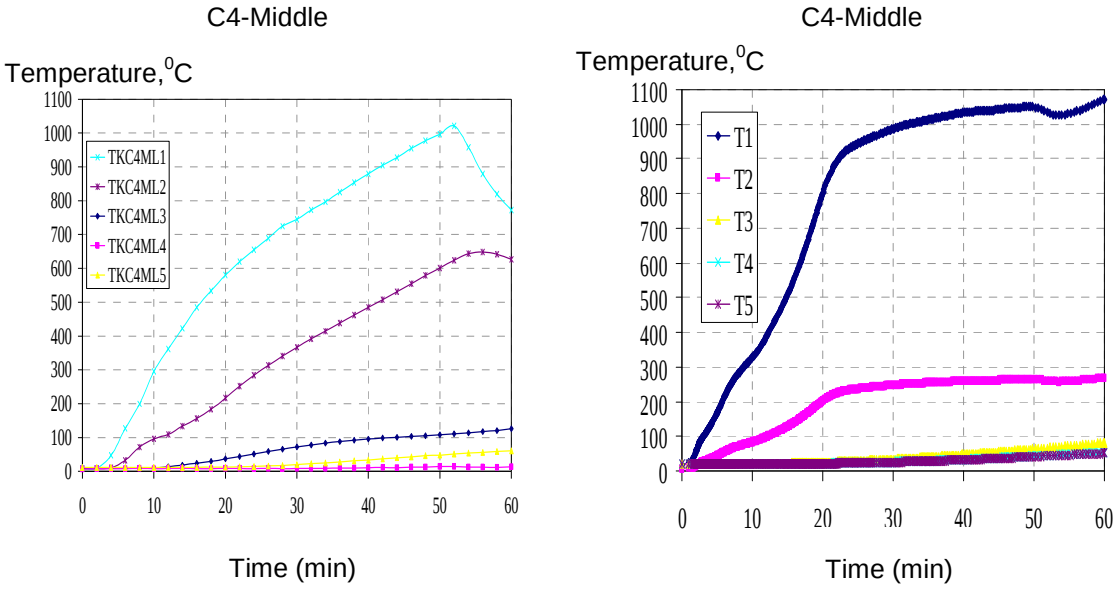

(a) (b)

Figure 6-23 Temperature distributions in the column, C4 at the middle along the height (a) Test (b) Heat Transfer using ABAQUS

6.4.4 Temperature Distribution through the Slab

The temperature distribution through the slab was captured at 5 locations from the slab area, A, B, C, D and O, as shown in

Figure 6-24. This was achieved by capturing the temperature through the depth of the slab section, at 5mm, 30mm, 60mm, 90mm and 115mm from the slab base, as shown in Appendices D.5 and E.5 for the test and heat transfer analysis. The maximum temperature obtained from the test at the end of 10 minutes was 1050^{o}C, which was captured at points A and D. At the middle of the slab, point O, the maximum temperature at the surface was 700^{o}C. The lowest temperature recorded was 440^{o}C, which was observed at point C.

Figure 6-25 shows the temperature distribution through the slab at point A obtained from both the test and heat transfer analysis. The temperature at the

slab surface obtained from heat transfer analysis shows that it gradually increased up to 20 minutes of heating. The temperature rose to its highest maximum temperature at the end of the heating time at locations A and B. At points C, D and O the temperature increased rapidly in the beginning, until 20 minutes, and was maintained at the same temperature until the end of 1 hour of heating. The minimum temperature at the slab surface from the heat transfer analysis was 800^{o}C at point B.

The temperature distribution within the slab at point A is chosen for comparison between the test and numerical analysis. This shows agreement between the test and numerical analysis at the end of heating. However, the temperatures obtained from the test are higher than those taken from the heat transfer analysis, for the first 50 minutes of heating. The difference might be due to the presence of a thicker smoke layer in the test which, using the emissivity value of 0.9829, takes effect at the end of the heating period.

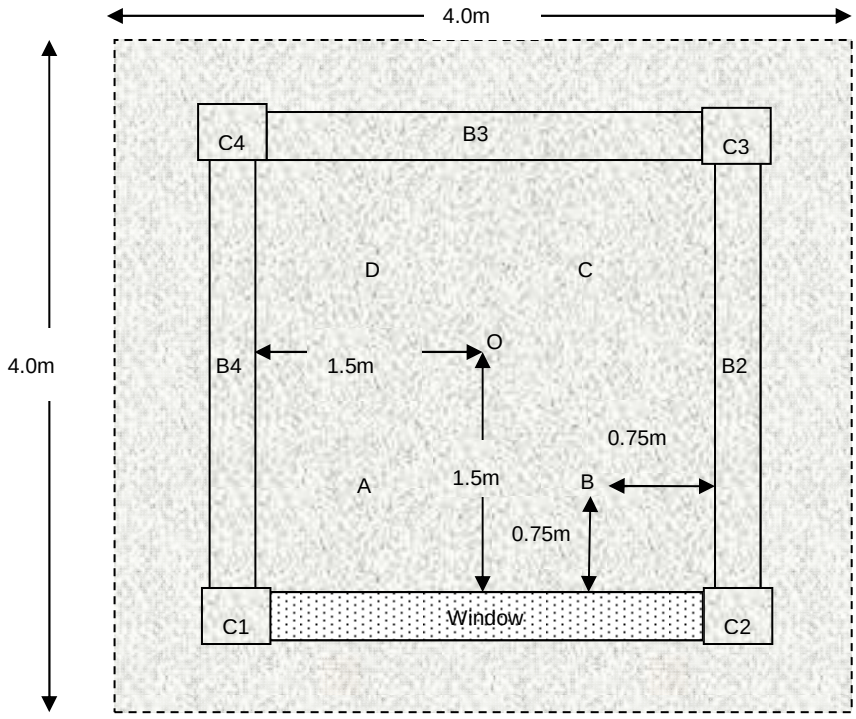

Figure 6-24 The five locations on the slab where the temperature distribution was recorded [117]

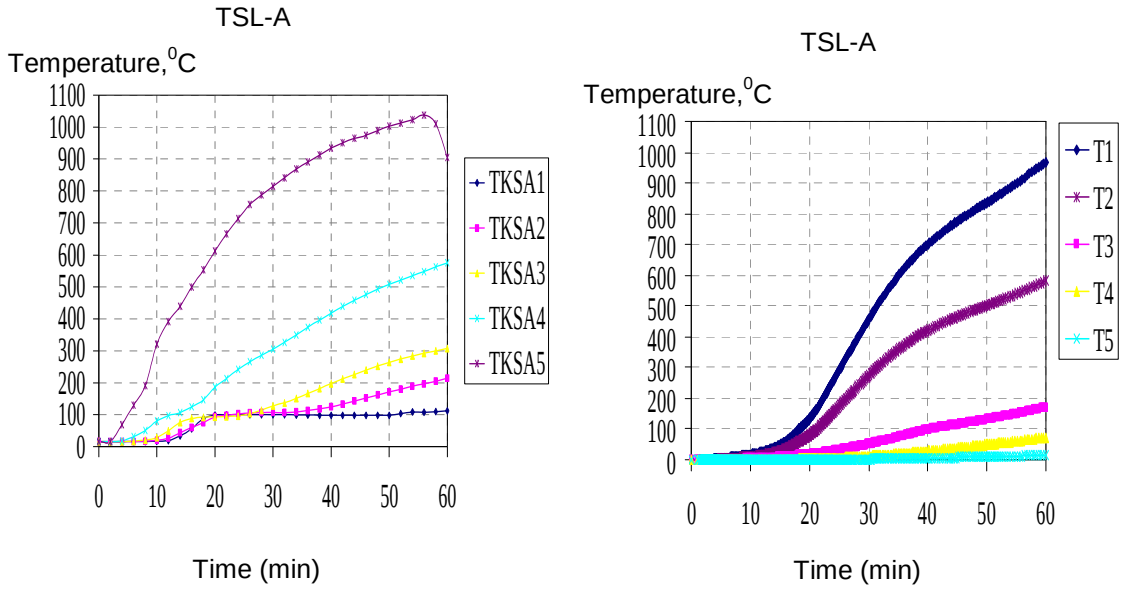

(a) (b)

Figure 6-25 Temperature distributions in the slab at A (a) Test (b) Heat Transfer using ABAQUS

6.5 Conclusions

- The temperature distribution within the frame was recorded in the test after the frame was subjected to fire.
- The thermocouples placed on some structural elements failed due to high temperatures.
- The failure of the thermocouples limited the temperature distribution data collected for some of the elements in the frame.
- Heat transfer analysis was done using ABAQUS 6.8 to capture the temperature distribution within the elements.

- The temperature data used in the heat transfer analysis was based on the temperature curve obtained from the compartment test.
- The temperature curves applied to the heat transfer analysis vary along the height of the columns.
- The emissivity value used in the heat transfer analysis is based on the effect of the smoke layer in the compartment.
- Two different emissivity values were used in the heat transfer analysis (CHT1 and CHT2), giving slightly different temperature distributions.
- The temperature distributions obtained from the heat transfer analysis CHT2 was used to compare with the test results.
- The temperatures from the heat transfer analyses are generally higher than corresponding temperatures from the test data. This is due to the temperature in the compartment in the test being higher than that calculated in the numerical analysis which is based on the emissivity value. It shows that the emissivity value, based on the fuel type and smoke layer, needs to be revised again.
- Due to the significant difference in the temperature distribution results from numerical analyses, the time- temperature curve from the test is used for the simulation of the response due to the thermo-mechanical loading of the Roorkee Frame Test 1.

7

Simulation of The Response Due to Thermo- Mechanical Loading

7.1 Introduction

This chapter presents an analysis of the behaviour of the pre-damaged Roorkee frame subjected to a one-hour compartment fire. For this, the temperature distributions used in the thermo-mechanical ABAQUS models were based on the temperatures obtained in the test with some modifications as discussed in the previous chapter.

This is because temperature distributions from the Roorkee frame test were not available for the entire frame due to the failure of the thermocouples in some areas and due to the loss of some of the data. Therefore assumptions had to be made for frame locations where temperature data was not available.

7.2 Thermal Loading

In the test, the temperature distributions were measured at three different locations along the height of the columns. The temperature distributions in the top and plinth beams were assumed to be uniform along the length. Table 7-1 shows the temperature loading which was used in the numerical simulation of the frame. Figure 7-1 to Figure 7-4 which were recorded in the Roorkee frame test. The hottest temperature distributions were recorded at 5mm from the surface. For the numerical simulation, the columns were divided into three sections to apply the different thermal loadings, as shown in Figure 7-5.

Table 7-1 Thermal loading details

Tested Frame	ABAQUS Models
B1	Plinth beam
B5	Top beam
C4	Column
TSLO	Slab

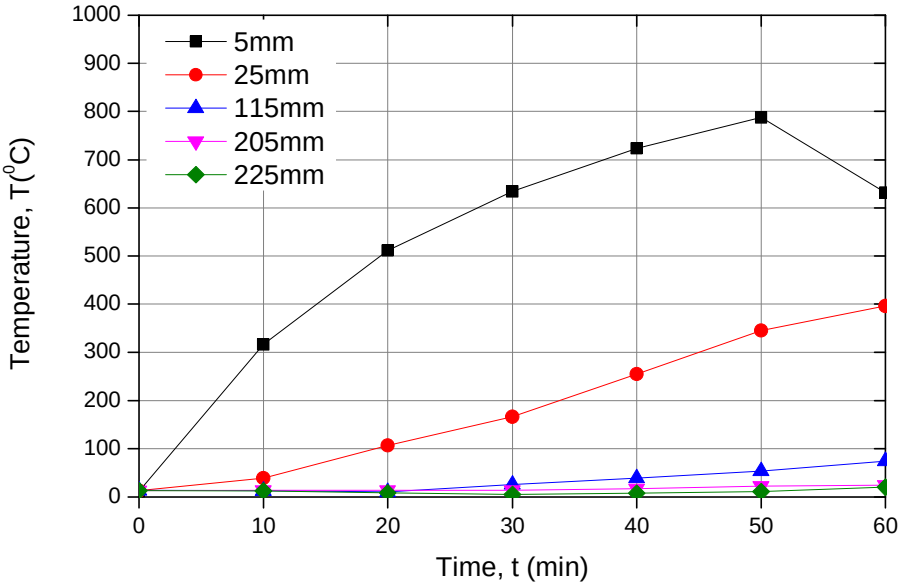

Figure 7-1 Temperature distributions in the plinth beam, B1 from the Roorkee test

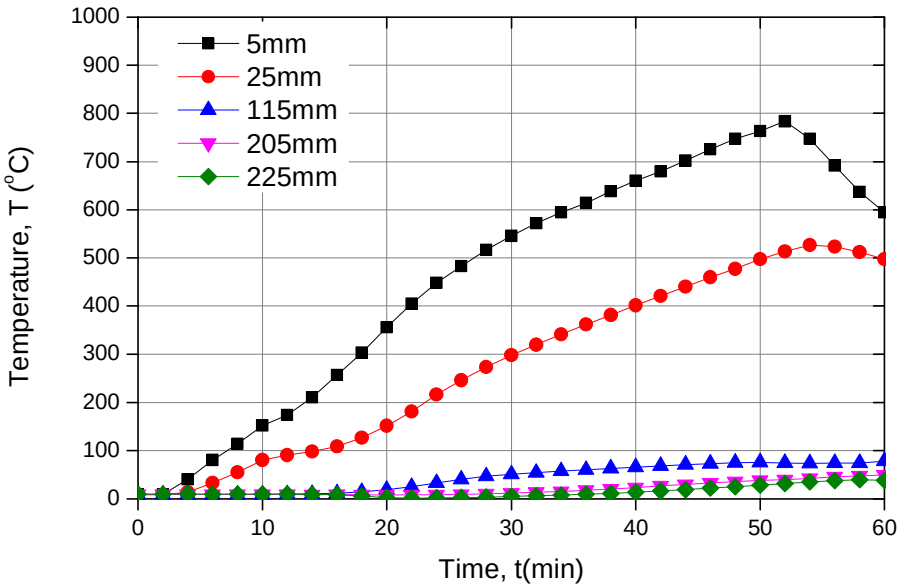

Figure 7-2 Temperature distributions in the top beam, B5 from the Roorkee test

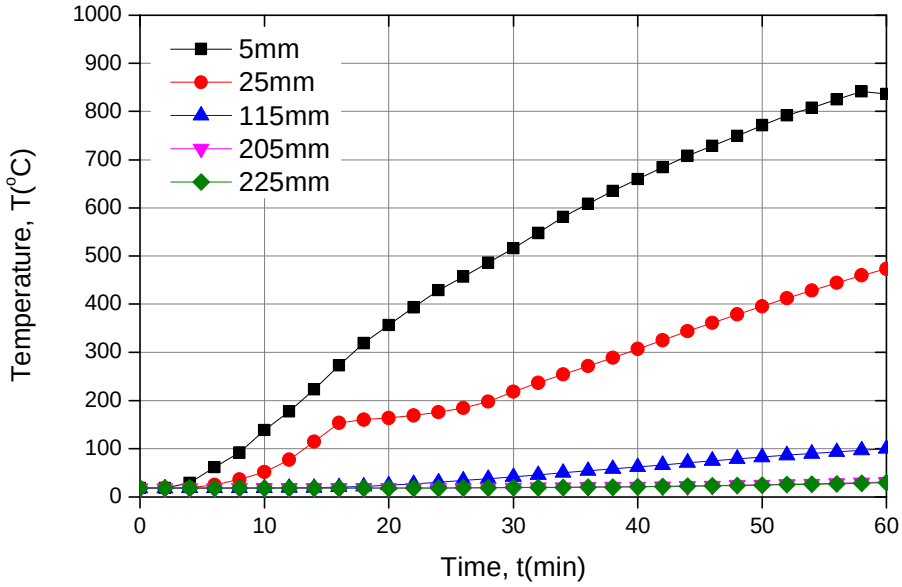

Figure 7-3 Temperature distributions in the column, C4 from the Roorkee test

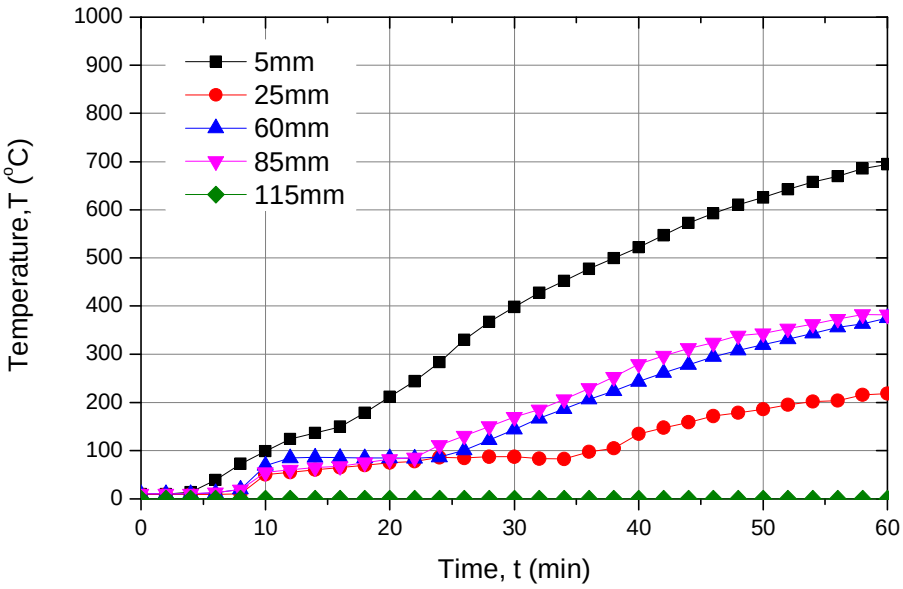

Figure 7-4 Temperature distributions in the slab, TSL-O from the Roorkee test

The temperature were input at three specific points in the beam section (for all beams and columns) as shown in Figure 7-6. The temperature values are presented in Table 7-2 and Table 7-3for the top beam and plinth beam respectively. Table 7-4 to Table 7-6 show the temperature values used at different heights in the columns.

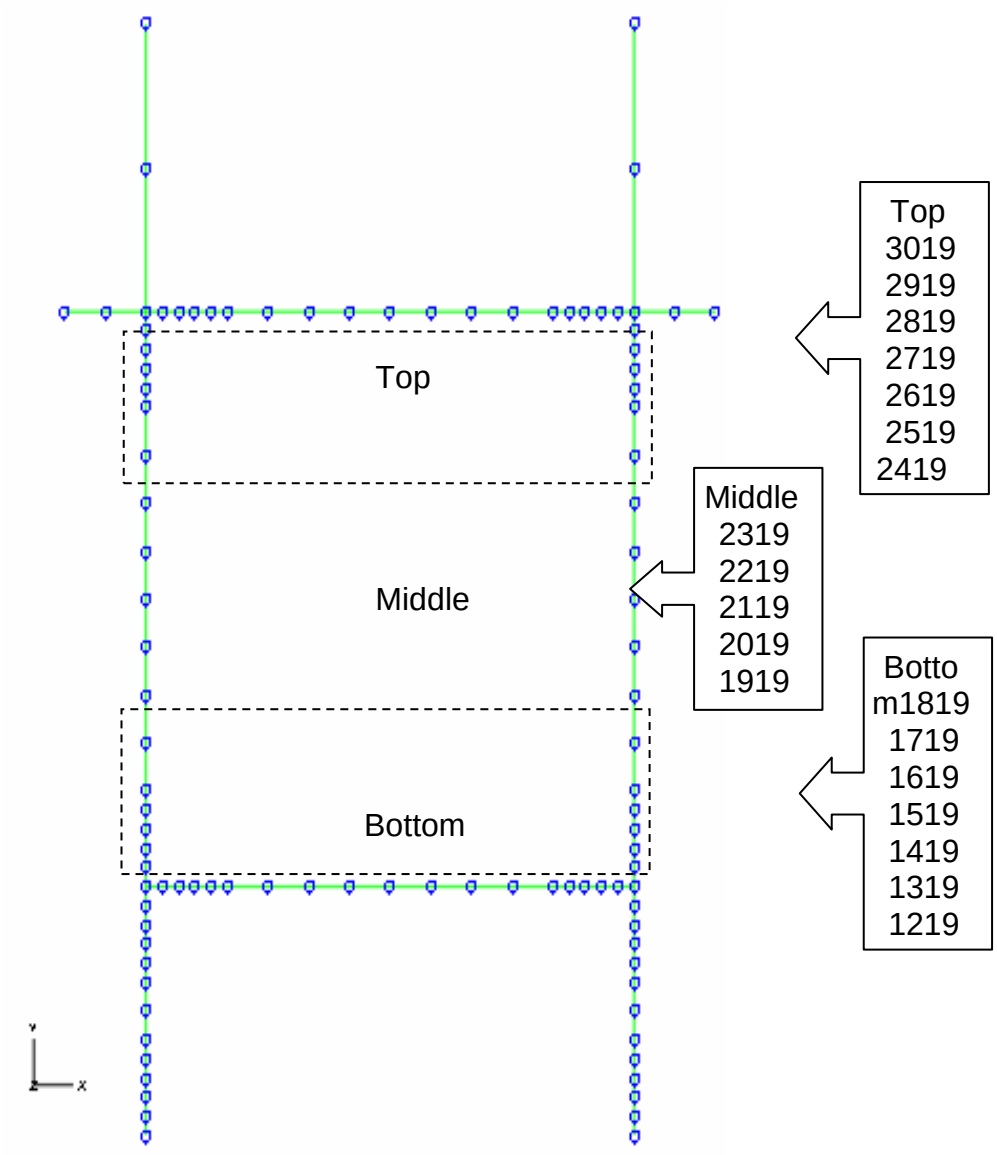

Figure 7-5 Nodes where the thermal loading applied at different heights of column

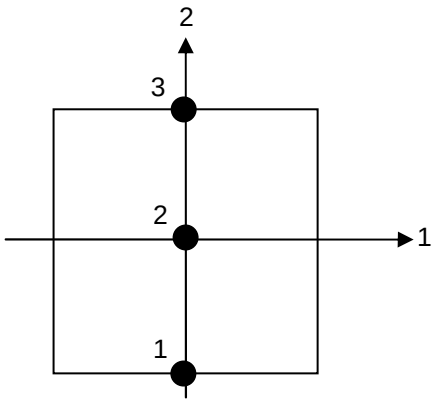

Figure 7-6 Temperature variable input at specific points in beam section

Table 7-2 Temperature values applied in the top beam

Time (Minutes)	Temperature Input at Specific Points for beam section		
	1	2	3
10	18	18	18
20	439	27	18
30	607	50	22
40	751	68	29
50	883	77	46
60	704	93	55

Table 7-3 Temperature values applied in the plinth beam

Time (Minutes)	Temperature Input at Specific Points for beam section		
	1	2	3
10	18	29	632
20	18	29	506
30	18	29	632
40	18	44	720
50	18	58	787
60	18	79	634

Table 7-4 Temperature values applied in the bottom level column

Time (Minutes)	Temperature Input at Specific Points for beam section		
	1	2	3
10	18	18	139
20	18	24	356
30	19	42	516
40	21	62	660
50	24	83	772
60	29	100	836

Table 7-5 Temperature values applied in the middle level column

Time (Minutes)	Temperature Input at Specific Points for beam section		
	1	2	3
10	12	12	296
20	13	37	580
30	20	72	745
40	34	96	880
50	49	108	997
60	61	126	772

Table 7-6 Temperature values applied in the top level column

Time (minute)	Temperature Input at Specific Points for beam section		
	1	2	3
10	10	13	259
20	24	49	538
30	57	88	703
40	66	89	839
50	71	90	954
60	75	90	699

Only half of the frame was modelled in the thermo-mechanical analysis to simplify the problem and reduce the analysis time – the Roorkee frame is symmetric in plan. Due to limited temperature points in the rectangular section, the columns and beams in the 3D model were designed as I-beam section types. This section was chosen to input the temperature values at the two

different surfaces in a more reasonable way compared to the rectangular section. ABAQUS is restricted to a maximum of five temperatures points through its beam section. The five temperatures input have been defined at specific points as shown in Figure 7-7. The web of the section has been modelled with a value the same as the width of the beams and columns in the frame. During heating, the temperatures are first interpolated linearly through the flanges based on the temperatures at points 1 and 2 and then 4 and 5, respectively. The temperatures are then interpolated parabolically though the web.

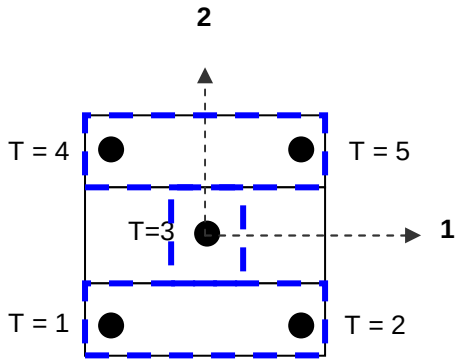

Figure 7-7 The I-beam section modelled with wider web and temperatures points

Figure 7-8 and Figure 7-9 show the temperatures input at specific points for the beam (B5) and column (C4), respectively. In both the beam and the column two faces are exposed to the fire and two faces are hidden front it. The temperature point 4 represents the lowest temperature in the section (assume to be 20^{o}C) and point 2 represents the highest temperature (based on recorded data. The temperature applied to each member is based on the temperature curve obtained from the test (B1 for plinth beam, B7 for top beam and C4 for columns), the same as in the 2D ABAQUS model. The temperatures within the slab are defined at five integration points through its depth as shown in

Figure 7-10. The temperature data applied at the beams, columns and the slab are shown in Appendix F.

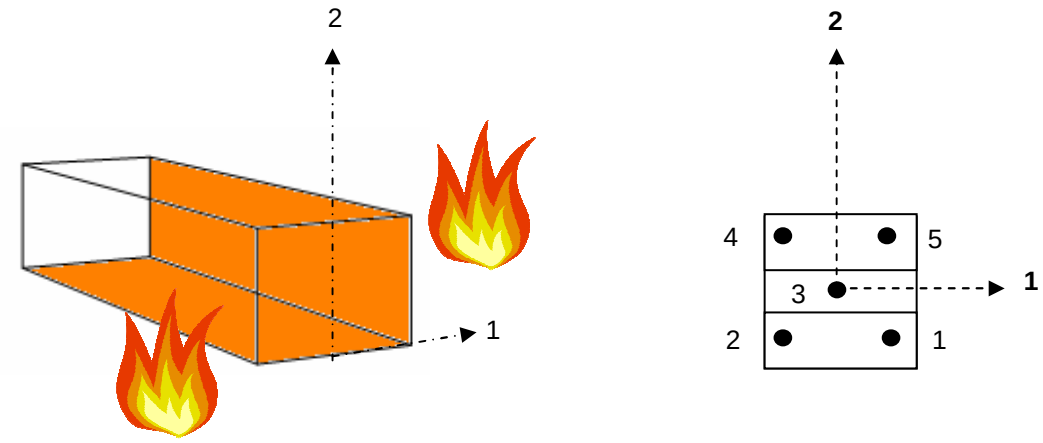

Figure 7-8 Representing beam B5 showing the location of the temperatures values at five points throughout the I-beam section

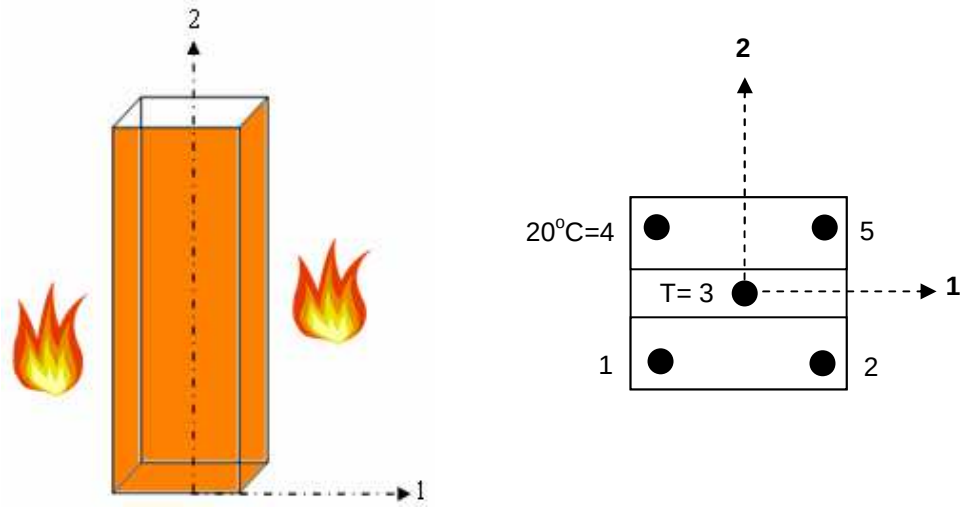

Figure 7-9 Representing column C4 showing the location of the temperatures values at five points throughout the I-beam section

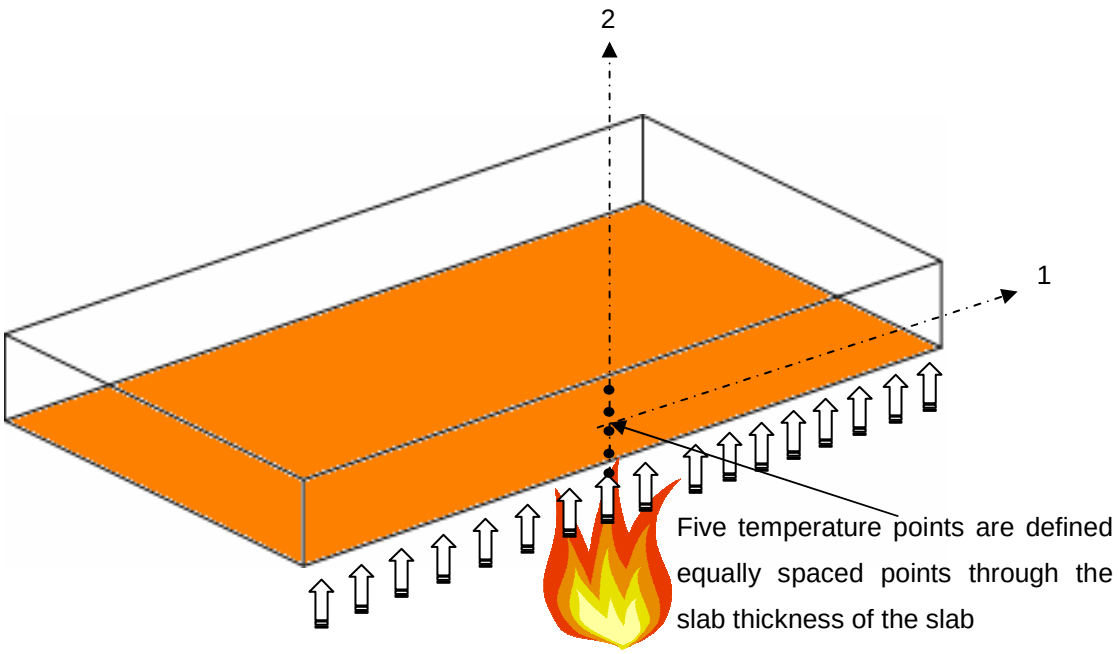

Figure 7-10 Cross section of the slab showing the temperature points through its thickness

7.3 Analysis of Result

7.3.1 Horizontal Displacements after Thermo-Mechanical Loading

Figure 7-11 illustrates the horizontal displacements of nodes 3001 and 3019 (see Figure 7-5) in the 2D ABAQUS model subjected to thermo-mechanical loading. It can be seen that both the nodes had an initial residual displacement of 55mm (towards the left of the frame) due to the cyclic lateral loading. As the thermal loading was applied both nodes moved to the right hand side from their initial position, but ten minutes before the end of heating cycle, both began to move towards the left again (suggesting an initial stiffening of the reinforcing steel because of thermally induced stresses followed by softening as the temperatures increase).

The comparative response of the frame from a 2D OpenSees analysis is shown in Figure 7-12. Both of the result is show a significant different between each other's subjected to thermo-mechanical loading, None of the numerical results is compared with the test except for vertical displacement in the slab due to the no available results were measured in the test. Therefore, the results presented throughout this chapter are only the results obtained from the numerical analysis.

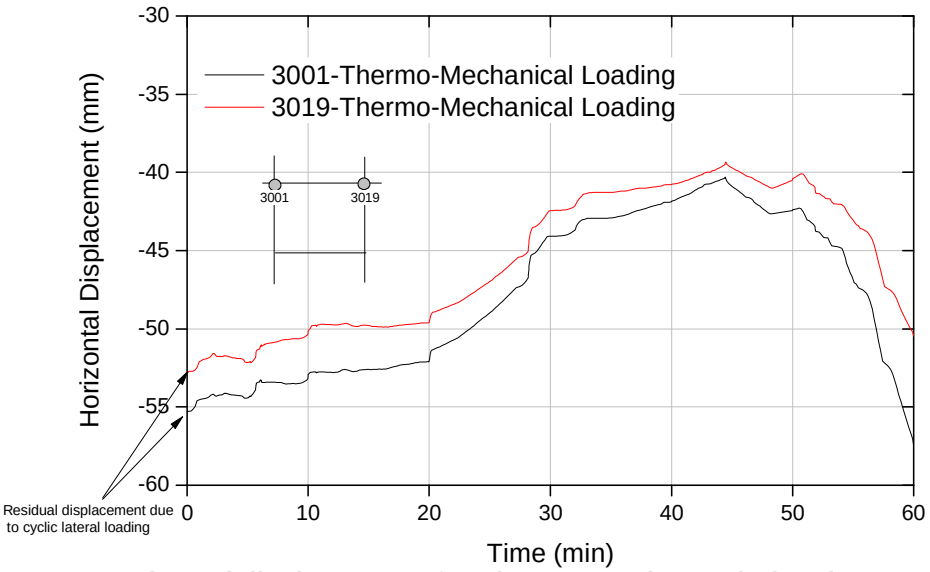

Figure 7-11 Horizontal displacement of Nodes 3001 and 3019 during thermo-mechanical loading-2D ABAQUS Model

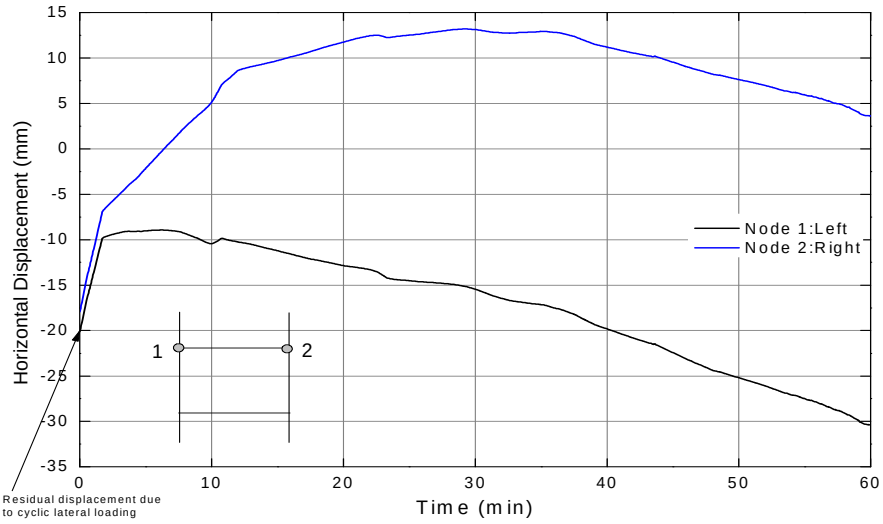

Figure 7-12 Horizontal displacement of Nodes 1 and 2 from 2D OpenSees model

Figure 7-13 shows the vertical displacement of the whole 3D ABAQUS model at the end of the thermo-mechanical analysis. Horizontal displacement at slab level (of nodes 3001 and 3019) is shown in Figure 7-14. It can be seen that two nodes plotted had residual displacements of 27mm to 29mm (towards the left) at the end of the lateral cyclic loading stage. After thermal loading was applied, the thermal expansion of the inner surfaces seem to have stiffened the frame causing both columns to displace towards the right hand side and reducing the residual displacement of after cyclic loading. Interestingly in this model the material degradation of the concrete and reinforcement at increased temperatures does not reverse the rightward displacement for the same period of heating. For comparison purposes, the horizontal displacement recorded from thermal loading of an equivalent undamaged frame (with no previous lateral cyclic loading stage) is shown in Figure 7-15. It can be seen both columns are gradually moving outward as the temperatures increase. The horizontal displacement of both columns (in the damaged test frame simulation) along their height is illustrated in Figure 7-16 and Figure 7-17.

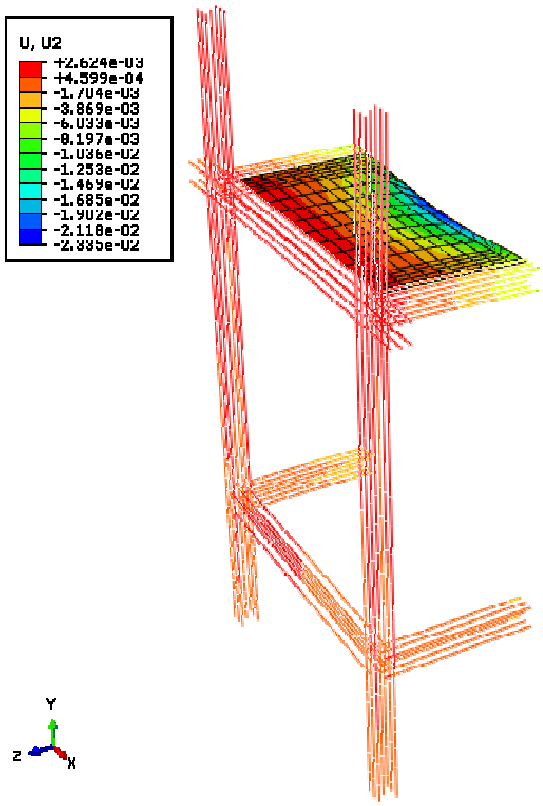

Figure 7-13 Vertical displacement (U2) from 3D ABAQUS model (magnified to 5)

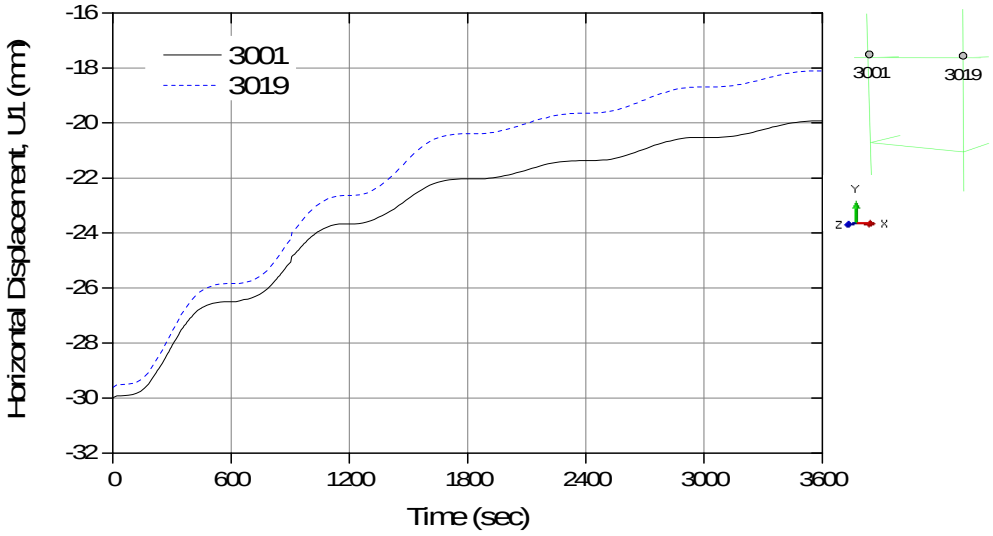

Figure 7-14 Horizontal displacement (U1) at slab level of node 3001 and 3019-3D ABAQUS Model

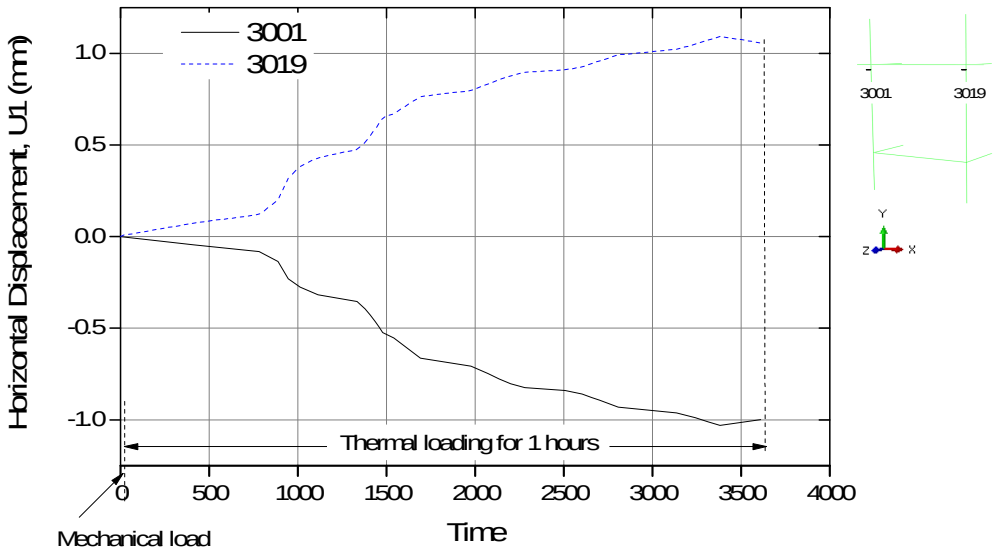

Figure 7-15 Horizontal displacement (U1) at slab level of node 3001 and 3019 from thermal analysis (undamaged frame)-3D ABAQUS Model

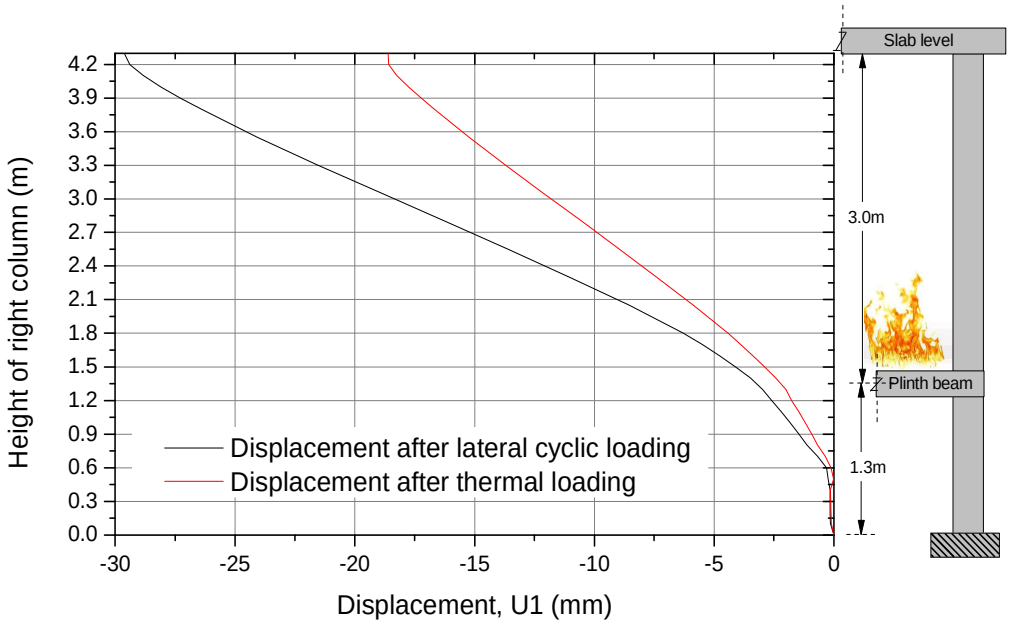

Figure 7-16 Horizontal displacement along the height of the right column

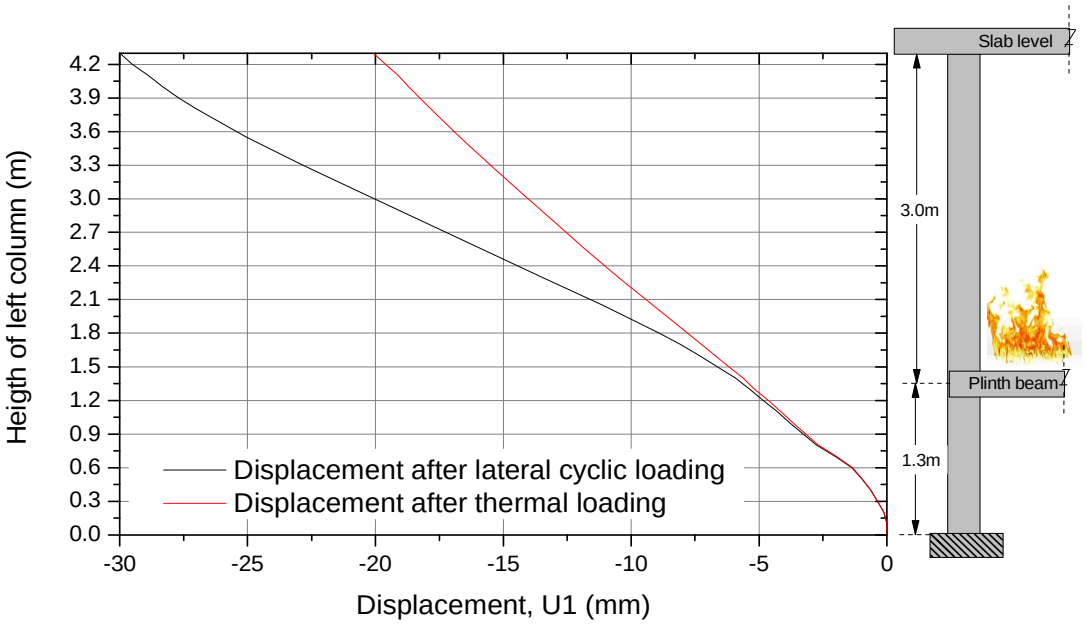

Figure 7-17 Horizontal displacement along the height of the left column

The vertical displacement of both columns is shown in Figure 7-18. It can be seen that both of the columns increase in height throughout the heating because of the thermal deformations. The initial vertical displacement due to the lateral cyclic loading applied is also shown in the plot. Figure 7-19 is shows the vertical displacement from thermal loading analysis on undamaged frame. Both columns were moved vertically in the similar rate during 1 hour of heating.

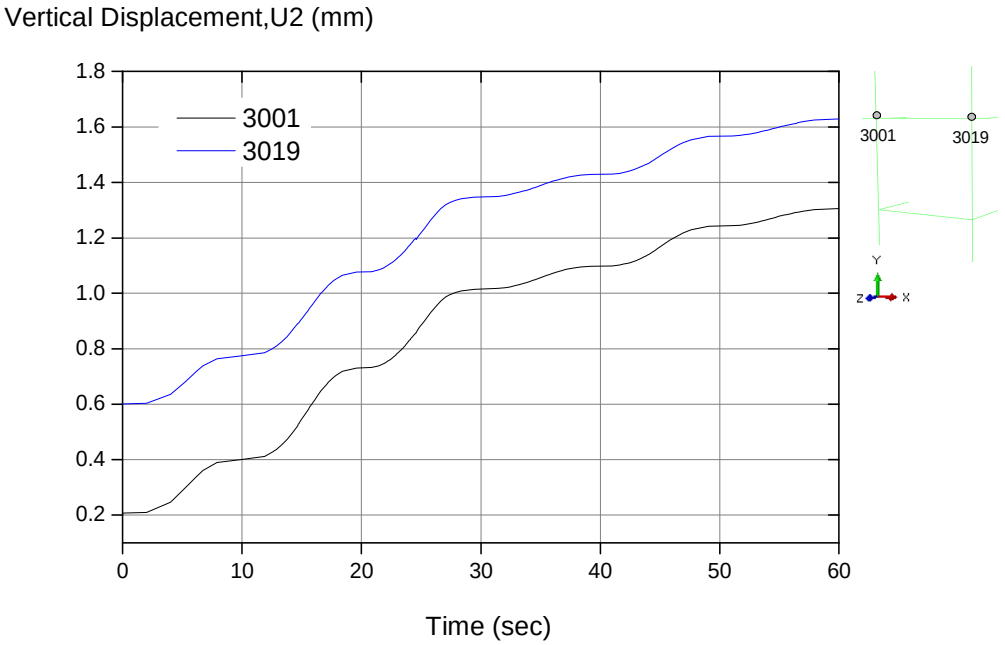

Figure 7-18 Vertical displacement (U2) at slab level of node 3001 and 3019

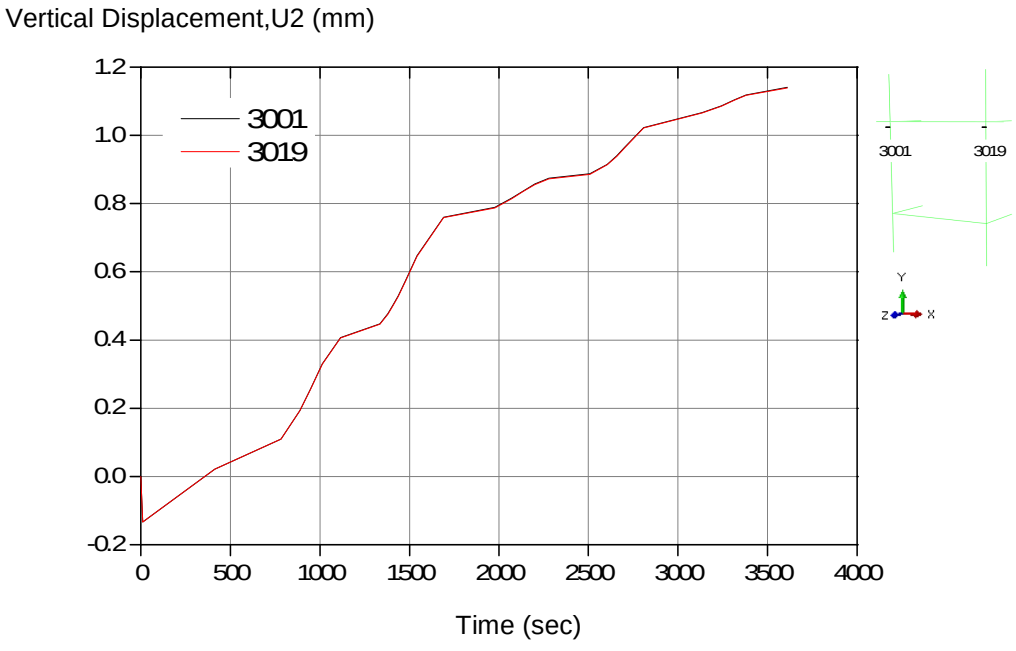

Figure 7-19 Vertical displacement (U2) at slab level of node 3001 and 3019 (thermal loading on undamaged frame)

Vertical deflection at node 3010 recorded from thermal loading analysis of undamaged frame is show in Figure 7-20.

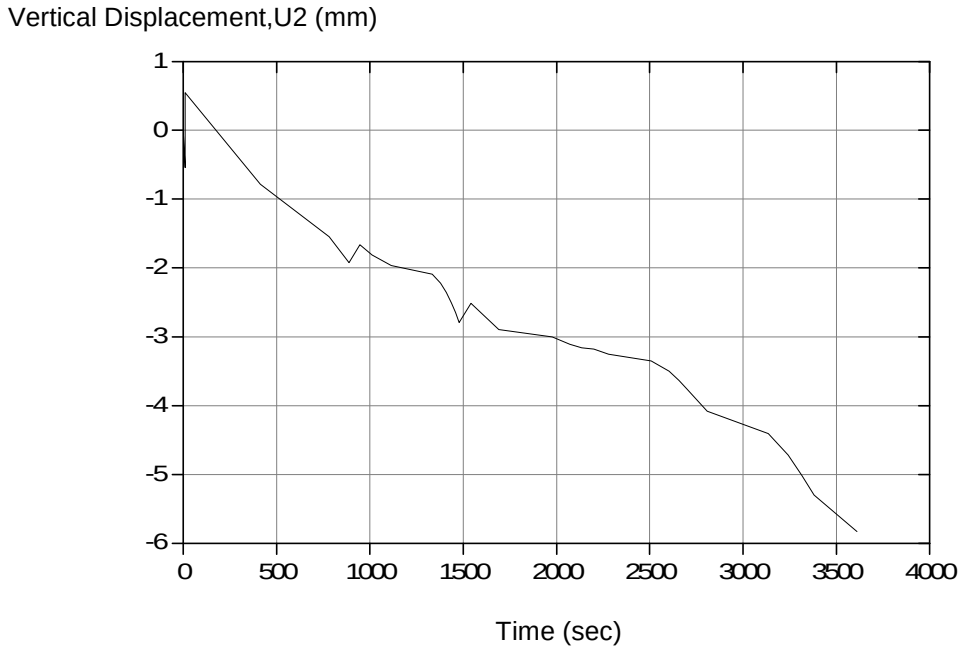

Figure 7-20 Vertical displacement (U2) at top beam of node 3010 (thermal loading analysis of undamaged frame)

Figure 7-21 shows the vertical displacement at the midspan of the plinth beam (node 1210). It can be seen that the initial deflection of 0.014mm (downwards) is due to the mechanical load applied. The plinth beam then begins to bow upwards due to heating of the top surface. A maximum deflection of 0.45mm was recorded during the fire. Figure 7-22 is show the vertical displacement of the plinth beam in thermal loading analysis of undamaged frame.

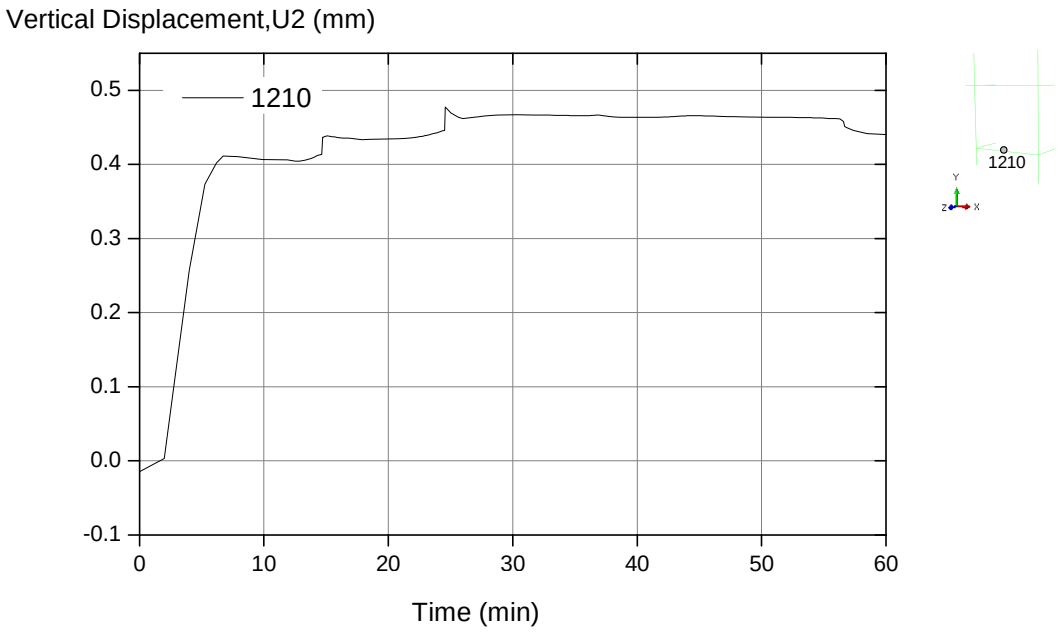

Figure 7-21 Vertical displacement (U2) at the plinth beam of node 1210

Figure 7-23 illustrates the midspan deflection of the slab at the top of the frame over the full history of the mechanical and thermal loading. An initial deflection of 0.54mm (downwards) is present due to the gravity and vertically applied loadings on the slab. A further downward deflection of up to 5mm occurred after the cyclic lateral loading. The slab deflected further downward during heating, due to thermally induced bowing (as a result of greater expansion of the inner, hotter surfaces than the top, cooler surfaces). A maximum deflection at midspan of 23.5mm was recorded at the end of the analysis. Vertical deflection recorded at the midspan of the slab for the undamaged frame is shown in Figure 7-24.

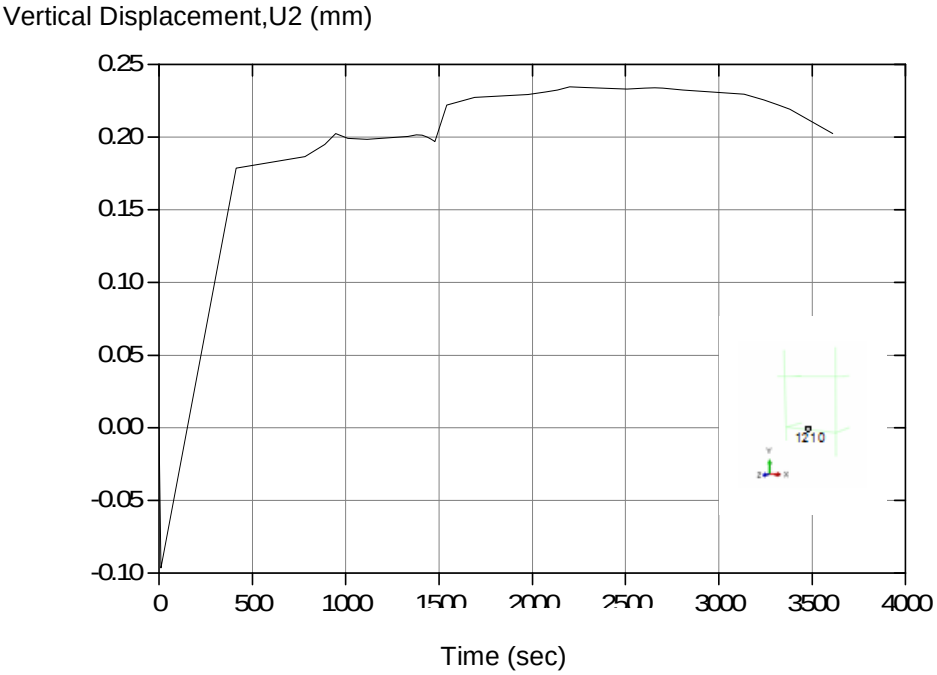

Figure 7-22 Vertical displacement (U2) at the plinth beam of node 1210 (thermal loading analysis of undamaged frame)

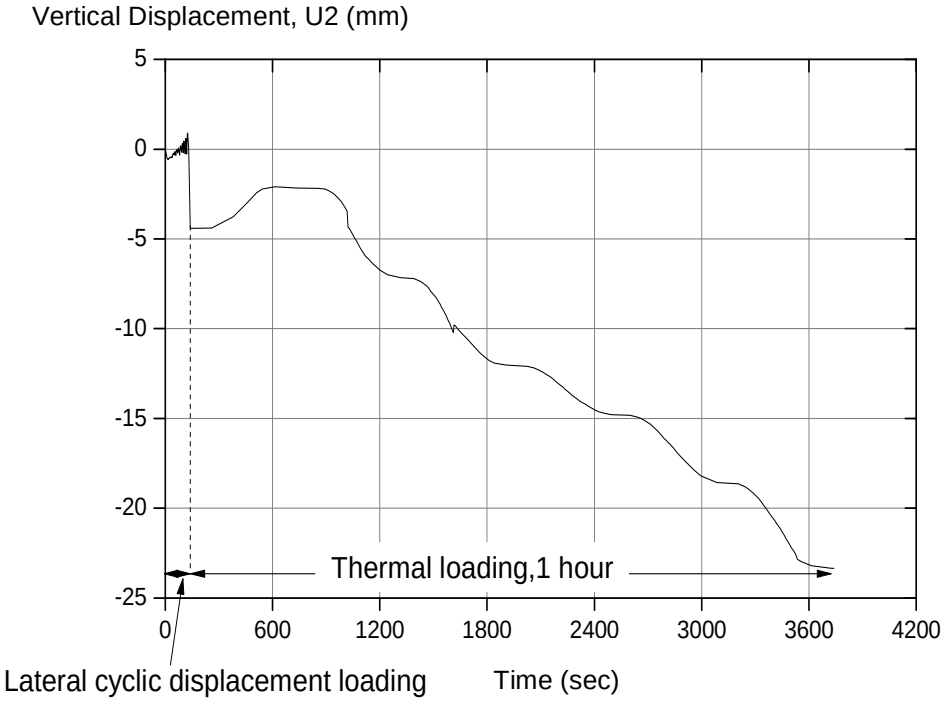

Figure 7-23 Vertical displacement (U2) at mid slab level due to thermo-mechanical loading

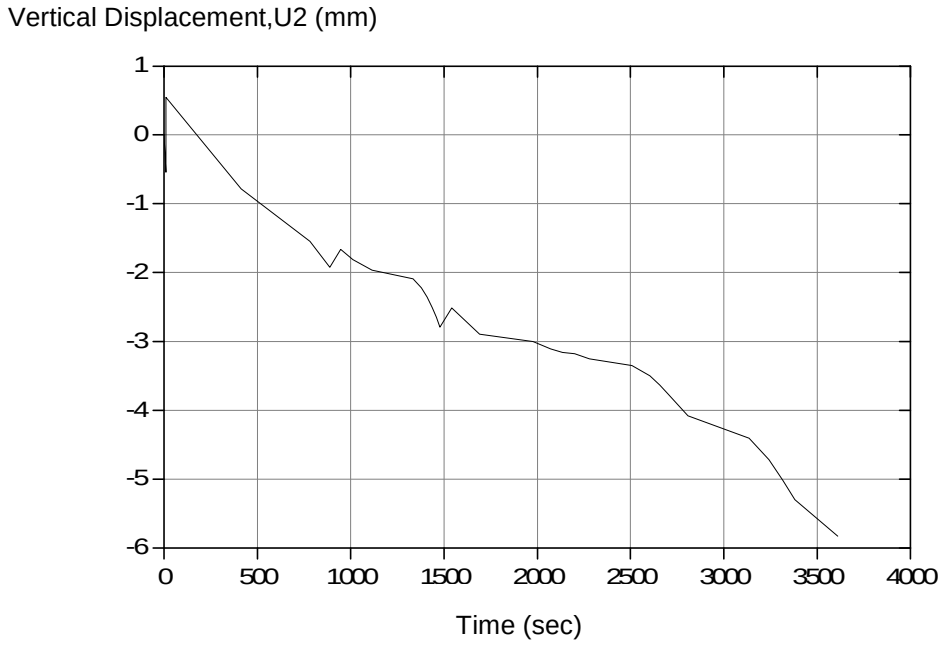

Figure 7-24 Vertical displacement (U2) at mid slab level (thermal loading analysis of undamaged frame)

7.3.2 Reaction Forces of the Frame Due to Thermo-Mechanical Loading

This section discusses the reaction forces at the base of the columns when subjected to thermo-mechanical loading. **Error! Reference source not found.**, **Error! Reference source not found.** and **Error! Reference source not found.** show the reaction force plot of the frame due to the heating. The reaction force was calculated from the column bases. There are initial forces in the x, y and z-directions due to the lateral displacement on the frame. At the end of the heating, the reaction force in the lateral loading direction (RF1) of the frame is 23kN. It is showing that the thermal loading induced forces to the frame. The horizontal reaction force in the z-direction (RF3) increases to 0.18kN (away the compartment) at the end of heating. It can be seen in the Figure 5-26 there are initial forces in vertical direction (in the y-direction, RF2) due to the gravity loading.

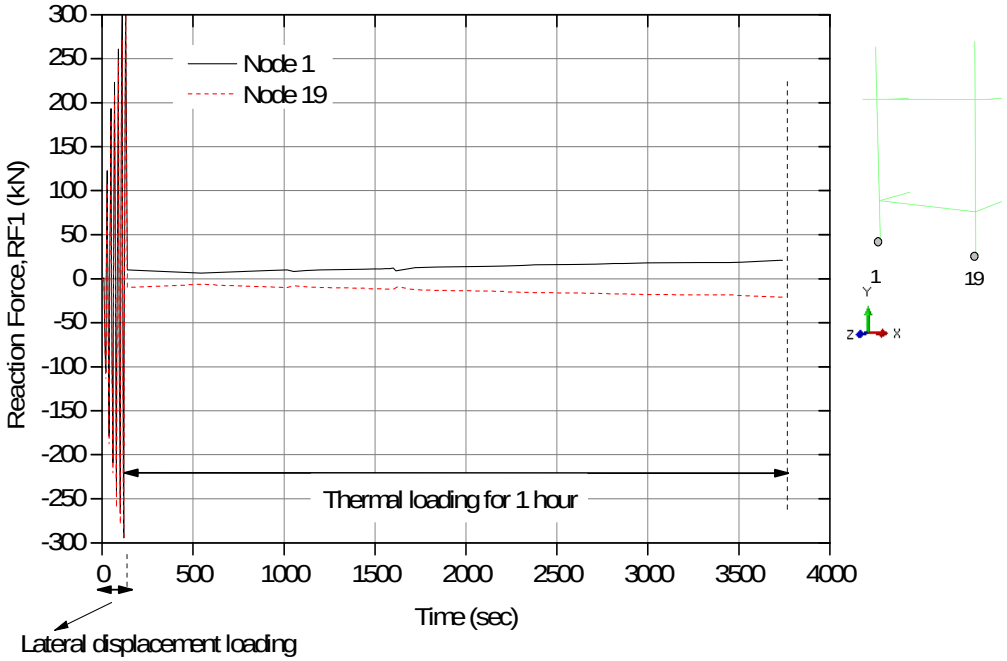

Figure 7-25 Reaction force (RF1) in x-direction of the frame due to thermo-mechanical loading

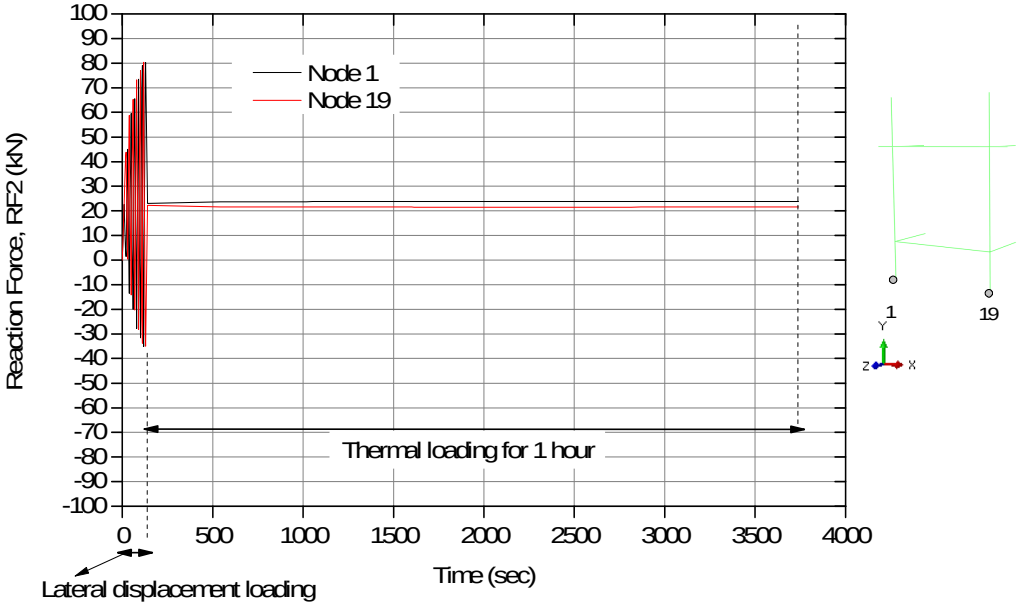

Figure 7-26 Reaction force (RF2) in y-direction of the frame due to thermo-mechanical loading

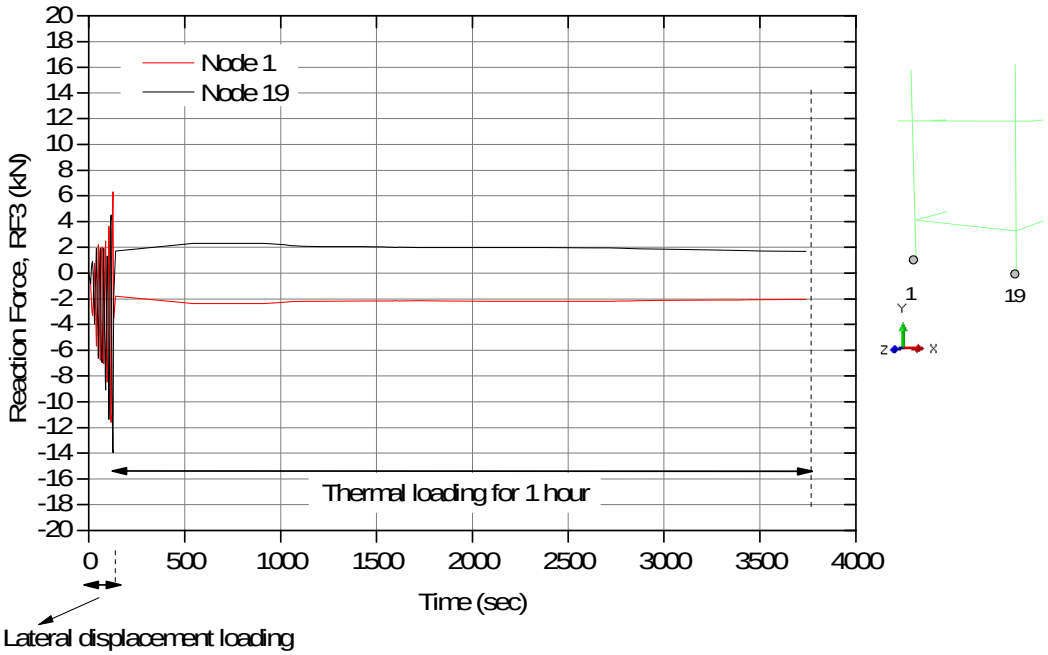

Figure 7-27 Reaction force (RF3) in z-direction of the frame due to thermo-mechanical loading

7.3.3 Forces in the Frame Due to Thermo-Mechanical Analysis

In to ABAQUS, the shear force present (SF3) is defined as the transverse shear force in the local x-direction. The variation of the shear force in both columns and the plinth beam are presented. For the column, the forces were measured at 200mm below the slab, and above the plinth beam. For the plinth beam it was measured at 400mm from the column.

Figure 7-28 and Figure 7-29 illustrate SF3 within both columns. As the thermal loading is applied, SF3 at the upper columns increases rapidly for the first 15 minutes of heating, before starting to reduce afterwards. The change in shear

force with temperature is from the thermally induced deformations (due to thermal bowing effect).

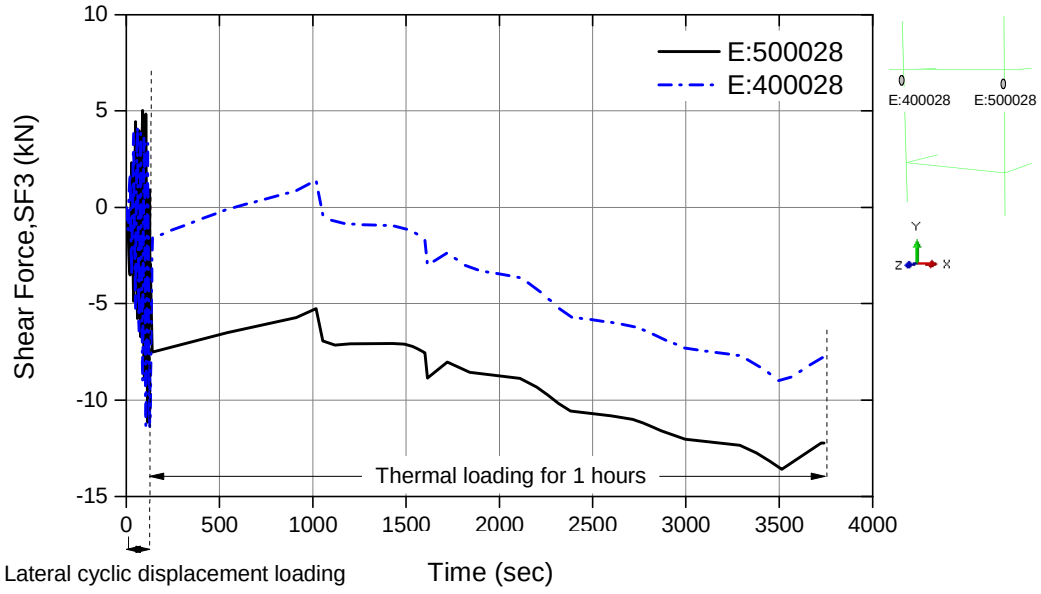

Figure 7-28 Shear force of both columns at 200mm below the slab

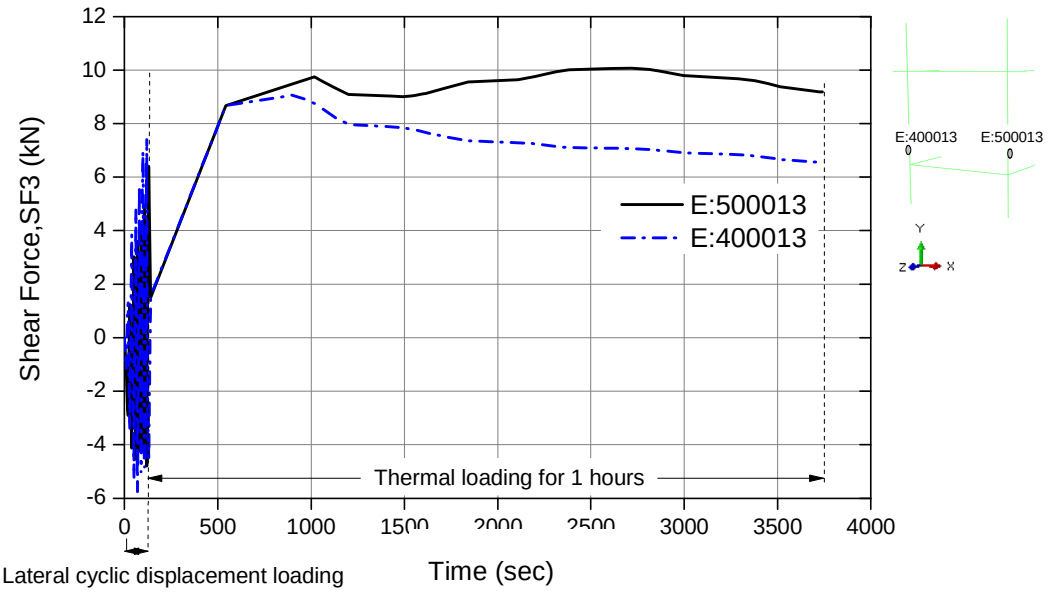

Figure 7-29 Shear force of both columns at 200mm above the plinth beam

Figure 7-30 and Figure 7-31 show SF3 of the plinth beam at 400mm from both columns. It can be seen that SF3 at the plinth beam is larger closer to the joints. The maximum SF3 value seen is 55kN at element E:300017.

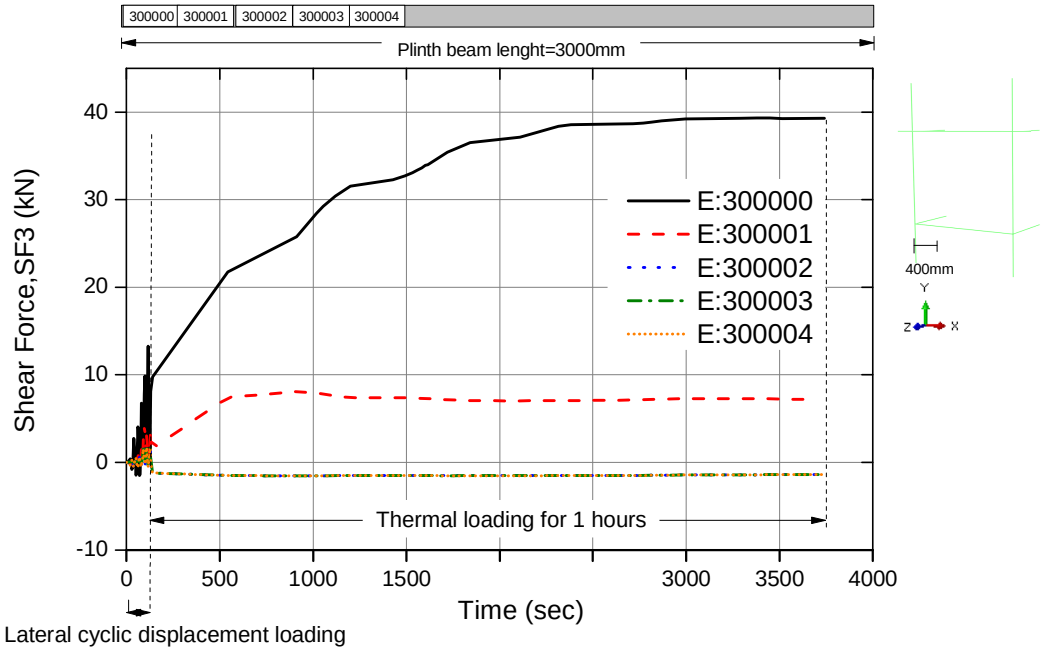

Figure 7-30 Shear force profile of the plinth beam at 400mm from left hand column

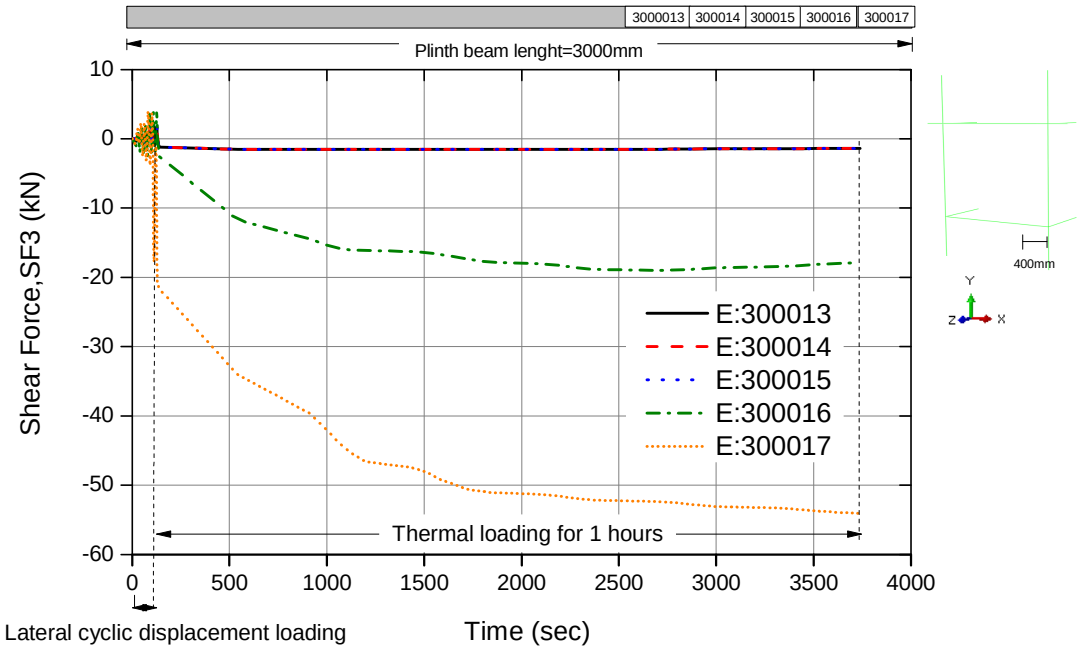

Figure 7-31 Shear force profile of the plinth beam at 400mm from right hand column

Figure 7-32 to Figure 7-34 illustrates the axial force (SF1) within the plinth beam. From those figures, it is seen that the SF1 increases rapidly (because of thermal expansion) as heating begins, but seems to stabilise in last 15 minutes of the analysis. The SF1 recorded at element E:300013 is larger than that seen in other elements.

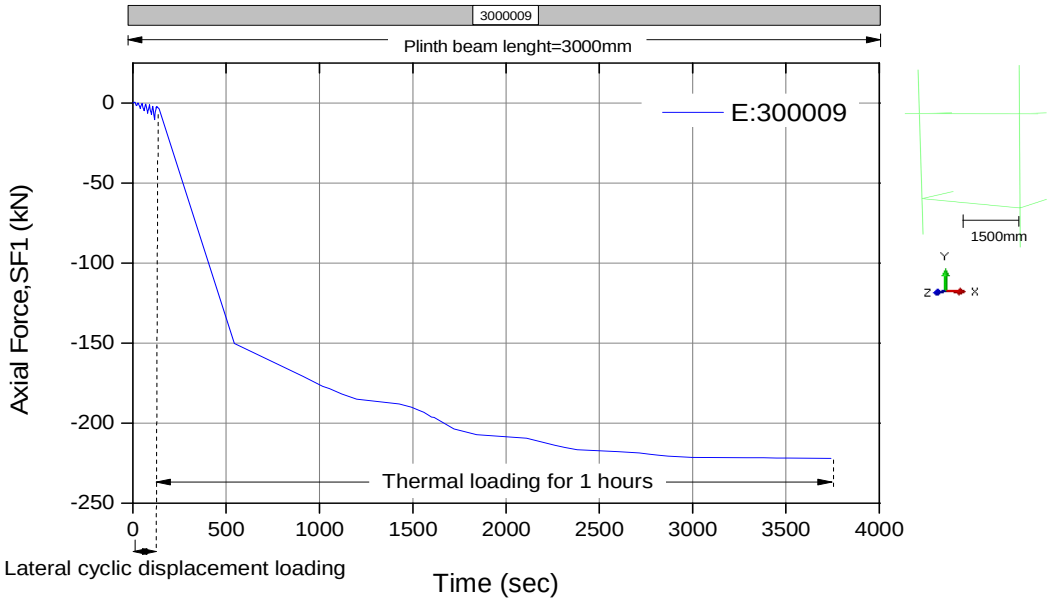

Figure 7-32 Axial force profile at mid span of the plinth beam

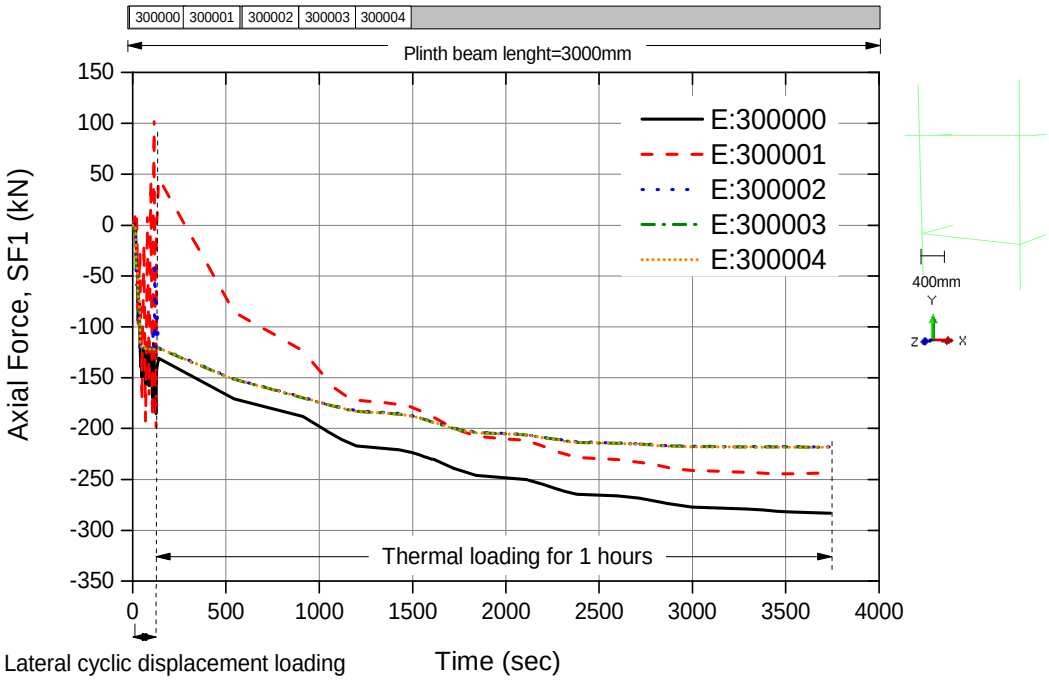

Figure 7-33 Axial force of the plinth beam at 400mm from left hand column

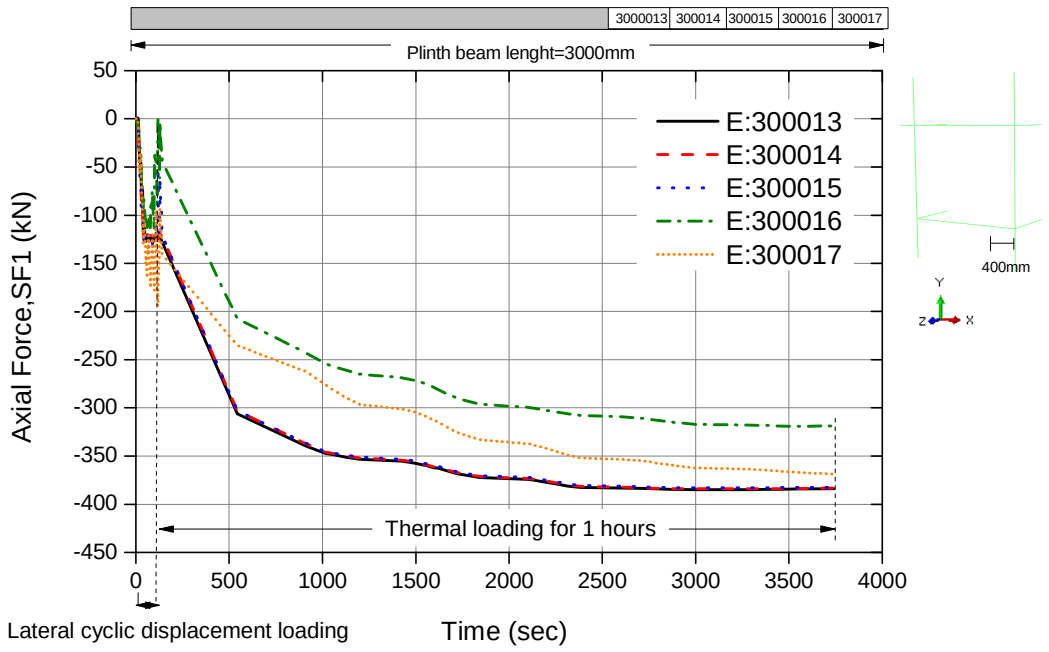

Figure 7-34 Axial force of the plinth beam at 400mm from right hand column

7.3.4 Bending Moment at Plinth Beam after Thermo-Mechanical Analysis

The bending moment (SM2) about the local y-axis of the plinth beam is shown in Figure 7-35 and Figure 7-37. It was measured at 400mm from the column. The SM2 value is 17kN.m larger at the left hand side than those values seen at mid span and the left hand side of the plinth beam. As the temperatures applied increase the plinth beam shows to bow downwards for the first 10 minutes. The plinth beam begins to bow upwards before returning to its initial shape by the end of the analysis.

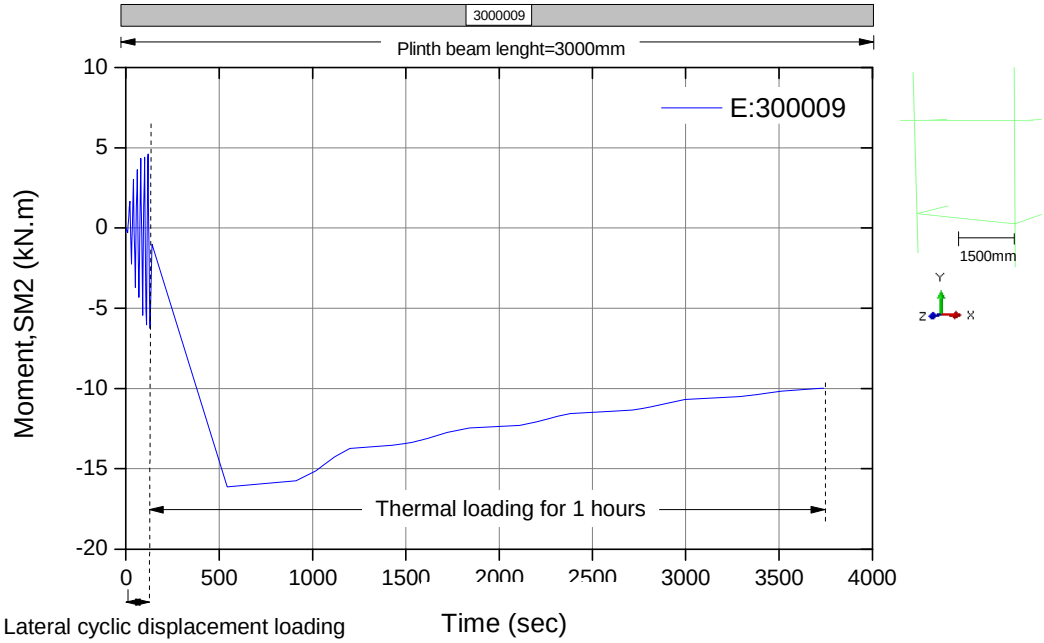

Figure 7-35 Bending moment profile at mid span of the plinth beam

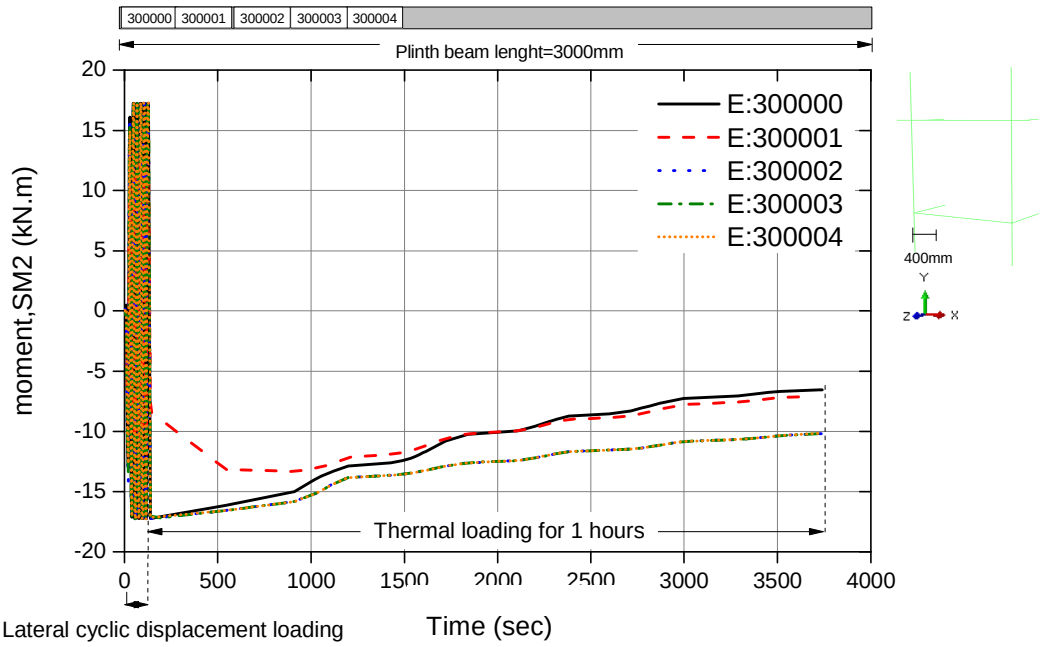

Figure 7-36 Bending moment profile of the plinth beam at 400mm from left hand column

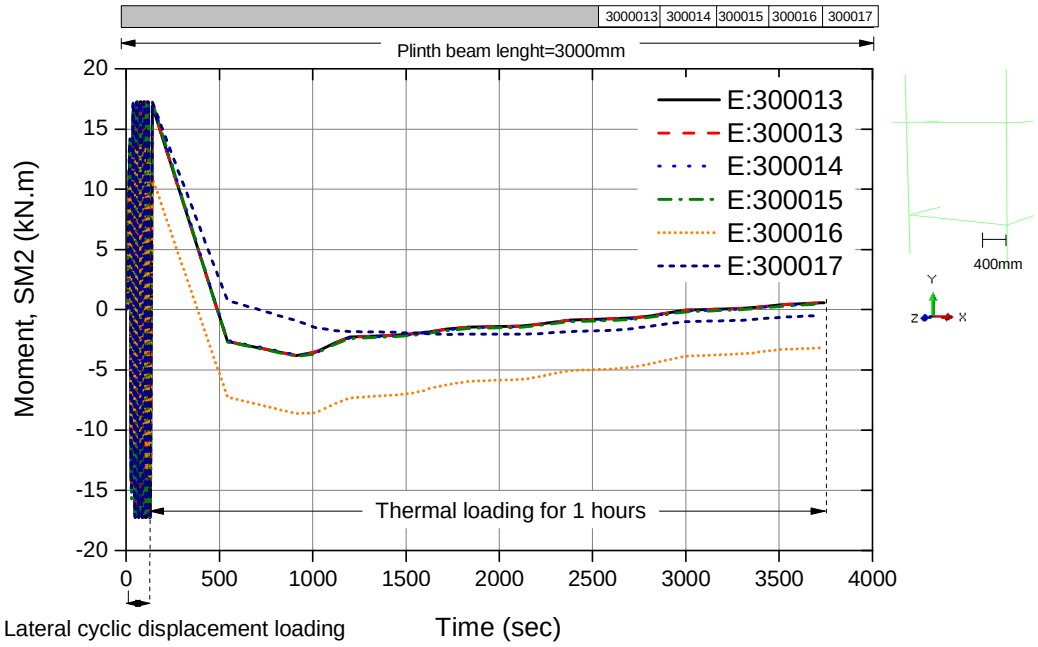

Figure 7-37 Bending moment profile of the plinth beam at 400mm from right hand column

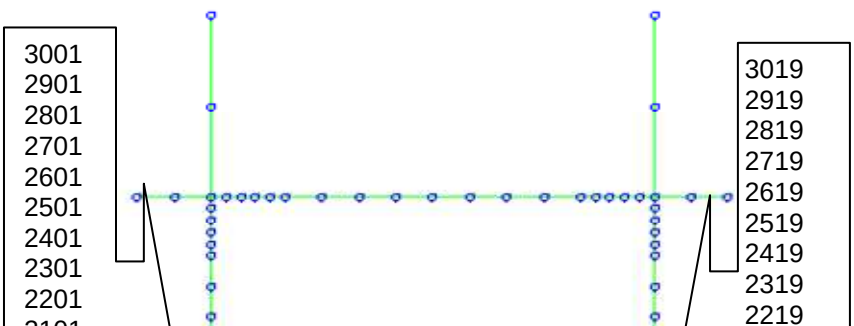

Figure 7-38 Nodes on the frame

Bending moments were measured along the height of both columns (see

Figure 7-38). Figure 7-39 and Figure 7-40 illustrates bending moment of both columns. In the beginning, the bending moment is increased and reduced after 1 hour of the heating.

The bending moment behaviour explained about end restraint effect in temperature. The initial increase in moment is because of the high rotation at ends-so the negative moment increases. At the same points there is some cracking or crushing of concrete at the ends which reduces the rotation restrain and the bending moment reduces.

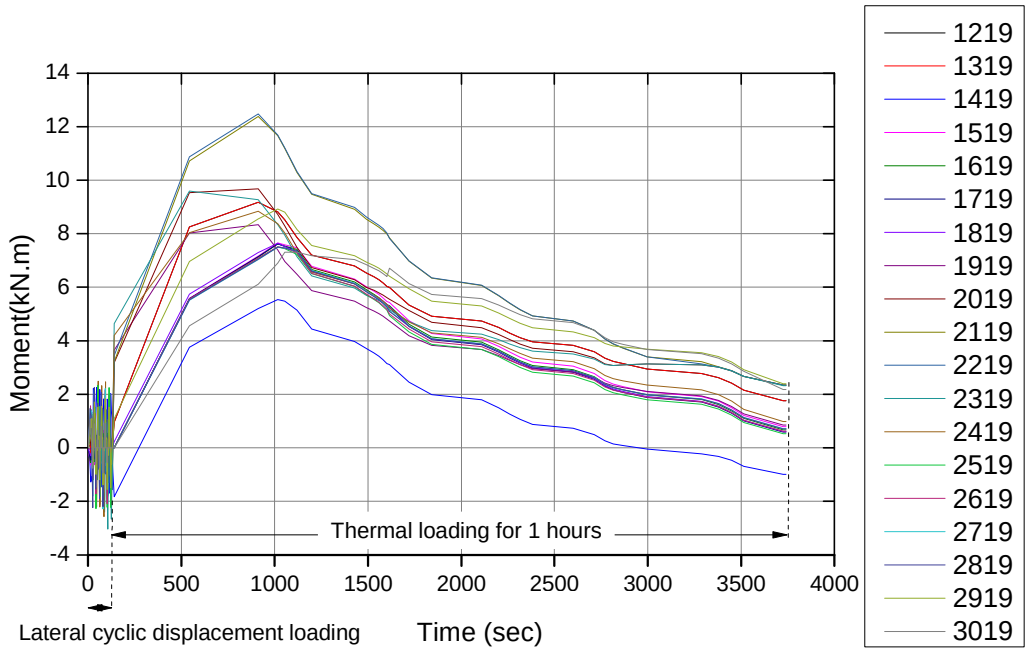

Figure 7-39 Bending moment profile of right hand column

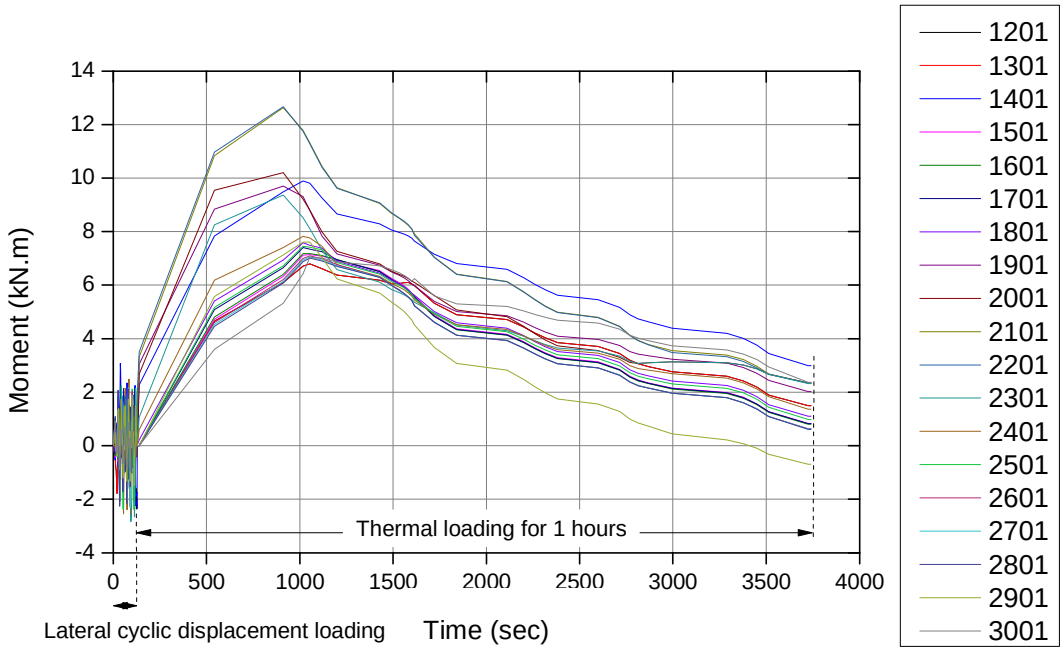

Figure 7-40 Bending moment profile of the left hand column

7.3.5 Horizontal Displacements Due to Monotonic Loading Followed by Fire

Monotonic lateral loading followed by fire is numerically examined using a 3D ABAQUS model of the reinforced concrete frame. In this section, the horizontal displacement obtained from the analysis is presented. Figure 7-41 to Figure 7-43 illustrate the horizontal displacements of nodes 3001 and 3019 when subjected to lateral displacements of 50mm, 70mm and 95mm followed by fire.

The frame was subjected to different levels of displacement and then released. After that, the frame was exposed to fire for one hour. The thermal loading used is the same used in other analyses. The figure shows that during the fire the frame moves back towards its original position. This suggests that the thermal expansion due to thermal loading plays a role in the frame's behaviour during the fire.

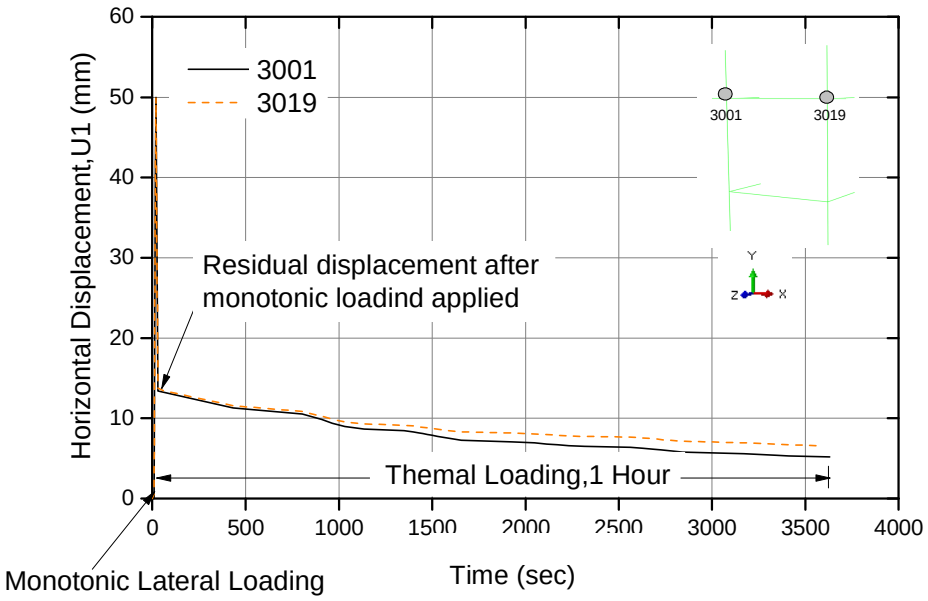

Figure 7-41 Horizontal displacement (U1) in x-direction of Nodes 3001 and 3019 subjected to monotonic lateral loading, 50mm followed by fire-3D Model

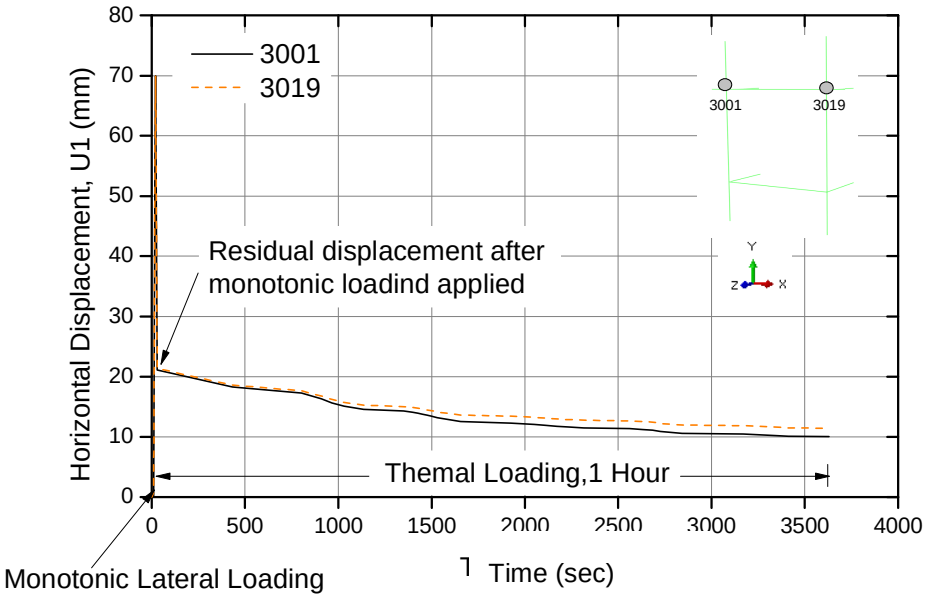

Figure 7-42 Horizontal displacement (U1) in x-direction of Nodes 3001 and 3019 subjected to monotonic lateral loading, 70mm followed by fire-3D Model

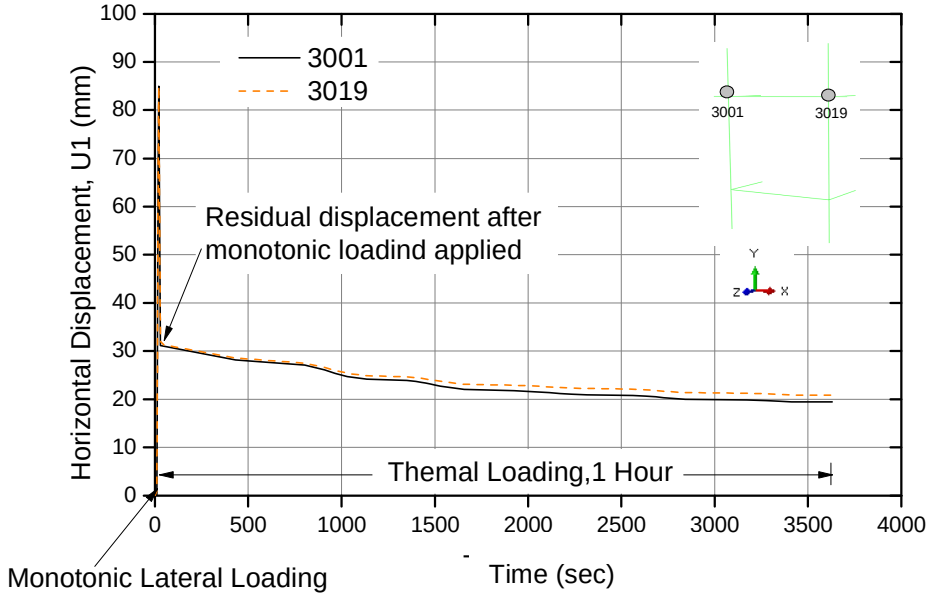

Figure 7-43 Horizontal displacement (U1) in x-direction of Nodes 3001 and 3019 subjected to monotonic lateral loading, 95mm followed by fire-3D Model

7.4 Discussion and Conclusions

A full 2D ABAQUS beam element analysis of the reinforced concrete frame has been conducted and compared with available test data and OpenSees results. The concrete damage plasticity model was used to model the concrete. The damage parameter in the concrete material was considered in order to take the effects of damage due to cyclic loading into account.

Only half of the frame was developed in the 3D ABAQUS model to simplify the problem and reduce the analysis time. The Drucker Prager concrete model was used to define concrete behaviour during the analysis. The pinching effect often seen in the reinforcing steel was not considered in this analysis. The temperatures applied to the elements in the thermo-mechanical analysis were based on the element temperatures obtained during the test, and used in previous numerical models.

Based on the target displacement obtained from the pushover analysis, 7 cyclic lateral displacements have been applied to simulate the ground motion behaviour of the frame. The displacement history used in the numerical analysis was taken from idealised values seen in the displacement history of the test.

After damage has been caused to the frame by cyclic lateral loading, it was exposed to elevated temperatures for 1 hour. At the end of the heating, there were decreasing temperatures seen as the fuel in the test ran out. However no cooling effects were considered in this study; loading was only applied to the frame after it had fully cooled over the course of a few hours.

The columns were considered to have different temperature distributions along their heights. The displacements of the frame base when subjected to elevated temperature and thermo-mechanical analysis were plotted for further

discussion. When the frame was subjected to elevated temperature, the horizontal displacement of the slab and columns reduced as the time exposure increased.

The 3D ABAQUS model shows a vertical deflection at the mid point of the slab of 23.5mm (downwards). This value does not match with the value of 46mm recorded during the test, Test 1 [120]. The difference is due to two main factors: the surface temperature used in the numerical analysis (which is taken at a depth of 5mm depth below the surface) was lower than those recorded in the test; and the fact that thermal spalling was not considered in the numerical simulations, even though this effect was physically observed in the test.

The horizontal displacements seen at nodes 3001 and 3019, at slab level of the frame, are plotted. For both of the ABAQUS models described, the displacements plotted suggested that the frame was moving back towards its original position at the end of heating. The stiffening effect of the reinforcing steel at elevated temperatures in the thermo-mechanical analysis was slightly evident. The displacements of the frame were recorded in thermal loading analysis of undamaged frame shown similarity and have smaller value compared to damaged frame.

End reactions effects with temperature clearly seen in bending moment diagram of the plinth beam. In the beginning, increased negative bending moment was recorded due to high rotation restraint at the ends. As the temperature increases there is some cracking or crushing of concrete at the ends of the element, leading to a reduction in the rotational restraints and a reduction in the bending moment present.

8

Summary, Conclusions and Recommendation for Further Work

8.1 Introduction

The research presented in this thesis is diverse and wide ranging. Some background information on engineering structural resistance to earthquakes and fires is presented in order to place this research in context. The research presented in this thesis makes an important contribution to furthering our understanding of the response of earthquake damaged reinforced concrete frames in fire.

The performance of earthquake damaged reinforced concrete frames was numerically examined. The sequence of analysis comprised of three main stages – gravity loading, followed by cyclic incremental lateral loading in displacement-control mode to simulate earthquake damage to the frame, and, finally, the thermal loading representing a fire. Static push over analysis and the heat transfer analysis were also performed to provide a detailed explanation of

the performance of the frame. Extensive studies on different modelling methods then followed.

The performance analysis methodology reviews the necessity of the background knowledge undertaken. The study touched on a number of the key points that concern structural earthquake and fire engineering, including the complexity of constitutive numerical modelling, and how it can be implemented. A combination of techniques for frame assessment when subjected to an earthquake followed by fire was developed. The study on the selection of emissivity parameters in a heat transfer analysis was presented.

The purpose of this chapter is to present the summary, review the specific conclusion from each of the areas studied, and discuss a more general conclusion from the work as a whole. At the end of this chapter, several remommendation for furher work is discussed.

8.2 Summary

The research conducted is briefly summarised as below.

8.2.1 Constitutive Models

One of the key factors affecting the accuracy of finite element models is the constitutive model chosen. Subtle changes to the constitutive modelling parameters produce significant differences in the results of the finite element model. A brief summary of the work on constitutive modelling of concrete is presented in bullet points.

- Concrete damage plasticity with damage parameters was used in the 2D ABAQUS beam element model. The concept of isotropic damaged

elasticity in combination with isotropic tensile and compressive plasticity was implemented to represent the inelastic behaviour of concrete. The damage parameter in compression was defined for the reduction effect to be taken into account in load reversal.

- In the 3D ABAQUS beam and shell element model, the Linear Drucker-Prager model with tension stiffening was used. The ratio of the compressive yield strength and the tensile strength of the concrete gave the value of the friction angle, β, and dilation angle, ψ.
- The two constitutive models are broadly similar in their trends and implementation. Neither of the constitutive models used in this study considered the pinching effect under cyclic loading.
- The pinching effect was clearly presented in the hysteresis curve of the test. As expected, this effect was not seen in the numerical analysis.
- Prior to fire loading, material properties were set to the ambient temperature. Once the fire loading had taken effect, the mechanical properties changed with time. The material constitutive calculations are in accordance with Eurocode 2 Part 1.2

8.2.2 Modelling and Analysis Methodology

The modelling of the earthquake damaged reinforced concrete frame followed by fire was developed using ABAQUS. Methods appropriate for analysing the structural behaviour both in ambient and at elevated temperatures were used. The details of the modelling and analysis methodology were presented in Chapters 4, 5, 6 and 7. Several conclusions can be drawn from the modelling and analysis methods:

- The 2D ABAQUS and the 3D ABAQUS models were used for numerically investigating the response of reinforced concrete frames subjected to an earthquake followed by fire, by considering the

appropriate material model and temperature loading applied to the elements.

- The gravity and lateral loading applied to the frame was based on the desired weak beam strong column behaviour. These load calculations are in accordance with the recommendations in the Indian Standard (IS 13920:1993). Several preliminary analyses were carried out using different to ensure that the desired frame behaviour was achieved during the experiments in IIT Roorkee.
- This study did not cover long-term effects, such as creep and shrinkage, and load duration was not important for either gravity or earthquake loads. Therefore, any arbitrary load duration could be chosen for these loads. The spalling effect is also not covered in this study.
- The study of the response to fire following an earthquake has been achieved using sequential nonlinear analysis carried out in three stages.
- The first stage was the application of a gravity load to the frame. This loading was assumed to be static and uniform.
- In the second stages, incremental cyclic lateral loading in displacement control mode was applied until the frame's peak displacement was reached (determined from pushover analyses earlier and from tests) and then released allowing the damaged frame to find its equilibrium displacement.
- Finally a compartment fire for 1 hour was applied in the third stage of the analysis. The temperatures were taken from the average recorded compartment temperatures.
- Heat transfer analysis was performed (see Chapter 6) to develop an understanding of the temperature distributions in the structural elements and to compare with the recorded compartment

temperatures. A 3D continuum solid element model was used to perform a heat transfer analysis based on the recorded compartment temperatures in the IIT frame test. This produced detailed temperature distributions in the heated structural elements against time.

- During the test, some of the thermocouples and displacement transducers failed due to high temperatures. Therefore insufficient data was available to fully compare the numerical results against the test results.
- The 2D ABAQUS model represented the peak response of frame under cyclic loading reasonably well and the fire load simulation, following the cyclic loading, produced convergent results in economical computational times. However in this analysis the response in the slab simplified and therefore compromised the quality of the results.
- In the 3D ABAQUS model, beam elements were used for the beams and columns and shell elements were used to model the slab. The 3D ABAQUS model presented the whole behaviour of the frame, including the slab deformation. The 3D model produced results that compared better agains the test results, particularly during the cyclic loading stage.

8.2.3 Thermal Loading

The temperature curves used in the analysis were based on the average compartment temperature. The parametric study on the heat transfer analysis was presented in Chapter 5. Several conclusions can be drawn from this study.

- The fire heated the frame primarily through a radiative flux emanating from a 1 meter square tray of kerosene fuel (maintained at constant head over one hour).

- The emissivity of the hot gases and smoke was calculated based on the fuel type and pool fire diameter. A study of emissivity values was set up on the basis of the smoke layer in the compartment fire. A parametric study concerning the various emissivity values was presented.
- Different temperature regimes were applied along the height of the compartment fire (along the height of the columns) to take the smoke layer height into account.
- The cooling effect was not included in this study.
- The results from the heat transfer analysis shows that the temperature distributions were significantly different to results from the recorded compartment temperature.
- This suggests that the assumptions made in the heat transfer analysis must be investigated further to obtain better agreement with the real temperatures.

8.2.4 Lateral displacement analysis

The displacement response of the structure was monitored during the application of the incremental cyclic lateral loading in displacement control mode. Several conclusions were drawn from this study.

- The capacity curve obtained from the numerical analysis and test was presented (see Chapter 5). At lower displacements, the strength of the frame obtained from the 2D ABAQUS model was lower than the test result, while the strength of the frame obtained from the 3D ABAQUS model was higher than the test result.
- The inelastic response of the frame was achieved earlier in the 3D ABAQUS model compared to the 2D ABAQUS model.

- At higher displacements, the frame responded similarly in both numerical analyses.
- Greater energy dissipation was obtained in the 2D ABAQUS model compared to the 3D ABAQUS model. The full model represents the rational response of the frame under cyclic loading and unloading. However, none of the hysteresis curves obtained from numerical analyses presented the pinching effect. This was expected since this effect was not considered in this study.
- Disregarding the pinching effect leads to higher relative displacements in the numerical analysis compared to the test data.
- The residual permanent displacement at the end of cyclic loading obtained from the 2D and the 3D ABAQUS models is 55mm and 27mm respectively. The ABAQUS models show a significantly higher result than that seen in the test (20mm).

8.2.5 Thermo-mechanical analysis

The thermo-mechanical analysis of the reinforced concrete frame was carried out for a one-hour compartment fire. The temperature distributions used were taken from average recorded structural member temperatures. Temperature was input at specific points in the beam section. The displacement response of the frame was presented in Chapter 7. Several conclusions from the analysis are presented as follows:

- The 2D ABAQUS model shows the thermal expansion effect, which leads to the frame moving inward during initial heating.
- The 3D ABAQUS model also shows the thermal expansion effect, leads to stiffen the frame causing both columns moving back towards its initial position at the end of heating. The slab deflection at the end of the analysis is 23.5mm which is significantly smaller than the test result

(46mm). The difference is due to thermal spalling which is not accounted for in the modelling and the temperature used in the analysis was lower compared to the test. The hotter surface temperature and greater loss of concrete cover within the slab has significant influence to the deflection of the heated slab.

- An increase in negative bending moment, due to high rotational restraints at the ends, can be seen. As the temperature increases, there is some cracking or crushing of concrete at the ends of the element. This leads to a reduction in the rotational restraint and the bending moment.

8.3 Conclusions

The key conclusions from the from this research is presented as following.

1. The finite element numerical modelling method, when parameters such as element type, material model, and analysis type are taken into consideration, is able to simulate the behaviour of reinforced concrete earthquake damage followed by fire.
2. The limitation in the material models used in ABAQUS is clearly presented in the hysteresis curve of the frame due to cyclic lateral loading. The bond between reinforcing steel and concrete is not considered in the analysis. Any interaction between the reinforcing steel and concrete is defined as the materials being perfectly attached to each other, with no bond slip.
3. Both 2D and 3D ABAQUS models are able to present the global behaviour of the frame when subjected to monotonic and cyclic lateral loading, producing a similar curve to that obtained in the Roorkee Frame Test 1.

4. The ABAQUS model gives results which match more closely the data from the Roorkee Frame test 1 than the 2D OpenSees model, when both are subjected to monotonic lateral loading.
5. The heat transfer analysis using ABAQUS is done by using the smoke layer method. The emissivity values used are based on the type of the fuel used in the enclosure and the smoke height. The temperature distribution found in the elements at the surface of the model is higher for the analysis than those seen in the test. This is due to the emmisisvity value used in the analysis not being able to represent the real heat transfer seen in the test. It suggests that not only fuel type, but smoke layer height plays a role in the heat transfer analysis when using ABAQUS. The enclosure temperature used might be lower than that seen in the real test. This is because the temperature in enclosure used in the analysis is taken from one of the three thermocouples in the enclosure in the test. This has the effect of lowering the surface temperature obtained in the analysis.
6. The simulation of the response due to thermo-mechanical analysis is solely carried out using the 3D ABAQUS model. In this analysis there is no valid result from the test to use for comparison. In the analysis, thermal loading causes the frame to move back towards its initial position (by the end of the heating phase) from its displacement at the end of cyclic lateral loading (when it has a residual horizontal displacement in the x-direction present). This is due to thermal expansion during the heating stiffening the reinforcing steel, back to its initial length. Thermal loading causes some cracking or crushing in the elements. This leads to a reduction in the rotational strain present during heating. Consequently, the bending moment present in the beam reduces at the end of the heating step.

8.4 Recommendation for Further Work

The study of fire following an earthquake on concrete structures can be considered to be in its early stages. There is a wide range of work that can be conducted on the response of reinforced concrete structures subjected to fire following an earthquake. The research described in this thesis has taken this understanding further, however, inevitably many issues remain unresolved.

Under cyclic loading and unloading, the pinching effect in either the material or structural elements was not considered in this study. For earthquake response, this behaviour is considered an important parameter and should not be ignored in future research. It can be seen in the hysteresis plot from the test.

It could be included by developing a constitutive model in ABAQUS for either the material or elements that include the pinching effect for frames structure subjected the cyclic loading

In this study, the temperature curve was applied based on the test data. A wide range of temperature loading could be applied to the frame in the future. In this study, the pool fire was considered in the middle of the compartment.

For the future, the pool fire could be considered at different locations and fuel pool size in the frame.

Different temperature durations could be considered. The response of the frame to different heating types is expected to vary.

The cooling effect could also be considered in future to show the response of the frame post-fire

.

References

[1] ABAQUS: *Abaqus Analysis User's Manual*. Providence, Dassault Systemes Simulia Corp, 2008

[2] Anderbergh Y: *Spalling Phenomena of HPC and OC*. Presented at the *NIST Workshop on Fire Performance of High Strength Concrete, Gaithersburg,* 1997

[3] Ansys, http://www.ansys.com/, 2010

[4] ASTM E119-95a *Standard test methods for fire tests of building construction and materials*, 1995

[5] ATC 40 *Seismic Evaluation and Retrofit of existing concrete buildings,* 1996

[6] Babrauskas V: *Burning Rates*. *SFPE Handbook of Fire Protection Engineering.National Fire Protection Association,Quincy, Massachusetts, 1995*

[7] Babrauskas V: *Estimating Large Pool Fire Burning Rates. Fire Technology*, 1983

[8] Bahn BY, Thomas HCT: *Stress-Strain behaviour of concrete under Cyclic Loading.* ACI Material Journal 1988, 95:178-193

[9] Bard P.-Y: *Effects of Surface Geology on Ground Motion: Recent Results and Remaining Issues Duma*. 10th European Conf. on Earthquake Eng., Vienna, 1994 1:305-323

[10] Bathe KJ: *Finite Element Procedures in Engineering Analysis.*Prentice-Hall Inc, 1982

[11] Bazant ZP, Kaplan MF: *Concrete at High Temperatures: Material Properties and Mathematical Models*. Harlow, Longman Group Limited, 1996

[12] Beattie GJ: *Seismic Restraint of Building Services*. Presented at the Australasian Structural Engineering Conference (ASEC),Australia, 2001

[13] Beattie GJ: *The Design of Building Services for Earthquake Resistance*. Presented at the 12th World Conference on Earthquake Engineering, Auckland, 2000

[14] Bernal D: *Amplification factors for inelastic dynamic P-delta effects in earthquake analysis*. *Earthquake Eng. Struct. Dyn.1987, 15:*635-651

[15] Bertero V V, et. al.: *Seismic Response of the Charaima Building.* Report No. EERC- 70/4 by Earthquake Engineering Research Center. University of California, 1970

[16] Bhargava P., et. al., Fire Testing of an Earthquake Damaged RC Frame, Seventh International Conference on Structures in Fire, Zurich, June (2012)

[17] Bhargava, P., et. al., Fire Testing of an Earthquake Damaged RC Frame, Sixth International Conference on Structures in Fire, Michigan, June (2010)

[18] Bird FF, Bommer JJ: *Earthquake Losses due to ground failure.*Engineering Geology Journal 2004, 75:147-179
[19] Blinov VI, and Khl GN: *Diffusion Burning of Liquids*. U.S. Army Translation, NTIS No. AD296762, 1961
[20] Bommer JJ, Boore DM: *Engineering seismology;Encyclopaedia of Geology*. New York, Academic Press, 2004
[21] Borcherdt RD: *Effects of Local Geology on Ground Motion Near San Francisco Bay.* Bull. Seismol Soc Am, 1970, 60:29–61
[22] Both C, Van De HP, Tan G, and Wolsink G: *Evaluation of Passive Fire Protection Measures for Concrete Tunnel Linings*. Proc. Int. Conf. on Tunnel Fires and Escape From Tunnels, France, May, 1999
[23] Botting R, Buchanan AH: *Building Design for Fire After Earthquake. Presented at the* 12th World Conference on Earthquake Engineering, Auckland, 2000
[24] Botting R: *The Impact of Post-Earthquake Fire on the Built Urban Environment.* Fire Engineering Report 98/1. University of Canterbury, Christchurch, 1998
[25] Bracci JM, Kunnath SK, Reinhorn AM: *Seismic performance and retrofit evaluation of reinforced concrete structures*. Journal of Structural Engineering (ASCE) 1997,123:3–10
[26] Brayn LJ: *SFPE Handbook of Fire Protection Engineering*. National Fire Protection Association, 2002
[27] Brunsdon D, Clark W: *Modern Multi-storey Buildings and Moderate Earthquakes.* Project No. EQC 93/173. Earthquake Commission Wellington, New Zealand, 2000
[28] BSI 476-20:1987: *Fire Tests on Buildings Materials and Structures-Part 20: Method for Determination of thefire Resistance of Elements of Construction*. British Standard Institution, UK, 1987
[29] Buchanan AH: *Structural Design for Fire Safety.Chichester*, WILEY, 2006
[30] Change YY, Deng HZ et al.: *A simplified Method for Nonlinear Cyclic Analysis of Reinforced Concrete Structures: Direct and Energy Base Formulations. Presented at* 13th World Conference on Earthquake Engineering, Vancouver Canada, 2004
[31] Chopra AK: *Dynamic of Structures:Theory and Application to Earthquake Engineering.* New Jersey, Prentice Hall,1995
[32] Drysdale D :*An Introduction to Fire Dynamic*. Second Edition. John Wiley&Sons,Chichester, UK, 1998
[33] Ellobody E, Bailey CG: *Testing and Modelling of Bonded and Unbonded Post-Tensioned Concrete Slabs in Fire*. Presented at the 5th International Conference on Structures in Fire. Singapore, 2008
[34] EN1991-1-1: *Eurocode 1: Action on Structures- Part 1-1: General Actions- Densities, Self-Weight and Imposed Loads*, 2009
[35] EN1992-1-2: *Eurocode 2: Design of concrete structures - Part 1-2: General rules - Structural Fire Design*, 2004

[36] EN1993-1-2: *Eurocode 3: Design of Steel Structures - Part 1-2: General Rules - Structural Fire Design,* 2005
[37] EN1998-1-1: *Eurocode 8: Design Provisions for Earthquake Resistance of Structures- Part 1-1:General Rules and Rules for Buildings,* 1998
[38] Evison FF: *On Occurrence of Volumes Change of The Earthquake Source.* Bull. Seism. Soc. Am., 1967, 57(1):9-25
[39] Evison FF:*Earthquake and Faults.*Bull.Seism.Soc. Am.,1963, 53(5):873-91
[40] Fajfar P, Gaspersic P: *The N2 Method for The Seismic Damage Analysis of RC Buildings*. Earthquake Engineering and Structural Dynamics Journal 1996, 25:31–46
[41] FEMA 273: *NEHRP Guidelines for The Seismic Rehabilitation of Buildings,* 1997
[42] FEMA 349: *NEHRP Action Plan for Performance Based Seismic Design,* 2000
[43] FEMA 356: *Prestandard and Commentary for the Seismic Rehabilitation of Buildings,* 2000
[44] FEMA 366 : *Estimating Losses with HAZUS*. Federal Emergency Management Agency, 2002
[45] Fleming RP: *Analysis of Fire Sprinkler Systems in the Northridge Earthquake.*Report No. NIST GCR-98-736. National Institute of Standards and Technology,Gaithersburg 1998
[46] Foster S, Chladná M, Hsieh C, et al.: *Thermal and Structural Behaviour of a Full-Scale Composite Building Subject to a Severe Compartment Fire.* Fire Safety Journal 2007, 42:183-199
[47] Franssen JM: *Safir. A Thermal/Strucutral Program Modelling Structures under Fire*. AISC Engineering Journal 2005, 42:143-58
[48] Gates WE, McGavin G : *Lessons Learned From the 1994 Northridge Earthquake on the Vulnerability of Non-Structural Systems*. Presented at the Seminar on Seismic Design, Retrofit and Performance of Non-Structural Components, San Francisco, 1998
[49] Georgali B, and Tsakiridis PE: *Microstructure of Fire-Damaged Concrete. A case study*. Journal Cement & Concrete Composites, 2005, 27:255-259
[50] Gillie M, Usmani A, Rotter M, et al.: *Modelling of Heated Composite Floor Slabs with Reference to the Cardington Experiments*. Fire Safety Journal 2001, 36:745-767
[51] Goel RK, Chopra AK: *Evaluation of Code Formulas for fundamental period of buildings. Presented at the 11*th World Conference on Earthquake Engineering,Mexico, 1996
[52] Grossi P, Kleindorfer P, Kunreuther H: *The Impact of Uncertainty in Managing Seismic risk: The Case of Earthquake Frequency and Structural Vulnerability. Report by* The Wharton Financial Institutions Center and The Whatron Risk Magement and Decision Processer Center 1998

[53] Hamburger RO: *A Framework for Performance-Base Earthquake Resistive Design*. Presented at the EERC-CUREe Symposium, California, 1997
[54] Handoo SK, Agarwal S, Agarwal SK: *Physicochemical, Mineralogical and Morphological Characteristics of Concrete Exposed to Elevated Temperatures*. Cement and Concrete Research 2002, 32:1009-18
[55] Hertz KD: *Concrete Strength for Fire Safety Design*. Magazine of Concrete Research 2005, 57:445-53
[56] Heskestad G: *Fire Plumes.SFPE Handbook of Fire Protection Engineering. National Fire Protection Association, Quincy, Massachusetts, 1995*
[57] Hottle HC; *Heat Transmission.*MacGraw-Hill, New York,1954
[58] Housner GW: *An Historical View of Earthquake Engineering*. Presented at the 8th World Conference on Earthquake Enignering,San Francisco,1984
[59] Hu Y, Burgess I, Davison B, et al.: *Modelling of Flexible End Plate Connections in Fire Using Cohesive Elements*. Presented at the 5th International Workshop Structure in Fire, Singapore, 2008
[60] Huang Z, Burgess IW, Plank RJ: *A Non-linear Beam-column Element for 3D Modelling of General Cross-sections in Fire. 3rd International Workshop Strcuctures in Fire, Ottawa, 2004*
[61] Husem M: *The Effects of High Temperature on Compressive and Flexural Strengths of Ordinary and High-Performance Concrete*. Fire Safety Journal 2006, 41:155-6
[62] International Conference of Building Officials: *Uniform Building Code.* Whittier, California, 1997
[63] IS 456: Indian Standard. Code of Practice for Plain and Reinforced Concrete,2000
[64] ISO 834:1975: *Fire Resistance Tests-Element of Building Construction*. ISO, 1975
[65] Johnston RG, Strand DR: Olive View Hospital in San Fernando, California, Earthquake of February 9, 1971. Vol. 1 Part A. U. S. Department of Commerce, Washington, 1973
[66] Kanamori H: *Magnitude Scale and Quantification of Earthquakes.* Tectonophysics Journal 1983, 93:185-199
[67] Kawagoe K: *Fire behaviour in Rooms*. Report No.27 by Building Research Institude,Tokyo, 1958
[68] Kent DC, and Park R: *Flexural Members with Confined Concrete*. Journal of Structural Division, Proceedings of the American Society of Civil Engineers, 1971, 97(ST7):1969-1990
[69] Khoury G: *Compressive Strength of Concrete at High Temperatures:A Reassessment*. Magazine of Concrete Research 1992, 44:291-309
[70] Khoury GA, Grainger BN, Sullivan PJE: *Transient Thermal Strain of Concrete: Literature Review, Conditions within Specimen and Behaviour of Individual Constituents*. Magazine of Concrete

Research 1985, 37:131-44
[71] Khoury GA: *Effect of Fire on Concrete and Concrete Structures*.Progress in Structural Engineering and Materials 2000, 2:429-447
[72] Khoury GA: *Strain of Heated Concrete During Two Thermal Cycles.Part 1: Strain over Two Cycles, During First Heating and at Subsequent Constant Temperature*. Magazine of Concrete Research 2006, 58:369-85
[73] Klote J.H, Milke J.A., Principles of Smoke Movement. American Society of Heating, Refrigerating and Air-Conditioning Engineers, Inc., Atlanta, GA., (2002)
[74] Kodur VKR, Harmathy TZ: *Properties of Building Materials*. SFPE Handbook of Fire Protection Engineering. Quincy, MA, 2008
[75] Kreger ME, Sozen MA: *Seismic Response of Imperial County Services Building in 1979*. Journal of Structural Engineering (ASCE) 1989, 15(12):3095-3111
[76] Kuchta JM, et al.:*Crash Fire Hazard RatingSystem for Controlled Flammability Fuels*. Report NA-69-17, Bureau of Mines, Pittsburgh, NTIS No. AD684089, 1969
[77] Kuntz, Gregory L, Browning J: *Reduction of Column Yielding During Earthquakes for Reinforced Concrete Frames*.ACI Structural Journal 2003, 100(5):573-580.
[78] Lamont S, Usmani AS, Drysdale DD: *Heat Transfer Analysis of the Composite Slab in the Cardington Frame Fire Tests*. Fire Safety Journal 2001, 36:815-39
[79] Lau A, Anson M: *Effect of High Temperatures on High Performance Steel Fibre Reinforced Concrete*.Cement and Concrete Research 2006, 36:1678-1707
[80] Law M*: A Basis for the Design of Fire Protection of Building Structures*. Structural Engineering 1893, 61A(1):25-33
[81] Lee J, and Fenves GL: *Plastic-Damage Model for Cyclic Loading of Concrete Structures*. Journal of Engineering Mechanics, 1998, 124(8):892-900
[82] Leet LD: *Cause of Catastrophe: Earthquakes, Volcanoes, Tidal Waves and Hurricanes.* New York, McGraw-Hill Book Co.,Inc, 1948
[83] Lie TT: Fire Temperature-Time Relations. SFPE Handbook of Fire Protection Engineering.Second Edition. Society of Fire Protection Engineers, USA, 1995
[84] Lin TT, Lie: *Structural Fire Protection*. ASCE Manuals and Reports of Engineering Practice, 1992, 78
[85] Macrae GA, Priestley MJN, Tao J: *P-Δ in Seismic Regions*. Reseach Project Report No. SSSRP-93/05. Department of Applied Mechanics and Engineering Sciences University of California. San Diego, 1991

[86] Magnusson SE, Thelandersson S: *Temperature-Time Curves of Complete Process of Fire Development; Theoretical Study of Wood Fuel Fires in Enclosed Spaces*. Civil Engineering and Building Construction 1970, Series No.65

[87] Mahin SA, et. al.: *Response of The Olive View Hospital Main Building During the San Fernando Earthquake.* Report No. EERC-76/22. Earthquake Engineering Research Center, University of California, Berkeley, 1976

[88] Mahin SA, Bertero VV, Chopra AK and Collins RG: *Response of the Olive View Hospital Main Building during the San Fernando Earthquake*. Report UCB/EERC-76/22, Earthquake Engineering Research Center, University of California, Berkeley, U.S.A, 1976

[89] Mahrenholtz O, Reddy DV and Bobby W :Limit analysis of internally pressurized cut-and-cover type underground reactor containments. ACI J 1982, 79:220–225

[90] Mander JB, Priestley JN, Park R: *Theoretical Stress Strain Model for Confined Concrete*. ASCE Journal 1989, 114(12):1804-1826

[91] Mariyana AAK, et al.; Modelling of an Earthquake Damaged RC Frame Subjected to Fire;7th International Conference on Structures in Fire, Zurich, Switzerland, June 2012

[92] Mariyana AAK, Zhang J, Usmani AS; Experimental and Numerical Study on softening and Pinching Effects of Reinforced Concrete; 8th Asia Pacific Structural Eningeeirng and Construction Conference (APSEC) and 1st International Conference on Civil Engineering Research (ICCER), Surabaya, Indonesia, October 2012

[93] Martínez-Rueda JE, Elnashai AS: *Confined Concrete Model Under Cyclic Load*. *Materials and Structures Journal 1997, 30:139-147*

[94] Mazzoni S, McKenna F, Scott MH and Fenves GL, *et al*.: *OpenSees Comand Language Manual*. Pacific Eathquake Engineering Research Center, University of California, Berkeley, 2007

[95] Moehle JP: *Displacement-Based Seismic Design Criteria*. Presented at the 11th World Conference on Earthquake Engineering, Mexico, 1996

[96] Mousavi S, Bagchi A, Kondur VKR: 2008. *Post-Earthquake Fire Hazard to Building Structures.* Canadian Journal of Civil Engineering 2008, 35:689-698

[97] Mwafy SM,Elnashai AS: *Static Pushover Versus Dynamic Collapse Analysis of RC Buildings*. Engineering Structure Journal 2001, 23:407-427

[98] Naeim F: *The Seismic Design Handbook*. International Conference of Building Officials, Structural Engineer Association National Council, Kluwer Academic Publishers, London, 2001

[99] NEHRP Recommended Provisions for the Development of seismic Regulations for New Buildings, Buildings Seismic Safety Council,Washington,D.C, 1991

[100] Ovando E, Ossa E, Romo MP: The Sinking of Mexico City; Its Effects on Soil Properties and Seismic Response. Soil Dynamic and Earthquake Eng. Journal 2007, 27:333-343
[101] Paulay T, Priestley MJN: *Seismic Design of Reinforced Concrete and Masonry Buildings.New York.* Johan Wiley&Son, 1992
[102] Pinho R, Crowley H: *Revisiting Eurocode 8 Formulae for Period of Vibration and Their Employment in Linear Seismic Analysis*. Earthquake Eng.. Struct. Dyn. Journal 2009, 39:223-235
[103] Poon CS, Azhar S, Anson M,Wong YL: *Comparison of the Strength and Durability Performance of Normal and High-Strength Pozzolanic Concretes at Elevated Temperatures*. Cement and Concrete Research 2001, 31:1291-1300
[104] Priestley MJ N, Calvi GM, and Kowalsky MJ: *Displacement-based seismic design of structures.* IUSS Press, Pavia, Italy 721pp.
[105] Purkiss JA: *Fire Safety Engineering Design of Structures*. Oxford, Butterworth-Heinemann, 2007
[106] *Recommended Lateral Force Requirements and Commentary.* Seismology Committee. Structural Engineers Association of California, San Francisco, California, 1989
[107] Richer CF: *An Instrumental Earthquake Magnitude Scale*. Bull. Seismol. Soc. Am 1935, 25:1-32
[108] Richer CF: *Elementary Seismilogy*.San Fransisco, Freeman WH, 1958
[109] Rojahn C: *Proc. of Seminar on Seismic Design, Retrofit and Performance of Non- Structural Components. ATC 29-1 Applied Technology Council,* Redwood City, CA. 1998
[110] Rose PS, Bailey CG, Burgess IW, et al.: *The Influence of Floor Slabs on the Structural Performance of the Cardington Frame in Fire*. Journal of Constructional Steel Research 1998, 46:310-311
[111] SAA 1990c: Fire Resistance Test of Elements of Structure. AS 1530.4-1990. Standards Association of Australia, 1990
[112] Saiidi M, Sozen MA: *Simple Nonlinear Seismic Analysis of R/C Structures*. Journal of The Structural Division, ASCE 198, 107(ST5):937–953
[113] Scawthorn C: *Fire Following Earthquakes*. New York, McGraw-Hill, 1992
[114] Schneider U: *Concrete at High Temperatures - a General Review*. Fire Safety Journal 1988, 13:55-68
[115] Schneider U: *Modelling of Concrete Behaviour at High Temperatures.Presented at the Design of Structures Against Fire*, Aston, Birmingham, 1986
[116] SEAOC: *Performance Based Seismic Engineering of Buildings.Vision 2000 Committee.* Structural Engineers Association of California,1995
[117] SEAOC: *Recommended Lateral Force Requirements*. Structural Engineers Association of California, San Francisco, 1996
[118] SeismoStruct,http//www,seismosoft.com, 2004

[119] Sekizawa A, Ebihara M, Notake H: *Development of Seismic-induced Fire Risk Assessment Method for a Building*. Presented at the 15th Meeting of the UJNR Panel on Fire Research and Safety, San Antonio, 2000

[120] Sharma UK, *et. al.:Full Scale Testing of a Damaged RC Frame in Fire.* Structures and Buildings.Proceedings of the ICE, in press, 2012

[121] Shibata A, Sozen M: *Substitute Structure Method for Sesmic Design in Reinforced Concrete*. Journal of Structure Div. (ASCE) 1976, 102(1):1-18

[122] Sullvan TJ, Phm TT, Carvi GM: *P-Delta Effects on Tall RC Frame-Wall Buildings*. Presented at the 14th World Earthquake Conference, Beijing, 2008

[123] Tenchev R, Purnell P: *An Application of a Damage Constitutive Model to Concrete at High Temperature and Prediction of Spalling*. International Journal of Solids and Structures 2005, 42(26): 6550

[124] Tentative Provisions for the Development of Seismic Regulations of Buildings. Report No. ATC-3-06 by Applied Technological Council, California, 1978

[125] Thomas PH, Heselden AJM: *Fully Developed Fire in Single Compartments*. CIB Report No 20. by Fire Research Station, UK, 1972

[126] Tien CL, Lee KY, and Stretton AJ:*Radiation Heat Transfer, SFPE Handbook of Fire Protection Engineering.National Fire Protection Association, Quincy, MA, 1995*

[127] Todd D, Carino N, et. Al.: *1994 Northridge Earthquake : Performance of Structures, Lifelines,and Fire Protection Systems*. NIST Special Publication 862. National Institute of Standards and Technology, Gaithersburg, 1994

[128] UBC-1:Admistrative Fire and Life Safety and Field Inspection Provision, United State, Delmar Cengage Learning, 1997

[129] USGS internet source http://earthquake.usgs.gov/learn/topics/mag_vs_int.php

[130] Usmani A, Zhang J, Jiang J, and Ian May I: *Using Opensees for Structures in Fire.* J. of Structural Fire Engineering 2009, 3:57-70

[131] Usmani AS, Rotter JM, Lamont S, Sanad AM, Gillie M: *Fundamental Prinsiples of Structural Behaviour under Thermal Effects*. Fire Safety Journal 2001, 36:721-744

[132] Walton WD, Thomas PH: *Estimating Temperatures in Compartment Fires*. SFPE Handbook of Fire Protection Engineering, 1995

[133] Welty JR, Wicks CE and Wilson RE:, *Fundamentals of Momentum, Heat and Mass Transfer.* John Wiley & Sons Inc., New York 1984

[134] Wen ZP, Hu YX, Chau KT: *Site Effect on Vulnerability of High Rise Shear Wall Buildings Under Near and Far Field Earthquakes*. Soil Dynamic and Earthquake Eng. Journal 2002, 22:9-12

[135] Wickstrom U, Palsson J: *A Scheme for Verification of Computer Codes for Calculating Temperature in Fire Exposed Structures*.

Boras,SP Swedish National Testing and Research Institute, 1999

[136] Williamson RB: *Manual of Evaluation Procedures for Passive Fire Prevention Following Earthquake. Report No. NIST GCR-99-768 by National Institute of Standards and Technology, Gaithersburg, 1999*

[137] Wood SL, Wight JK,Moehle JP: *The 1985 Chile Earthquake: Observations on Earthquake-Resistant Construction in Vina del Mar.* Structural Research Series No. 532. University of Illinois at Urbana-Champaign, Urbana, 1987

[138] Yang H, Lin Y, Hsiao C, et al.: *Evaluating Residual Compressive Strength of Concrete at Elevated Temperatures Using Ultrasonic Pulse Velocity*. Fire Safety Journal 2009, 44:121-30

Appendix A

Preliminary design details

A.1 Loading combination calculation

Load distribution for this frame can be divided into two cases, the non-earthquake and the earthquake case. The main difference between these two cases is the reduction factor for live load, which is about 25% for the earthquake case with no load for the roof taken into consideration; while for the non-earthquake case, about 75% is used for the live load at the roof floor. The load distribution on the building is calculated as follows:

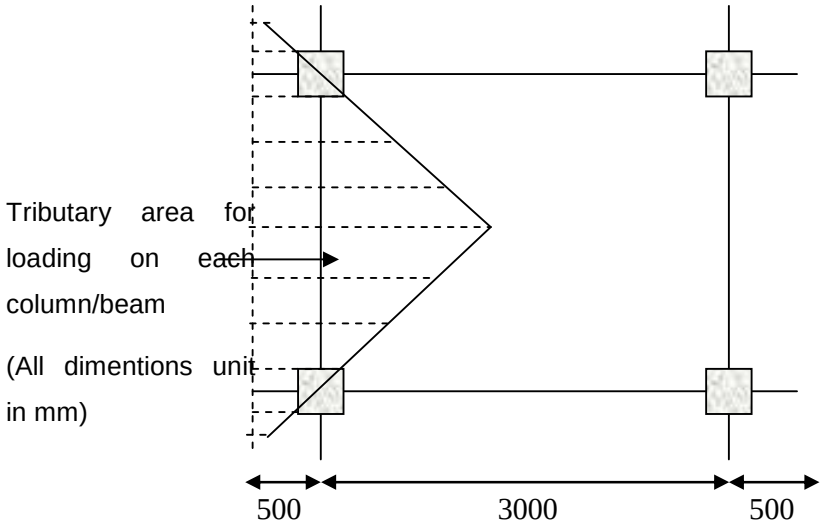

Figure A.1 Plan view of the Roorkee frame (all units in mm)

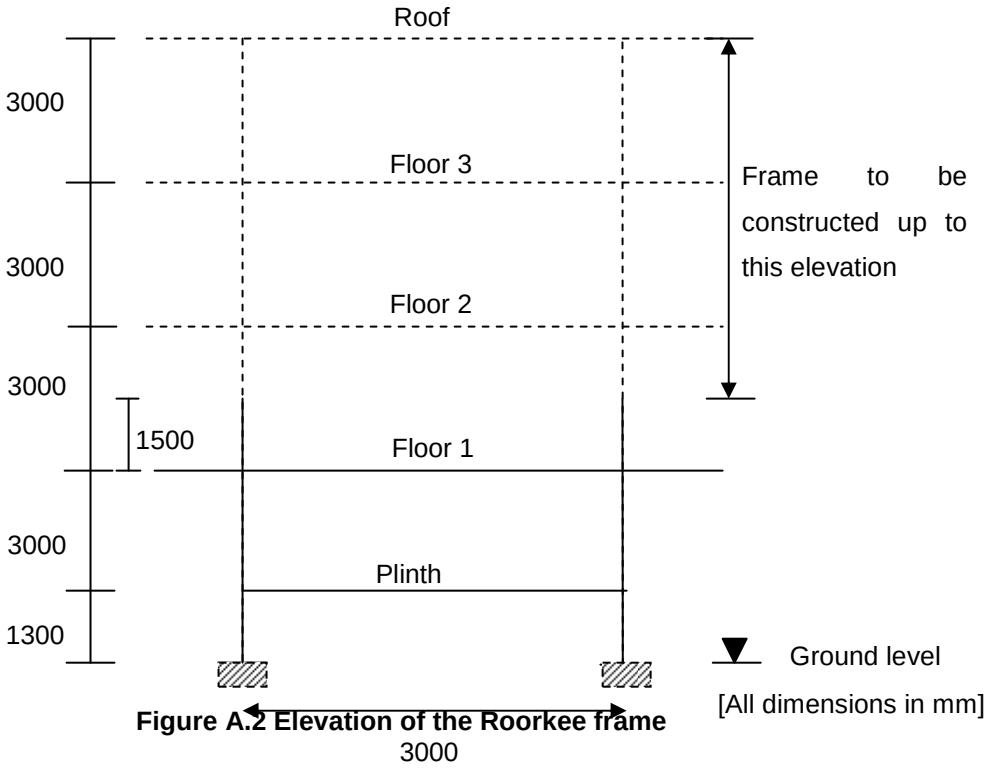

Figure A.2 Elevation of the Roorkee frame

A.1.1 Columns loads

Tributary area for each column = $\frac{1}{4}x5x5 = 6.25m^2$

Dead loads ;

Roof slab= $6.25x[1+(0.12x25)] = 25kN$

Floor 3= $25kN$

Floor 2= $25kN$

Column= $0.3x0.3x25x7.5 = 16.875kN$

Beam from Roof, Floor 3, Floor 2= $4x5x\left(\frac{0.23-0.12}{4}\right)x0.23x25x3 = 9.4875kN$

Total dead load reaction on each column= $101.3625kN$

Live load

Loading from Roof, Floor 3 and Floor 2= $0.25x2x6.25 = 3.125kN$

$\therefore$ Total load on each column= $104.5kN$

A.1.2 Beam loads

Dead load

a) Total floor dead load= $0.12x25 + 1 = 4kN/m^2$

b) Equivalent UDL on framing beams = $\frac{5x5x4}{4x5} = 5kN/m$

Total UDL on beam = $(0.23x0.12)x0.23x25 = 0.6325kN/m$

Live load

Total floor loads = $2.0x0.25 = 0.5kN/m^2$

Equivalent UDL on framing beams: 5x5x0.5/(4x5)= 0.625kN/m

$\therefore$ Total UDL on beams = $6.2575kN/m$

A.2 Plastic Hinge Calculation

Following are presents the analytical solution using plastic analysis and numerical analysis method to identify the location of plastic hinge at the frame.

A.2.1 Stiffness method

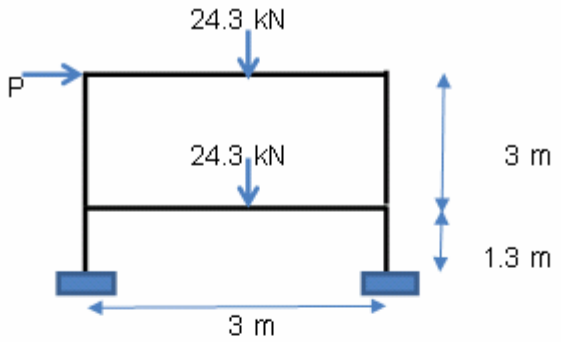

Hogging Moment

Mp beam :	140 kN.m
Mp Column :	85 kN.m

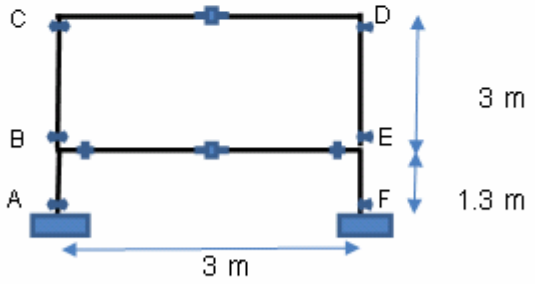

Redundancy 6-3 = 3
Hinges location = 10
So,separates Elementary Mechanism are 10-3 =7

Beam Mechanisms :2
Sway Mechanisms : 1
Combination : 7-3 =4

Beam

2nd-storey

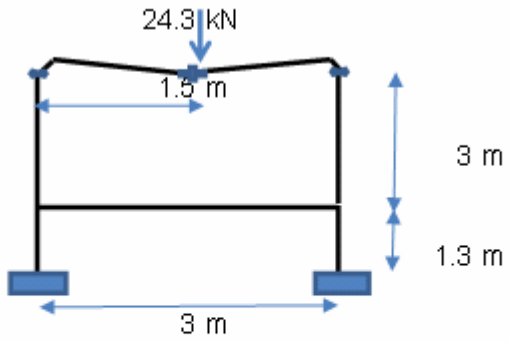

a) Work done by load = 24.3λ x 1.5 θ

= 36.45 λθ

Energy absorbed in hinges = sum of elementary - elimanted hinges

= 2θx140 + 2θx85

= 450 θ

Equating these two, λ = 12.35

1st-storey

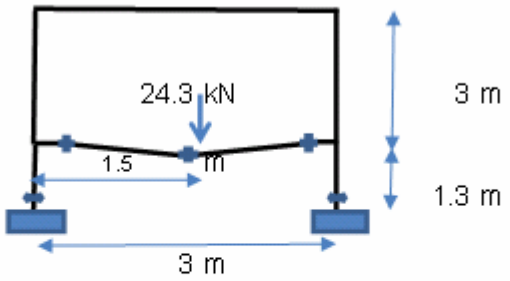

b) Work done by load = 24.3λ x 1.5 q

= 36.45 λθ

Energy absorbed in hinges = sum of elementary - elimanted hinges

= 560 θ

Equating these two, λ = 15.36

Sway

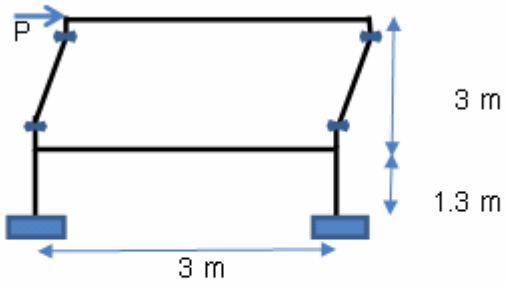

c) Work done by load = 5λ x 3 θ

= 15 λθ

Energy absorbed in hinges = sum of elementary - elimanted hinges

= 340 θ

Equating these two, λ = 22.67

Combination

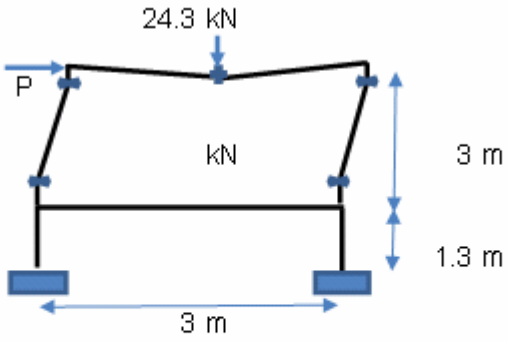

d=a+c Work done by load = 5λ x 1.3 q + 24.3λ x 1.5 q

= 51.45 λθ

Energy absorbed in hinges = sum of elementary - elimanted hinges

= 480 θ

Equating these two, λ = 9.33

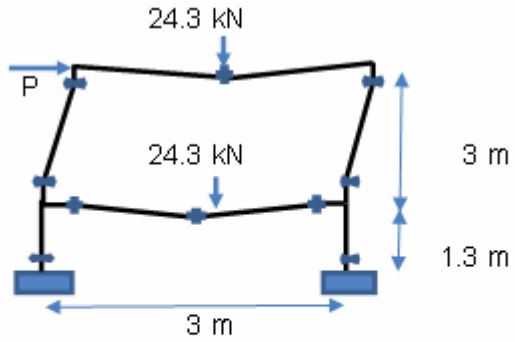

e=d+b

Work done by load = 87.9 λθ

Energy absorbed in hinges = sum of elementary - elimanted hinges

= 1040 θ

Equating these two, λ = 11.83

e' =modify this collapse mechanism if joint B is allowed to rotate

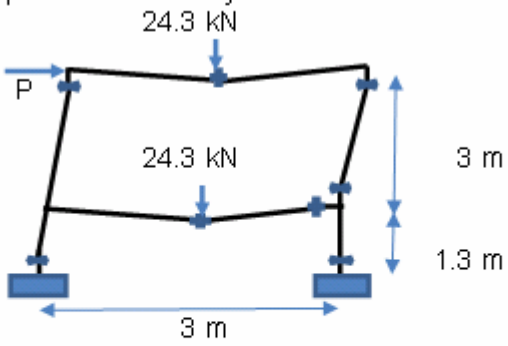

Work done by load = 87.9 λθ

Energy absorbed in hinges = sum of elementary - elimanted hinges

= 815 θ

Equating these two, λ = 9.27

f =modify this collapse mechanism if joint E is allowed to rotate

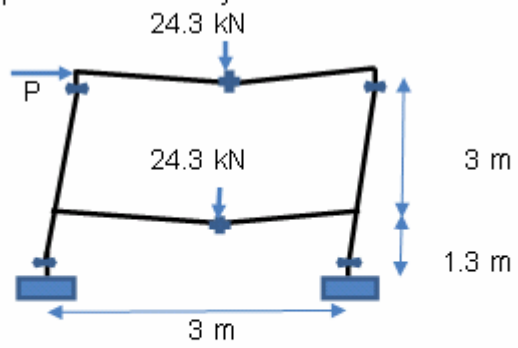

Work done by load = 87.9 λθ

Energy absorbed in hinges = sum of elementary - elimanted hinges

= 590 θ

Equating these two, λ = 6.71

A.2.2 Numerical analysis results

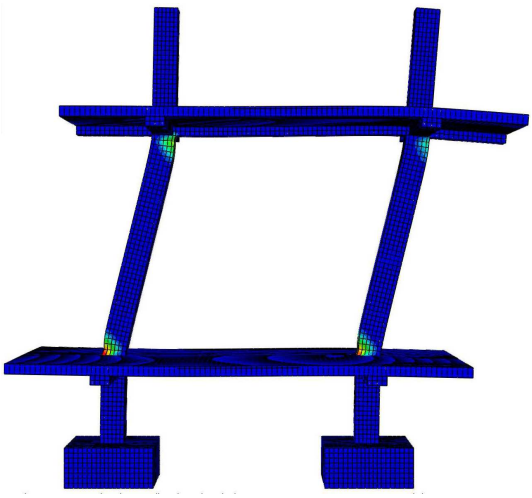

Figure A.3 Finite element model ABAQUS of the frame showing hinges in columns [17]

A.3 Load displacement curve

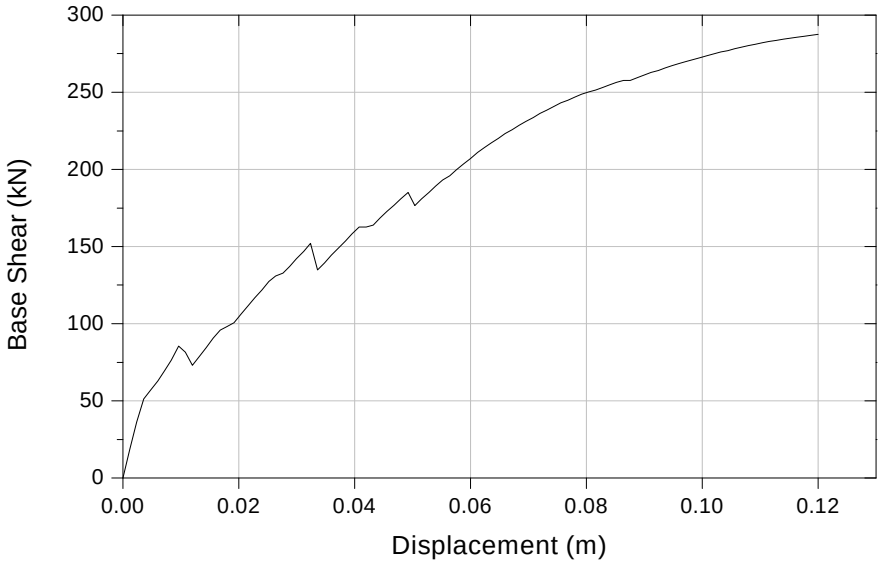

Figure A.4 Base shear against displacement curve obtained from SeismoStruct

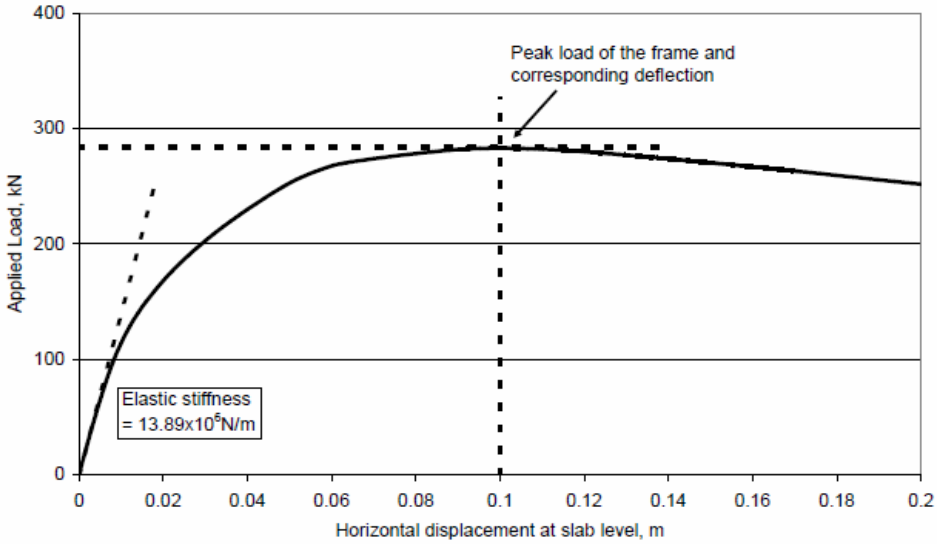

Figure A.5 Base shear against displacement curve obtained from ABAQUS [17]

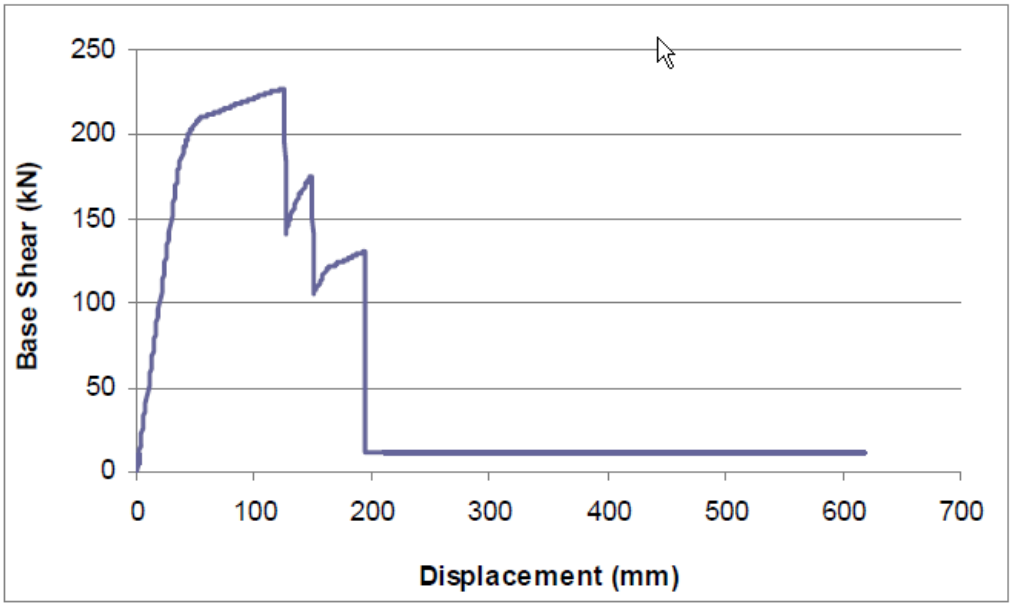

Figure A.6 Base shear against displacement curve obtained from SAP2000 [17]

Appendix B

Numerical Modelling of material inputs

This section presents the material properties used for the numerical modelling in a finite element programme.

For the mechanical analysis, the concrete properties used in the 2D beam and 3D beam-shell models included softening behaviour in both compression and tension. For the unloading part, the damage parameter in compression, dc, is implemented to consider the degradation of the elastic stiffness.

In the thermal properties, the conductivity and specific heat capacity are defined and take into account temperature effects in the numerical modelling. The material properties which vary with temperature follow relationships defined in Eurocode 2 Part 1-2 (2004).

B.1 Material Properties for Concrete

Table B.1 Concrete Damage Plasticity Parameter

Dilation angle, ψ (^{o})	15
Flow Potential Eccentricity, ε	0.1
Ratio of initial equibiaxial compressive yield stress to initial uniaxial compressive yield stress, σ_{b0}/σ_{c0}	1.16
Ratio of the second stress invarinat on the tensile meridian, K_c	0.667
Viscosity Parameter, μ	0

Table B.2 Young's Modulus of Concrete

Young's Modulus, E (N/m^2)	Poission's Ratio	Temperature, T (^oC)
2.03E+10	0.25	20
1.27E+10	0.25	100
8.96E+08	0.25	200
6.60E+09	0.25	300
4.32E+09	0.25	400
2.51E+09	0.25	500
1.90E+09	0.25	600
1.28E+09	0.25	700
7.62E+08	0.25	800
4.01E+08	0.25	900
1.52E+08	0.25	1000

Table B.3 Expansion Coefficients of Concrete

Expansion Coefficient, α ($/^oC$)	Temperature, T (^oC)
0	20
6.20E-06	100
6.60E-06	200
7.40E-06	300
8.40E-06	400
9.70E-06	500
1.12E-05	600
1.31E-05	700
1.52E-05	800
1.36E-05	900
1.22E-05	1000

Table B.4 Concrete Compression Hardening

Yield stress in Compression, σ_c (N/m^2)	Inelastic Yield Strain	Temperature, T (^oC)
1.02E+07	0	20
3.40E+07	0.00083	20
102000	0.01994	20
0	0.02	20
1.02E+07	0	100
3.40E+07	0.00132	100
0	0.0225	100
9.85E+06	0	200
3.30E+07	0.00182	200
0	0.025	200
9.25E+06	0	300
3.09E+07	0.00231	300
0	0.0275	300
8.64E+06	0	400
2.89E+07	0.00331	400
0	0.03	400
7.52E+06	0	500
2.52E+07	0.00496	500
0	0.0325	500
6.10E+06	0	600
2.04E+07	0.00529	600
0	0.035	600
4.37E+06	0	700
1.46E+07	0.00562	700
0	0.0375	700
2.74E+06	0	800
9.18E+06	0.00595	800
0	0.04	800
1.52E+06	0	900
5.10E+06	0.00628	900
0	0.0425	900
610000	0	1000
2.04E+06	0.00661	1000
0	0.045	1000

Table B.5 Density of Concrete

Density,ρ (kg/m^3)	Temperature, T (^oC)
2400	All temperatures

Table B.6 Concrete Tension Stiffening

Yield Stress in Tension, σ_t (N/m^2)	Inelastic Yield Strain	Temperature, T (^oC)
3.40E+06	0	20
3.40E+06	1.00E-05	20
3.40E+06	0.00173	20
30000	0.00190767	20
3.40E+06	0	100
3.40E+06	0.000510044	100
3.40E+06	0.00144927	100
30000	0.0018027	100
2.91E+06	0	200
2.91E+06	0.000433699	200
2.91E+06	0.00155158	200
29100	0.00193742	200
2.73E+06	0	300
2.73E+06	0.000386168	300
2.73E+06	0.001718	300
27300	0.00212522	300
2.55E+06	0	400
2.55E+06	0.000245699	400
2.55E+06	0.00186024	400
25500	0.00229495	400
2.22E+06	0	500
2.22E+06	4.71E-05	500
2.22E+06	0.00125197	500
22200	0.0016935	500

TableB.7 Compression Damage Properties of Concrete

Compressive Damage, d_c	Inelastic Yield Strain	Temperature, T (^oC)
0	0	20
0	0.0008	20
0.8	0.02	20
0	0	100
0	0.00132	100
0.8	0.0225	100
0	0	200
0	0.00182	200
0.8	0.025	200
0	0	300
0	0.00231	300
0.8	0.0275	300
0	0	400
0	0.00331	400
0.8	0.03	400
0	0	500
0	0.00496	500

Table B.8 Compression Damage Properties of Concrete: continued

Compressive Damage, d_c	Inelastic Yield Strain	Temperature, T (^oC)
0.8	0.0325	500
0	0	600
0	0.00529	600
0.8	0.035	600
0	0	700
0	0.00562	700
0.8	0.0375	700
0	0	800
0	0.00595	800
0.8	0.04	800
0	0	900
0	0.00628	900
0.8	0.0425	900
0	0	1000
0	0.00661	1000
0.8	0.045	1000

Table B.9 Thermal Conductivity Properties of Concrete

Conductivity, K (W/m.K)	Temperature, T (^{o}C)
1.951	20
1.766	100
1.553	200
1.361	300
1.191	400
1.042	500
0.915	600
0.809	700
0.724	800
0.661	900
0.619	1000

Table B.10 Specific Heat of Concrete

Specific Heat capacity (J/kg.K)	Temperature, T (^{o}C)
900	20
900	100
1000	200
1050	300
1100	400
1100	500
1100	600
1100	700
1100	800
1100	900
1100	1000

B.2 Material Properties for Reinforcing Steel

Table B.11 Young's Modulus of Reinforcing Steel

Youngs's Modulus, E (N/m^2)	Poission's Ratio	Temperature, T (^oC)
2.10E+11	0.3	20
2.10E+11	0.3	100
1.80E+11	0.3	200
1.50E+11	0.3	300
1.20E+11	0.3	400
8.40E+10	0.3	500
5.00E+10	0.3	600
1.68E+10	0.3	700
1.26E+10	0.3	800
1.05E+10	0.3	900
6.30E+09	0.3	1000

Table B.12 Expansion Coefficients of Reinforcing Steel

Expansion Coefficient, α ($/^oC$)	Temperature, T (^oC)
0	20
1.25E+00	100
1.29E-05	200
1.33E-05	300
1.37E-05	400
1.41E-05	500
1.45E-05	600
1.49E-05	700
1.50E-05	800
1.41E-05	900
1.34E-05	1000

Table A.13 Density of Reinforcing Steel

Density,ρ (kg/m^3)	Temperature, T (^oC)
7580	All temperatures

Table B.14 Compression Hardening of Reinforcing Steel

Yield stress in Compression, σ_c (N/m^2)	Inelastic Yield Strain	Temperature, T (^oC)
4.50E+08	0	20
4.50E+08	0.002	20
6.60E+08	0.5	20
4.50E+08	0	100
4.50E+08	0.002	100
6.60E+08	0.5	100
4.50E+08	0	200
4.50E+08	0.002	200
6.00E+08	0.5	200
4.50E+08	0	300
4.50E+08	0.0029	300
6.00E+08	0.5	300
4.23E+08	0	400
4.23E+08	0.0035	400
5.40E+08	0.5	400
3.02E+08	0	500
3.02E+08	0.0035	500
3.85E+08	0.5	500
1.80E+08	0	600
1.80E+08	0.0035	600
2.30E+08	0.5	600
5.40E+07	0	700
5.40E+07	0.003	700
7.07E+07	0.5	700
4.95E+07	0	800
4.95E+07	0.0039	800
6.20E+07	0.5	800
3.60E+07	0	900
3.60E+07	0.003	900
4.64E+07	0.5	900
2.25E+07	0	1000
2.25E+07	0.0035	1000
2.88E+07	0.5	1000

Appendix C

Parametric Study of Beam Elements using ABAQUS

A benchmark problem made up of beam elements is present in this section. All the solutions have been done by writing the ABAQUS script for each of the cases separately and then running them with the ABAQUS program. The numerical results and analytical results are compared.

The ABAQUS script for the simple supported beam loaded with UDL and fire is presented.

C.1 Rectangular Section

The beam is divided by 9 nodes and 8 elements. The naming of the nodes starts from the left of the beam. Beam element type B21 has been chosen as the element for all of the cases below. In all of the analyses, values are recorded at node 9 which is located at the end of the beam on the right side, except for the displacement at y-axis which is measured at mid-span of the beam length. Figure C.1 shows the temperatures input at specific points though the depth of the beam.

General details of the beam;

Cross-section of the beam (rectangular) = 300mm x 300mm

Elastic Modulus,E = 10 GPa (kN/mm^2)

Thermal expansion, $\alpha = 12 \times 10^{-6} / {}^{o}C$

Temperature at the bottom,T_{bot}= 800 ^{o}C

Temperature at the bottom,T_{top}= 20 ^{o}C

Average temperature, ΔT=390 ^{o}C

Thermal Gradient, T,y = 2.6 ^{o}C/mm

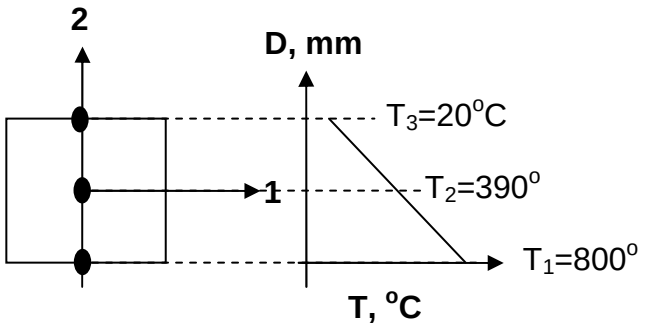

Figure C.1 Temperatures input at specific points trough the depth of the beam

C.1.1 Determine the value of δx and δy for the simply supported beam with small UDL and temperatures points at three specific points through its depth.

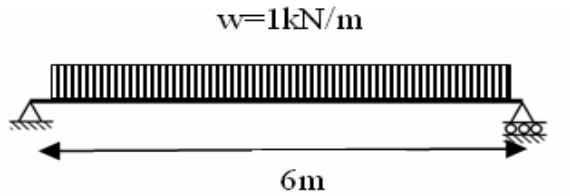

Figure C.2 Simply supported Beam

Table C.1 Result of benchmark B1

Benchmark	B1		
	UDL	Fire	UDL & Fire
δx (mm)	-2.60E-03	19.2685	18.9596
δy (mm)	-2.51063	-142.712	-144.162
θz (rad)	1.33E-03	9.40E-02	9.54E-02

C.1.2 Determine the value of δy and R for the axially restrained beam with small UDL and temperatures points at three specific points through its depth.

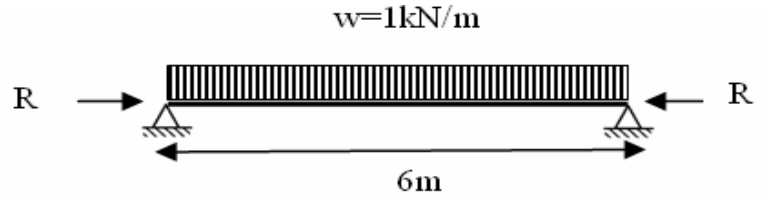

Figure C.3 Axially restrained Beam

Table C.2 Result of benchmark B2

Benchmark	**B2**		
	UDL	**Fire**	**UDL & Fire**
δx (mm)	0.0000	0.0000	0.0000
δy (mm)	-2.5101	-233.3060	-233.8800
θz (rad)	0.0013	0.1424	0.1427
R (kN)	0.3901	-710.3300	-693.5040

C.1.3 Determine the value of δy, R and M for the fixed end beam with small UDL and temperatures points at three specific points through its depth.

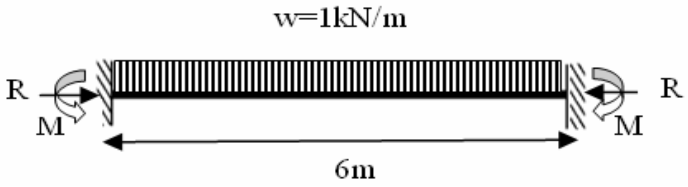

Figure C.4 Fixed end beam

Table C.3 Result of benchmark B3

Benchmark	B3		
	UDL	**Fire**	**UDL & Fire**
δx (mm)	0.0000	0.0000	0.0000
δy (mm)	-0.5114	0.0000	-1.2024
R (N)	0.0156	-4212.	-4212
M(KN.mm)	-2998.8	-210600.	-216222.

C.2 I-Beam Section

This section shows the study on the same beam with I-section, with the temperature variation applied. The I-beam section with a wider web is modelled to idealise the section of the original beam. The beam was divided by 9 nodes and 8 elements, with beam element type B22 used as the element for all the cases below. The temperature input at five specific points is shown in Figure C.5.

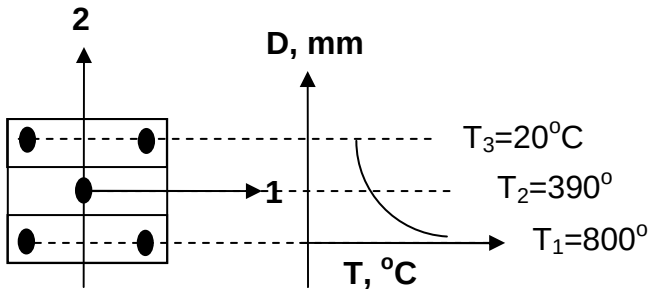

Figure C.5 Temperatures input at specific points trough the depth of the beam

Table C.4 Result of benchmark B1

Benchmark	B1		
	UDL	Fire	UDL & Fire
δx (mm)	-2.60E-03	19.2685	18.9596
δy (mm)	-2.51063	-141.616	-144.162
θz (rad)	1.33E-03	9.40E-02	9.54E-02

C.3 Analytical Solution

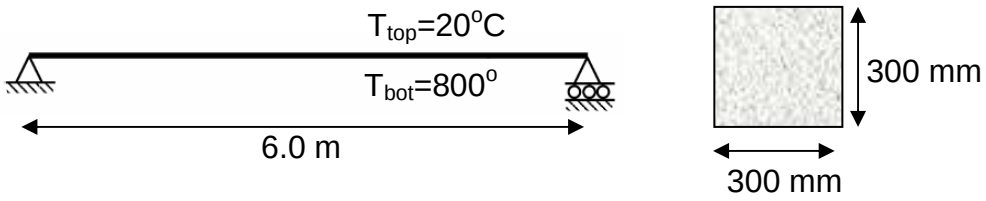

Figure C.6 The simply supported beam and its cross-section details

Design Properties

Elastic Modulus, $E = 10kN/mm^2$

Expansion Coefficient, $\alpha = 1.2x10^{-5}/^0 C$

Uniform distribution load (UDL), $w = 1x10^{-3} kN/mm$

Length of the beam, $l = 6000mm$

Width of the beam cross-section, $b = 300mm$

Depth of the beam cross-section, $d = 300mm$

Spring translation stiffness, $K_T = 100kN/mm$

Spring rotation stiffness, $K_R = 3.0x10^5 kN/mm$

Uniform temperature, $\Delta T = \frac{T_{bot-}T_{top}}{2} = 390^0 C$

Temperature gradient, $T_{,y} = \frac{T_{bot-}T_{top}}{d} = 2.6^0 C/mm$

Thermal expansion strain, $\varepsilon_T = \alpha\Delta T = 4.68x10^{-3}$

Uniform curvature, $\phi = \alpha T_{,y} = 3.12x10^{-5}/mm$

Thermal curvature strain, $\varepsilon_\phi = 1 - \frac{\sin\left(l\frac{\phi}{2}\right)}{l\frac{\phi}{2}} = 1.46x10^{-3}$

C.3.1 Simply supported beam (see Figure B.2)

Calculating δx:

UDL:

Horizontal displacement is negligible.

Thermal loading:

Horizontal displacement is given by: $\varepsilon_T l = 28.08mm$.

Horizontal pulling in of the beam due to curvature is given by:

$$R_\theta = l\left(1 - \frac{\sin\left(\frac{\phi l}{2}\right)}{\frac{\phi l}{2}}\right) = 8.757mm$$

Thus the total horizontal deflection is given by $\varepsilon_T l - R_\theta = 19.323mm$

Calculating δy :

- UDL:

Vertical displacement given by: $\delta y_{\omega} = \frac{5\omega l^4}{384EI} = 2.5mm$

- Thermal loading:

Vertical displacement given by: $\delta y_T = \frac{2l}{\pi}\sqrt{\varepsilon_{\phi} + \frac{\varepsilon_{\phi}^{\ 2}}{2}} = 146mm$

Calculating θ_z :

- UDL:

Rotation given by: $\theta_{z,\omega} = \frac{\omega l^3}{EI} = 1.33\times10^{-3}$

- Thermal loading:

Rotation given by: $\theta_{z,T} = \frac{l\phi}{2} = 0.0936$

B.3.2 Axially restrained beam (see Figure B.3)

Calculating δx :

- UDL:

Horizontal displacement is negligible.

- Thermal loading:

Horizontal displacement is given by: $\varepsilon_T l = 28.08mm$.

Horizontal pulling in of the beam due to curvature is given by: $R_{\theta} = l\left(1 - \frac{\sin\left(\frac{\phi l}{2}\right)}{\frac{\phi l}{2}}\right) = 8.757mm$

Thus the total horizontal deflection is given by $\varepsilon_T l - R_{\theta} = 19.323mm$

Calculating δy :

- UDL:

Vertical displacement given by: $\delta y_{\omega} = \frac{5\omega l^4}{384EI} = 2.5mm$

- Thermal loading:

Vertical displacement given by: $\delta y_T = \frac{2l}{\pi}\sqrt{\varepsilon_{\phi} + \frac{\varepsilon_{\phi}^{\ 2}}{2}} = 146mm$

Calculating θ_z :

- UDL:

Rotation given by: $\theta_{z,\omega} = \frac{\omega l^3}{EI} = 1.33\times10^{-3}$

- Thermal loading:

Rotation given by: $\theta_{z,T} = \frac{l\phi}{2} = 0.0936$

B.3.3 Fixed end beam (see Figure B.4)

Calculating δy :

- UDL:

Vertical displacement given by: $\delta y_{\omega} = \frac{5\omega l^4}{384EI} = 2.5mm$

- Thermal loading:

Vertical displacement given by: $\delta y_T = \frac{2l}{\pi}\sqrt{\varepsilon_T + \frac{\varepsilon_T^{\ 2}}{2}} = 262mm$

Calculating *R*:

- UDL:

Horizontal restraining force is negligible.

- Thermal loading:

Thermally induced force is given by: $R_T = EA\alpha\Delta T = 4212kN$

Calculating *M*:

- UDL:

Load induced moment is given by: $M_\omega = \frac{\omega l^2}{12} = 3000kNmm$

- Thermal loading:

Thermally induced moment is given by: $M_T = EA\phi = 210600kNmm$

Calculating *M*:

- UDL:

Load induced moment is given by: $M_\omega = \frac{\omega l^2}{12} = 3000kNmm$

- Thermal loading:

Thermally induced moment is given by: $M_T = EA\phi = 210600kNmm$

C.4 Input ABAQUS for Simply supported beam (see Figure C.2)

```
**********************************************************
****       Simply supported beam model              ****
**            Loading-UDL&Fire                      **
**   Pin & roller at the end of the beam length      **
***          Structural Elements B21                ***
*****        Units kN, mm, GPa (kN/mm2)           *****
**********************************************************
*HEADING
SIMPLY SUPPORTED BEAM,B21,STRUCTURAL ELEMENTS
*PREPRINT,HISTORY=YES,MODEL=YES
************************************************
**                NODE                        **
************************************************
*NODE,NSET=NBEAM
1,0.,0.
9,6000.,0.
*NGEN,NSET=NBEAM
1,9,1
************************************************
**              ELEMENT TYPE              **
************************************************
*ELEMENT,TYPE=B21
1,1,2
*ELGEN,ELSET=EBEAM
1,7,1,1
*ELSET,ELSET=EMID
5
************************************************
**                      SECTION               **
************************************************
*BEAM
SECTION,MATERIAL=STEEL,ELSET=EBEAM,SECTION=RECT,TEMPERAT
URE=VALUES
300,300

3
******************************************************
** SECTION BEHAVIOUR OF THE BEAM    **
******************************************************
*MATERIAL,NAME=MATERIAL-I
 *ELASTIC
10
*EXPANSION
0.000012,0
************************************************
**      BOUNDARY CONDITIONS       **
************************************************
*BOUNDARY
1,1,2
9,2
```

C inued

```
**********************************************
**        LOADING CASES - UDL           **
**********************************************
*STEP
*STATIC
0.1,1,,0.1
*DLOAD
EBEAM,PY,-0.001

**********************************************
**              OUTPUT                  **
**********************************************
*OUTPUT,FIELD
*ELEMENT OUTPUT
1,2,3,4,5,6,7,8,9
TEMP
*NODE OUTPUT
U,UR,RF,RM
*OUTPUT,HISTORY
*NODE OUTPUT
U,UR,RF,RM
*ELPRINT,ELSET=EMID
1,2,3,4,5,6,7,8,9
TEMP
*END STEP
**********************************************
**          LOADING CASES - FIRE          **
**********************************************
*STEP
*STATIC
0.1,1,,0.1
*TEMPERATURE
NBEAM,390,-2.6,0
**********************************************
**                PRINTING              **
**********************************************
*OUTPUT,FIELD
*ELEMENT OUTPUT
1,2,3,4,5,6,7,8,9
TEMP
*NODE OUTPUT
U,UR,RF,RM
*OUTPUT,HISTORY
*NODE OUTPUT
U,UR,RF,RM
*ELPRINT,ELSET=EMID
1,2,3,4,5,6,7,8,9
TEMP
*END STEP
**********************************************
```

upported beam analysis

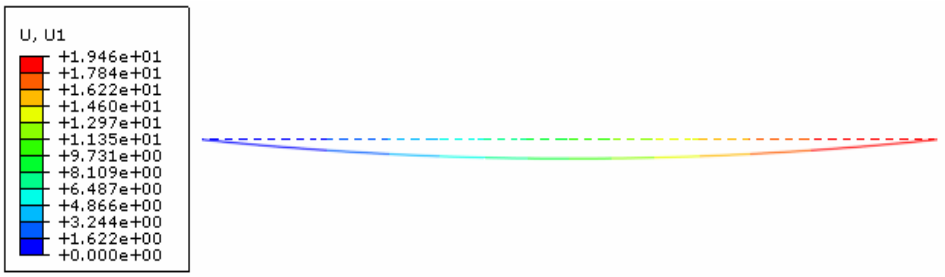

Figure C.8 Horizontal displacement obtained from ABAQUS for simply supported beam analysis

Appendix D

Temperature distributions from the Roorkee frame Test

D.1: Temperature Distributions of bottom Beam (B1 – B4)

B1-left

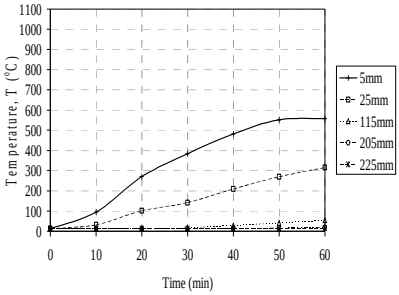

B1-mid

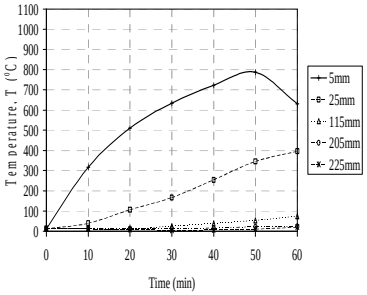

B1-right

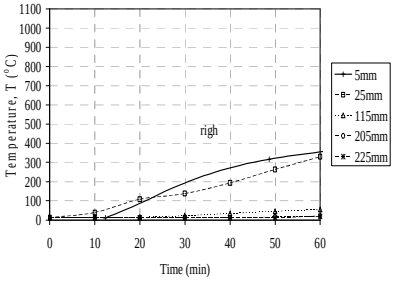

B2-left

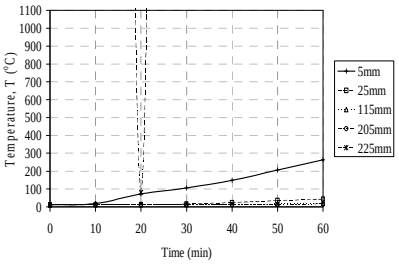

B2-mid

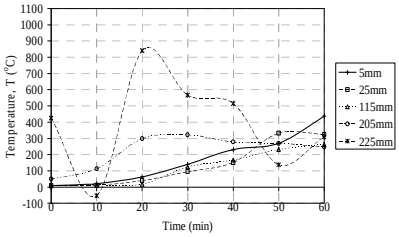

B2-right

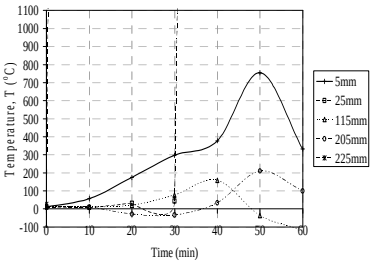

B3-left

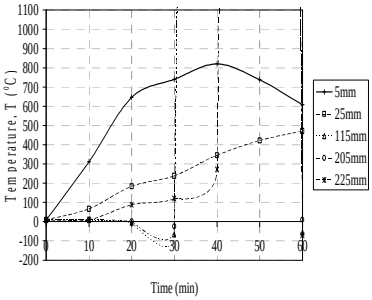

B3-mid

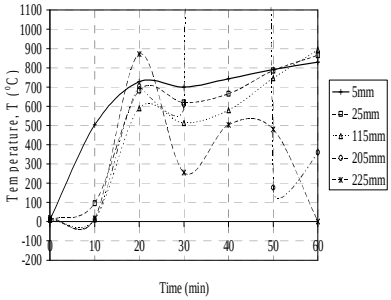

B3-right

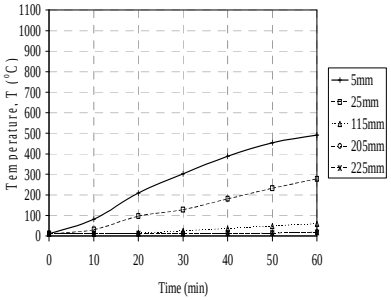

B4-left

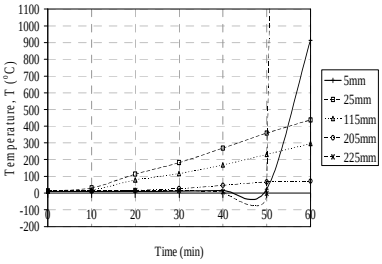

B4-mid

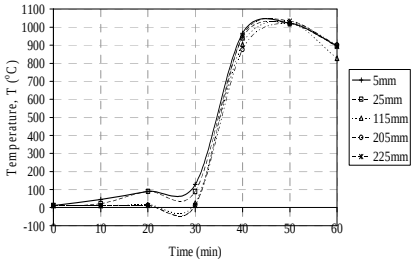

B4-right

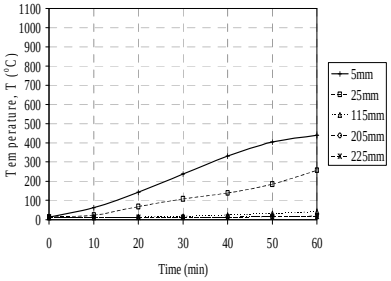

D.2 : Temperature Distributions of Top Beam (B7 and B8)

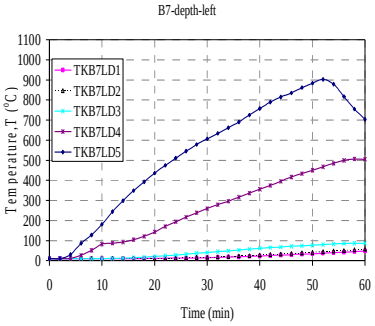

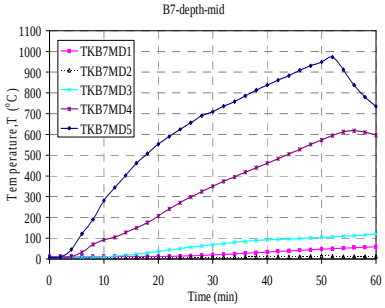

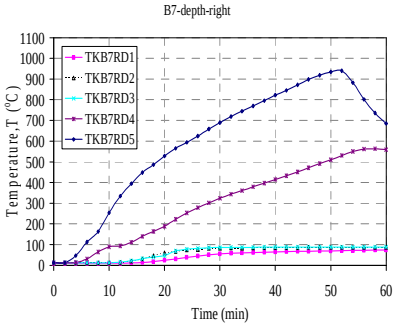

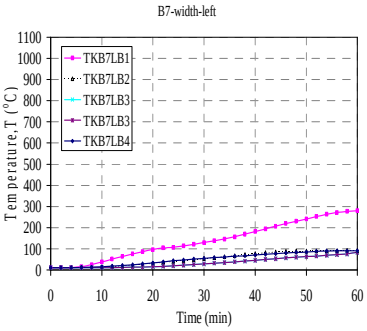

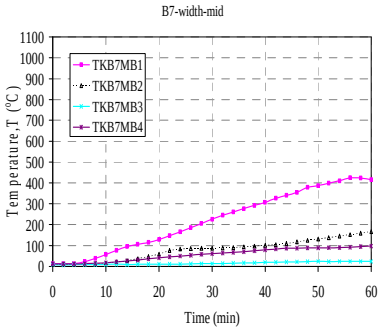

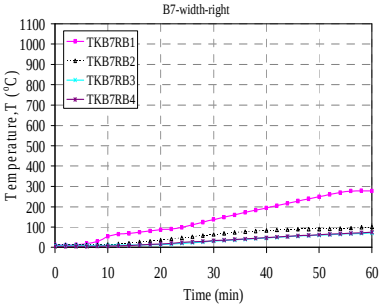

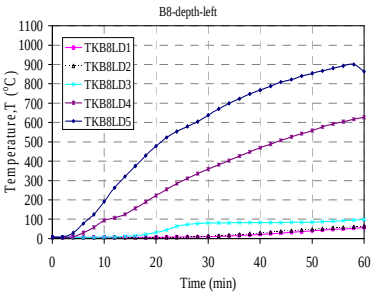

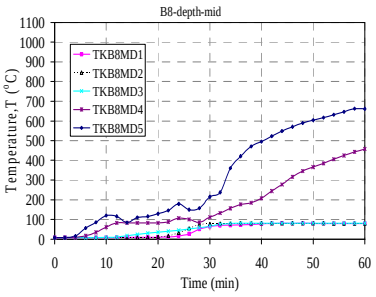

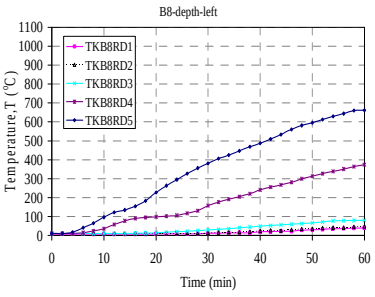

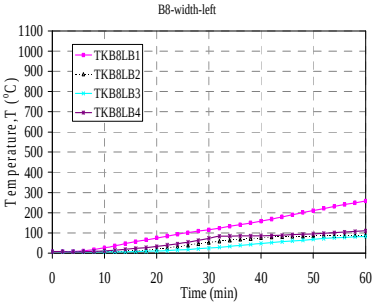

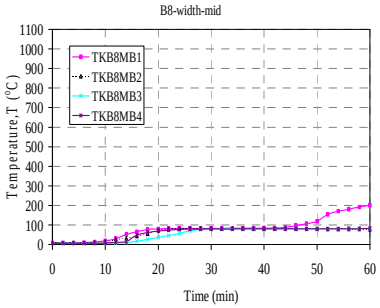

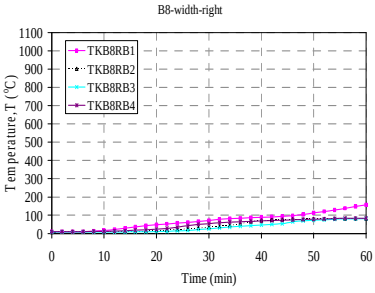

D.3: Temperature Distributions of columns (C1 and C2)

C1-bot;loading direction

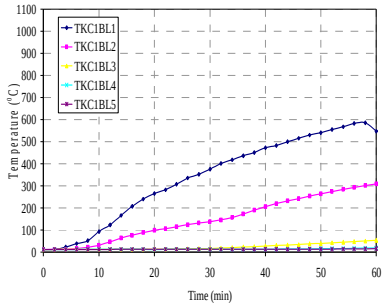

C1-mid;loading direction

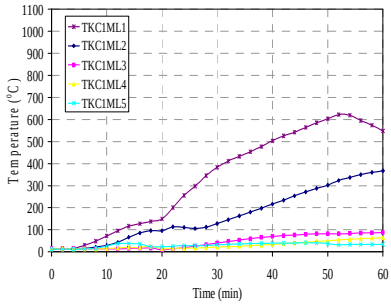

C1-top;loading direction

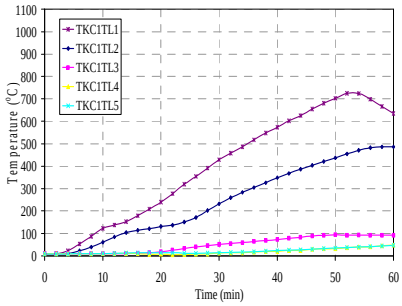

C1-bot;perp loading direction

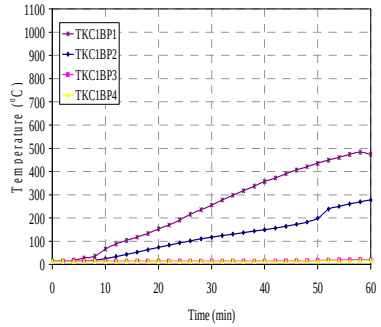

C1-mid;perp loading direction

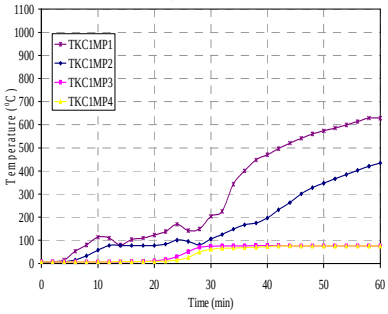

C1-top;perp loading direction

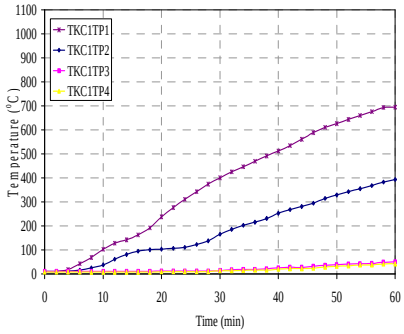

C2-bot;loading direction

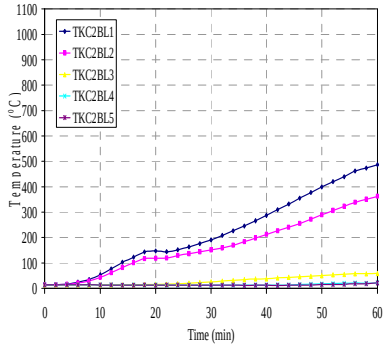

C2-bot;loading direction

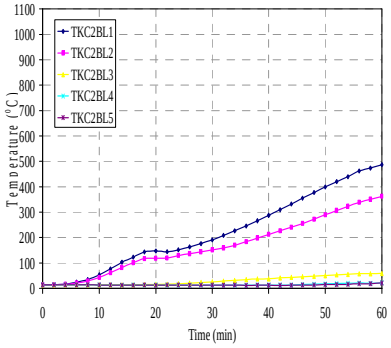

C2-top;loading direction

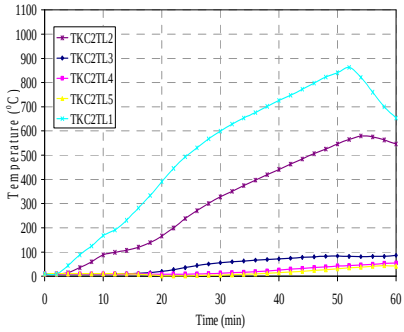

C2-bot;perp loading direction

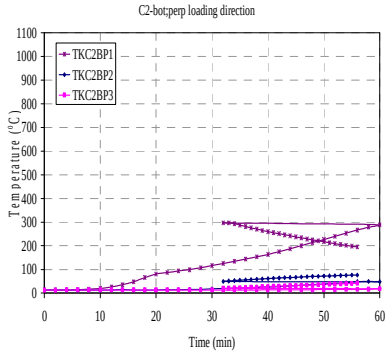

C2-mid;perp loading direction

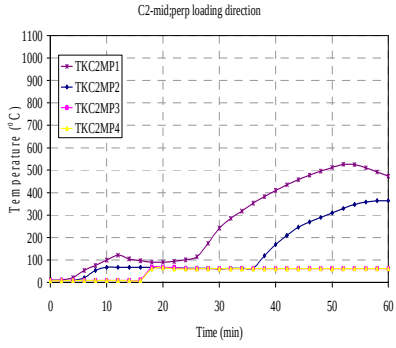

C2-top;perp loading direction

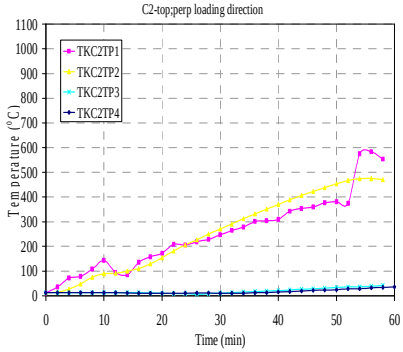

D.4: Temperature Distributions of columns (C3 and C4)

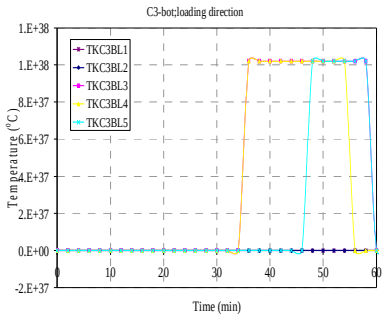

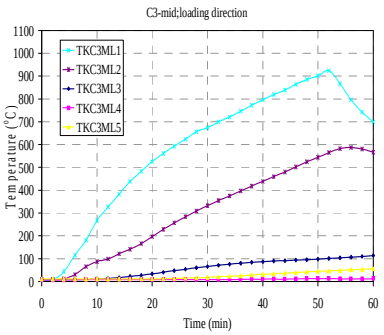

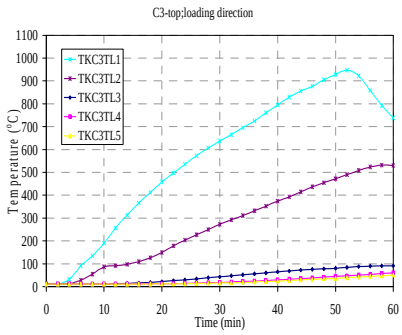

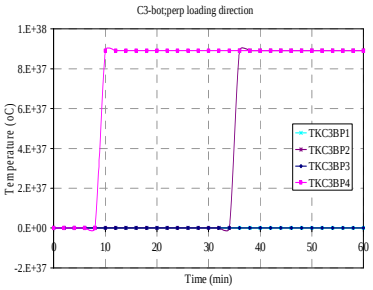

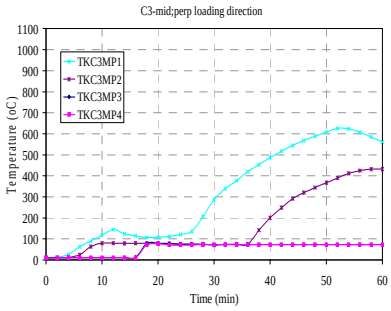

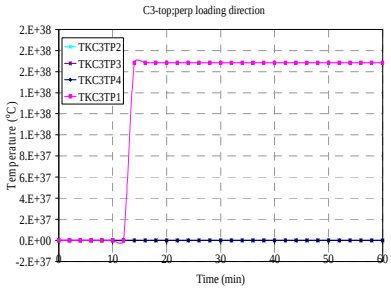

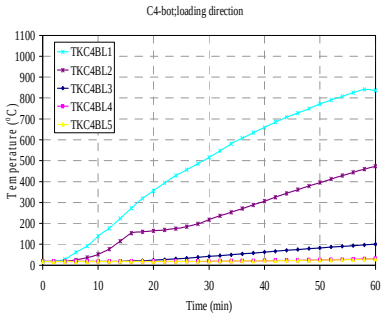

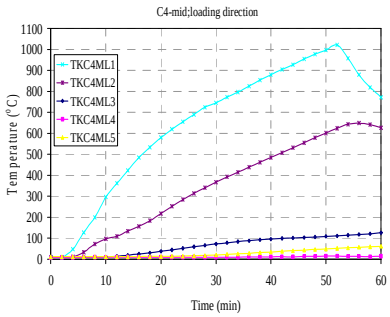

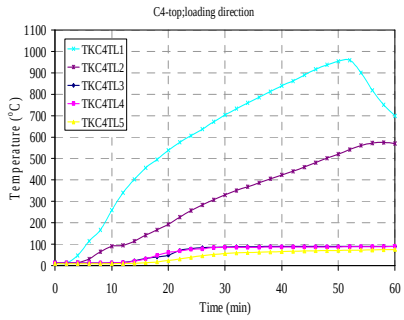

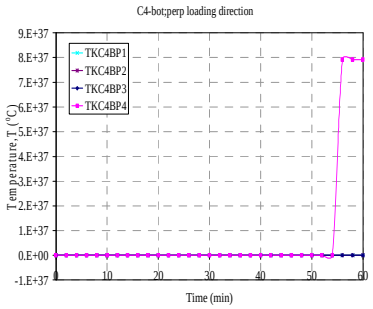

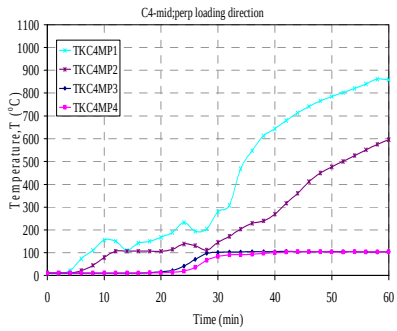

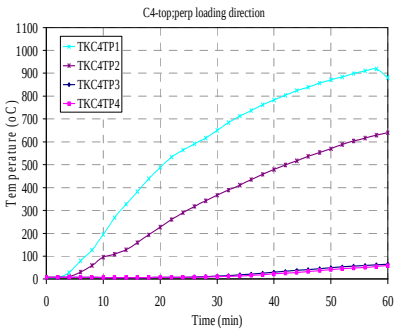

D.5: Temperature Distributions of Slab at point A, B, C, D and O

TKSA

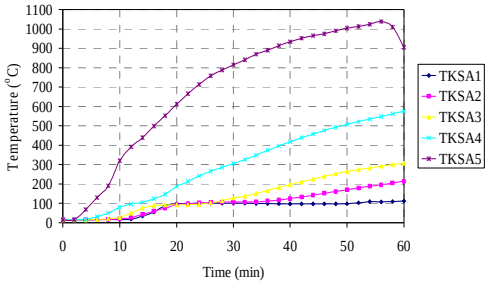

TKSB

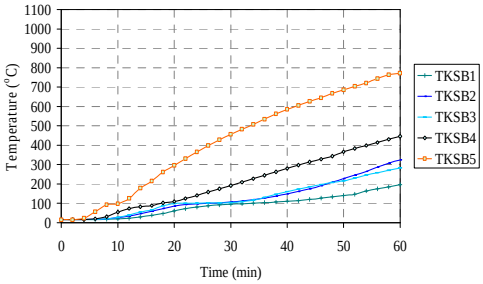

TKSC

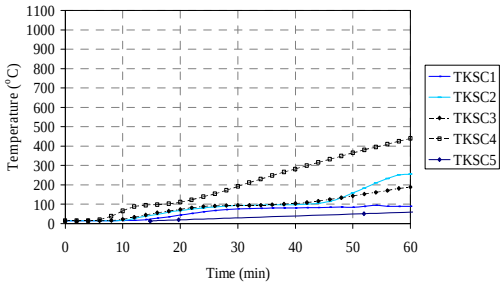

TKSD

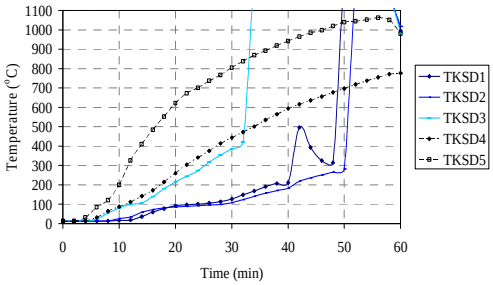

TKSO

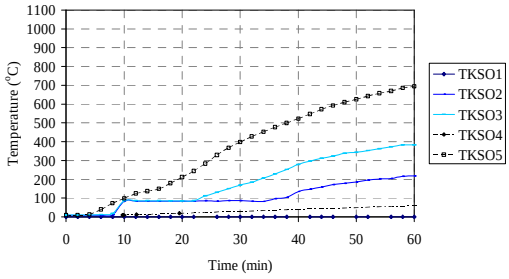

Appendix E

Temperature distributions from the Heat Transfer Analysis

E.1: Temperature Distributions of Top Beam (B1 – B4)

B1-Left

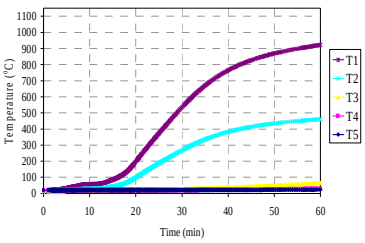

B1-Mid

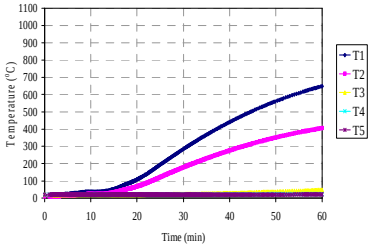

B1-Right

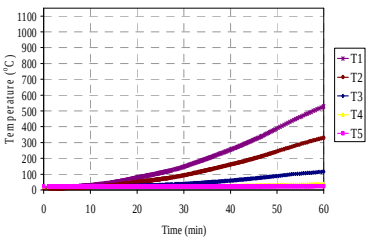

B2-Left-H

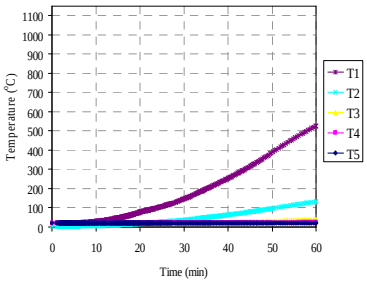

B2-Mid-H

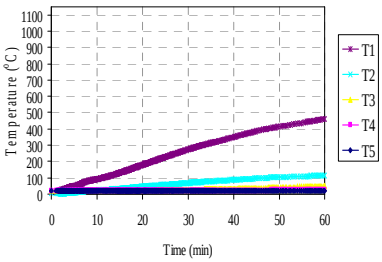

B2-Right-H

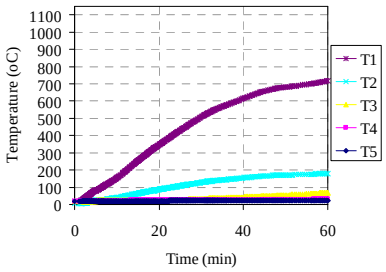

B3-Left-H

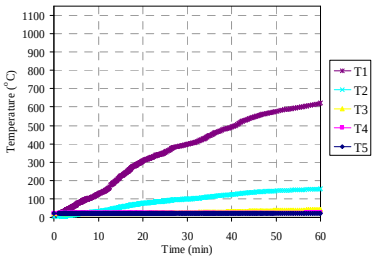

B3-Mid-H

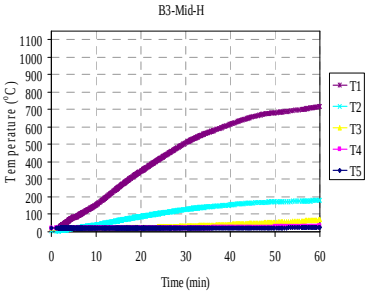

B3-Right-H

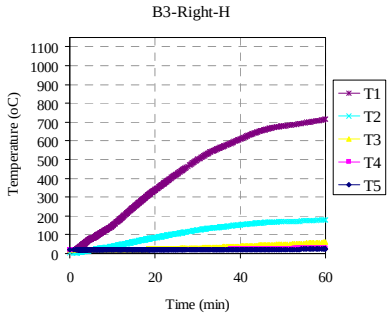

B4-Left-H

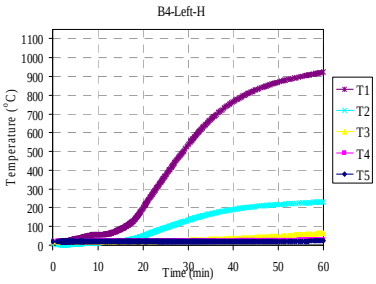

B4-Mid-H

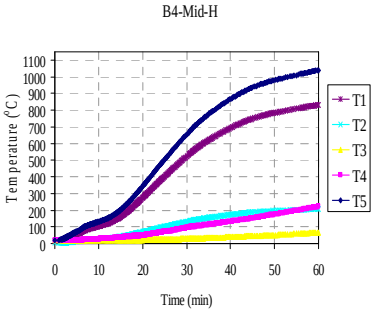

B4-Right-H

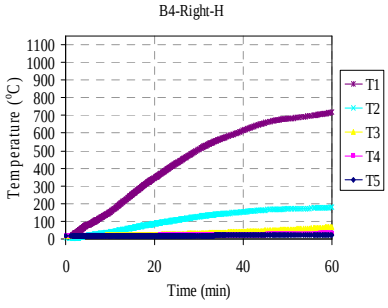

E.2 : Temperature Distributions of Top Beam (B7 and B8)

B7-Left-H

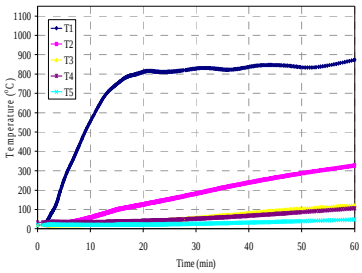

B7-Mid-H

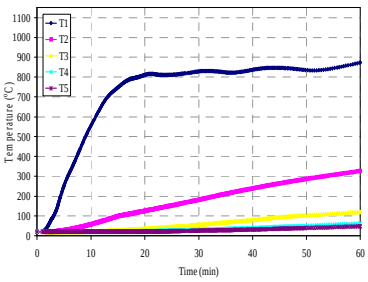

B7-Right-H

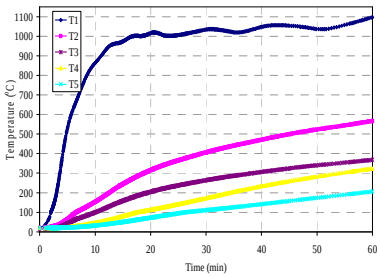

B7-Mid-H

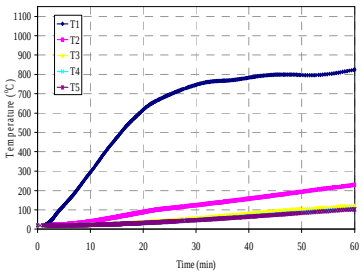

B7-Mid-H

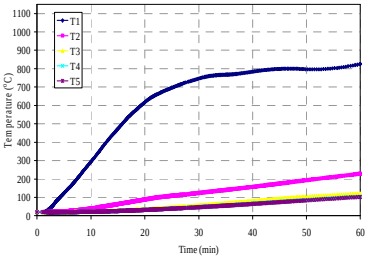

B7-Right-W

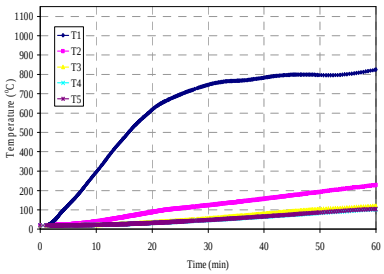

B8-Left-H

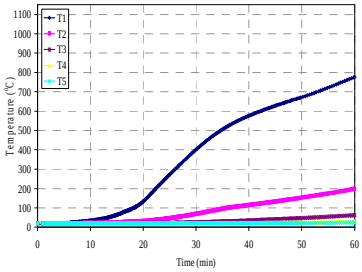

B8-Mid-H

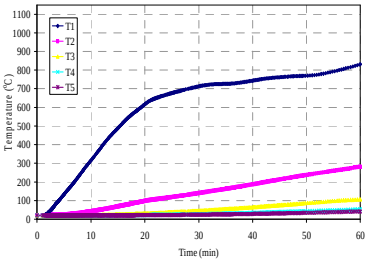

B8-Right-H

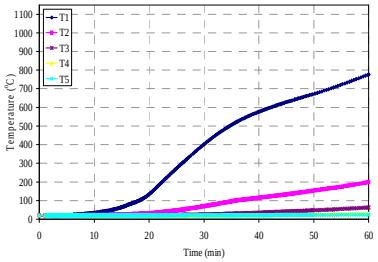

B8-Left-W

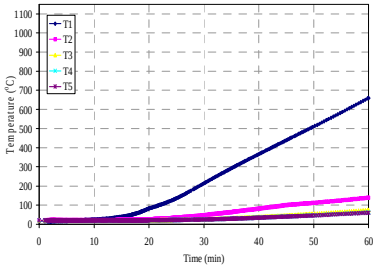

B8-Mid-W

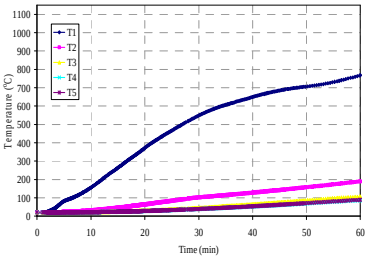

B8-Right-W

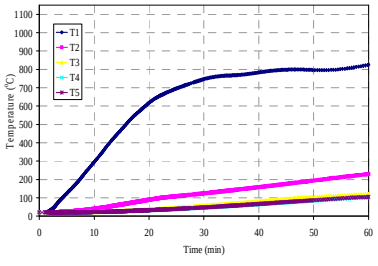

E.3: Temperature Distributions on Column (C1 and C2)

C1-Bottom-X-CHT2

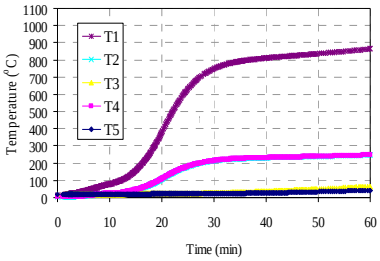

C1-Middle-X-CHT2

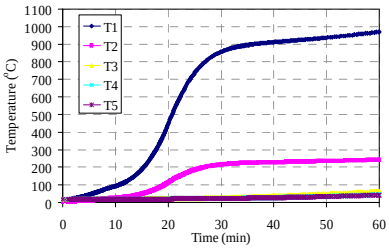

C1-Top-X-CHT2

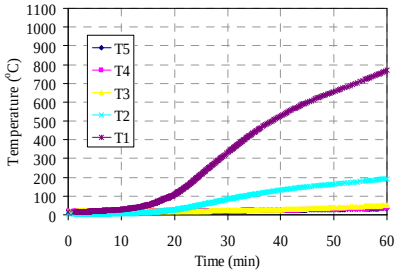

C1-Bottom-Z-CHT2

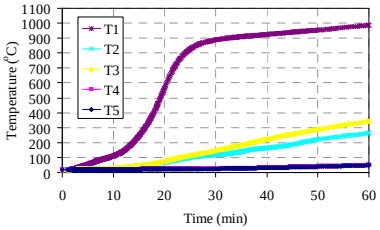

C1-Middle-Z-CHT2

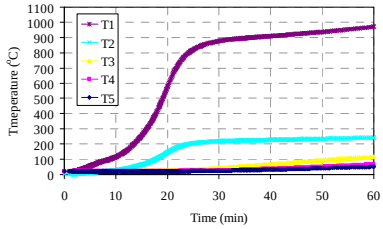

C1-Top-Z-CHT2

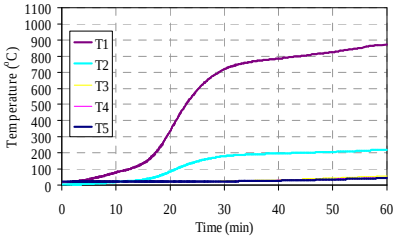

C2-Bottom-X-CHT2

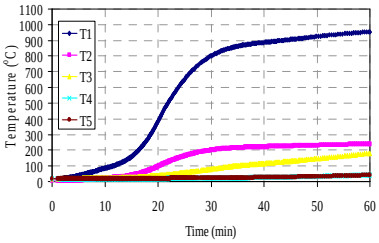

C2-Middle-X-CHT2

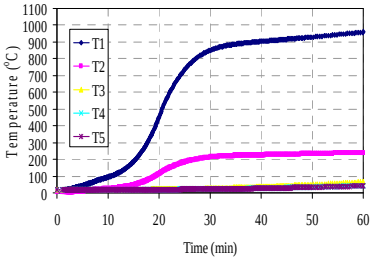

C2-Top-X-CHT2

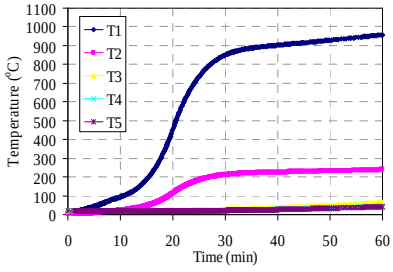

C2-Bottom-Z-CHT2

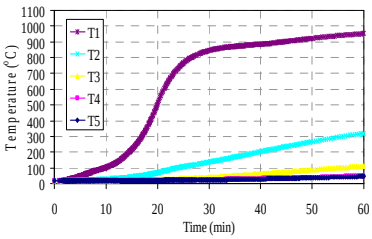

C2-Middle-Z-CHT2

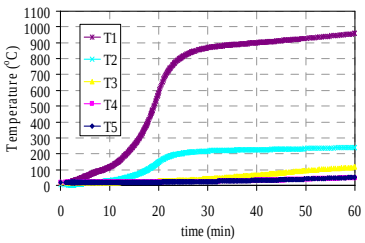

C2-Top-Z-CHT2

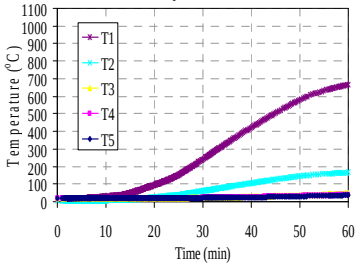

E.4: Temperature Distributions on Column (C3 and C4)

C3-Bottom-X-CHT2

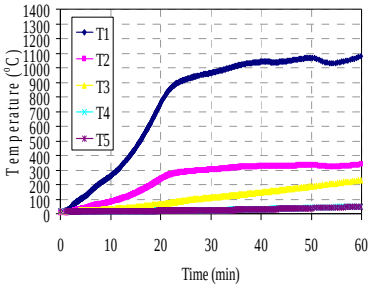

C3-Middle-X-CHT2

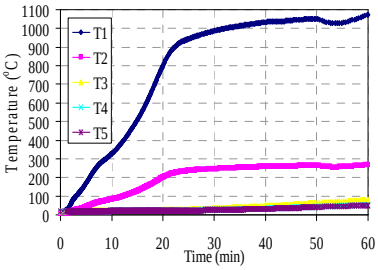

C3-Top-X-CHT2

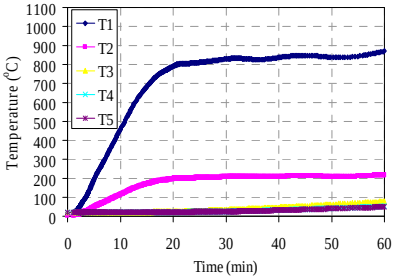

C3-Bottom-Z-CHT2

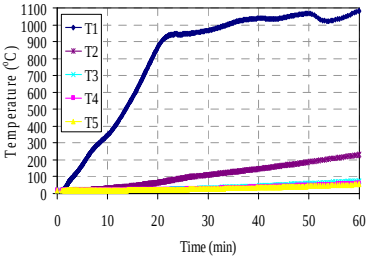

C3-Middle-Z-CHT2

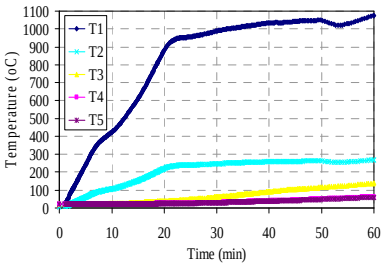

C3-Top-Z-CHT2

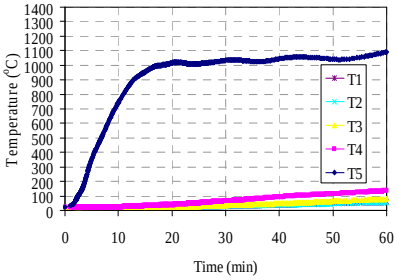

C4-Bottom-X-CHT2

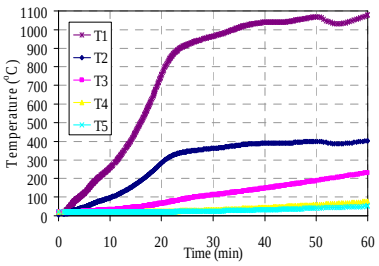

C4-Middle-X-CHT2

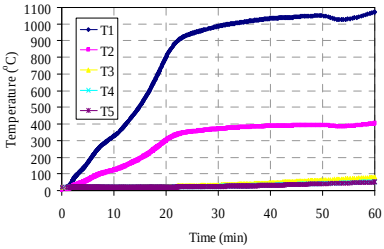

C4-Top-X-CHT2

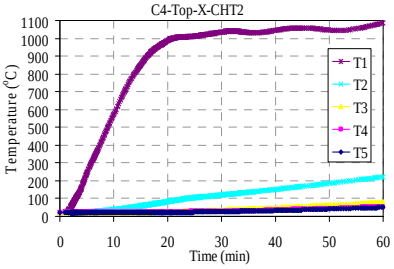

C4-Bottom-Z-CHT2

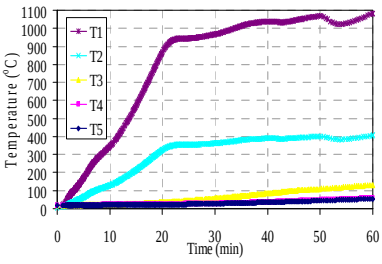

C4-Middle-Z-CHT2

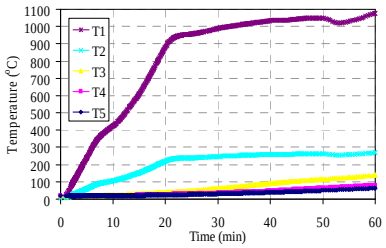

C4-Top-Z-CHT2

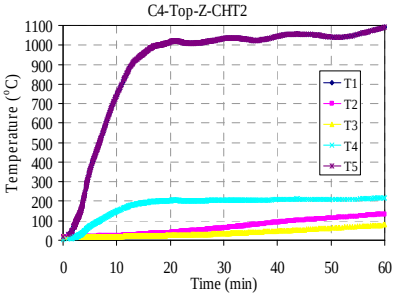

E.5: Temperature Distributions of Slab at point A, B, C, D and O

TSL-A

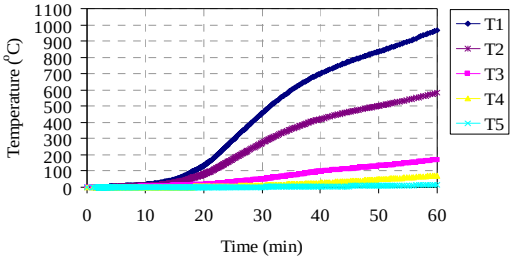

TSL-B

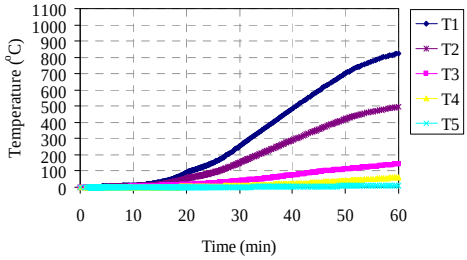

TSL-C

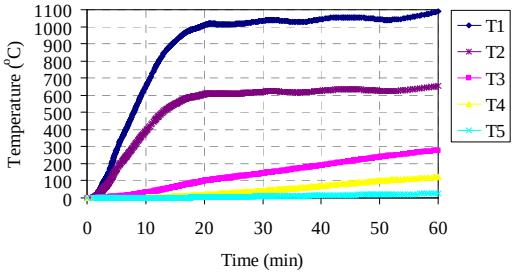

TSL-D

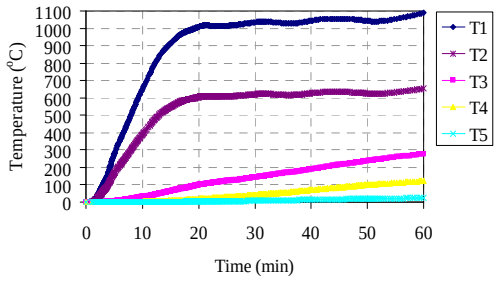

TSL-O

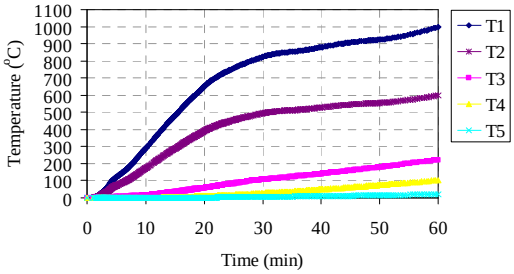

Appendix F

Temperature distribution details used for I-Section

This section presents the temperature input used for the beams and columns in the 3D ABAQUS beam-shell model. The temperature input at five specific points throughout the I-beam cross-section is given.

F.1 Temperature details at specific points for an I-beam section used for columns in the 3D ABAQUS beam-shell model.

The temperature values used in numerical modelling are taken from average temperatures in the test. Temperature distributions seen in C4 during the test are used for the columns. The temperature input for the columns varies depending on the time and the column's height. Figure F.1 shows the temperature points used in each column. The temperature details used for the columns are listed in Tables F.1 to F.3

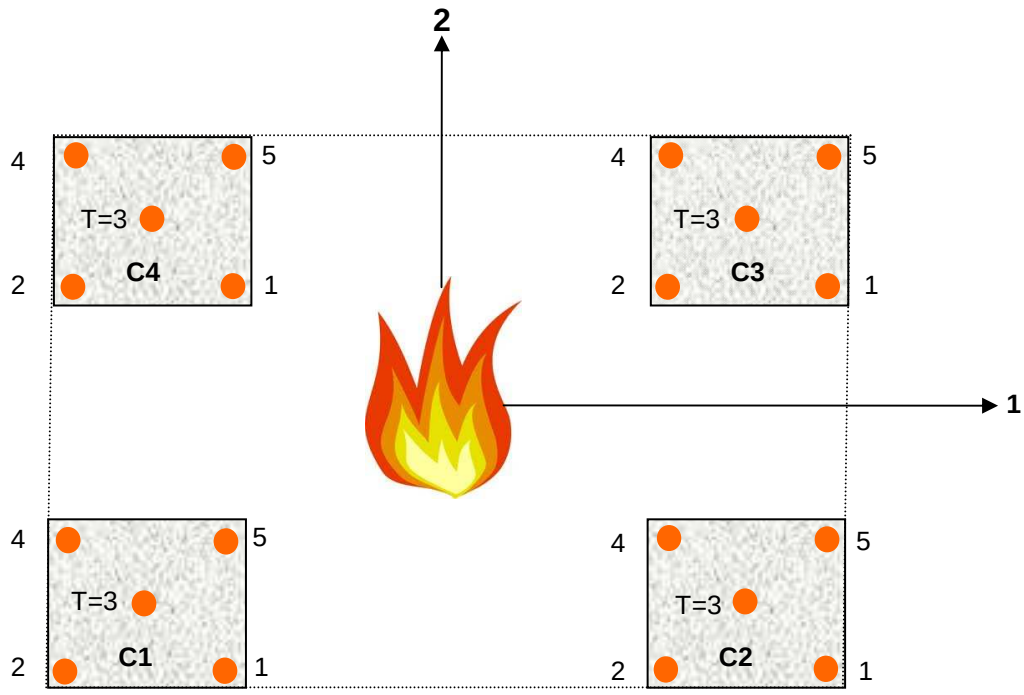

Figure F.1 Diagram of columns and the temperatures points

Table F.1 Temperatures input at specific points at the bottom of the column C1

Temperature points (^{o}C) / Time (min)	C1 (Reference)	1	2 (Cool)	3	4	5
	C2	2	1 (Cool)	3	5	4
	C3	2	5 (Cool)	3	4	1
	C4	1	4(Cool)	3	2	5
10		150	20	18	150	150
20		350	20	24	350	350
30		520	20	42	520	520
40		610	20	62	610	610
50		760	20	83	760	760
60		840	20	100	840	840

Table F.2 Temperatures input at specific points at the middle of the column C1

Temperature points (^{o}C) / Time (min)	C1 (Reference)	1	2 (Cool)	3	4	5
	C2	2	1 (Cool)	3	5	4
	C3	2	5 (Cool)	3	4	1
	C4	1	4 (Cool)	3	2	5
10		300	20	12	160	300
20		580	20	24	170	580
30		750	20	42	280	750
40		880	20	62	650	880
50		1000	20	83	780	1000
60		780	20	100	860	780

Table F.3 Temperatures input at specific points at the top of the column C1

Temperature points (^{o}C) / Time (min)	C1 (Reference)	1	2 (Cool)	3	4	5
	C2	2	1(Cool)	3	5	4
	C3	2	5(Cool)	3	4	1
	C4	1	4(Cool)	3	2	5
10		270	190	12	20	270
20		550	480	24	20	550
30		700	650	42	20	700
40		840	780	62	20	840
50		960	870	83	20	960
60		700	880	100	20	700

F.2 Temperatures details at specific points for I-beam section use for plinth beams in 3D beam-shell model.

The temperature distributions in the plinth beams used in the numerical modelling follow the temperatures seen in B1 during the test. For the plinth beams, the heating is from the top surface to the bottom of the beam section. Temperature points 4 and 5 are defined with the highest temperature and 1 and 2 experience the coolest temperature. Temperature point 3 is defined as having the temperature at the middle of the section depth. Figure F.2 shows the details of the temperature points in each beam. Table F.4 shows the temperature distribution seen throughout the plinth beams over the course of 1 hour exposure.

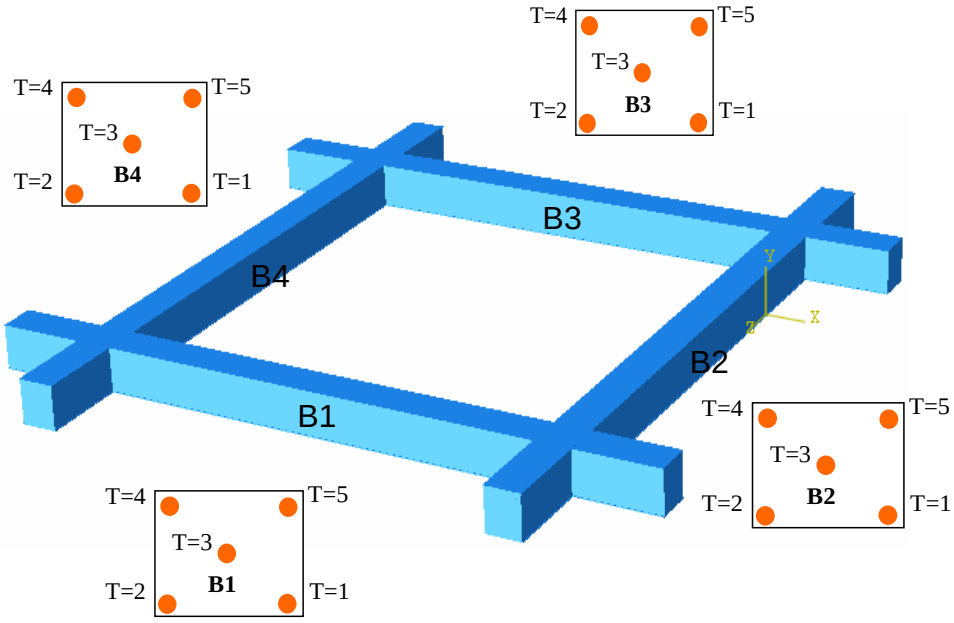

Figure F.2 Diagram of plinth breams and the temperatures points

Table F.4 Temperatures input at specific points at the plinth beam

Temperature points (^{o}C) / Time (min)	B1 (Reference)	1 (Cool)	2 (Cool)	3	4	5
	B2	1 (Cool)	2 (Cool)	3	4	5
	B3	1 (Cool)	2 (Cool)	3	4	5
	B4	1(Cool)	2 (Cool)	3	4	5
10		20	20	29	325	325
20		20	20	23	520	520
30		20	20	29	640	640
40		20	20	44	730	730
50		20	20	58	780	780
60		20	20	79	630	630

F.3 Temperatures details at specific points for I-beam section use for top beams in 3D beam-shell model.

The temperature distribution through the top beams used in numerical modelling follows the temperatures of beam B7 from the test. The temperatures are defined at the two different surfaces: at the bottom surface, and at the inner side of the beams. The hottest surfaces experienced by B1 and B8 are defined at the temperature points 1,2, and 5. For beam B6 and B7, the hot surfaces are defined at temperature points 1,2 and 4. The outer surface of the beams is defined with a lower temperature than the inner surface. The details of the temperature points within each top beam are shown in Figure F.3. The temperature distributions seen in the top beams are shown in Table F.5.

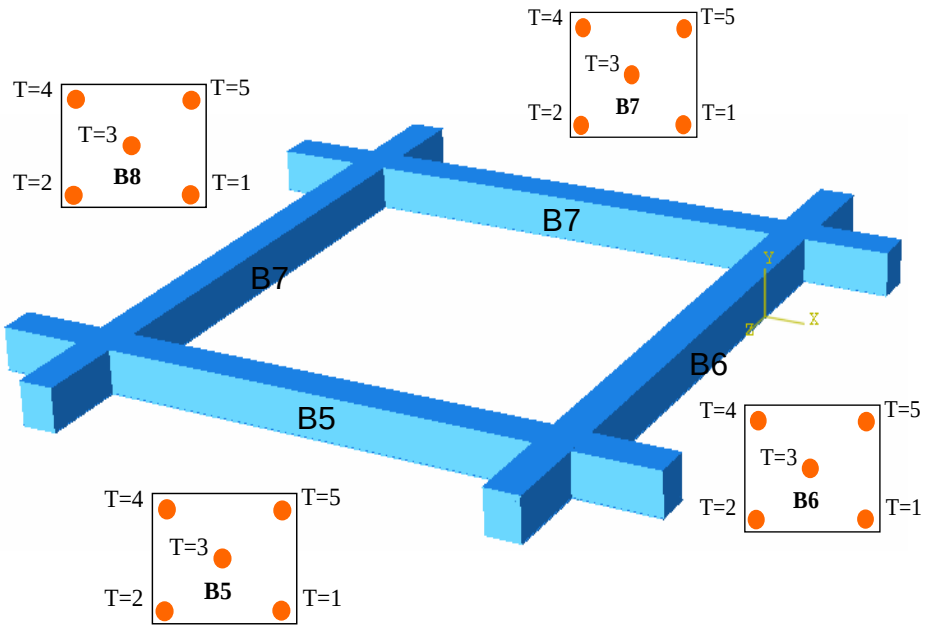

Figure F.3 Diagram of top breams and the temperatures points

Table F.5 Temperatures input at specific points at the top beam

Temperature points (^{o}C) / Time (min)	B5 (Reference)	1	2	3	4 (Cool)	5
	B6	1	2	3	5 (Cool)	4
	B7	1	2	3	5 (Cool)	4
	B8	1	2	3	4 (Cool)	5
10		300	300	18	20	300
20		560	560	27	20	560
30		700	700	50	20	700
40		850	850	68	20	850
50		950	950	77	20	950
60		700	700	93	20	700

F.4 Temperatures details at specific points for I-beam section use for slab in 3D beam-shell model.

Table F.6 shows the temperature distribution through the thickness of the slab. Five temperature points are defined at equally spaced points through the depth of each layer of the shell's thickness. Temperature point 1 is defined at the bottom surface of the slab and 5 is the top surface of the slab. The distance between each temperature point is 30mm. The bottom surface of the slab is hottest, while the top surface of the slab remains coolest.

Table F.6 Temperatures input at specific points at the slab

Temperature points (^{o}C) / Time (min)	1	2	3	4	5 (Cool)
10	100	50	30	20	20
20	210	80	80	20	20
30	400	170	80	40	20
40	520	280	140	45	20
50	630	350	180	50	20
60	700	380	220	60	20

Appendix G

Selected Publications

This section presents three papers which have resulted from the work throughout the thesis.

1. Mariyana A. Ab-Kadir, J.Zhang, Asif S. Usmani; Experimental and Numerical Study on softening and Pinching Effects of Reinforced Concrete; 8th Asia Pacific Structural Eningeeirng and Construction Conference (APSEC) and 1st International Conference on Civil Engineering Research (ICCER), Surabaya, Indonesia, October 2012

2. Mariyana A. Ab-Kadir, Jian Zhang, Jian Jiang, Asif S. Usmani, Martin Gillie, Umesh K. Sharma, Pradeep Bhargava; Modelling of an Earthquake Damaged RC Frame Subjected to Fire;7th International Conference on Structures in Fire, Zurich, Switzerland, June 2012 (Accepted for Oral Presentation)

3. Ab.Kadir M A, A.S Usmani, M. Gillie; Modelling of Reinforced Concrete Frames in Fire Following an Earthquake; Applications of Structural Fire Engineering, Prague, April 2011 (Accepted for Oral Presentation)

EXPERIMENTAL AND NUMERICAL STUDY ON SOFTENING AND PINCHING EFFECTS OF REINFORCED CONCRETE FRAME

Mariyana A. Ab-Kadir[1,2], J.Zhang[1], Asif S. Usmani[1]

[1]School of Engineering, University of Edinburgh

[2]Faculty of Civil Engineering, Universiti Teknologi Malaysia

Abstract—**The response analysis of reinforced concrete (RC) structures subjected to strong earthquake motions requires material models that are able to simulate cyclic deformation and damage realistically. This paper presents the results of a study of pinching and softening behaviour in an RC frame subjected to cyclic loading. The experiment was conducted on a full-scale RC frame at Indian Institute of Technology Roorkee in India. The hysteretic curve representing the response of the frame was generated. Finite element analyses were performed to predict the response of the frame under cyclic loading both before and after the test using different computer codes, ABAQUS and OpenSees. Although the experiment was conducted using load control, the finite element simulations were performed using displacement control. The result from both models are compared to the experiment and to each other and a detailed discussion is provided on the modelling capabilities of the two software in capturing the pinching and softening behaviour observed in the test.**

Keywords- Finite element models, Hysteretic behaviour, Pinching, Softening

Introduction

According to present building code, reinforced concrete buildings are designed to withstand certain earthquake intensity and expected to deformed well into the inelastic range and dissipate a large part of the energy input through stable hysteretic behaviour of their structural components [3]. The hysteretic behaviour of the buildings structures reflects the ability of energy dissipation and collapse resistance of a structure at different levels, such a material, member and structure as a whole.

Experimental on single reinforced concrete members is of major importance for understanding the complete structure behaviour subjects to either monotonic or cyclic loading conditions. Even though the experimental do not exactly match the actual condition of members in a real structure, the source of relevant phenomenal remains essentially the

same, therefore experimental result could be valuable information on nonlinear response mechanisms. However, experimental for the whole buildings will consume cost and time, therefore numerical analysis is become more applicable.

In over the last two decades, many rigorous and computationally complex methods for predicting of response of reinforced concrete structures subjected to cyclic loading have been developed. The first record of used the nonlinear finite element model (FEM) to simulate reinforced concrete members was in 1967 [8]. The finite element model created broadly to all structure analysis, and not all purposely for an earthquake analysis. Hence, for the general purposes of finite element model for example ABAQUS, SAP2000. It always has to validate with the test data or any finite element model.

In this paper, the response of RC frame subject to cyclic loading is numerically studied using ABAQUS [1] and OpenSees [6]. The results of hysteretic curve from the modeling have been used to compare against experimental result to determine the capability of the modeling

Experimental study

A single storey of reinforced concrete frame was carried out at Indian Institute of Technology (IIT) Roorkee, India. The height of the frame is 5.0m and the distance between plinth beam and roof beam is 3.0m. The test frame consist of four column with cross-section of the columns is 300mm x 300mm and that of the beams is 230mmx230mm. Slabs thickness is 120mm. Reinforcing steel details in beam and column as shows in Figure 1 and 2. The frame was subjected to cyclic lateral load in load control manner using pair of double acting hydraulics jack acting in tendem with each other against a stiff reaction wall at the slab level of the frame [9]. Front view of schematic test frame as shows in Figure 3. Each column was loaded with an 80kN load coming from upper storey and the slab was loaded with a uniformly distributed load of 2.3 kN/m^2.

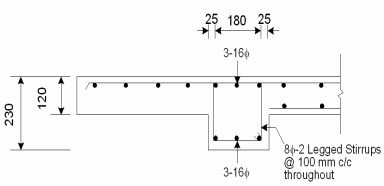

Figure 1. Detailing of beam reinforcement

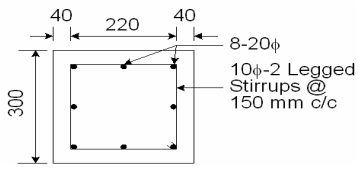

Figure 3. Detailing of column reinforcement

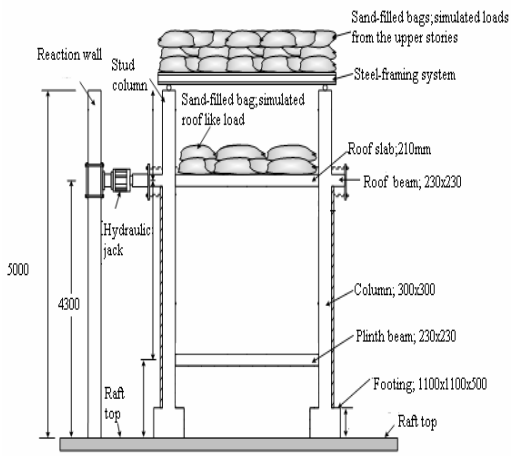

Figure 2. Schematic of the test frame and loading

Finite element analysis

To study the behaviour of RC frame under earthquake excitation loading, the numerical modeling of the RC frame was investigated. The numerical analysis was carried out using the general purpose of finite element software ABAQUS and the open source software framework OpenSees.

A 2D beam element is modeled using ABAQUS. All the elements are simulated using beam elements. In order to reduce computational time the slab was modelled as apart of the overall beam cross section in 2D beam element model. Timoshenko beam element (B21) that allows transverse shear strain is used in this. The 2D beam element model of RC frame as shows in Figure 4. The compressive strength of concrete is 34MPa and tensile strength is 3.4MPa. Material properties is used according to Eurocode [2]. The stress-strain relationship for both concrete and reinforcing steel as shows in Figure 5 and 6. Continuum plasticity – based damage model known as concrete damaged plasticity in ABAQUS is used to simulate the behaviour of concrete. The concrete damage plasticity model take into consideration of degradation of strength of the concrete under both compression and tension. It assumes that the two main failure mechanisms are tensile cracking and compressive crushing of the concrete material and

that the uniaxial tensile and compressive response of concrete is characterized by damaged plasticity[4]. Due to the limitation of using shell element in simulation of the pinching and softening effects, the structural response will be compared with the results using OpenSees.

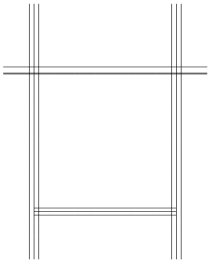

Figure 4. 3D shell element model

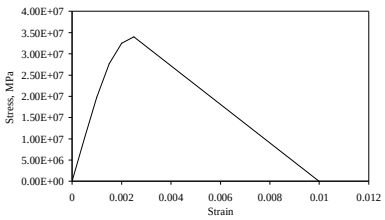

Figure 5. Stress strain relationship of concrete

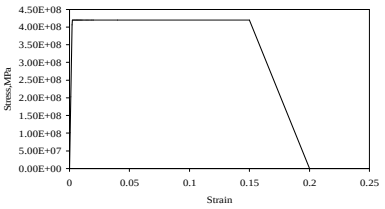

Figure 7. Stress strain relationship of steel

In OpenSees, Euler- Bernoulli beam element is used to model the RC frame. To take into account the pinching and softening behaviour, pinching material have been used at the end of the joint. The pinching material is a uniaxial material that represents a 'pinched' load-deformation response and exhibits degradation under cyclic loading. Cyclic degradation of strength and stiffness occurs in three ways: unloading stiffness degradation, reloading stiffness degradation, strength degradation [7,5]. The degradation of the stiffness and strength of the pinching material under cyclic loading is shown in Figure 7

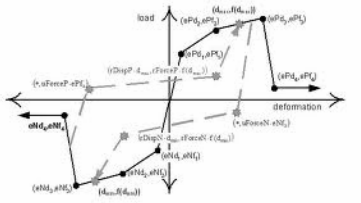

Figure 8. Pinching material in OpenSees

Cyclic loading analysis

In numerical analysis, the displacement control scheme was used to generate hystretic behaviour of the frame. A step-by step procedure in increasing displacement to reach the maximum displacement capacity (about 90mm) obtained the hysteretic behavior the frame. The displacement is applied the slab level of the frame. The displacement history applied as shows in Figure 8.

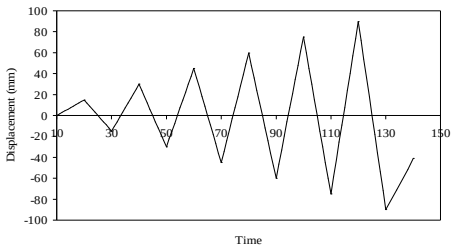

Figure 9. Displacement history

Figure 9 is illustrates the hysteretic behavior of the frame obtained in the test. Stiffness degradation and pinching effects clearly shows in the curve. Figure 10 and 11 shows the hysteretic curve of the frame obtained from ABAQUS and OpenSees , respectively.

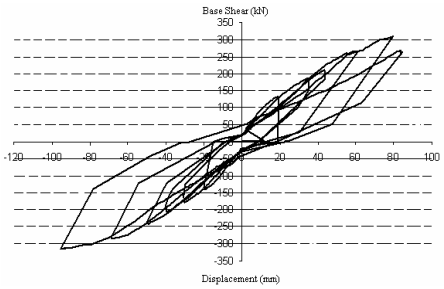

Figure 10. Hysteretic curve of tested frame

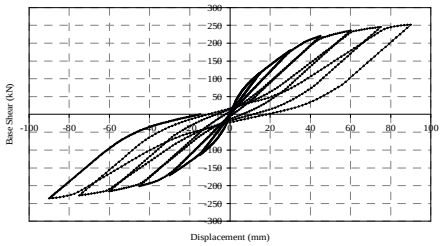

Figure 10. Hysteretis curve of OpenSees analysis

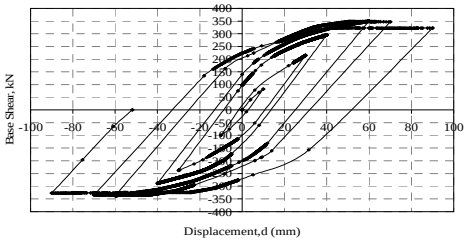

Figure 11. Hysteretis curve of ABAQUS analysis

From the figure, it can be clearly observed that the results obtained from ABAQUS can find the strength envelop (or capacity curve) precisely .But, when the deformation increases, the area under the loop varies dramatically. OpenSees results can simulate the hysteretic behavior much better than ABAQUS.

Summary and conclusion

From this study, it is found that by using numerical simulation to study the cyclic response of RC frame, OpenSees can take both pinching and softening effect into account. The hysteresis curve looks close using OpenSees than using ABAQUS. By using ABAQUS, the beam element was used to simulate the RC frame behaviour. However this type of element shows the effects of strength and stiffness degradation but not reflect the pinching behaviour

Acknowledgment

This studies which are presented herein have been carried out as part of a research project involving the University of Edinburgh and Indian Institute of Technologi (IIT) Roorkee, India. Thanks to the researchers from Department of Civil Engineering, IIT Roorkee for providing the testing results of full-scale RC frame.

References

[1] ABAQUS, ABAQUS 6.8 (2008) Dassault Systemes Simulia Corp: Providence

[2] EN1992-1-2: Eurocode 2 (2004) Design of concrete structures

[3] Filip C.F, and Issa A. (1988) Nonlinear Analysis of Reinforced Concrete Frames Under Cyclic load Reversals. Report No. UCB/EERC-88/12, Earthquake Engineering Research Center, University of California Berkeley

[4] Lee, J., and G. L. Fenves (1998) Plastic-Damage Model for Cyclic Loading of Concrete Structures, Journal of Engineering Mechanics,124: 892-900

[5] http://nisee.berkeley.edu/elibrary/Text/1288878

[6]http://opensees.berkeley.eduhttp://opensees.berkeley.edu/wiki/index.php/OpenSees_User

[8] Ngo, D. and Scordelis, A.C. (1967) Finite Element Analysis of Reinforced Concrete Beams, Journal of ACI,64: 152-163.

[9] Sharma, U.K. et. al., Full scale testing of a damaged RC frame in fire, Structures *and Buildings, Proceedings of the ICE, in press, 2012*

MODELLING OF AN EARTHQUAKE DAMAGED RC FRAME SUBJECTED TO FIRE

Mariyana A. Ab-Kadir*, Jian Zhang*, Jian Jiang*, Asif S. Usmani*, Martin Gillie*, Umesh K. Sharma and Pradeep Bhargava****

*School of Engineering, University of Edinburgh, Edinburgh, UK EH9 3JF e-mails: m.ab-kadir@ed.ac.uk, j.zhang@ed.ac.uk, asif.usmani@ed.ac.uk, M.Gillie@ed.ac.uk

** Department of Civil Engineer, Indian Institute of Technology, Roorkee, Roorkee, India 247667 e-mails: umuksfce@iitr.ernet.in, bhpdpfce@iitr.ernet.in

Keywords: Fire following an earthquake, finite element modelling, reinforced concrete frame

Abstract. Fires are a relatively likely event consequent to earthquakes in urban locations and in general are an integral part of the emergency response strategies focussed on life safety in most developed economies. Similarly building regulations in most countries require engineers to consider the effect of seismic and fire loading on the structures to provide an adequate level of resistance to these hazards, however only on a separate basis. To the authors knowledge there are no current regulations that require buildings to consider these hazards in a sequential manner to quantify the compound loading and design for the required resistance. This paper offers a preliminary report of a modelling exercise undertaken to simulate a novel test on a full-scale RC frame subjected to simulated earthquake and fire loads. The results from the first test indicate that the test frame could withstand a pre-damage corresponding to a seismic performance level and subsequent one-hour fire exposure without collapse. The modelling has been carried out using the ABAQUS and OpenSees finite element software and the results from the models are compared against observed data from the experiment.

INTRODUCTION

Earthquakes are natural hazards in seismic region and can cause devastating damage to urban infrastructure and lifelines. Buildings constructed in seismic regions are vulnerable not only to earthquakes but also to subsequent secondary hazards such as fires and flooding etc. This study is concerned with the effect of fires on structures damaged in an earthquake. Botting reported that a significant conflagration occurred following 15 out of 40 of major earthquakes [1]. For example, a significant proportion of the damage to infrastructure and facilities in the 1994 Northridge and the 1995 Kobe earthquakes could be attributed to fires following the earthquake [2]. The damaged buildings due to earthquakes are more vulnerable to fire effects than undamaged buildings [2,3]. In design, these two events are considered to occur separately and no current regulations explicitly require consideration of this load combination for civil infrastructure. This situation may change with increasing acceptance of performance based options in building standards, however considerable new research is required in this area before these options can be fully exploited in the profession [4].

This paper presents results from 2D and 3D modelling of a full-scale reinforced concrete test frame subjected to a severe fire following cyclic lateral loading applied to simulate realistic seismic damage. The test was carried out as part of the collaborative UK-India research programme and preliminary results and modelling have been reported in [5], this paper builds on that work. The modelling was carried out using the commercial software package ABAQUS and the open source software framework OpenSees [6]. The results from the modelling have then been compared against selected measured data from the test.

BUILDING CONFIGURATION

A four-storey reinforced concrete building was designed using the Indian Building Code [7]. For the purpose of this study, a single storey frame from this building was constructed for the test which considers the loading from the storeys above. The total height of the constructed frame was 6.0m with the distance between the plinth and top beams being 3.0m. The cross section of the columns was 300mm x 300mm and that of the beams was 230mm x 230mm topped up further by 120mm thick slab. Eight steel bars of 20 mm diameter were used as main reinforcement for columns and six steel bars of 16mm diameter were used for beams (3 each on the top and bottom). The slab was

reinforced with 8mm reinforcing steel in the tension zones in both directions on top and bottom. Each column was loaded with an 80kN load coming from upper storey and the slab was loaded with a uniformly distributed load of 2.3kN/m^2.

STRUCTURAL MODELLING

ABAQUS models

Finite element software ABAQUS [8] was used to analyse both the thermal and mechanical response of the frame. For the 2D model, beams, columns and slab are modelled using beam elements as shown in Figure 1(a). The slab was modelled as apart of the overall beam cross section in the 2D beam element model. Linear Timoshenko beam element (B21) that allows transverse shear strain is used in this model. In the 3D model the whole frame is constructed using shell elements as shown in Figure 1(b). Shell elements (S4R) are used. Only a half of the frame is modelled assuming symmetry to reduce computation time. Both the 2D and 3D analyses were fully nonlinear. The reinforcing steel in the 2D model is modelled as truss elements (T2D2) that only allow axial forces. In the 3D model, reinforcing steel is modelled as discreet rebars. The rebars are defined by specifying the size and distribution of the reinforcing steel in the cross section.

The mechanical properties of the reinforcing steel and the concrete at elevated temperatures is assumed to comply with Eurocode 2 [9]. The ambient compressive strength of concrete is 34MPa and tensile ambient strength is 3.4MPa. Mechanical properties of reinforcing steel are shown in Table 1. The applied loading on the frame was constant throughout the analysis. Continuum plasticity based damage model known as “concrete damaged plasticity” in ABAQUS is used to simulate the material nonlinearity of concrete. This model takes into consideration of degradation of strength of the concrete under both compression and tension. It assumes that the two main failure mechanisms are tensile cracking and compressive crushing of the concrete material and that the uniaxial tensile and compressive response of concrete is characterized by damaged plasticity [10]. The analysis is implemented using implicit integration (ABAQUS/Standard) which more computationally efficient and reliable for highly nonlinear problems than explicit dynamics (ABAQUS/Explicit), however it is also more difficult to obtain convergent results using this approach.

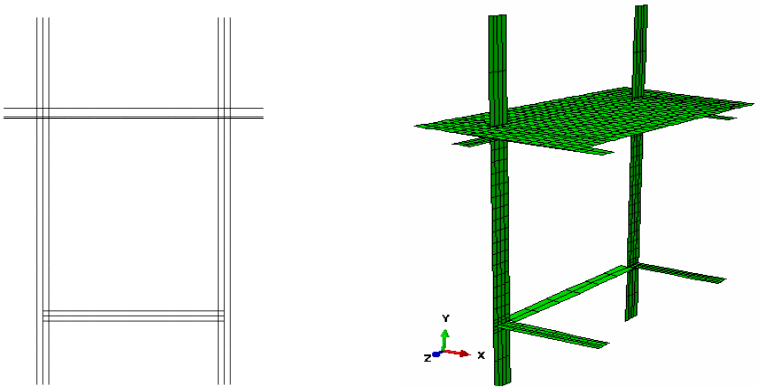

(a) (b)

Figure 1: 2D (a) and 3D (b) finite element models using ABAQUS

Table 1. Mechanical properties of reinforcing steel

Diameter of reinforcing steel (mm)	Yield stress (MPa)	Ultimate Stress (MPa)	Yield Strain (mm/mm)	Ultimate Strain (mm/mm)	Elongation (%)	Young’s Modulus (x10^5 MPa)
8	551	643	0.0047	0.207	20.7	2.14
10	447	538	0.0042	0.196	19.6	2.13
16	420	541	0.0023	0.1389	16.9	2.03
20	449	568	0.0021	0.1458	14.6	2.1

OpenSees models

OpenSees is an open source object oriented software framework developed at UC Berekeley and currently supported by PEER and Nees. It has been further developed by a team at the University of Edinburgh to perform thermo-mechanical analyses. More details can be found in the reference [11].

The numerical model of the original frames is shown in Figure 2. Due to the simplification to the 2D frame, the slab and roof beams are considered as one structural member (see Section 1-1 in Figure 2). Similarly, two lower beams are regarded as one beam (see Section 2-2 in Figure 2), and the cross section of "the double column" is Section 3-3. Non-linear beam-column elements are used in the modelling. To get sufficient precision in the calculation and to obtain values of displacement, deflection, stress and at different sections, each frame member in the model is divided into many elements. This would also help in comparing the deformed shapes of the model to the frame shape in the tests at various loading stages.

FIRE LOADING

The result of mock fire tests done in IIT, Roorkee, India is shows in Figure 3. The height was measured from the plinth beam. Based on the temperature curve in Figure 3 (obtained from mock fire test carried out in a compartment without the concrete frame), a heat transfer analysis was done using ABAQUS in order to capture the distribution of the temperature in the element cross-section. The temperature distributions obtained were used in the thermo-mechanical analysis for the 2D and 3D models using ABAQUS and OpenSees.

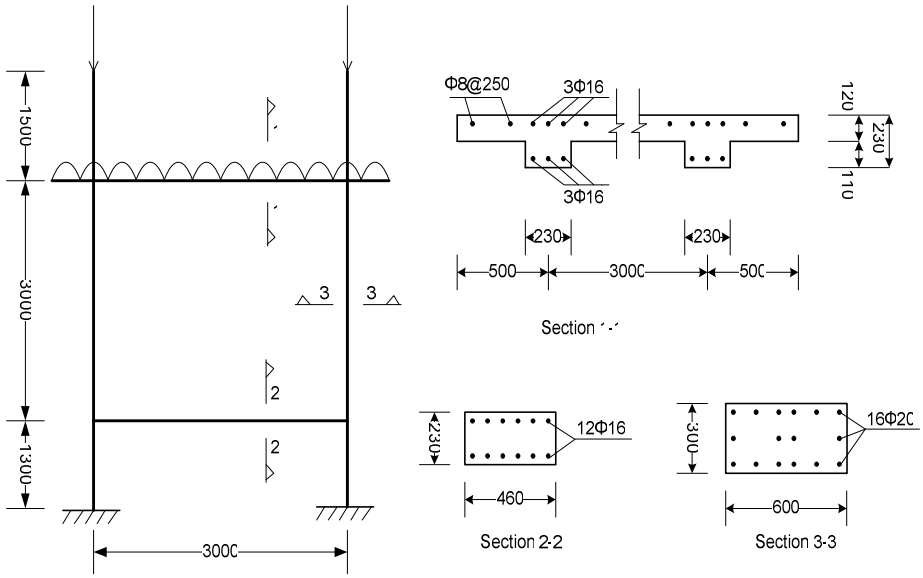

Figure 2. 2D frame model and member sections

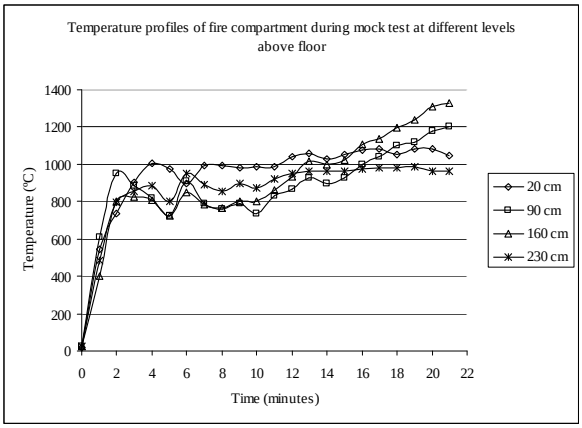

Figure 3. Temperatures curves from the mock test

RESULTS AND COMPARISON WITH TESTED DATA

Base Shear versus roof displacement curve (capacity curve)

The capacity curve is plotted to represent the first mode response of the building based on the structural response to a seismic input predominantly in its fundamental mode of vibration. Incremental lateral loading in displacement control mode is applied until nonlinear static capacity curve is reached. Target displacement at which seismic performance evaluation of the structure is to be performed can be obtained from the capacity curve. The peak loads against corresponding displacement from hysteretic curve of the test and 2D numerical modelling using ABAQUS and OpenSees are plotted in Figure 4. Target displacement of 90mm corresponding to 2% drift ratio is chosen for further analysis.

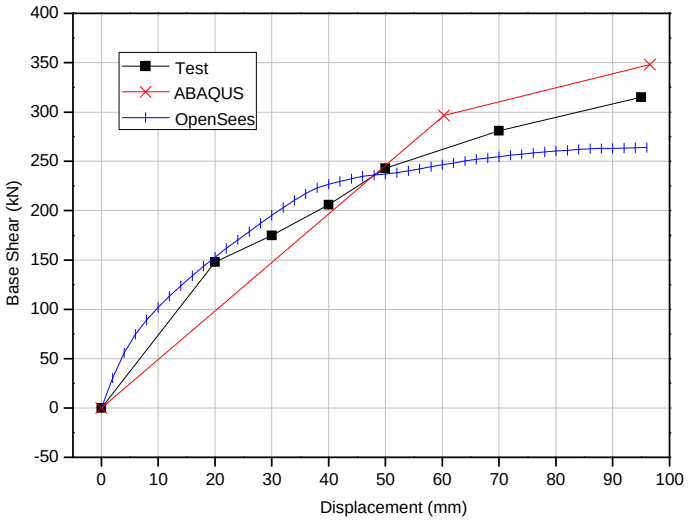

Figure 4. Base shear-roof plotted against roof displacement

Cyclic Analysis

Cyclic lateral loading was applied in the test to simulate the earthquake damage to the frame. Based on the target displacement obtained from the capacity curve, the frame is loaded with horizontal cyclic displacements at the slab level in negative and positive directions. The displacement history applied is shown in Figure 5.

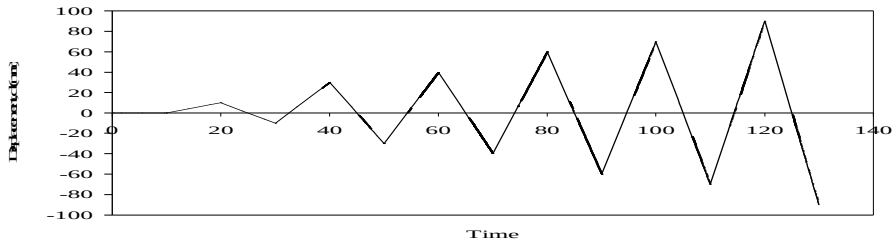

Figure 5. Displacements history for cyclic loading analysis

Figure 7 shows the hysteresis curve obtained from tested frame after seven cycles of loading. The cyclic loading in the test were applied in a quasi-static manner in load controlled mode. The peak load was about 316 kN and 267kN corresponding to a 95mm displacement in one and 85mm displacement in the other direction respectively. The residual displacement of the frame at end of the cyclic loading phase was approximately 19mm (towards the left). Figure 7 shows hysteresis curves from the 2D and 3D OpenSees models. The peak load from 2D model is 250kN corresponding to a displacement of 90mm and the peak load from the 3D model is 350kN corresponding to a displacement of 90mm. Permanent residual displacements of approximately 15mm are predicted by both OpenSees models.

Figure 8 (a) shows the hysteresis curve obtained from ABAQUS for 2D model. The peak load is approximately 350kN and the permanent residual displacement is 44mm. The hysteresis curve of 3D shell element model is shows in Figure 8 (b). The peak load from the analysis is 230kN is lower than obtained in 2D beam element model and the permanent residual displacement is 38mm. Pinching behaviour due to bonding effects is not considered in both 2D and 3D ABAQUS model.

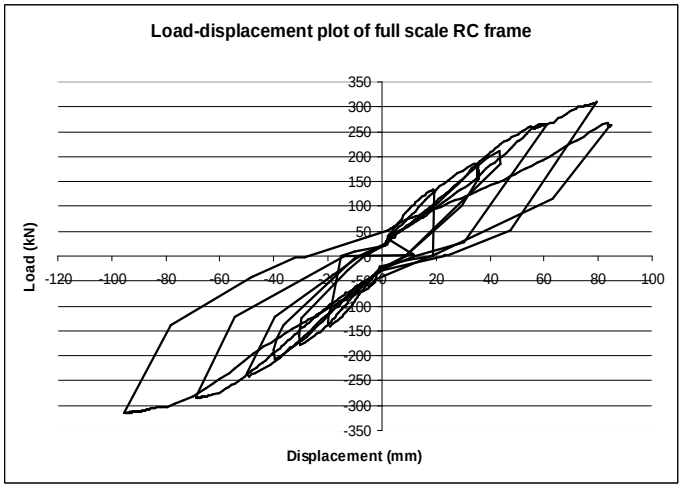

Figure 6. Hysteresis curve tested frame

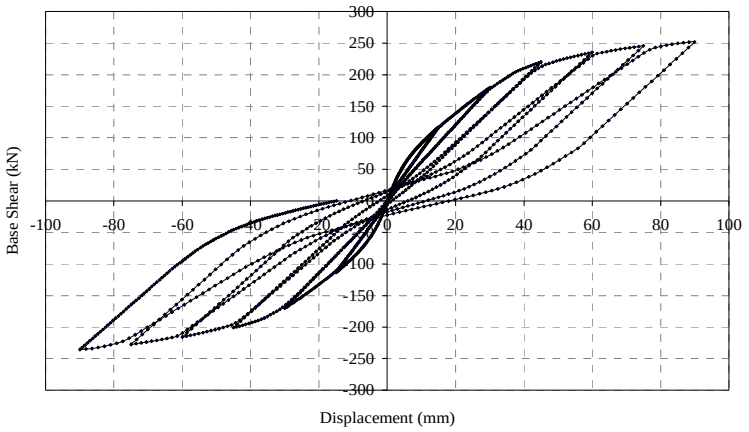

(a)

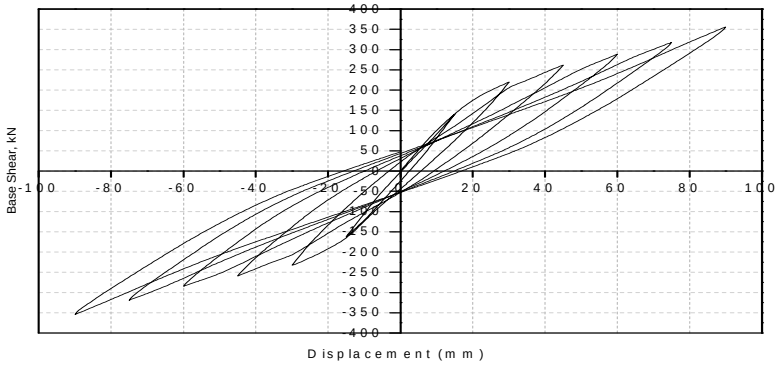

(b)

Figure 7. Hysteresis curve from OpenSees Model (a) 2D model (b) 3D model

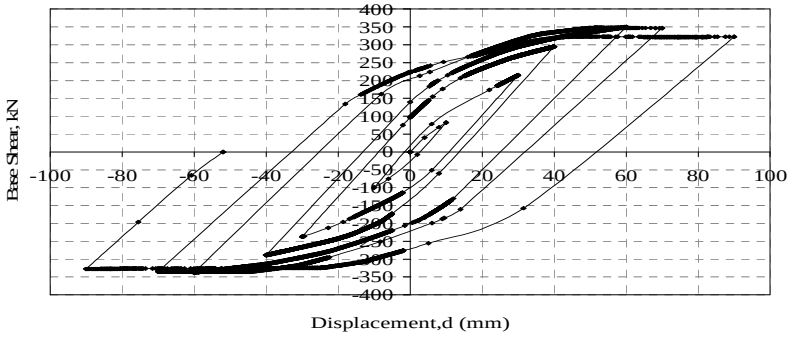

(a)

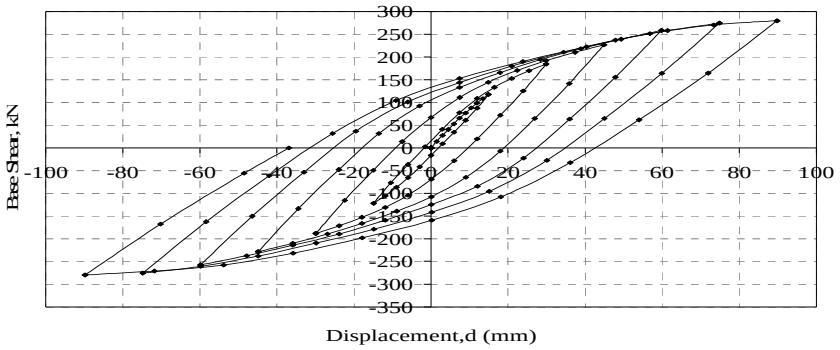

(b)

Figure 8. Hysteresis curve of ABAQUS analysis(a) 2D beam element model (b) 3D shell element model

Result of thermo-mechanical analysis

After simulating damage from cyclic loading the frame was subjected to a 1 hour compartment fire with a fixed ventilation opening [5]. A maximum displacement of 46mm at the middle of slab was recorded. The 3D OpenSees model showed maximum slab vertical displacement of 23mm as shows in Figure 9. The horizontal displacement of the columns as a result of the fire (starting from the point of permanent residual displacement) predicted by the 2D and 3D OpenSees models are shown in Figure 10. There is a mismatch in these results as the 2D model suggests a small recovery in the residual displacement but this is absent in the 3D model, which corresponds better with the test where no such recovery was recorded.

Figures 11 and 12 show the horizontal displacement of the column along the height of the columns from 2D and 3D models using ABAQUS. The height is measured from the plinth beam. The both columns appear to stiffen under the heating and the residual displacement seems to recover slightly.

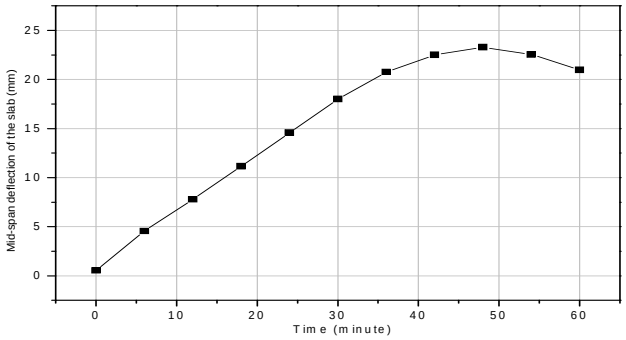

Figure 9. Vertical displacement of the slab from 3D OpenSees model

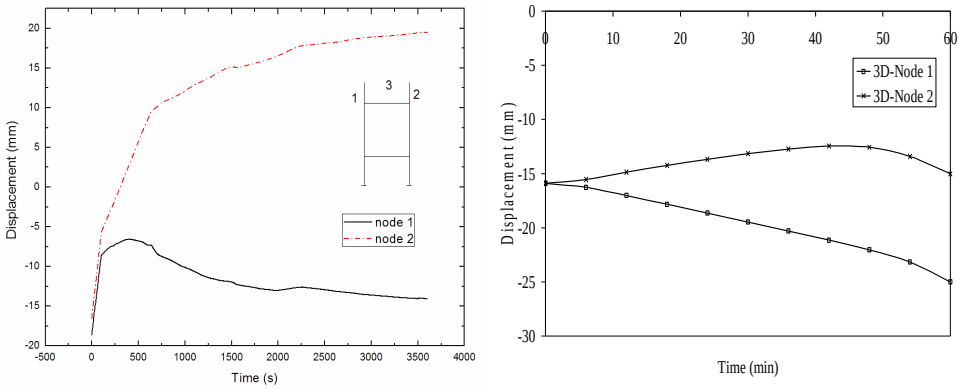

(a) 2D model (b) 3D model

Figure 10. Horizontal displacement of columns of model by OpenSees

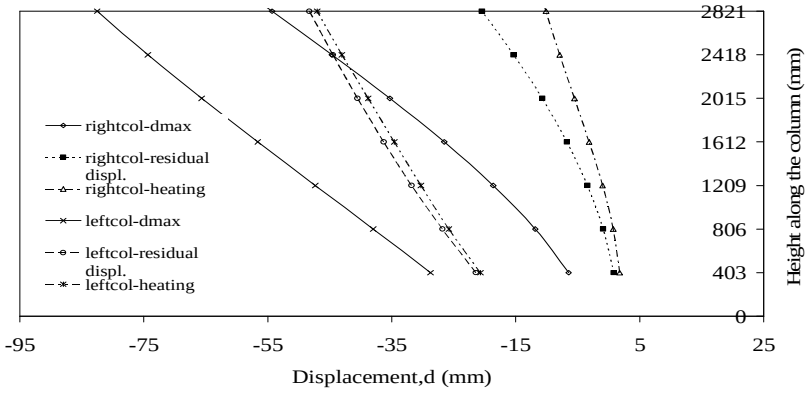

Figure 11. Horizontal displacement of the column along the height (ABAQUS 2D model)

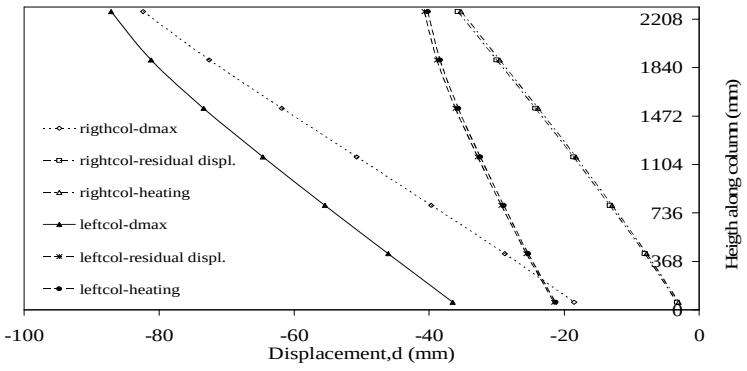

Figure 12. Horizontal displacement of the column along the height (ABAQUS 3D model)

DISCUSION AND CONCLUSION

2D and 3D analyses of a damaged reinforced frame subjected to fire carried out using ABAQUS and OpenSees has been presented and compared with selected test results. Temperature distributions obtained from a heat transfer analysis (based on a mock compartment fire) are used as an input (applied at integration points of the elements).

The tested frame was reported to withstand the mechanical damage and subsequent fire without collapse. The observed capacity curve using ABAQUS and OpenSees predicted the test reasonably in terms of peak load and the target displacement, however there were some large differences between models. A permanent residual displacement in the tested frame of approximately 20mm after the cyclic loading phase seems to agree well with the OpenSees predictions, suggesting that the simulated damage was modelled reasonably well. The residual displacements from ABAQUS models showed much larger values than the test results. The phenomenon of 'pinching' during cyclic loading was clearly observed in the test results. The OpenSees model using a "pinching material" and could capture this effect in the analysis, it was not possible to capture it in the ABAQUS model. Considerable differences were observed between individual models and the test and work is going on to understand the reasons for these differences which should help understand the behaviour of earthquake damaged RC frames subjected to a subsequent fire.

ACKNOWLEDGEMENTS

This studies were carried out as part of a research project involving the University of Edinburgh and Indian Institute of Technology (IIT) Roorkee, India with the financial support of the UK-India Education and Research Initiative (UKIERI).

REFFRENCES

[1] Botting, R. The Impact of Post-Earthquake Fire on the Built Urban Environment. Fire Engineering Report 98/1. University of Canterbury, Christchurch,New Zealand, (1998).

[2] Scawthorn, C., Eidinger J.M. and Schiff, A.J., editors, Fire Following Earthquake, ASCE Publications (2005)

[3] Botting, R. and Buchanan, A. H. Building Design for Fire After Earthquake.Proc 12th World Conference on Earthquake Engineering (Auckland) Jan 13 to Feb 4.paper 1569, (2000.

[4] Usmani, A.S., Research priorities for maintaining structural fire resistance after seismic damage, The 14th World Conference on Earthquake Engineering, Beijing, China, October 12–17, (2008).

[5] Sharma, U.K. *et. al.*, Full scale testing of a damaged RC frame in fire, Structures and Buildings, Proceedings of the ICE, in press, 2012.

[6] Mazzoni, S., F. McKenna, and G.L. Fenves, OpenSees command language manual. Pacific Earthquake Engineering Research (PEER) Center, 2007.

[7] Bhargava, P., *et. al*., Fire Testing of an Earthquake Damaged RC Frame, Sixth International Conference on Structures in Fire, Michigan, June 2010

[8] ABAQUS, ABAQUS 6.8. 2008, Dassault Systemes Simulia Corp: Providence

[9] European Committee for Standardisation, Eurocode 2: Design of Concrete Structures- Part 1-2: General Rules - Structural Fire Design. 2004, BS EN 1992-1-2:2004.

[10] Lee, J., and G. L. Fenves, Plastic-Damage Model for Cyclic Loading of Concrete Structures, Journal of Engineering Mechanics, vol. 124, no.8, pp. 892-900, (1998).

[11] Usmani, A., Zhang, J., Jiang, J. Jiang, J. and Ian May, I., Using Opensees for Structures in Fire, J. of Structural Fire Engineering, vol. 3, no. 1, pp. 57-70, (2012).

Modelling of Reinforced Concrete Frames in Fire Following an Earthquake

Ab.Kadir M A[a], A.S Usmani[b], M. Gillie[c]

[a]PhD student, School of Engineering, The University of Edinburgh, Edinburgh EH9 3JF, United Kingdom

[b]Professor, School of Engineering, The University of Edinburgh, Edinburgh EH9 3JF, United Kingdom

[c]Lecturer, School of Engineering, The University of Edinburgh, Edinburgh EH9 3JF, United Kingdom

INTRODUCTION

Earthquakes are natural hazards which occur in seismic areas and can cause devastating damage in urban infrastructure and facilities. Sometimes earthquake events are followed by fires which may cause more damage than the earthquake itself. Essentially, seismic design codes are relevant for designing a structure for an expected level earthquake and do not consider fire safety. In general, these two events are considered to occur separately.

A large number of post-earthquake building fires result in the collapse of the buildings. As a result of earthquake damage the fire resistance of a structure may be significantly impaired. In their study of the 1906 San Francisco earthquake and the 1923 Tokyo earthquake, Scawtorn *et.al.* (2005) have shown that about 80% of the building damage was due to the fires following the earthquake rather than the earthquake itself. This may pose a serious threat to the structural integrity and be detrimental to the life safety of the occupants and rescue workers. Hence, it is prudent to consider such scenarios in the design of buildings constructed in seismic zones (Mousavi et al. 2008). Consequently,

understanding the performance and response of structures in a fire following an earthquake is important at the design stage.

The aim of this study is to model a number of experiments being conducted on 2D reinforced concrete frames exposed to fire following simulated cyclic pushover. Increasing cyclic displacements are applied at the slab level in a pushover analysis to simulate the damage to the structure as a result of an earthquake.

2. REINFORCED CONCRETE FRAME MODELLING

A number of preliminary analyses were carried out on a 2D finite element model of the frame to determine its capacity under lateral pushover and its behaviours under cyclic loads. Based on the results, from the preliminary analyses, increasing cyclic displacements was applied to the frame as a second loading step (after applying all gravity loading in the first step). The columns and beam cross-sections were then exposed to temperature distributions obtained from a heat transfer analysis also carried out in the preliminary stage.

The temperature distributions were the result of radiative hear fluxes from a one hour compartment fire applied to the internal surfaced of the frame.

A computational analysis for this study was performed using ABAQUS. The reinforced concrete frame consisted of four columns supporting four beams and a slab on top floor and four beams at plinth level. The frame was modelled as a 2D frame with beam elements assigned for columns, beams and slab. Truss elements were used to model reinforcement bars. The frame model is shown in Figure 1 The total height of the frame

is 6.0m with the distance between the plinth and top beams being roughly 3m. The cross section of the columns is 300mm x 300mm and that of the beams is

230mm x 230mm. Slabs thickness is 120mm. In order to reduce computational time the slab was modelled as apart of the overall beam cross section in 2D. Eight steel bars of 20 mm diameter were used for the columns and six steel bars of 16mm diameter were used for beam (3 each on the top and bottom). Node and element numbering of the model was as shown in Figure 2 and Figure 3.

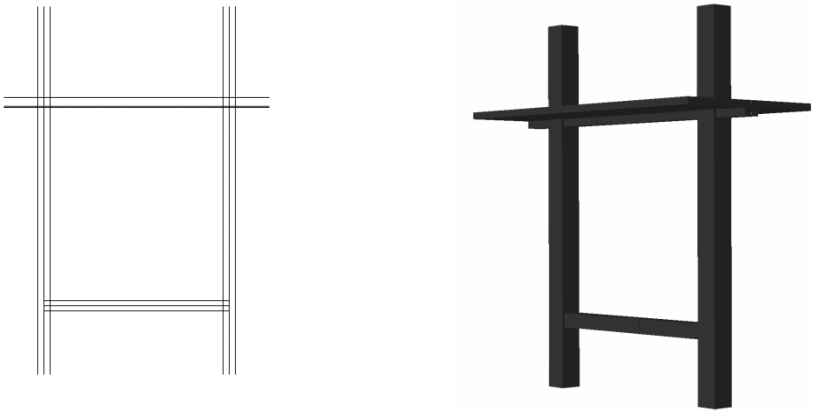

Fig. 1 2D The Analytical model

Temperature dependent material properties for concrete and steel were assigned according to the Euro Code 2. Concrete strength of 34MPa and steel strength 415 MPa was used. Permanent loads of 100kN on each column and 2.3kN/m^2 on the slab are applied. This load was constant throughout the analysis. Due to loading and unloading cycles on the frame, degradation of strength of the concrete and reinforcing bars was considered. Therefore, the concrete damaged plasticity was used in the analysis.

In the thermo-mechanical analysis, temperatures were assigned at the integration points of the elements at node locations. Five temperatures were assigned to the beam and three node temperatures to the column. The temperature exposures were assumed to occur only between the plinth beams

and the top beam slab. The compartment temperatures were increased from 20^{o}C to 1000^{o}C in 5 minutes and maintained for another 55 minutes, as in Figure 4.

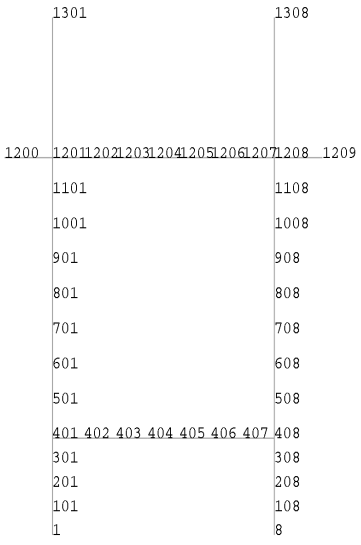

Fig. 2 Node Numbering

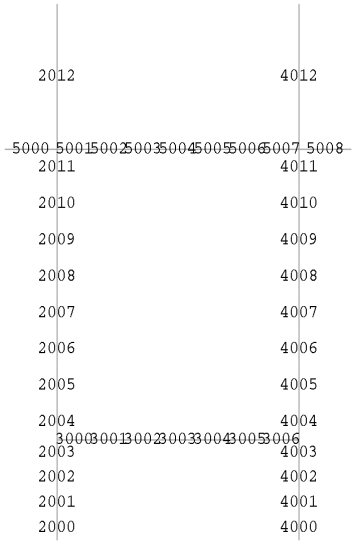

Fig. 3 Element Numbering

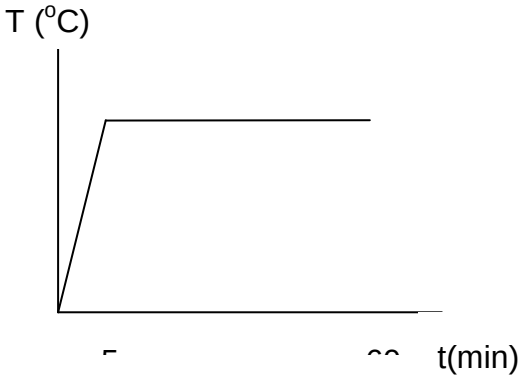

Fig. 4 Temperature Amplitude

3.0 PERFORMANCE OF RC FRAME

An analysis was performed to get an overview of the capacity of the frame. Figure 5 shows the hysteresis curve after a 7 cycle displacement load was applied at the slab level of the frame. Displacement was also observed at the slab level (node number 1208). The maximum base shear is around 300kN corresponding to a displacement of the frame of approximately 90mm. Three further cases were studied. A maximum displacement of 100mm was applied over 4 cycles for case I, 70% of this for case II and 30% for case III.

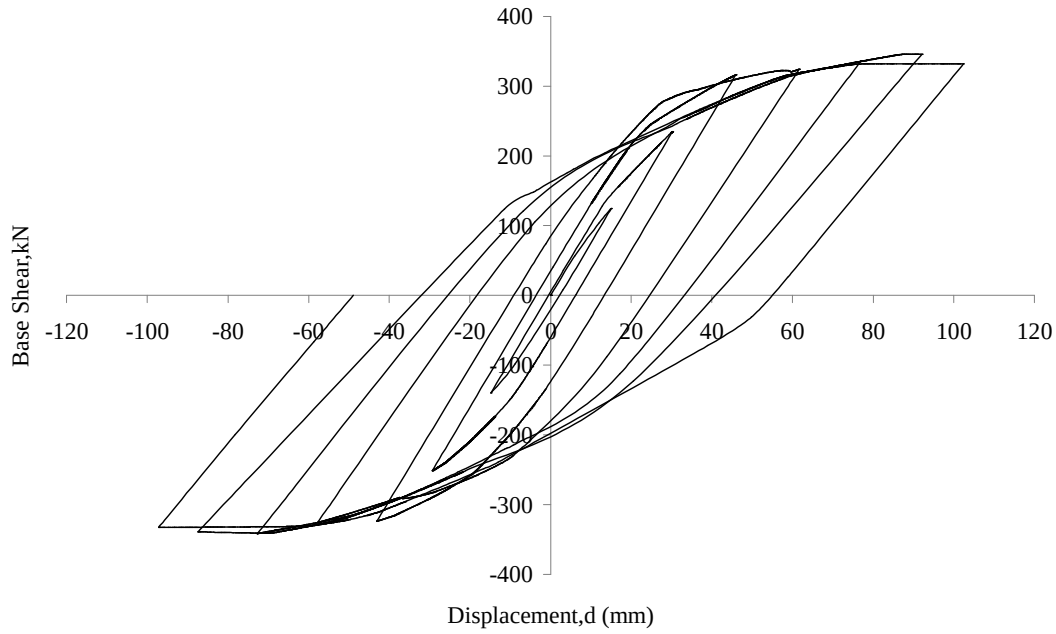

Fig. 5 Hysteresis Curve

Figure 6 illustrates the displacement history for the three cases. The results in this figures show that there are residual displacements after when the base shear is brought to zero at the end of the loading cycles. The residual

displacements are seen to increase with increasing magnitudes of the applied cyclic displacements.

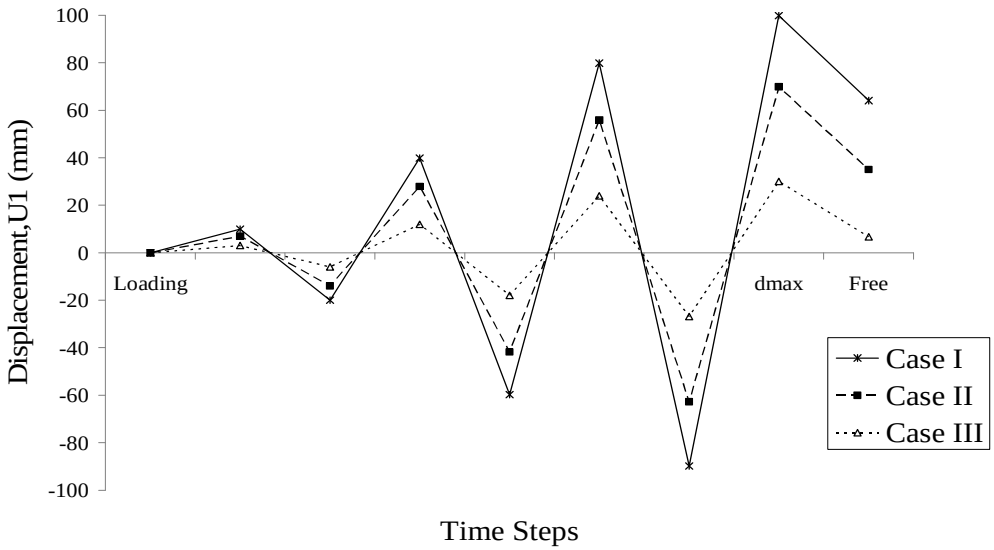

Fig. 6 Displacement history

Figure 7 shows the displacement history when after the frame is subjected to heating for all the three cases. The frame appears to stiffen under the heating and the residual displacements seem to recover. The reaction forced of the frame for the cases was observed in this study as shown in Figure 8.

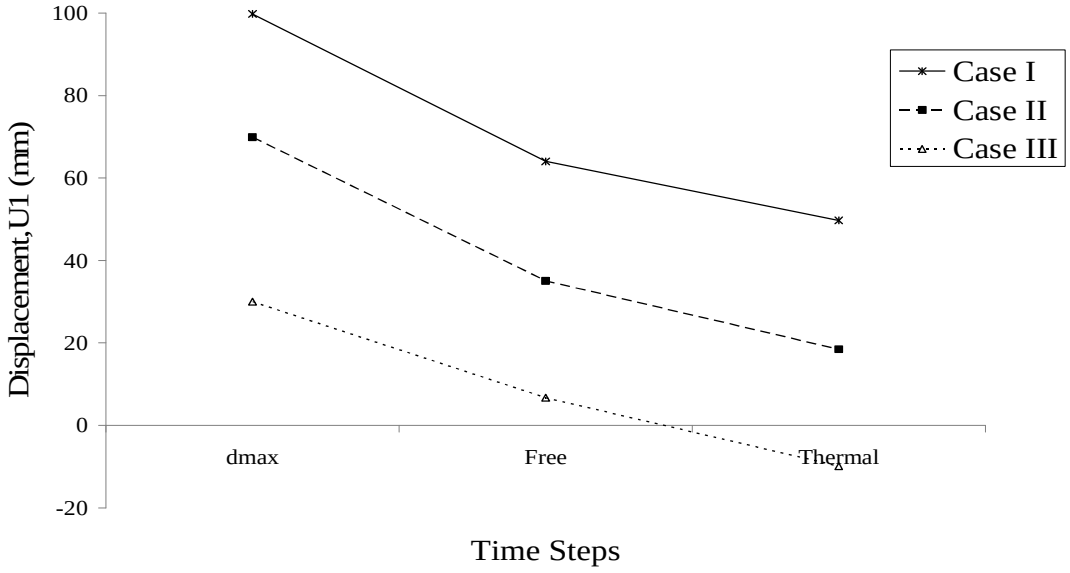

Fig. 7 Displacement of the frame after the temperature applied

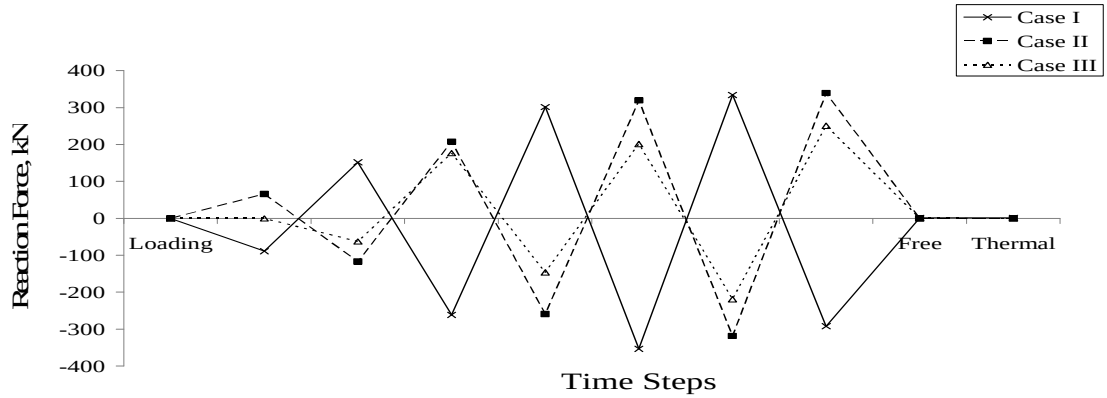

Fig. 8 Reaction force of the frame for the three cases

4. COMPARISONS

The eventual aim of this work is to compare the computational results with the test results on real frame currently being carried out at IIT Roorkee in India..

Both the model development and the tests are currently incomplete and full finding will be reported in future papers.

5. CONCLUSION

This study was carried out to model a number of experiments being conducted on 2D reinforced concrete frame exposed to the fire following simulated cyclic pushover. The computational analysis shows there is a reduction in the residual displacement of the frame after heating. Further studies need to be implemented to compare the computational analysis with the test results.

6. ACKNOWLEDGEMENTS

This study has been funded by Universiti Teknologi Malaysia. We would like to thank all members in the UK-India Education and Research Initiative (UKIERI) project group which has contributed the data.

REFERENCES

Abaqus: Abaqus Analysis User's Manual. Providence, Dassault Systemes Simula Corp,2008

EN1992-1-2. Eurocode 2: Design of concrete Structures-Part 1-2: General Action-Actions on Structures Exposed to Fire, 1999.

Mousavi, S. Bagchi, A. Kodur, V.K.R. Post-Earthquake Fire Hazard to Building structures, Canadian Journal of Civil Engineering, 35: 689-698, 2008

Scawthon, C., Eidinger J.M. and Schiff, A.J., editors, Fire Following Earthquake, ASCE Publications, 2005.